Department of Electrical and Computer Engineering

Correction and Compensation of I/Q Imbalance and Multipath Channel

Khandker Nadya Haq

This thesis is presented for the Degree of

Doctor of Philosophy
of
Curtin University

January 2015

DECLARATION

To the best of my knowledge and belief, this thesis contains no material previously published by any other person except where due acknowledgement has been made.

This thesis contains no material which has been accepted for award of any other degree or diploma in any university.

Signature: …….

Date: ……

ACKNOWLEDGEMENT

I would like to express my deepest appreciation and earnest gratitude to my retired supervisor, Professor Kah-Seng Chung for his constant guidance and advice throughout the course of this research.

I would also like to express my heartfelt gratitude to my supervisor, Professor Sven Nordholm for his supervision, support and enormous help. Also I would like to thank my co-supervisor Dr. Ba Tuong Vo for his direction and support.

In addition, I would like to thank all the members in the Communication Technology Research Group (CTRG) especially my friend Xiaolin Wu, for providing a friendly and supportive working environment.

I would also like to express my thankfulness to my parents Khandker Mozaharul Haq and Farida Yasmeen and my brother Khandker Azimul Huq for their constant love and prayers. I would like to thank my husband Shakhawat Hossain Molla for his relentless support and care. A special thanks to my best friend Tanzim Faruque Aditi from Newcastle University, for her rigours review which helped me to write this thesis with more precision.

Last but not least, I would like to dedicate this thesis to my 3 years old daughter, Fiona Shamseen Molla, whose smile always brings joy in my life.

ABSTRACT

Superheterodyne receivers with one or more stages of frequency down translation are the most well established and commonly used receiver architectures in contemporary radio communication systems. Their proper operation, however, demands the use of high performance bandpass filters for image rejection and channel selectivity. The stringent specifications required for such bandpass filters are not yet able to be met by means of monolithic integration. On the other hand, the relatively simpler direct conversion receiver (DCR) architecture, which down translates the incoming radio frequency (RF) signal directly to a zero intermediate frequency (IF) signal, does not suffer from any image problems. This direct down-conversion is carried out by a quadrature demodulator comprised of an in-phase (I) and a quadrature (Q) signal branches. However, for such a dual branch receiver to operate perfectly, it requires the I and Q signal branches to have exactly the same gain and be precisely 90^{o} out of phase. Any deviations from these perfect conditions will give rise to what is commonly referred to as I/Q imbalance. The presence of an I/Q imbalance will result in degradation of the signal quality caused by a self-image of the signal. Nonetheless, due to practical circuit imperfections and component tolerances, mismatch in the two signal paths often becomes unavoidable. Hence, I/Q imbalance problem is considered to be the key stumbling block to adopting DCR architecture for monolithic integration of a complete single chip receiver. As the data rates in wireless communications continue to increase, the need to adopt higher order modulation schemes becomes mandatory. Moreover, the performance of such modulation schemes is more susceptible to the presence of any signal distortion. Now, as a broadband radio signal is also known to suffer from intersymbol interference (ISI) caused by multipath propagation, this further aggravates any attempt to overcome the I/Q imbalance problem. Any effective solution would require the two forms of signal impairment, caused by I/Q imbalance and multipath propagation, to be distinguished and acted upon. This difficult technical challenge forms the basis of this research. At present, the I/Q imbalance problem is not likely to be solved by means of better circuit design. Therefore, digital processing is required in order to correct and compensate for the effect of I/Q imbalance and channel.

The aim of this thesis is to deliver an in-depth study of I/Q imbalance and multipath propagation. In order to fulfil this aim, this thesis presents correction and compensation schemes to mitigate the joint effect of these two impairments on orthogonal frequency division multiplexing (OFDM) and single carrier modulation. For OFDM, an adaptive combined correction and compensation (ACCC) scheme has been presented which is capable of correcting and compensating for the effects of the frequency-selective I/Q imbalance and multipath propagation. The performance of the proposed scheme has been extensively studied by means of computer simulations using MATLAB. With the proposed ACCC scheme, the signal to noise ratio (SNR) degradation is approximately 2 dB higher than the reference symbol error rate (SER) obtained for no I/Q imbalance and channel condition, at a specified symbol error rate (SER) of 10^{-3}. Next, in order to assess the robustness of the proposed ACCC scheme, it has been compared with three other previously published schemes, under different simulation conditions. For a low level of I/Q imbalance with an image rejection ratio (IRR) of 25.93 dB, almost all tested schemes show similar performances. On the other hand, for moderate and high level of I/Q imbalance condition with an average IRR of 17.1 dB and 8.6 dB respectively, the proposed ACCC scheme achieves the lowest symbol error rate (SER). The results depict that the ACCC scheme significantly outperforms the three other existing schemes by expending less than 2% of the subcarriers as pilots. For single carrier modulation, two methods for correcting and compensating for I/Q imbalance and channel have been presented. Both of these two proposed methods share the same I/Q imbalance and channel parameters estimation technique. Parameter estimation has been carried out with the assistance of a known reference signal using least mean square (LMS) adaptive filters. As the unknown parameters are estimated, Method 1, referred to as the adaptive time domain correction method, carries out I/Q imbalance correction followed by equalization of the multipath channel in the time domain. On the other hand, Method 2, employs frequency domain compensation to jointly mitigate the I/Q imbalance and channel imperfections. A 2 dB signal to noise ratio (SNR) degradation, compared to the reference SER, is obtained for a specified SER 10^{-3}. This has also been achieved in the presence of a 20% gain and 10^{o} phase deviation, provided that the gain and phase remain relatively flat over the entire bandwidth.

Robust schemes for correcting and compensating for the adverse effects of I/Q imbalance and multipath channel distortions, have been proposed in this thesis. The effectiveness of the schemes has been verified by means of simulation performances. It has been shown that even a severe level of I/Q imbalance can be corrected and compensated for by means of the proposed schemes.

TABLE OF CONTENTS

DECLARATION i

ACKNOWLEDGEMENT ii

ABSTRACT iii

TABLE OF CONTENTS vi

LIST OF FIGURES x

LIST OF TABLES xviii

LIST OF SYMBOLS AND NOTATIONS xix

LIST OF ACRONYMS xxv

CHAPTER 1 INTRODUCTION 1

1.1 Scope of the thesis 1

1.2 Objectives and original contributions of the thesis 3

1.3 Organization of the thesis 5

CHAPTER 2 BACKGROUND AND LITERATURE REVIEW 8

2.1 Introduction 8

2.2 Introduction to the popular receiver architecture 9

2.2.1 Superheterodyne receivers 9

2.2.2 Direct conversion receivers 11

2.3 Introduction to I/Q Imbalance 13

2.4 Compensation and correction of I/Q imbalance and multipath channel 16

2.4.1 Compensation and correction of I/Q imbalance for single carrier modulation 18

2.4.1.1 I/Q imbalance compensation by generating test sinusoid 18

2.4.1.2 I/Q imbalance compensation using known training sequences 20

2.4.1.3 I/Q imbalance and channel compensation using no reference signal 20

2.4.2 Compensation and correction of I/Q imbalance and channel for OFDM 22

2.4.2.1 I/Q imbalance compensation using pilot subcarriers 23

2.4.2.2 I/Q imbalance compensation by non-data aided or blind method..... 27

2.5 I/Q imbalance schemes presented in the dissertation..... 29

2.6 Summary 30

CHAPTER 3 MODELLING OF I/Q IMBALANCE..... 31

3.1 Introduction..... 31

3.2 Representation of bandpass waveforms and systems..... 31

3.3 Complex envelope and baseband equivalent representation of transmit signal, received signal and channel 32

3.4 General mathematical model of I/Q imbalance for single carrier modulation 35

3.5 OFDM transmission..... 38

3.6 I/Q imbalance modelling for OFDM..... 41

3.7 Effects of frequency-flat I/Q gain and phase imbalance and channel on an OFDM system 46

3.7.1 Signal constellations 47

3.7.2 Symbol error rate (SER)..... 54

3.8 Summary 60

CHAPTER 4 ADAPTIVE COMBINED CORRECTION AND COMPENSATION (ACCC) SCHEME FOR I/Q IMBALANCE AND MULTIPATH CHANNEL FOR OFDM RECEIVERS..... 62

4.1 Introduction..... 62

4.2 I/Q imbalance values used 64

4.2.1 Frequency-flat I/Q imbalance values used..... 65

4.2.2 Frequency-selective I/Q imbalance..... 65

4.3 Adaptive Combined Correction and Compensation Scheme (ACCC) 67

4.3.1 System model..... 67

4.3.2 Pilot pattern adopted for this proposed method 69

4.3.3 Estimation of I/Q imbalance and channel parameters..... 70

4.3.4 Estimation of nominal gain and phase 73

4.3.5 Interpolation for I/Q and channel parameters 76

4.3.6 Correction and compensation for the data period 77

4.4 Evaluation of the proposed ACCC scheme..... 78

4.4.1 Simulation platform used for the evaluation of the proposed scheme 78

4.4.2 Pilot detection 80

4.4.3 Estimated I/Q and channel parameters for different constant gain and phase84

4.4.4 Estimated I/Q and channel parameters for different variable I/Q models ... 87

4.4.5 Estimated nominal gain and phase..... 90

4.4.6 Signal constellations 93

4.4.7 Error vector magnitude (EVM)..... 101

4.4.8 Average Symbol error rate (SER) performance..... 104

4.4.9 Evaluation of the proposed scheme for different channel scenario 107

4.4.10 Evaluation of the proposed scheme for frequency-flat I/Q imbalance 111

4.5 Summary 115

CHAPTER 5 PERFORMANCE COMPARISON FOR DIFFERENT CORRECTION AND COMPENSATION SCHEMES 116

5.1 Introduction..... 116

5.2 The joint compensation scheme..... 117

5.3 The separate/de-coupled compensation scheme 119

5.4 The adaptive LMS compensation scheme..... 123

5.5 Performance comparison of different schemes..... 125

5.5.1 Performance comparison under different frequency-selective I/Q imbalance126

5.5.2 Performance comparison under various frequency-flat gain and phase 138

5.5.3 Performance comparison under different IRR level 142

5.5.4 Performance comparison under different number of pilots 148

5.6 Summary 151

CHAPTER 6 CORRECTION AND COMPENSATION OF I/Q IMBALANCE FOR SINGLE CARRIER MODULATIONS 152

6.1 Introduction 152

6.2 I/Q imbalance for the single carrier modulation 153

6.3 Method 1: An Adaptive time domain estimation and correction method 155

6.3.1 Simulation results for time domain correction method 160

6.4 Method 2: A frequency domain compensation method by adding CP 178

6.4.1 Simulation results for the frequency domain compensation 184

6.5 Comparison of time domain correction and frequency domain compensation schemes 191

6.6 Summary 196

CHAPTER 7 CONCLUSION AND FUTURE WORKS 197

7.1 Conclusion 197

7.2 Future work 202

APPENDIX A PROPOSED ACCC FOR SC-FDE 203

Step 1: Pre-FFT Correction 203

Step 2: Nominal gain and phase estimation 205

Step 3: Frequency domain compensation 208

APPENDIC B PARALLEL CORRECTION AND EQUALIZATION OF I/Q IMBALANCE AND CHANNEL FOR SINGLE CARRIER MODULATIONS 209

APPENDIX C LIST OF PUBLICATIONS 214

REFERENCES 215

LIST OF FIGURES

Figure 2-1 Superheterodyne receiver 10
Figure 2-2 Direct conversion or zero-IF receiver 12
Figure 2-3 Quadrature down-conversion by a) Shifting the RF signal by 90^o b) Shifting the LO output by 90^o 14
Figure 2-4 Ideal complex down-conversion 17
Figure 2-5 Effects of self-image caused by I/Q imbalance in direct conversion receivers 17

Figure 3-1 Down-conversion in dual branch receiver represented in baseband ... 34
Figure 3-2 The model of a DCR incorporating I/Q imbalance 36
Figure 3-3 OFDM Spectrum 39
Figure 3-4 Block diagram of a general OFDM system 40
Figure 3-5 Simulation Set-up 46
Figure 3-6 Constellations of the received signal after being distorted by a) I/Q gain only, b) I/Q phase only c) I/Q gain and phase, for 64-QAM ... 48
Figure 3-7 Constellations of the received signal after being distorted by a) I/Q gain only, b) I/Q phase only c) I/Q gain and phase, for 16-QAM ... 49
Figure 3-8 Constellations of the received signal after being distorted by a) I/Q gain only, b) I/Q phase only c) I/Q gain and phase, for QPSK 50
Figure 3-9 Constellations of the received signal after being distorted by a) channel only, b) channel and I/Q, for 64-QAM 51
Figure 3-10 Constellations of the received signal after being distorted by a) channel only, b) channel and I/Q, for 16-QAM 52
Figure 3-11 Constellations of the received signal after being distorted by a) channel only, b) channel and I/Q, QPSK 53

Figure 3-12 SER for uncompensated received signal for 64-QAM..... 55
Figure 3-13 SER for uncompensated received signal for 16-QAM..... 56
Figure 3-14 SER for uncompensated received signal distorted by different I/Q gain and phase combinations, for 64 QAM 57
Figure 3-15 SER for uncompensated received signal distorted by different I/Q gain and phase combinations, for 16-QAM 58
Figure 3-16 SER for uncompensated received signal distorted by I/Q and channel for 64-QAM 59
Figure 3-17 SER for uncompensated received signal distorted by I/Q and channel for 16-QAM 60

Figure 4-1 Frequency-selective I/Q imbalance for Model 1 (a) Gain imbalance = $20log_{10}\left|\frac{A_I[k]}{A_Q[k]}\right|$., (b) Phase imbalance =$Arg\left\{\frac{A_I[k]}{A_Q[k]}\right\}$..... 66
Figure 4-2 Frequency-selective I/Q imbalance for Model 2. (a) Gain imbalance = $20log_{10}\left|\frac{A_I[k]}{A_Q[k]}\right|$., (b) Phase imbalance =$Arg\left\{\frac{A_I[k]}{A_Q[k]}\right\}$..... 66
Figure 4-3 Block diagram of the ACCC scheme 68
Figure 4-4 Pilot and data arrangement 70
Figure 4-5 Signal constellations for the pilot tones for Model 1 for a) first frame b) second frame and c) third frame, for 30 dB SNR 80
Figure 4-6 Signal constellations for the pilot tones for Model 2 for a) first frame b) second frame and c) third frame, for 30 dB SNR 80
Figure 4-7 Signal constellations for the pilot tones for Model 1 for a) first frame b) second frame and c) third frame, for 20 dB SNR 82
Figure 4-8 Signal constellations for the pilot tones for Model 2 for a) first frame b) second frame and c) third frame, for 20 dB SNR 82
Figure 4-9 Estimated I/Q and channel parameters for Model 1 for first frame 88
Figure 4-10 Estimated I/Q and channel parameters for Model 1 for third frame . 88

Figure 4-11 Estimated I/Q and channel parameters for Model 2 for first frame .. 89
Figure 4-12 Estimated I/Q and channel parameters for Model 2 for third frame . 90
Figure 4-13 Estimated a) Nominal gain and b) Nominal phase for Model 1 for different number of frames..... 91
Figure 4-14 Estimated a) nominal gain and b) nominal phase for Model 2 for different number of frames..... 92
Figure 4-15 Constellations for 64-QAM signal for Model 1 for a) uncompensated b) first frame and c) third frame..... 95
Figure 4-16 Constellations for 16-QAM signal for Model 1 for a) uncompensated b) first frame and c) third frame..... 96
Figure 4-17 Constellations for QPSK signal for Model 1 for a) uncompensated b) first frame and c) third frame 97
Figure 4-18 Constellations for 64-QAM signal for Model 2 for a) uncompensated b) first frame and c) third frame..... 98
Figure 4-19 Constellations for 16-QAM signal for Model 2 for a) uncompensated b) first frame and c) third frame..... 99
Figure 4-20 Constellations for QPSK signal for Model 2 for a) uncompensated b) first frame and c) third frame..... 100
Figure 4-21 EVM for different OFDM frames for Model 1 102
Figure 4-22 EVM for different OFDM frames for Model 2 103
Figure 4-23 SER for different OFDM frames for Model 1..... 104
Figure 4-24 SER for different OFDM frames for Model 2..... 105
Figure 4-25 SER for different frequency-flat gain and phase combination for tenth frame for Model 2 106
Figure 4-26 SER for different numbers of pilots for tenth frame for Model 2 ... 107
Figure 4-27 Signal constellation of pilot tones, for Ricean channel for delays of a) 1Ts b) 7Ts and c) 14Ts 108

Figure 4-28 SER for ETU and Ricean channel for first and tenth frames for Model 2 109
Figure 4-29 SER for ETU and Ricean channel for first frame, corresponding to different delays..... 110
Figure 4-30 SER for ETU and Ricean channel for tenth frame, corresponding to different delays..... 111

Figure 5-1 Constellations of a) Uncompensated b) Decoupled compensation c) Joint compensation d) adaptive LMS compensation e) ACCC Frame 1 f) ACCC Frame 3, for 64-QAM, for Model 1 128
Figure 5-2 Constellations of a) Uncompensated b) Decoupled compensation c) Joint compensation d) Adaptive LMS compensation e) ACCC Frame 1 f) ACCC Frame 3, for QPSK, for Model 1..... 129
Figure 5-3 Constellations of a) Uncompensated b) Decoupled compensation c) Joint compensation d) Adaptive LMS compensation e) ACCC Frame 1 f) ACCC Frame 3 ,for 64-QAM, for Model 2 131
Figure 5-4 Constellations of a) Uncompensated b) Decoupled compensation c) Joint compensation d) Adaptive LMS compensation e) ACCC Frame 1 f) ACCC Frame 3, for QPSK, for Model 2..... 132
Figure 5-5 EVM for different I/Q imbalance compensation schemes, for Model 1, for 64-QAM 133
Figure 5-6 EVM for different I/Q imbalance compensation schemes, for Model 2, for 64-QAM 135
Figure 5-7 SER for different I/Q imbalance compensation schemes, for Model 1, for 64-QAM 136
Figure 5-8 SER for different I/Q imbalance compensation schemes, for Model 2, for 64-QAM 137

Figure 5-9 SER for different frequency-flat gain and phase for Model 1, for joint and decoupled compensation schemes..... 139
Figure 5-10 SER for different frequency-flat gain and phase for Model 2, for joint and decoupled Compensation schemes..... 140
Figure 5-11 SER for different frequency-flat gain and phase for Model 1, for adaptive LMS and proposed ACCC schemes. 141
Figure 5-12 SER for different frequency-flat gain and phase for Model 2, for adaptive LMS and proposed ACCC schemes. 142
Figure 5-13 IRR corresponding to low I/Q..... 143
Figure 5-14 SER performance under low I/Q..... 144
Figure 5-15 IRR corresponding to moderate I/Q..... 145
Figure 5-16 SER performance under moderate I/Q..... 145
Figure 5-17 IRR corresponding to high I/Q..... 146
Figure 5-18 SER performance under high I/Q..... 147
Figure 5-19 SER for different pilots for Model 1 for the joint compensation scheme..... 149
Figure 5-20 SER for different pilots for Model 1 for the decoupled compensation scheme..... 149
Figure 5-21 SER for different pilots for Model 1 for the adaptive LMS compensation scheme 150
Figure 5-22 SER for different pilots for Model 1 for the proposed ACCC scheme150

Figure 6-1 Adaptive estimations of I/Q imbalance and channel parameters with an In-phase and Quadrature filter network..... 156
Figure 6-2 A frame structure that incorporates a preamble for the reference training signal in each frame..... 156
Figure 6-3 Simulation setup for the time domain correction method..... 157

Figure 6-4 MSE for different SNR level for 64-QAM 162
Figure 6-5 MSE for different step size μ, for 64-QAM 163
Figure 6-6 Estimated nominal gain for 64-QAM..... 165
Figure 6-7 Estimated nominal phase for 64-QAM 165
Figure 6-8 Estimated nominal gain for16-QAM..... 166
Figure 6-9 Estimated nominal phase for 16-QAM 166
Figure 6-10 Constellation of the uncorrected signal, for 64-QAM..... 168
Figure 6-11 Constellation of the received signal after being corrected by the time domain correction method, for 64-QAM 168
Figure 6-12 Constellation of the uncorrected signal, for 16-QAM..... 169
Figure 6-13 Constellation of the received signal after being corrected by the time domain correction method, for 16-QAM 169
Figure 6-14 Constellation of the uncorrected signal, for QPSK 170
Figure 6-15 Constellation of the received signal after being corrected by the time domain correction method, for QPSK..... 170
Figure 6-16 EVM for different frames of the received signal corrected by the time domain correction method, for 64-QAM 172
Figure 6-17 EVM for different frames of the received signal corrected by the time domain correction method, for 16-QAM 173
Figure 6-18 EVM for different gain and phase after being corrected by the time domain correction method, for 64-QAM 174
Figure 6-19 EVM for different gain and phase after being corrected by the time domain correction method, for 16-QAM 175
Figure 6-20 SER for different frames of the received signal corrected by the time domain correction method, for 64-QAM 176
Figure 6-21 SER for different frames of the received signal corrected by the time domain correction method, for 16-QAM 177

Figure 6-22 SER for different gain and phase combinations after being corrected by the time domain correction method, for 64-QAM and 16-QAM178
Figure 6-23 Simulation set-up for the frequency domain compensation method179
Figure 6-24 MSE for different SNR levels 185
Figure 6-25 Constellation of the uncompensated signal, for 64-QAM..... 186
Figure 6-26 Constellation of the received signal after being compensated by the frequency domain compensation method, for 64-QAM 186
Figure 6-27 Constellation of the uncompensated signal, for 16-QAM..... 187
Figure 6-28 Constellation of the received signal after being compensated by the frequency domain compensation method, for 16-QAM 187
Figure 6-29 Constellation of the uncompensated signal, for QPSK 188
Figure 6-30 Constellation of the received signal after being compensated by the frequency domain compensation method, for QPSK..... 188
Figure 6-31 EVM for different gain and phase combinations after compensation by the frequency domain compensation technique for 64-QAM... 189
Figure 6-32 EVM for different gain and phase combinations after compensation by the frequency domain compensation technique for 16-QAM... 190
Figure 6-33 SER for different gain and phase combinations after being compensated by the frequency domain compensation technique, for 64-QAM and 16-QAM..... 191
Figure 6-34 EVM representation for the time domain correction and frequency domain compensation, for 64-QAM 192
Figure 6-35 EVM representation for the time domain correction and frequency domain compensation, for 16-QAM 193
Figure 6-36 SER representation for the time domain correction and frequency domain compensation..... 194

Figure A-1 Block diagram of the ACCC scheme on SC-FDE 203
Figure B-2 Block diagram for parallel correction and equalization 211

LIST OF TABLES

Table 4-1 Simulation Parameters 78

Table 4-2 A 9 path Extended Typical Urban (ETU) LTE channel 79

Table 4-3 Percentage of pilots detected in error for Model 1 83

Table 4-4 Percentage of pilots detected in error for Model 2 83

Table 4-5 Estimated parameters for different gain and phase combination for the first frame 85

Table 4-6 Estimated parameters for different gain and phase combination for the third frame 86

Table 4-7 Nominal gain and phase for different frequency-flat gain and phase ... 93

Table 6-1 Simulation Condition 160

Table 6-2 Channel Parameters 161

LIST OF SYMBOLS AND NOTATIONS

In the following, the principal mathematical notations are listed. For notation, all the time domain signals have been denoted by lower case ($x[n]$) and frequency domain signal has been denoted as upper case ($X[f]$). Vectors are represented by bold cases (**X**). Matrices are denoted as bold cases with a bar ($\overline{\mathbf{X}}$).

$\lvert . \rvert$	Absolute value
$w_I[n]$	Adaptive filter coefficients of the In-phase branch for single carrier modulation
$w_Q[n]$	Adaptive filter coefficients of the Quadrature branch for single carrier modulation
$\acute{\eta}[k]$	Additive white Gaussian noise in frequency domain with I/Q imbalance after being corrected
$\eta[k]$	Additive white Gaussian noise in frequency domain with I/Q imbalance
$\varepsilon_T[n]$	Additive white Gaussian noise in time domain with I/Q imbalance
$\varepsilon[n]$	Additive white Gaussian noise in time domain without I/Q imbalance
$z(t)$	Analogue received signal in time domain with frequency-flat I/Q imbalance
$r(t)$	Analogue received signal in time domain without any I/Q imbalance
$x(t)$	Analogue transmit signal in time domain
$y(t)$	Analogue uncompensated/uncorrected received signal in time domain with frequency-flat and frequency-selective I/Q imbalance
$h_p(t)$	Bandpass equivalent of channel's impulse response
$z_p(t)$	Bandpass equivalent of the received signal with only frequency-flat I/Q imbalance

$r_p(t)$	Bandpass equivalent of the received signal without I/Q imbalance
$x_p(t)$	Bandpass equivalent of the transmit signal
f_c	Carrier frequency
$H[k]$	Channel transfer function
$\circledast$	Circular convolution
$\widehat{W}_k$	Compensation coefficients of decoupled compensation
$[.]^*$	Conjugate of a vector
$z[n]$	Digital received signal with frequency-flat I/Q imbalance and channel in time domain
$y[n]$	Digital received uncompensated/uncorrected signal in time domain with frequency-flat and frequency-selective I/Q imbalance and channel
$c[n]$	Digital received signal with I/Q imbalance and channel in time domain after undergone correction
$r[n]$	Digital received signal without I/Q imbalance in time domain
$\mathbf{X}$	Digital transmitted OFDM block in frequency domain
$\mathbf{x}$	Digital transmitted OFDM block in time domain
$X[k]$	Digital transmitted signal in frequency domain
$x[n]$	Digital transmitted signal in time domain
$\bar{\mathbf{F}}$	Discrete Fourier transform matrix (NxN)
$\bar{\mathbf{F}}^*$	Discrete inverse Fourier transform matrix (NxN)
d_p	Distance between two pilot subcarriers
$\hat{g}$	Estimate of frequency-flat gain g
$\hat{\varphi}$	Estimate of frequency-flat phase φ
$\hat{X}[k]$	Estimate of $X[k]$
$\hat{x}[n]$	Estimate of $x[n]$
f	Frequency in Hz
$A_I[n]$	Frequency response of the In-phase signal branch
$A_Q[n]$	Frequency response of the Quadrature signal branch

$u[n]$	I/Q impulse response for the desired signal
$v[n]$	I/Q impulse response for the image signal
$\check{U}[k]$	I/Q transfer function after correction for desired signal
$\check{V}[k]$	I/Q transfer function after correction for image signal
$U[k]$	I/Q transfer function for the desired signal
$V[k]$	I/Q transfer function for the image signal
$h[n]$	Impulse response of channel
$a_I[n]$	Impulse response of the frequency-selective I/Q imbalance in In-phase branch
$a_Q[n]$	Impulse response of the frequency-selective I/Q imbalance in Quadrature branch
k	Index for frequency
m	Index for OFDM frame
i	Index for OFDM symbol/block
k_p	Index for pilot subcarrier
$\acute{\imath}$	Index for single carrier frame
l	Index of propagation path
G_k	Initial value of adaptive filter coefficients
$z_{p,I}(t)$	In-phase component of $z_p(t)$
$r_I(t)$	In-phase component of $r(t)$
$r_I[n]$	In-phase component of $r[n]$
$x_I(t)$	In-phase component of $x(t)$
$x_I[n]$	In-phase component of $x[n]$
$y_I(t)$	In-phase component of $y(t)$
$y_I[n]$	In-phase component of $y[n]$
$z_I(t)$	In-phase component of $z(t)$
$z_I[n]$	In-phase component of $z[n]$
$\otimes$	Linear convolution
$\bar{\mathbf{Z}}$	Matrix (2x2) containing channel and I/Q parameters
$\bar{\mathbf{H}}_s$	Matrix (2x2) containing channel parameters
$\bar{\mathbf{Z}}_s$	Matrix (2x2) containing I/Q parameters

$\bar{\boldsymbol{\eta}}_{\mathbf{p}}$	Matrix (2x2) containing noise corresponding to the pilot tones
$\bar{\mathbf{X}}_{\mathbf{p}}^{\mathbf{c}}$	Matrix $(2x2)$ containing mirrored conjugate pilot tones
$\bar{\mathbf{X}}_{\mathbf{p}}$	Matrix $(2x2)$ containing pilot tones
$\bar{\mathbf{w}}_{\mathbf{Q}}^{\mathbf{c}}$	Matrix (circulant $\acute{N}x\acute{N}$) containing $w_I[n]$
$\bar{\mathbf{w}}_{\mathbf{I}}^{\mathbf{c}}$	Matrix (circulant $\acute{N}x\acute{N}$) containing $w_Q[n]$
$\mathbf{h}^{\mathbf{c}}$	Matrix (circulant $\acute{N}x\acute{N}$) containing $h[n]$
$\bar{\mathbf{u}}^{\mathbf{c}}$	Matrix (circulant $\acute{N}x\acute{N}$) containing $u[n]$
$\bar{\mathbf{v}}^{\mathbf{c}}$	Matrix (circulant $\acute{N}x\acute{N}$) containing $v[n]$
$\bar{\boldsymbol{\Delta}}_{\boldsymbol{w_I}}$	Matrix (diagonal NxN) containing Fourier transform of $w_I[n]$
$\bar{\boldsymbol{\Delta}}_{\boldsymbol{w_Q}}$	Matrix (diagonal NxN) containing the values of Fourier transform of $w_Q[n]$
$\bar{\boldsymbol{\Delta}}_{\mathbf{h}}$	Matrix (diagonal NxN) containing $H[k]$
$\bar{\boldsymbol{\Delta}}_{\mathbf{u}}$	Matrix (diagonal NxN) containing $U[k]$
$\bar{\boldsymbol{\Delta}}_{\mathbf{v}}$	Matrix (diagonal NxN) containing $V[k]$
$\acute{M}_l$	Number of filter taps for the frequency domain correction method for single carrier modulation
M_l	Number of filter taps for the time domain correction method for single carrier modulation
L	Number of propagation paths
p_o	Power of LOS path
p_l	Power of the l^{th} path
$z_{p,Q}(t)$	Quadrature component of $z_p(t)$
$r_Q(t)$	Quadrature component of $r(t)$
$r_Q[n]$	Quadrature component of $r[n]$
$x_Q(t)$	Quadrature component of $x(t)$
$x_Q[n]$	Quadrature component of $x[n]$
$y_Q(t)$	Quadrature component of $y(t)$
$y_Q[n]$	Quadrature component of $y[n]$

$z_Q(t)$	Quadrature component of $z(t)$
$z_Q[n]$	Quadrature component of $z[n]$
$C[k]$	Received signal in frequency domain after undergone correction
$Y[k]$	Received uncompensated signal in frequency domain
T_s	Sampling time
μ	Step size for LMS adaptation
$\overline{\mathbf{u_n}}$	Toeplitz matrix containing I/Q parameters for desired signal
$\overline{\mathbf{v_n}}$	Toeplitz matrix containing I/Q parameters for image signal
$[.]^T$	Transpose of a matrix
$\mathbf{C_p^c}$	Vector containing $C^*[-k]$ for pilot subcarriers
$\mathbf{C_p^c}$	Vector containing $C^*[-k]$ for pilot subcarriers
$\mathbf{w_I}$	Vector containing $w_I[n]$
$\mathbf{w_Q}$	Vector containing $w_Q[n]$
$\boldsymbol{\varepsilon_T}$	Vector containing $\varepsilon_T[n]$
$\boldsymbol{w}_k$	Vector containing adaptive filter coefficients for the adaptive LMS compensation method
$\boldsymbol{\beta_p}$	Vector containing channel and residue I/Q parameters
$\mathbf{W_I}$	Vector containing Fourier transform of $w_I[n]$
$\mathbf{W_Q}$	Vector containing Fourier transform of $w_Q[n]$
$\boldsymbol{\eta}$	Vector containing Fourier transform of $\boldsymbol{\varepsilon_T}$
$\mathbf{U}$	Vector containing Fourier transform of $u[n]$
$\mathbf{V}$	Vector containing Fourier transform of $v[n]$
$\boldsymbol{\lambda_p^c}$	Vector containing I/Q and channel parameters in frequency domain for mirrored conjugate pilot tones
$\boldsymbol{\lambda_p}$	Vector containing I/Q and channel parameters in frequency domain for pilot tones
$\boldsymbol{\beta_p^c}$	Vector containing mirrored frequency conjugates of channel and residue I/Q parameters

$\mathbf{y}$	Vector containing received uncompensated OFDM signal in time domain
$\mathbf{H}^{\#}$	Vector containing mirrored frequency conjugate of $\mathbf{H}$
$\mathbf{X}^{\#}$	Vector containing mirrored frequency conjugate of $\mathbf{X}$
$\mathbf{Y_p}$	Vector containing uncompensated received signal for the pilot subcarriers
$\mathbf{C_p}$	Vector containing $C[k]$ for pilot subcarriers
$\mathbf{u}$	Vector containing $u[n]$
$\mathbf{v}$	Vector containing $v[n]$
$\boldsymbol{\varepsilon}$	Vector containing $\varepsilon[n]$

LIST OF ACRONYMS

ACCC	Adaptive Combined Correction and Compensation
ADC	Analogue to digital converter
AGC	Automatic gain controller
AWGN	Additive white Gaussian noise
BLUE	Best linear unbiased estimator
BPSK	Binary phase shift keying
BSS	Blind source separation
CDMA	Code division multiple access
CFO	Carrier frequency offset
CMOS	Complementary metal-oxide-semiconductor
CP	Cyclic prefix
CR	Capacitor-resistor
DAC	Digital to analogue converter
DC	Direct current
DCR	Direct conversion receiver
DFT	Discrete Fourier Transfer
DVB-H	Digital video broadcasting-handheld
DVB-T	Digital video broadcasting-terrestrial
EASI	Equivariant adaptive separation via independence
ETU	Extended typical urban
EVM	Error vector magnitude

FFT	Fast Fourier transform
GSM	Global system for mobile communications
HF	High frequency
I	In-phase
I/Q	In-phase and quadrature
ICI	Inter carrier interference
IDFT	Inverse discrete Fourier transform
IEEE	Institute of Electrical and Electronics Engineers
IF	Intermediate frequency
IFFT	Inverse fast Fourier transform
IQ imbalance	Gain and phase imbalances between the in-phase and quadrature
IR	Image rejection
ISI	Inter symbol interference
LMS	Least mean square
LNA	Low noise amplifier
LO	Local oscillator
LOS	Line of sight
LPF	Low pass filter
LS	Least square
LTE	Long term evolution
MATLAB	Matrix laboratory
MBWA	Mobile broadband wireless access
MMSE	Minimum means square estimation

Model 1	Frequency-selective gain and phase described in Section 4.2.2
Model 2	Frequency-selective gain and phase described in Section 4.2.2
MSE	Mean squared error
No I/Q	The reference error vector magnitude or symbol error rate obtained without any gain or phase imbalances
OFDM	Orthogonal frequency division multiplexing
OFDMA	Orthogonal frequency division multiple access
Q	Quadrature
QAM	Quadrature amplitude modulation
QPSK	Quadrature phase shift keying
RC	Resistor capacitor
RF	Radio frequency
RF-SOC	Radio frequency-system on chip
RLS	Recursive least square
SC-FDE	Single carrier-frequency domain equalization
SC-FDMA	Single carrier-frequency domain multiple access
SER	Symbol error rate
SNR	Signal to noise ratio
UHF	Ultra high frequency
UL	Uplink
VHF	Very high frequency
WCDMA	Wideband code division multiple access

Wi Fi	Local area wireless technology
Wi Max	Worldwide Interoperability for Microwave Access
WLS	Weighted least square

CHAPTER 1

INTRODUCTION

1.1 Scope of the thesis

There are many receiver architectures used in present days. Among them, superheterodyne receivers are the most popular. These architectures are mostly used, especially for the OFDM based wireless transceivers, where the radio frequency (RF)/ bandpass signal is down-converted to one or two intermediate frequencies (IF). At IF stages, high quality passive image rejection, channel selectivity filtering and amplifications are executed to maintain selectivity and sensitivity. One major discrepancy of this architecture is that it requires a large number of analogue filters and amplifiers to achieve an acceptable signal quality, which increases the overall power consumption and cost [1, 2]. Moreover, in recent years, radio frequency–system-on-chip (RF-SOC) designs are promising as they provide a compact, efficient yet low-cost receivers [1, 3] . In RF-SOC, the RF analogue front end and digital baseband all are integrated on a single chip. However, due to the necessity of a large number of image rejection and channel selectivity filters in superheterodyne architectures, these receivers cannot be integrated as a system on-chip [1].

On the other hand, the superheterodynes' counterpart, zero-IF receivers or DCRs, down convert the bandpass/RF signal straight into the baseband. They do not suffer from image frequency problem, which means a number of sensitive image rejection filters are not required for this case. In addition, channel selectivity in DCRs could be readily realized with the assistance of integrated low-pass filters (LPF), which discards

the requirement of additional sensitive channel selectivity filters as well. It is also suitable for system on chip integration. It is capable of providing low power consumption, low computational complexities and low cost [1, 2, 4]. Therefore, in recent years, this receiver architecture has received lot of attention and interests.

However, the DCRs have one major problem that creates distortion and degrades signal quality. Ideally, use of these receivers dictates that the In-phase (I) and Quadrature (Q) branches must maintain equal gain and be exactly 90^{o} out of phase which is rarely the case in practice. Any deviation from these ideal gain and phase conditions will give rise to an imbalance that is commonly known as the In-phase (I)/Quadrature (Q) imbalance or I/Q imbalance. Due to this mismatch, a self-image of the desired signal which is mathematically the conjugate of the desired signal is produced and the self-image is added to the desired part. It is an analogue front end imperfection, which is caused due to fabrication process variation and is very difficult to control or predict [5]. Also, it is almost impossible to cancel the I/Q imbalance problem completely in the analogue domain due to power area cost trade-offs [5].
This thesis proposes I/Q imbalance correction and compensation schemes for both OFDM and single carrier modulation techniques. Although there are lots of compensation and correction techniques available in literature for OFDM, many of them are not suitable for frequency-selective I/Q imbalance and multipath channel conditions (details in Section 2.4). Some methods require a large number of reference symbols whereas other methods are blind that do not use up many symbols as references but are very computationally complex (details in Section 2.4). To our best knowledge, to date all the blind compensation techniques available in literature, considers a very low level of I/Q imbalance. On the other hand the pilot based methods are capable of compensating for a severe level of I/Q imbalance. However, all of the pilot based methods, published so far, are based on the assumption that the known pilot subcarriers have been detected accurately. Nonetheless, when the system suffers high level of I/Q imbalance and channel, this assumption would no longer be valid. This leads to the necessity of investigation of an effective I/Q imbalance correction/compensation scheme for OFDM, which is robust enough to function even when faulty pilots are detected. Furthermore, a scheme is required that is suitable for

a high level of frequency-flat and frequency-selective I/Q imbalance and; frequency-selective multipath channel, uses less pilots and is less computationally complex.

Compared to the schemes suitable for OFDM, in the case of the single carrier modulations, less research has been done in recent years to mitigate the I/Q imbalance and channel. In most cases, the level of I/Q imbalance has been considered very low such as, [6-9]. Also, some of the iterative process uses a large number of training symbols to train the system such as [2, 10]. In addition, many of the available schemes uses low order modulation schemes like BPSK, QPSK, and 16-QAM [6-9, 11-13]. However, the higher the modulation order, the more severe the effect of the I/Q imbalance. Thus the motivation arises to examine the joint effect of I/Q imbalance and channel distortion for a higher order modulation. A correction/ compensation scheme is needed in order to mitigate the joint effect of these two impairments using fewer numbers of known reference symbols. Furthermore, it should be suitable for handling a high level of I/Q imbalance.

1.2 Objectives and original contributions of the thesis

The primary objectives of this research are the following:

a) To investigate the phenomena of I/Q imbalance and channel on both single carrier and OFDM, and explore its adverse effect on the received signal.
b) To design robust correction and compensation schemes to mitigate the effect of I/Q imbalance and multipath channel that are suitable for the OFDM and single carrier modulations.
c) To study the performance of the proposed correction/compensation scheme by comparing the proposed scheme with some of the previously published methods for portraying the robustness and effectiveness of each scheme.

In order to achieve these aims, the following novel contributions are the highlights of this research:

a) The effects of I/Q imbalance on the performance of the single carrier modulation signal and the OFDM signal has been presented in Section 3.4 and 3.6, respectively.
b) An adaptive combined correction and compensation (ACCC) scheme has been proposed in Chapter 4 in order to mitigate the I/Q and channel imperfection in OFDM receivers. The scheme makes use of pilot subcarriers. Some parts of the I/Q imbalance are corrected using a feedback loop when the signal is still in time domain, i.e. before the frequency transfer. The rest of the I/Q imbalance along with the channel imperfection is compensated afterwards through a post processing in the frequency domain. Unlike the other pilot based schemes available in the literature, in this scheme the pilot sub carriers have been extracted from the received signal rather than assuming it has been extracted perfectly. At the beginning of each frame, the number of incorrectly detected pilots are quite high. As the system estimates the coefficients corresponding to the imperfections and adapts itself with time, the chances of detecting wrong pilots become less likely. The ACCC scheme is less computationally complex and can correct/compensate a relatively large level of frequency-selective I/Q imbalance with an average image rejection ratio (IRR) of 17.1 dB by using 1.56% subcarriers as pilots.
c) The performance of the proposed ACCC scheme has been compared with three other well-known schemes to assess the robustness of each scheme in Chapter 5. These three methods used pilot subcarriers for I/Q and channel compensation purposes. They have been tested under different conditions, such as various frequency-flat and frequency-selective I/Q imbalances, various numbers of pilots, various levels of IRR, etc.
d) Two methods have been proposed in Chapter 6 in order to perform the mitigation of I/Q imbalance and channel for single carrier modulation. A joint I/Q imbalance and channel parameter estimation technique has been obtained. After the estimation, Method 1, which is referred to as the time domain correction scheme, uses an adaptive feedback loop-based time domain correction. Method 2, which is referred to as the frequency domain

compensation scheme, uses a frequency domain post processing, which is suitable for single carrier frequency domain equalization (SC-FDE).

1.3 Organization of the thesis

This thesis is organized into seven chapters.

i) Chapter 2 comprises the background and literature review relevant to the thesis title. It briefly describes some of the popular receiver architecture, such as superheterodyne receivers, direct conversion, or zero-IF receivers along with the advantages and disadvantages of each. One of the biggest disadvantages in DCR architecture is the I/Q imbalance problem, which is the main topic of this thesis. The I/Q imbalance phenomena and the reason for this imbalance have been presented in this chapter. It also provides an up-to-date literature review in the field of I/Q imbalance and channel mitigation. Digital and analogue domain I/Q imbalance correction and compensation schemes have been presented. The correction and compensation schemes available in literature for OFDM and single carrier modulations have been described separately. Also, the compensation/correction methods based on known reference signals, such as pilots, preambles, training sequences, and methods that are non-data aided, such as the blind method, have been presented as well. As the thesis focuses on I/Q imbalance and channel mitigation, the previously published works that have considered these two distortions have been discussed.

ii) A mathematical representation of the bandpass waveforms and systems for a DCR has been described in Chapter 3. At the beginning, the impact of I/Q imbalance and the channel has been modelled for the single carrier modulation system. Afterwards, the impact of I/Q imbalance has been presented in the case of the OFDM system. This chapter also includes some simulations performed by MATLAB to demonstrate the effects of the I/Q imbalance and multipath channel on the received signal. The resultant

distorted received signal clearly shows that the impact of the I/Q imbalance and channel can be severe, and correction and compensation is necessary to mitigate the distortion and achieve a good SNR.

iii) Chapter 4 includes a novel ACCC to mitigate the I/Q imbalance and channel distortion for OFDM receivers. The unknown distortion parameters generated due to the I/Q imbalance and channel can be estimated by utilizing pilot tones. These estimated parameters are used to obtain the frequency-flat gain and phase, which have been referred in this thesis as 'nominal gain' and 'nominal phase', respectively. The nominal gain and phase has been corrected in the time domain, whereas the remaining frequency-selective I/Q imbalance, which has been referred to here as 'the residue I/Q imbalance', and the channel distortion have been mitigated in the frequency domain. The various requirements necessary for the ACCC scheme, such as pilot pattern, modulation, and stability have also been discussed. The performance of the system has been observed in terms of various conditions, such as different frequency-flat and frequency-selective I/Q imbalances, different channel parameters, different modulation schemes, different number of pilots, etc.

iv) In Chapter 5, a performance comparison of three other different schemes and the proposed ACCC scheme has been presented. The three other well-known I/Q imbalance and channel mitigation methods that have been discussed in this chapter are i) the joint compensation method [14] ii) the decoupled compensation method [15], and iii) the compensation method by adaptive filtering [2]. All of these methods are applicable to the OFDM system. Under various conditions extensive research has been done to compare the output of these methods with the ACCC scheme to observe the robustness of each scheme.

v) Chapter 4 and 5 present compensation/correction schemes and the results for the OFDM only. In Chapter 6, two novel methods have been presented

in order to mitigate the I/Q imbalance and channel parameters for the single carrier modulation, such as 64-QAM and 16-QAM. These two methods are based on a single channel and I/Q parameter estimation technique that has also been presented in this chapter. In addition, the performance of the outputs retrieved from these two methods have been presented.

vi) Chapter 7 provides the conclusion and future work to be carried out based on the results of the thesis.

CHAPTER 2

BACKGROUND AND LITERATURE REVIEW

2.1 Introduction

In-phase quadrature imbalance or I/Q imbalance occurs in dual branch receivers. It is a type of impairment that creates distortion at the receiver output. It must be corrected and compensated from the received signal. In this chapter, some important queries regarding the I/Q imbalance (for example, why this impairment is significant, how it is produced, what the impacts of the impairment are, or how bad it can affect the signal) will be answered.

The chapter starts with a brief discussion about modern receiver architecture, which lends insight into how the I/Q problem arises. Then, a general mathematical model of an I/Q imbalance for a single carrier modulation is presented. As the thesis mainly takes OFDM into consideration, a brief discussion about OFDM transmission has been presented in this chapter as well. Next, the model for I/Q imbalance has been further extended for the OFDM signal. Finally the effects of I/Q imbalance in the presence of multipath channel and additive white Gaussian noise (AWGN) are discussed by means of signal constellation and SER; to portray the necessity of I/Q correction and compensation for dual branch receivers.

2.2 Introduction to the popular receiver architecture

The RF receiver is responsible for performing the following three important tasks; down-conversion, demodulation and filtering. Conventional heterodyne receivers are very popular and widely used in many applications. However, these receivers require expensive image rejection filters and channel selective filters. Also, their integration in a single chip requires high performance which is difficult to achieve with current integration technology [1]. More recently direct conversion or homodyne receivers have become attractive due to its simple architecture and cost effective functionality [2]. Yet, a DCR is not commonly used because of the unsolved I/Q imbalance problem associated with its theoretically simple architecture.

The recent progress of the wireless industry has been in exploring advanced and innovative receiver architectures, which are appropriate for monolithic integration. In this regard, several improvements on conventional receiver architectures have been made. In present days, there are various receiver architectures, such as superheterodyne receivers, DCRs, the integrable image rejection receivers, Hartley image rejection receivers, Weaver image rejection receivers, polyphase filter based image rejection receivers, RF/IF sampling receivers, etc. [1]. This section provides a brief description of the two most popular receiver architectures known as the superheterodyne receiver and the DCR.

2.2.1 Superheterodyne receivers

Superheterodyne receiver architecture was invented by Armstrong in 1917 and is currently the most widely used architecture in wireless transceivers [1]. Figure 2-1 shows the block diagram of a dual-conversion superheterodyne receiver with two IF stages. In this receiver architecture, the incoming RF frequency is first frequency translated to one or more intermediate frequencies (IF) before demodulation [4]. As can be seen from Figure 2-1, the RF signal is applied to a low noise amplifier (LNA) and afterwards to an image rejection filter. The IF is produced by mixing the resultant signal out of the image rejection filter with the LO output [16]. The channel selectivity

is carried out by means of a bandpass filter with a practical quality factor [1].The last IF stage is used to retrieve the modulating information.

The advantages and drawbacks of this architecture have been stated below.

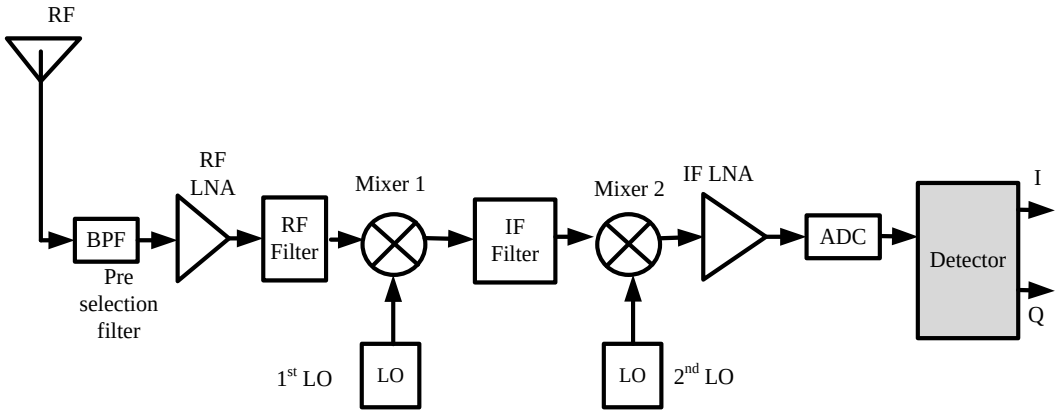

Figure 2-1 Superheterodyne receiver

Advantages

- Superheterodyne receivers have better immunity from interfering signals compared to the zero-IF receivers [4].
- Usually the narrow bandwidth passive IF filtering is done by the help of crystal, ceramics, or surface acoustic wave (SAW) filters, which provide better protection than the gyrator filters used for the DCRs, against signals close to the desired signal [4]. The reason for better protection is that because passive filters are not degraded by the compression of large signals [4].
- It has good sensitivity and selectivity.
- It suffers DC offset to a lesser extent, as DC offsets occur in later stages after the incoming signal has already been adequately amplified.

Drawbacks

- Superheterodyne architecture deals with channel selectivity and image rejection. If the IF is high, then the image can be greatly attenuated, however, the close interferes remain in a significant level. On the other hand if the IF is low, interferes can be supressed but the image distorts the down converted signal [16]. For this reason, this architecture requires high precision image rejection and channel selectivity filters [1, 4, 16].
- They require stable oscillators with high frequency accuracy and low phase noise.
- They require additional oscillators and passive filters. These increase the size of the receiver. Also the requirements of additional components make the superheterodyne receiver architecture more expensive than the DCRs.
- Low noise and high dynamic range are essential for LNA.
- They are unable to achieve high performance, in terms of linearity over a sufficiently large dynamic range and noise, with current integration technology

2.2.2 Direct conversion receivers

A DCR, also known as a zero IF or homodyne receiver translates the desired incoming RF signal directly to the baseband. Baseband refers to the frequency band occupied by modulating signal. The block diagram of a zero-IF receiver is shown in Figure 2-2, obtained from [8].

It contains mixers and a local oscillator (LO). The LO signal is tuned to the same frequency as the desired RF signal. The LO output is mixed with the RF signal. After low pass filtering (LPF), the baseband signal is obtained. The baseband filtering is done often by active op-amp filters which are commonly known as gyratos [4]. Also DCRs do not require image rejection filters. This forms an important advantage of this architecture.

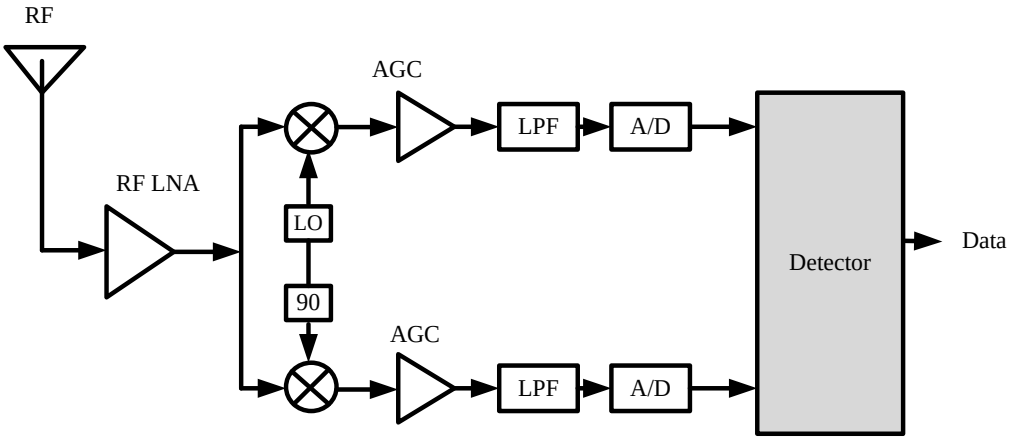

Figure 2-2 Direct conversion or zero-IF receiver

Advantages

- Theoretically, DCRs require less hardware compared to its superheterodyne counterpart [4].
- DCRs do not require image rejection filters as there is no image present [1, 16].
- Gyrators are much less expensive than the expensive Ceramic or crystal IF filters [4].
- As there is no IF stage, LPFs are used for channel selectivity.
- Most of the signal amplification may be carried out at baseband frequencies. This could potentially lead to lower power dissipation.
- This architecture is more suitable for single chip integration, thus leading to a more cost effective manufacturing of receivers.

However, DCR architecture comes with its limitations. Some of the drawbacks are listed below:

Drawbacks

- I/Q imbalance

During the quadrature down-conversion, if the gains of the In-phase (I) and Quadrature (Q) branches are not equal and their respective phases are not differed by exactly 90^{o} , then the phenomenon commonly known as I/Q imbalance occurs. IQ imbalance causes an unwanted self-image signal to appear at the demodulator output. This is

considered the most serious problem associated with any DCR. For this reason, it will be discussed in greater details in Section 2.3.

- LO Leakage

Leakage of the LO signal to the antenna as well as radiation from the antenna creates interference [16]. This leakage is not very effective in the case of superheterodyne architectures, as the LO frequency is usually out of the reception band [16].

- Second-order Intermodulation

Another known problem of DCR is the second-order intermodulation (IM2) or second-order intercept point (IP2). Large blocking signals cause DC in the direct conversion receiver. The DC is produced at the mixer output and amplified by the baseband stages. It is due primarily to second-order nonlinearity of the mixer, characterized by the IM2 or IP2. It can be alleviated by extremely well-balanced circuit design. However, the mixer and LNA used to require a single-ended design because the antenna and a hypothetical preselect filter were usually single-ended

- DC offsets

As DCRs convert the bandpass signal directly to baseband, often the front end has a low level of amplification [1]. That is why; the downconverted baseband signal needs large level of amplification by means of DC coupled amplifier [1]. The use of DC amplifiers required to handle the down-converted baseband signals, can give rise to significant DC offsets due to non-precise components matching of differential amplifying stages.

2.3 Introduction to I/Q Imbalance

For most phase and frequency modulation schemes, The DCR adopts the quadrature down-conversion shown in Figure 2-3. This requires shifting either the RF signal (Figure 2-3 (a)) or the LO output (Figure 2-3 (b)) by 90° [16]. Since shifting the RF signal generally entails severe noise-power-gain trade-offs, it is much more convenient

to shift the LO output by 90^0. Again the requirement is quite strict for this impairment as well. The In-phase (I) and Quadrature (Q) branches of the dual branch receiver represent the real and imaginary parts of the baseband equivalent model.

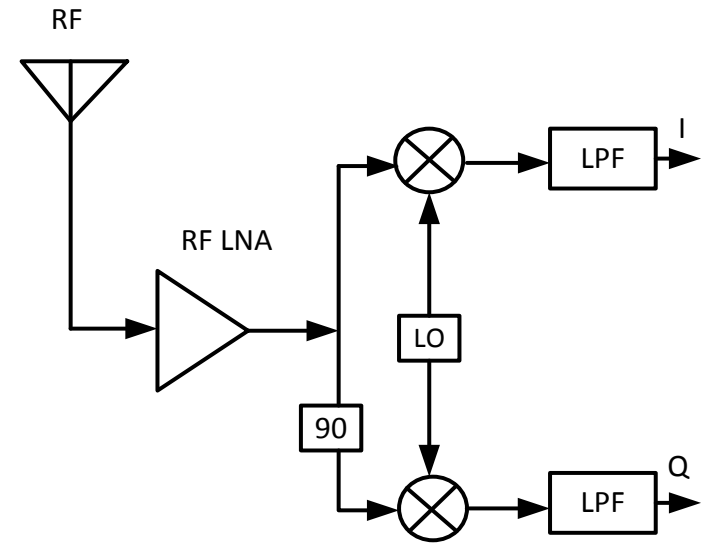

a)

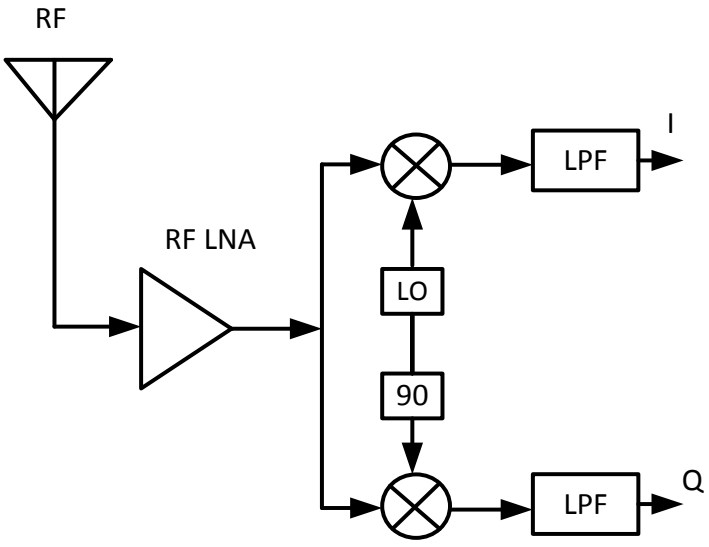

b)

Figure 2-3 Quadrature down-conversion by a) Shifting the RF signal by 90^o b) Shifting the LO output by 90^o

The key fact is, the gain of the I and Q branches should be exactly equal and the phase should be exactly 90^{o}. Any variation from the above gain and phase introduces distortion that is responsible for the phenomenon commonly known as I/Q imbalance. An I/Q imbalance can degrade system performance significantly.
The reason that I/Q imbalance is produced is analogue front end discrepancies. Achieving orthogonal waveform at radio frequencies is a very difficult job for silicon implementation [2]. Some circuit technologies, such as complementary metal oxide semiconductor (CMOS) produces quite a considerable amount of I/Q mismatch in the components. It can happen due to the fabrication process which includes doping concentration, oxide thickness, mobility and geometrical size of the chip, etc. [2].

Also, gain and phase mismatch may occur from any part of the dual branch receiver. It could be the RF splitter, the LO, mixers, automatic gain controller (AGC) , or the LPFs. For an ultra-high frequency (UHF) integrated receiver, stray reactive components are often present in the RF splitting junction as well as the input port of the quadrature mixing stage [1, 17].These stray reactive components are difficult to control in the semiconductor integration process. Their presence affects phases of the RF signals at the inputs of the quadrature mixers. Additionally, the mixers may not be ideal and can contribute to the overall I/Q imbalance. The quadrature LO signals also play an important role in this regard. Suppose a 90^{o} phase shifter has been used to generate the I and Q signals. These phase shifters are first order resistor capacitor (RC) low-pass in conjunction with a capacitor resistor (CR) high pass network [1, 16]. These sorts of networks are able to provide a 90^{o} phase shift over a large bandwidth but the amplitudes of the quadrature outputs are only equal at the cut off frequency [1, 18]. Therefore maintaining equal gain over a wide service band is not possible. The I/Q imbalance can be divided into the following two groups: frequency-flat I/Q imbalance and frequency-selective I/Q imbalance. For the frequency-flat case, I/Q imbalance does not vary with the frequency.

On the other hand, for the frequency-selective case, it differs with frequency. For many practical applications (particularly broadband applications) the assumption of a frequency-flat I/Q imbalance may not be very realistic. Normally, the mismatch

arrived from the RF splitter, LO and Mixers are considered frequency-flat. Yet the gain and phase mismatch associated with the LPFs, digital to analogue converters (DAC) and analogue to digital converters (ADC) are usually frequency-selective [5]. Alteration of temperature and process mismatch also play an important role in I/Q imbalance. Figure 2-4 represents the ideal down-conversion. Figure 2-5 shows down-conversion in presence of the I/Q imbalance. The occurrence of I/Q imbalance gives rise to a self-image of the incoming signal arising in the output of a dual-branch receiver. The negative frequency component of the desired signal at $-f_c$ has also been down converted to baseband, as shown in the figure. This down-converted negative frequency component is known as the self-image. Hence, the resulting signal has a desired component and a self-image.

2.4 Compensation and correction of I/Q imbalance and multipath channel

The I/Q imbalance and channel have an adverse effect on the received signal. From the Figure 2-5, it is shown that I/Q imbalance creates a self-image which is imposed on the desired down-converted signal. This self-image creates distortion and it is needed to be corrected or compensated for by some technique. There are many techniques available in literature for the purpose of I/Q imbalance compensation and correction. As I/Q imbalance starts in the analogue domain, the compensation can be done both in the digital and analogue domain. While estimating the gain and phase in analogue domain, the estimations are often based on many approximations. These approximations need to be simple and realistic. Generally the approximations are valid only when the gain and phase imbalances are very small.

Also the accuracy can be biased by the DC offsets present in the DC amplifiers used to implement the scheme [1]. However, as this dissertation only focuses on the digital domain compensation and correction techniques, analogue domain techniques have not been covered here. Moreover, the I/Q imbalance problem is normally dealt with some other impairments such as multipath channel, DC offsets, frequency offsets, etc.

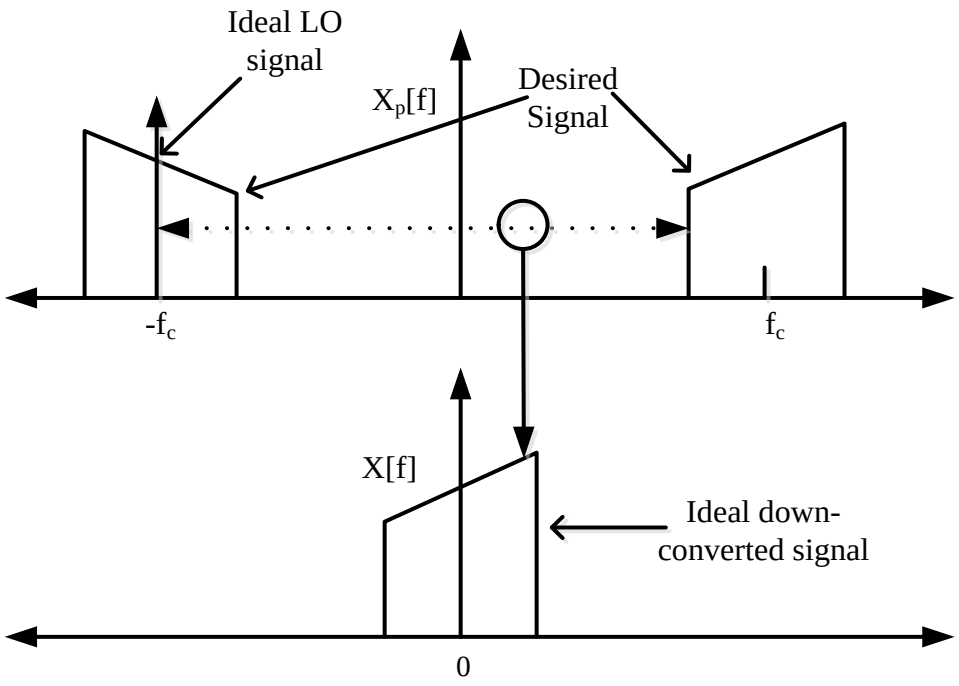

Figure 2-4 Ideal complex down-conversion

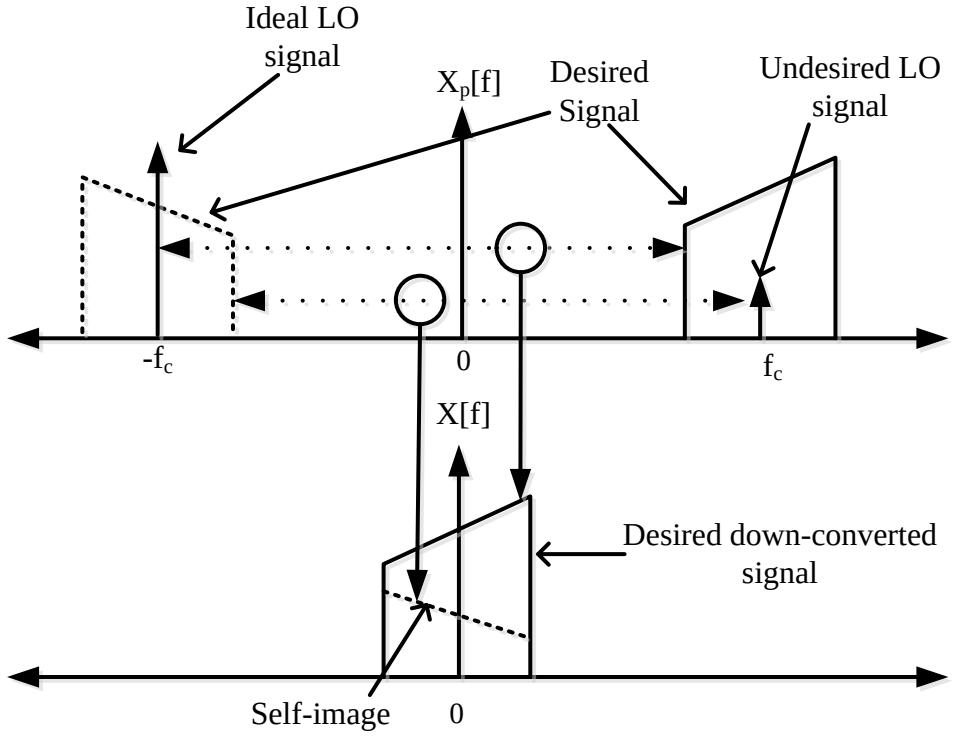

Figure 2-5 Effects of self-image caused by I/Q imbalance in direct conversion receivers

Only the compensation and correction schemes present for I/Q imbalance and multipath channel have been discussed, as the thesis mainly emphasises these two impairments. In many cases, correction or compensation techniques used for single carrier modulation are not suitable for a multicarrier modulation and vice versa. So, the available schemes can be divided into two main groups; a) compensation and correction schemes for the single carrier modulation system and b) compensation and correction schemes for OFDM systems.

2.4.1 Compensation and correction of I/Q imbalance for single carrier modulation

For single carrier modulation, there are plenty of compensation and correction techniques available in literature. Nevertheless, most recent papers focus on OFDM. In past years, one of the most popular methods of compensating for and correcting I/Q imbalance for single carrier modulation was using a locally generated test signal. Later, using a reference signal instead of a locally generated test sinusoid has been suggested and adopted. In addition, there are methods available to compensate and correct the I/Q imbalance and channel without the help of any reference signal, based on the statistical property of the signal. These methods are known as the blind methods. In the following section, a general review of these compensation methods have been discussed.

2.4.1.1 I/Q imbalance compensation by generating test sinusoid

This is one of the earliest methods for mitigating I/Q problem which was first proposed in 1981 by [19]. Similarly, [20, 21] invented methods that use a test signal. Using these methods, the goal is to measure the mismatch in two branches. Once the mismatches are determined, they can be corrected from the received signal. Sometimes the correction scheme is through the Grahm Schmidt procedure, which produces

orthonormal basis from an arbitrary set of vectors [22, 23]. This correction can be applied to one frequency at a time [24].

This test signal is generally a sinusoid that is transmitted to evaluate and estimate the I/Q imbalance. These estimated parameters are used afterwards to remove the I/Q from the system. For example, in Glas's research [20]; a test sinusoid is used and mathematical solution has been done to estimate the gain and phase imbalance. Down-conversion was performed in two stages. At first the signal is down-converted to a low-IF and afterwards into DC. One limitation of this scheme is; that during the second down-conversion stage; an assumption is made that the LO, mixers and filters involved are free from any I/Q distortion. However, these equipment used in the second stage down-conversion can also produce a different value I/Q imbalance which would not only affect the signal but also double the number of unknown parameters. So this assumption is somewhat unrealistic.

Another example, in [25], a correction method has been proposed that estimates the gain and phase imbalance values in the frequency domain. Then, these values are used to remove the I/Q imbalance in the time domain. Different probe signals have been used for different frequencies. However, this sort of solution is suitable for the frequency-flat I/Q imbalance. For correcting the frequency-selective I/Q imbalance, estimation of I/Q imbalance needs to be carried out by making use of a number of test sinusoidal signal covering the entire bandwidth. Furthermore, this approach requires accurate test signals that have been generated over the entire bandwidth.

Moreover, schemes depending on the test signal are not suitable for the time variant I/Q imbalance, either. After the I/Q parameters have been estimated, one method is; calibrating the I and Q branch according to the estimated values. However, by doing this, the system will not be able to cope with the change of I/Q imbalance with time. The other method is, continuously adapting and correcting the gain and phase with time. This way; the system needs to send the test signal quite often to estimate and remove all I/Q parameters, which will definitely interrupt a steady flow of transmission.

2.4.1.2 I/Q imbalance compensation using known training sequences

As the I/Q correction by off-line test signal has some limitations, a different approach that can handle the time variant and frequency-selective I/Q imbalance; has been adopted since the early 1990s. This approach makes use of known reference symbols to do the estimation and compensation of the unknown I/Q and channel parameters. Generally, time domain estimation and compensation technique is applied in the case of single carrier modulation [24, 26, 27].

In [26], a scheme was first introduced which used a training sequence instead of an offline test signal to compensate the I/Q and channel. In this method, an adaptive LMS technique has been used to perform the compensation of the I/Q and the channel. The equalizer works as the compensator in this case. Later other researchers used the adaptive filtering method by using the known reference signal [24, 27]. In the work of [24], an adaptive complex LMS algorithm has been proposed and a modified adaptive noise canceller has been used to separate the desired signal and the image caused due to I/Q imbalance. The noise canceller is also capable of solving the signal leakage problem. In the work of [27], a specially designed training pattern or pre amble has been used to estimate I/Q and channel parameters. The pilot pattern has been chosen on the basis of the minimum mean squared error. This method is also suitable for compensating for the DC offset. In case of the applications where time domain signals are not readily available, these methods will not be very attractive.

2.4.1.3 I/Q imbalance and channel compensation using no reference signal

The I/Q and channel can also be estimated and compensated for without the help of any special reference signal or offline test sinusoids. This is also a well-known method to determine the I/Q and channel parameters. With a no reference signal aided method, it is possible to extract the desired signal from a mixture of other signals based on the statistical properties of these signals. A way to perform this estimation of I/Q imbalance parameters is by; taking the output from each branch and comparing the power and rotation of one branch with another. This comparison of branches gives an

idea regarding the imbalance present, which can be used to obtain the unknown parameters through a mathematical solution [6].

Otherwise, the signal's statistical property can be utilized to do the estimation. For example, I/Q imbalance has been modelled as a linear mixture of the desired signal and the image signal in the work of [28]. The interference due to the image signal is cancelled using adaptive filtering technique. Instead of using a training signal as an input to the adaptive filter, the input to the adaptive filter has been chosen blindly. Filters have been updated according to the LMS and RLS method. In the work of [29, 30], the authors have used the maximum likelihood estimation technique in order to obtain the channel and I/Q parameters. Similarly, in the work of [7], I/Q has been compensated for by means of blind source separation (BSS). It is based on higher order statistics, which involves computational complexities. Moreover, in the work of [7] a technique called equivariant adaptive separation via independence (EASI) [31] has been used to do the estimation and compensation. In the work of [28] a comparison and performance analysis of the other three methods; (i.e., the interference canceller based method, the BSS method and the EASI method) have been described. The comparison portrays that the adaptive interference cancellation scheme is much more robust than the blind source separation based scheme when additive noise effect and symbol timing error are high. On the other hand the BSS and EASI methods are more suitable for different receiver imbalance properties and different received signal levels. In the case of the method involving EASI, it has been assumed that the desired signal and the image signal are mutually independent. This is true for image rejection architecture as the desired signal and image comes from two different sources. However, in the case of DCRs, the image introduced by the I/Q imbalance is the complex conjugate of the received signal, so there is no way they can be mutually independent from each other. Therefore, this method is not appropriate to be adopted for the DCR architectures.

Additionally, all of these methods mentioned in this section are suitable for the frequency-flat I/Q imbalance only. Later, blind methods proposed by various authors [12, 32] deal with more practical situations as the methods are suitable for frequency-

selective I/Q condition. In the work of [32], two blind compensation techniques have been proposed. The proposed methods are based on the circular or proper concept of the random signal.

The I/Q imbalance is often expressed by means of a term known as the front end image rejection ratio (IRR) [12, 33, 34]. This term has also been referred to [28] as image attenuation and in [13] as image power rejection. It is the ratio of the desired signal's coefficient to its self-image or complex conjugate's coefficient. Suppose, u and v are the coefficients of the desired signal and its complex conjugate, respectively, then the front end IRR can be expressed as, $20\log\left(\left|\frac{u}{v}\right|\right)$. High levels of I/Q yields low IRR and vice versa.

To our best knowledge, all current methods that involve no reference signal; available in the literature; consider quite a low level of I/Q imbalance. For most of the non-data aided methods, this IRR is quite high corresponding to a very low level of gain and phase imbalance. For example, in the work of [6-9], the static IRR was 30 dB, 33.95 dB, 34 dB and 30 dB, respectively. The IRR is static in these cases, as the I/Q was considered frequency-flat. In other work [12], the IRR has been varied from 25 to 40 dB. Although the I/Q is frequency-selective in this case, the lowest IRR has started from 25 dB. On the other hand, in Chapter 6, we have proposed two compensation techniques based on the reference signal, for the single carrier modulation which is capable of compensating for 20% of gain imbalance and 10^{o} of the phase imbalance corresponding to an IRR of 17 dB.

2.4.2 Compensation and correction of I/Q imbalance and channel for OFDM

The OFDM based physical layers have been selected for several standards, such as IEEE 802.11, IEEE 802.11g, IEEE 802,16, IEEE 802.20 etc [2]. Furthermore, the OFDM technique has been applied in most of the wireless applications, such as LTE, DVB-T, DVB-H, WiFi, WiMax etc [1]. In recent years, the effect of I/Q imbalance on

OFDM receivers has been studied extensively. The adverse effect of I/Q imbalance and channel on OFDM receivers were first described by [35]. Later, several techniques have been proposed to reduce the degradation caused by I/Q imbalance and channel on OFDM signal. Comprehensive research has been done in order to mitigate these two impairments with the aid of known reference signals such as pilot subcarriers. Additionally, there are several examples of compensation techniques where no such reference symbols have been used.

2.4.2.1 I/Q imbalance compensation using pilot subcarriers

Often channel estimation for OFDM is performed by means of pilot subcarriers [36-43]. These pilot subcarriers can also be used to mitigate both I/Q imbalance and channel parameters. There are many research studies where pilot subcarriers have been utilized in order to do I/Q parameter estimation and compensation [2, 5, 10, 14, 15, 33, 44-61].

We have divided all the compensation techniques into the two following groups: 1) joint compensation of I/Q imbalance and channel and 2) separate/decoupled compensation of I/Q imbalance and channel.

- ***Joint Compensation of I/Q imbalance and Channel***

For the OFDM signal, the I/Q imbalance and channel are often compensated for together in the frequency domain. In this case, the equalizer acts as a compensator for both I/Q and channel. These sorts of compensation schemes are known as joint compensation schemes [5, 14, 33, 44, 45, 47, 49-55].

In this section, only the joint compensation schemes that have used known pilot subcarriers have been discussed. Usually the pilot subcarriers are used for the purpose of estimating the unknown parameters associated with I/Q imbalance and channel. During the data symbol, these unknown parameters are used to compensate the effects of the I/Q imbalance and channel. The distribution of pilots may differ for various scheme. Pilots can be distributed along the time or along the frequency depending on

the channel property. In the works of [5, 14, 51, 52], it has been assumed, that the channel's coherence bandwidth is more than the bandwidth between two pilot subcarriers. This means the channel and I/Q property remain unchanged for two pilot subcarriers in one OFDM symbol. However, this sort of method suffers in degradation in the presence of highly frequency-selective channels.

On the other hand, in method B described by [14] and [2], it has been assumed that the channel coherence time is more than the duration between the pilots. These sorts of methods work well for frequency-selective channel but suffer if the channel's property changes quickly with time. Similarly, due to the high mobility of the receiver, the channel property may change completely. The OFDM system suffers in inter carrier interference (ICI) in this case. In [5] a pilot based scheme has been proposed that is capable of mitigating the channel and I/Q when the subcarriers have ICI.

Sometimes, it is much more convenient to use a special pilot pattern for joint compensation purposes, so that the I/Q and channel parameter can be obtained easily with the help of some mathematical evaluation. For example, in research work by [56] the image subcarriers have been kept purposely unmodulated. This is because the effect of I/Q generates an undesired self-image signal at the location of the unmodulated image frequency; this undesired signal could then serve as a measure of I/Q imbalance. Later, similar sort of pilot pattern has been used in [2] for imbalance coefficients estimation purpose. However, this approach is not capable of providing an accurate estimation, as the parameters that correspond to the null subcarriers have less average power and thus are greatly affected by the noise.

The joint compensation of the I/Q imbalance and channel can be also executed by means of adaptive equalization [2, 10, 48]. For OFDM signals, compensation of I/Q imbalance and channel by adaptive filtering has been first introduced by [10]. As the resultant signal is distorted by its additive image, a two way filter network has been presented to do the equalization. One filter takes the received signal whereas the other takes the mirror frequency conjugate of the received signal as input. Later, this method also has been used by [2, 48]. Both of these methods are suitable for compensating for

the frequency-selective I/Q imbalance and channel. In [2, 10] an adaptive least mean square (LMS) method has been used to perform the iteration. Some authors preferred to use recursive least square (RLS) method for this purpose [48].

In [48], an extended version of the adaptive method proposed by [2, 10] has been proposed after making it suitable for time varying channel. A 'V' shaped pilot pattern has been used to remove the channel and I/Q effects. However, one major drawback of these adaptive filtering methods stated above is; that all of them have performed in the presence of frequency-flat I/Q imbalances only. The method described in [48] would not work in the presence of frequency-selective channel and I/Q imbalance.

On the other hand, schemes described in [2, 10] should be useful in the case of frequency-selective channel and I/Q conditions, since the iteration progresses in the time axis. However, these methods use up huge amount of resources in form of pilots which is a major disadvantage from the throughput point of view. For example, in [10] , all the subcarriers have been used as pilots. Moreover, it takes 100 iterations to obtain the unknown parameters and complete the compensation. As each iteration is carried out once in every fourth OFDM symbol, it takes 400 OFDM symbols to obtain the imbalance coefficients. In addition, another 30 iteration is required in the decision directed stage. Assuming one OFDM symbol is 231 μs long, this iteration process takes almost 92 ms which is a long duration. Also, assuming that the channel property would remain steady for 92 ms; is not quite realistic. Similarly, in [2], all the subcarriers in one OFDM block/symbol have been used as pilots and required at least 40 OFDM symbols for training purposes, which would also take approximately 9.2 ms.

- ***Separate/ Decoupled Compensation of I/Q imbalance and channel***

The I/Q imbalance and channel are often dealt with separately. This is because the properties of I/Q and channel are different in nature. The I/Q mainly is caused for the imperfection in the analogue front end, whereas the channel property depends on many variables such as the environment, the relative speed of the transmitter and the receivers as well as; the number of reflective, refractive, and shadowing elements present, etc. Most of the time, the channel property changes more frequently than the

I/Q imbalance. Therefore, it is sometimes much more convenient to estimate and update the I/Q less frequently than the channel. In the work of [62], a scheme has been proposed where the transmitter caused I/Q imbalance is minimised by the assistance of a specially designed pilots on the receiver side. The I/Q and channel parameters are estimated separately here. The preambles are used to determine the unknown parameters corresponding to I/Q imbalance. The pre-distortion technique is used so that during the subsequent channel estimation, the deviation caused by the I/Q imbalance can be minimised. However, the scheme has quite a number of limitations. The scheme solves the I/Q imbalance of the transmitter on the receiver side assuming the receiver side is free from any I/Q imbalance. Nevertheless, if the receiver side has an I/Q imbalance, then number of unknown parameters will be doubled, which will lead to an incorrect estimation of the unknown parameters. Furthermore, for the iterative solution, the estimated channel parameter is required and the authors have assumed the channel estimation is perfect, which is also quite an unrealistic assumption especially when the signal has already been distorted by the I/Q imbalance.

In the research work by [2], another separate/decoupled compensation technique has been proposed as well. The unknown parameters are estimated with the assistance of known pilot subcarriers. Then, these parameters are used to determine a self-image cancellation coefficient which has been multiplied with the image signal (conjugate of the received signal) and subtracted from the received signal. Hence the received signal can remove the self-image. The subtraction of the image signal takes place in the time domain. For the frequency-selective I/Q imbalance parameters, the unknown I/Q parameters are convolved with the received signal. So the cancellation operation in the time domain would not be possible for the frequency-selective case. Therefore, this method is not useful in the case where I/Q variation is frequency-selective.

However, the decoupled compensation of frequency-selective I/Q and channel has been done by [15]. This method is more practical, as it takes few pilots and is suitable for frequency-flat and frequency-selective I/Q imbalances and channels. The known pilots have been used to determine the I/Q and channel parameters. Then certain mathematical solution and assumptions have been made to discover the cancellation

coefficient, which has been referred to as the ‘compensator coefficient’. Unlike using the compensator coefficient in the time domain, it has been used in the frequency domain to remove the mirror frequency interference. The compensator coefficients are different for each subcarrier; therefore, it is suitable when the I/Q parameters change along the whole bandwidth. However, this scheme also has some drawbacks. First, it has been assumed in this scheme that the frequency-selective I/Q imbalance filters corresponding to the I and Q branches, referred to as $G_1[k]$ and $G_2[k]$, maintain some specific conditions such as, $G_1[k] >> G_2[k]$ and $G_1[k] = 1$; when the I/Q variation is higher, such assumption no longer remains valid. This assumption plays a crucial part in correcting the interference signal from the desired signal. In case of a large gain and phase imbalance such as a 20% gain and a 10^o phase imbalance, the above estimation is no longer valid. Thus the estimated compensator coefficients would have errors. Therefore, the estimated desired signal output would contain errors as well. Moreover, it has been observed from this scheme’s result section, that the SER from the resultant corrected output and the SER of the uncompensated signal’s output hardly show any difference when the SNR is less than 25 dB, which means this scheme also requires a low noise environment.

2.4.2.2 I/Q imbalance compensation by non-data aided or blind method

A number of blind I/Q imbalance and channel compensation schemes have been proposed for OFDM receivers [63-70]. This thesis focuses mainly on the schemes that are based on pilot subcarriers. Therefore, a brief discussion about the blind estimation and compensation technique has been presented.

In the work of [70] a less computationally complex scheme for obtaining the I/Q gain and phase has been described. The I/Q parameters have been estimated by two statistics of the received signal, one is the cross correlation and the other is the power of the sum. This estimated gain and phase has been used afterwards to compensate for the signal. However, it is suitable only for the frequency-flat I/Q imbalance. A

maximum likelihood approach has been obtained to estimate the I/Q and channel in [69]. Similarly, a time domain blind adaptive technique has been described in the work of [66]. Generally, in the case of the OFDM the I/Q is compensated in the frequency domain. However, in this case an adaptive time domain method has been proposed. In the work of [65], another blind method for the I/Q compensation has been described. The self-image due to I/Q imbalance has been considered here as an interference. An optimum coefficient that discards the interference has been obtained by a blind method. A similar method has been used in the work of [15] for compensation purpose. The difference is that in research by [15] known pilot subcarriers have been used for the estimation purpose.

However, all of the non-data aided compensation methods have considered very low variation of I/Q imbalance compared to the pilot aided methods. For example, in several studies [65, 66, 69, 70] the IRR has been chosen as 17.65 dB, 25 to 40 dB, 20 dB and 26 dB, respectively. It is evident from the above references that there is no example of a non-data aided method, for the case of a single carrier and OFDM modulation, which is capable of mitigating a high level of I/Q (IRR lower than 10 dB) imbalance in presence of channel.

Likewise, some of the pilot based methods also considered a very low variation of I/Q. For example, in several studies [15, 33, 34] the IRR values have been considered as 27 to 33 dB, 35 dB and 25 dB, respectively. In some pilot aided methods, a moderate I/Q level has been chosen; for example, in [53, 54], the IRRs are 12.42 dB and 13.86 dB, respectively. On the other hand, some of the pilot aided methods such as those in the works of [2, 14] have compensated for quite severe I/Q with corresponding IRR of 5.72 dB and 4.64 dB, respectively. That is why these two methods have been chosen in this thesis to perform a comparison with the proposed ACCC method in Chapter 5.

2.5 I/Q imbalance schemes presented in the dissertation

In this thesis, compensation/correction schemes for I/Q imbalance and channel for the case of OFDM and single carrier modulations; have been proposed. It is to be noted that, 'correction' refers to where the I/Q imbalance has been fixed before channel equalization. On the other hand, 'compensation' is the term that refers to the post processing, which has been performed on the received signal along with channel equalization.

The compensation scheme ACCC has been presented in Chapter 4. It is suitable for OFDM and SC-FDE systems. It uses pilot subcarriers to perform the compensation and correction. It is capable of mitigating the frequency-selective channel and I/Q imbalance. It is a combination of joint and decoupled compensation. Additionally, it uses both correction and compensation techniques. The joint compensation techniques presented in the works of [14, 52] are very simple and less computationally complex. However, it requires updating the I/Q and channel parameters quite often. As the properties of I/Q and channel are different, the frequency-flat I/Q does not tend to change as frequently as the channel. Dealing with these two distortion properties separately seems more logical. However, it is not always easy to separate these two impairments from each other. We have used mathematical solutions to obtain the frequency-flat gain and phase from the received signal, which has been used as a feedback to do the correction. At the same time, the frequency-selective I/Q and the channel, which requires more frequent updates, are dealt with together. Two frequency-selective models, 'Model 1' and 'Model 2', have been used. Also, a variety of frequency-flat I/Q imbalances ranging from 1% gain and 1^{o} phase to 20% gain and 10^{o} phase have been considered for the simulation. The IRR has been varied approximately from 10 to 33 dB for the entire signal bandwidth.

In Chapter 5, we have selected one joint compensation method described in the work of [14], one separate compensation method presented in the work of [15] and one LMS compensation by adaptive filtering method described in the work of [2], to compare the performance with the proposed ACCC method. These methods have been compared considering different scenarios, such as; different frequency-flat gain and

phase, different frequency-selective I/Q imbalance models, different numbers of pilots etc., to assess the robustness of each scheme. All of these methods have been tested for both models of frequency-selective I/Q and a large variety of frequency-flat I/Q. Depending on the values of the frequency-flat and frequency-selective gain and phase, three different I/Q imbalance levels have been chosen as follows; a) low I/Q level with a corresponding IRR ranging from 20-30 dB, b) Moderate I/Q level with an IRR ranging from 10-20 dB and c) High I/Q level with an IRR less than 10 dB. The proposed ACCC method and the other three methods have been compared for different levels of I/Q imbalance as well.

In Chapter 6, two methods have been proposed, which are suitable for single carrier modulation. These two methods use the same technique in order to estimate the unknown channel and I/Q parameters. After that, one method performs a time domain correction on the received signal. The second method converts the received signal into frequency domain and perform a frequency domain compensation. The time domain correction can be classified as a separate/decoupled correction technique, whereas the frequency domain compensation can be referred as a joint compensation technique. Both of these methods are capable of mitigating the I/Q imbalance and channel imperfection. Moreover, a comparison between these two proposed methods has been discussed afterwards. All the compensation/correction methods proposed in this thesis, have used known pilot subcarriers and known training signals.

2.6 Summary

The inherent circuit impairment I/Q imbalance has been discussed in this chapter. The chapter presents a brief description regarding the zero IF and superheterodyne receivers. This explains how the I/Q imbalance is produced. Some well-known compensation/correction methods that are capable of mitigating I/Q imbalance and channel have also been discussed.

CHAPTER 3

MODELLING OF I/Q IMBALANCE

3.1 Introduction

I/Q imbalance has adverse effects on both single carrier and multi carrier modulations such as OFDM. These effects can be modelled mathematically and used subsequently for analysis. This chapter begins with a brief description about band-pass waveforms and systems. Then the baseband equivalent model of the band-pass signal has been presented. After that, a general mathematical model of I/Q imbalance for single carrier modulation has been developed. A brief discussion about OFDM transmission/reception has been presented in this chapter as well. Next, the model for the I/Q imbalance has been further extended for the OFDM signal. Finally, the effect of I/Q in the presence of multipath channel and AWGN has been shown by means of signal constellation, error vector magnitude (EVM) and SER, to portray the necessity of I/Q imbalance correction and compensation for dual branch receivers.

3.2 Representation of bandpass waveforms and systems

This thesis uses the definitions from [71]: baseband, bandpass and modulation.

Baseband waveform: A baseband waveform has a spectral magnitude that is non zero for frequencies in the vicinity of the origin (i.e., $f = 0$) and negligible elsewhere [71].

Bandpass waveform: A bandpass waveform has a spectral magnitude that is non zero for frequencies in some band concentrated about a frequency $f = \pm f_c$ where, $f_c >> 0$. The spectral magnitude is negligible elsewhere; fc is called the carrier frequency [71]. For a bandpass waveform f_c may be arbitrarily assigned for mathematical convenience in some problems. In others, such as modulation, f_c is the frequency of an oscillatory signal in the transmitter circuit and is the assigned frequency of the transmitter, such as for example 900 MHZ for GSM. In communication system the bandpass signal which has a bandpass spectrum that is concentrated at $\pm f_c$, will propagate across the communication channel [71].

Modulation: Modulation is the process of imparting the source information onto a bandpass signal with a carrier frequency f_c by the introduction of amplitude and or phase perturbations. This bandpass signal is called a modulated signal and the baseband signal is called modulating signal. The modulation can be explained as a mapping technique that maps the message or source information onto the bandpass signal. As the modulated signal goes through the channel, it becomes distorted by the channel. The resultant signal is received by the receiver, and the receiver retrieves the message/source information from the corrupted modulated signal.

3.3 Complex envelope and baseband equivalent representation of transmit signal, received signal and channel

In typical wireless applications, communication occurs in a bandpass $[-f_c - \frac{W}{2}, f_c + \frac{W}{2}]$ of bandwidth W around a centre frequency f_c, the spectrum having been specified by regulatory authorities. However, most of the processing, such as coding/decoding, modulation/demodulation, synchronization, etc., is actually done at the baseband. At the transmitter, the last stage of the operation is to “up-convert” the signal to the carrier frequency and transmit it via the antenna. Similarly, the first step at the receiver is to “down-convert” the RF signal to the baseband before further processing. Therefore from a communication system design point of view, it is most useful to have a baseband and a bandpass equivalent representation of the system. We first start with

defining the baseband equivalent representation of signals. The expression, $x[n]$ denotes the digital domain baseband representation of the transmitted signal. After the digital to analogue conversion $x[n]$ becomes the analogue domain transmitted baseband signal, given by, $x(t)$. The complex bandpass equivalent is defined as $x_p(t)$ and its Fourier transform is $X_p(f)$, band limited in $[f_c - W/2, f_c + W/2]$ with $W << 2f_c$. The basband signal $x(t)$ has a Fourier transform given by,

$$X(f) = \begin{cases} X_p(f + f_c) & f + f_c > 0 \\ 0 & f + f_c \leq 0 \end{cases} \tag{3.1}$$

If $x_p(t)$ is real, its Fourier transform becomes, $X_p(f) = X_p^*(-f)$ which means that $x(t)$ contains information as $x_p(t)$. Note that $x(t)$ is band-limited in $\left[-\frac{W}{2}, \frac{W}{2}\right]$. To reconstruct $x_p(t)$ from $x(t)$, we observe that,

$$X_p(f) = X(f - f_c) + X^*(-f - f_c) \tag{3.2}$$

Taking inverse Fourier transforms, we obtain [72],

$$x_p(t) = x(t)e^{j2\pi f_c t} + x^*(t)e^{-j2\pi f_c t} \tag{3.3}$$

$$x_p(t) = 2Re\{x(t)e^{j2\pi f_c t}\}$$

or
$$x_p(t) = 2x_I(t)cos2\pi f_c t - 2x_Q(t)\, sin2\pi f_c t \tag{3.4}$$

here, $x_I(t) = Re\{x(t)\}$ and $x_Q(t) = Im\{x(t)\}$, where $Re\{.\}$ and Im represent the real and imaginary component of the signal, respectively. Also, $x(t) = x_I(t) + jx_Q(t)$. Thus by equation (3.4) the real signal $x_p(t)$ can now be represented by its complex envelope. In terms of real signals, the down-conversion of the dual branch receiver is shown in Figure 3-1.

The bandpass signal $x_p(t)$ is obtained by modulating $Re\{x(t)\}$ by $cos2\pi f_c t$ and $Im\{x(t)\}$ by $-sin2\pi f_c t$ and by summing up $x_I(t)cos2\pi f_c t$ and $-x_Q(t)\, sin2\pi f_c t$, we

obtain $Re\{x(t)e^{j2\pi f_c t}\}$ (up-conversion). The expression, $x_I(t)$ is known as the In-phase component and $x_Q(t)$ (rotated by 90^0) is known as the Quadrature component. Similarly, the baseband signal is obtained by demodulating the $x_p(t)$ by $cos2\pi f_c t$ and $-sin2\pi f_c t$ followed by ideal low-pass filtering at the baseband $[-W/2,\ W/2]$ (down-conversion). The channel impulse response in bandpass is given by $h_p(t)$. The expressions, $x(t)$ and $r(t)$ are the complex baseband equivalents of the transmitted signal $x_p(t)$ and the received signal $r_p(t)$, respectively. Now as $x_p(t)$ passes through the channel, it gets distorted by multipath channel and AWGN. The resultant signal $r_p(t)$ is then obtained by,

$$r_p(t) = x_p(t) \otimes h_p(t) + \varepsilon_p(t) \tag{3.5}$$

where,' $\otimes$' stands for linear convolution and $\varepsilon_p(t)$ is the bandpass noise component. The expression, $x_p(t)$ is given by equation (3.4), and $r_p(t)$ and $h_p(t)$ can be written in a similar manner as:

$$h_p(t) = 2Re\{h(t)e^{j2\pi f_c t}\} \tag{3.6}$$

$$r_p(t) = 2Re\{r(t)e^{j2\pi f_c t}\} \tag{3.7}$$

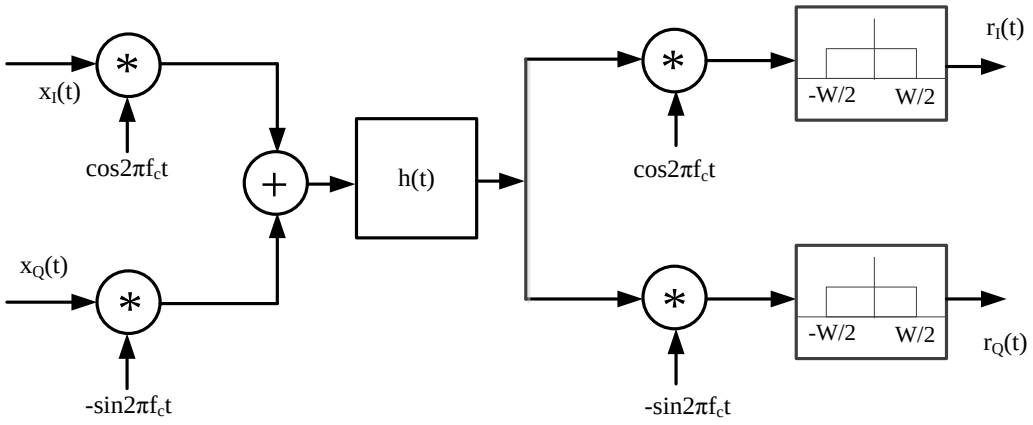

Figure 3-1 Down-conversion in dual branch receiver represented in baseband

So the baseband equivalent model of the transmit signal, received signal, channel and noise are $x(t)$, $r(t)$ $h(t)$ and $\varepsilon(t)$, respectively. After $r(t)$ is passed through the ADC

and the digital domain output $r[n]$ is obtained. The digital domain baseband equivalent of $x(t)$, $r(t)$, $h(t)$ and $\varepsilon(t)$ are denoted as, $x[n]$, $r[n]$, $h[n]$ and $\varepsilon[n]$, respectively and their relationship is as follows;

$$r[n] = x[n] \otimes h[n] + \varepsilon[n] \tag{3.8}$$

3.4 General mathematical model of I/Q imbalance for single carrier modulation

Mismatches in gain and phase that occurred between the I and Q signal branches of a dual-branch receiver are often modelled in several ways for mathematical analysis. For example, in the research by [2, 52], equal portions of gain and phase mismatches are assigned to the two signal branches. In some cases, it may be more convenient to consider the entire gain and phase deviations to occur in one branch, either I or Q branch, relative to the other [7, 12, 28]. In our study, it is assumed that the entire gain deviation to occur in the I branch with reference to the Q branch. On the other hand, all the phase deviation is present in the Q branch. In this section, a general I/Q imbalance model has been presented. Although I/Q imbalance may arise from different components of the analogue front end, for mathematical explanation, often frequency-flat I/Q imbalance has been assumed to be generated due to the gain and phase mismatch of the local oscillator [1]. The block diagram of a general I/Q imbalance model on DCR has been shown in Figure 3-2. It is an extension of Figure 3-1, containing the I/Q imbalance components. The frequency-selective I/Q imbalance is often assumed to be arrived from the mismatch of the low pass filters shown in Figure 3-2 [1]. From equations (3.1) to (3.8), the transmission of the signal has been described. Also, we have assumed that the transmitter is completely I/Q imbalance free. So only the I/Q imbalance corresponding to the receiver part, has been modelled here. The received bandpass signal to be downconverted can be written as (3.4) where,

$$r_p(t) = 2Re\{r(t)\}cos2\pi f_c t - 2Im\{r(t)\}sin2\pi f_c t \tag{3.9}$$

Let, $Re\{r(t)\} = r_I(t)$ and $Im\{r(t)\} = r_Q(t)$. Now, equation (3.9) can be written as,

$$r_p(t) = 2r_I(t)cos2\pi f_c t - 2r_Q(t)sin2\pi f_c t \qquad (3.10)$$

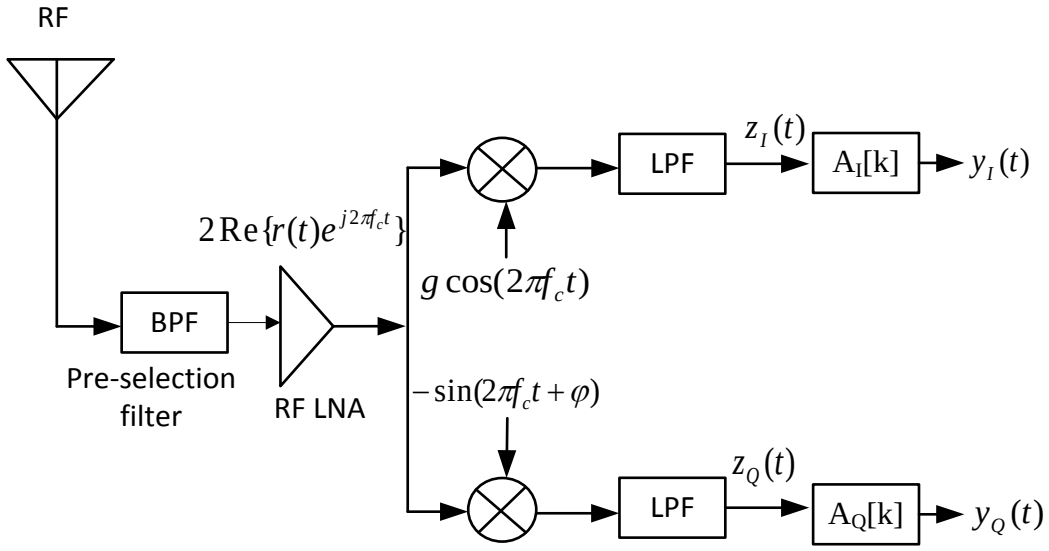

Figure 3-2 The model of a DCR incorporating I/Q imbalance

Let $z_p(t) = z_{p,I}(t) + jz_{p,Q}(t)$; denotes the bandpass signal after $r_p(t)$ has experienced a frequency-flat I/Q imbalance before the low pass filtering process. The In-Phase (I) and Quadrature (Q) component of $z_p(t)$ are given as follows:

$$z_{p,I}(t) = r_p(t)gcos(2\pi f_c t) \qquad (3.11)$$

$$z_{P,Q}(t) = -r_p(t)sin(2\pi f_c t + \varphi) \qquad (3.12)$$

Now, inputting the value of $r_p(t)$ in equations (3.11) and (3.12), we get

$$z_{p,I}(t) = (2r_I(t)cos2\pi f_c t - 2r_Q(t)sin2\pi f_c t)(gcos2\pi f_c t)$$

or, $$z_{p,I}(t) = gr_I(t)(1 + cos4\pi f_c t) - gr_Q(t)sin4\pi f_c t \qquad (3.13)$$

Similarly, we obtain,

$$z_{P,Q}(t) = -r_p(t)sin(2\pi f_c t + \varphi)$$

or, $$z_{P,Q}(t) = \{-r_I(t)(cos\varphi)(sin4\pi f_c t) - r_I(t)sin\varphi(1 + cos4\pi f_c t) + r_Q(t)cos\varphi(1 - cos4\pi f_c t) + r_Q(t)sin\varphi sin4\pi f_c t\} \quad (3.14)$$

After the LPF operation, the terms including $4\pi f_c t$ gets filtered out and the resultant baseband signals is given by,

$$z_I(t) = g r_I(t) \quad (3.15)$$

and $$z_Q(t) = cos\varphi\, r_Q(t) - sin\,\varphi\, r_I(t) \quad (3.16)$$

Also, $z(t) = z_I(t) + jz_Q(t)$. Next, the signal $z(t)$ becomes distorted by the frequency-selective I/Q imbalance. Given that the transfer function of the frequency-selective mismatch in discrete form is denoted by $A_I[k]$ and $A_Q[k]$ for the I and Q branches, respectively, the resultant signal $y(t) = y_I(t) + jy_Q(t)$ can be denoted as;

$$y_I(t) = z_I(t) \otimes a_I(t) \quad (3.17)$$

and $$y_Q(t) = z_Q(t) \otimes a_Q(t) \quad (3.18)$$

Consequently,

$$y(t) = \frac{1}{2}\{g a_I(t) \otimes (r(t) + r^*(t))\} + \frac{1}{2} a_Q(t) \otimes \{\left(r(t)e^{-j\varphi} - r^*(t)e^{j\varphi}\right)\}$$

or, $$y(t) = \frac{g a_I(t) + e^{-j\varphi} a_Q(t)}{2} \otimes r(t) + \frac{g a_I(t) - e^{j\varphi} a_Q(t)}{2} \otimes r^*(t) \quad (3.19)$$

thus, $$y(t) = u(t) \otimes r(t) + v(t) \otimes r^*(t) \quad (3.20)$$

where, $$u(t) = \frac{g a_I(t) + e^{-j\varphi} a_Q(t)}{2}, \quad (3.21)$$

and $$v(t) = \frac{g a_I(t) - e^{j\varphi} a_Q(t)}{2}. \quad (3.22)$$

Using discrete notations the equations can be denoted as,

$$y[n] = u[n] \otimes r[n] + v[n] \otimes r^*[n] \tag{3.23}$$

as
$$r[n] = h[n] \otimes x[n] + \varepsilon[n] \tag{3.24}$$

Thus
$$y[n] = u[n] \otimes h[n] \otimes x[n] + v[n] \otimes h^*[n] \otimes x^*[n] + u[n] \otimes \varepsilon[n] + v \otimes \varepsilon^*[n] \tag{3.25}$$

where,
$$u[n] = \frac{g a_I[n] + e^{-j\varphi} a_Q[n]}{2} \tag{3.26}$$

and
$$v[n] = \frac{g a_I[n] - e^{j\varphi} a_Q[n]}{2} \tag{3.27}$$

3.5 OFDM transmission

Due to the necessity of a high data rate, most broad band systems, such as worldwide interoperability for microwave access (WiMax), Wi-Fi, long term evolution (LTE), European digital video broadcasting–terrestrial (DVB-T), mobile broadband wireless access (MBWA) use the OFDM. However, OFDM is very sensitive to the RF front end impairments such as I/Q imbalance. In this section, a brief description about the OFDM transmission system has been presented. Later, a mathematical model of frequency-selective I/Q imbalance on an OFDM system has been derived. The OFDM system divides the signal frequency band into a number of overlapping sub channels. The spectrum of OFDM is given in Figure 3-3. Each sub channel is represented by a sinc function. These sub channels or subcarriers are harmonically related to each other. Thus, the peak of one sub carrier coincides with the nulls of other subcarriers, and they remain orthogonal to each other. Figure 3-4 shows a general block diagram of the OFDM system. The output of the mapping block is a signal stream that is modulated by using a typical modulation scheme, such as BPSK, QPSK, or QAM. By serial to parallel conversion, a number of parallel blocks are obtained from the serial signal stream.

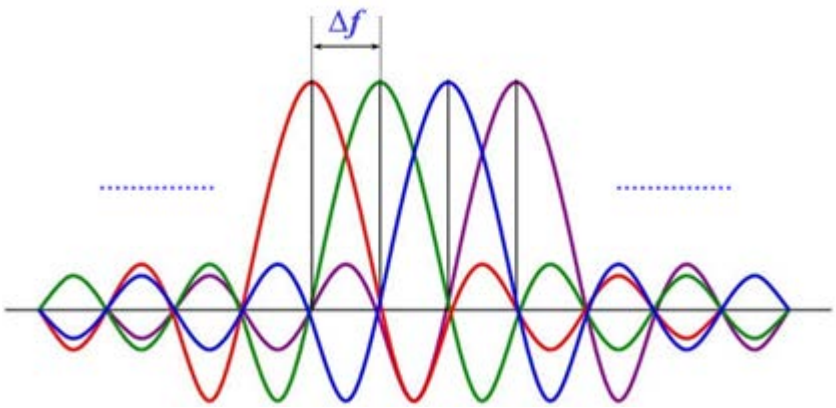

Figure 3-3 OFDM Spectrum

Each parallel block contains a number of samples. If $\{X\left[-\frac{N}{2}\right], X\left[-\frac{N}{2}+1\right], \ldots \ldots X[k], [X[\frac{N}{2}-1]]\}$; denote the data mapped onto the N subcarriers of an OFDM signal; an inverse Fourier transform (IFFT) is performed on these N data modulated symbols to yield a discrete time signal in time domain given by,

$$x[n] = \frac{1}{\sqrt{N}} \sum_{k=-\frac{N}{2}}^{\frac{N}{2}-1} X[k] e^{j2\pi kn/N} \qquad (3.28)$$

Here, k is the subcarrier index relative to the centre frequency and is set such that $k = [-N/2\ to\ N/2-1]$, where $k = 0$ is the centre frequency that represents the DC sub carrier (when N is even). One of the principal benefits of an OFDM system is that it is realistically robust against multipath channel conditions. The OFDM is effective against inter symbol interference (ISI) and inter carrier interference (ICI). In OFDM, N serial data values are sampled at a rate of $1/T_s$ are converted into N parallel streams, which are transmitted at a rate of $1/NT_s$. Therefore, the symbol duration can be increased to a larger period [1]. This decreases the multipath delay with respect to the OFDM symbol duration which results in less ISI. Moreover, the ISI can be entirely removed from the signal by introducing an appropriate guard interval provided that the length of the guard interval is greater than the delay spread of the channel. A set of nulls were used as guard intervals and added in front of each OFDM symbol; in early

OFDM systems as mentioned in the work of [1]. However, guard intervals reduce the chance of becoming affected by ISI; the interference caused by the adjoining sub carriers still remains in the system. Alternatively, inter sub carrier interference could be avoided by cyclically extending the signal rather than using a set of null as a guard period.

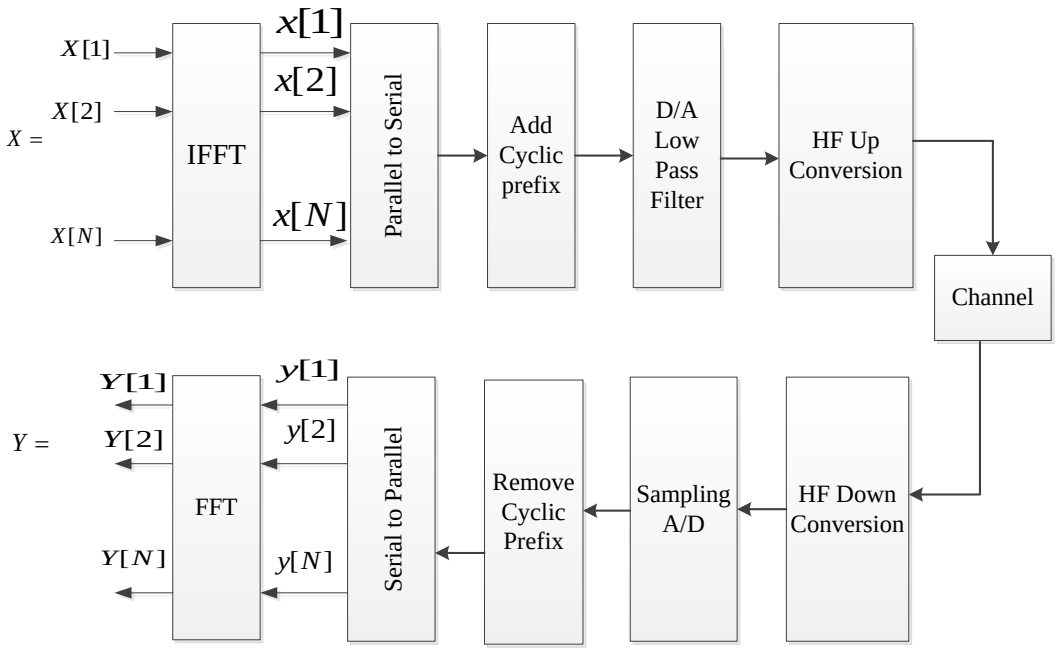

Figure 3-4 Block diagram of a general OFDM system

For adding a cyclic prefix (CP), an appropriate number of samples are appended from the latter part of the signal to the beginning. By doing this the periodicity of the signal is preserved provided that the CP length N_{cp} is greater than the delay spread. The total symbol length then becomes, $N + N_{cp}$ samples. At the receiver, the first N_{cp} samples of the received OFDM signal are discarded and the FFT is performed on the original N number of received sample. As N_{cp} is greater than the delay spread, the phase continuity is maintained, and thereby the inter sub carrier interference is eliminated.

The real and imaginary parts of $x[n]$ in equation (3.28) is $x_I[n]$ and $x_Q[n]$, respectively. They go through the DAC, and after the analogue conversion they become, $x_I(t)$ and $x_Q(t)$. The expressions, $x_I(t)$ and $x_Q(t)$ are up converted using

equation (3.4). Combining equations (3.4) and (3.28), the bandpass signal can be written as,

$$x_p(t) = 2Re\left\{\left(\frac{1}{\sqrt{N}}\sum_{k=-\frac{N}{2}}^{\frac{N}{2}-1} X[k]e^{j2\pi kn/N}\right)e^{j2\pi f_c t}\right\} \qquad (3.29)$$

3.6 I/Q imbalance modelling for OFDM

In this section, we apply the I/Q imbalance model described in Section 3.4 to the OFDM signal. In an OFDM transmission, a block of data is transmitted as an OFDM symbol. The transmitted OFDM symbol can be written in vector form as, $\mathbf{X} = \left[X\left[-\frac{N}{2}\right], X\left[-\frac{N}{2}+1\right], \ldots\ldots X\left[\frac{N}{2}-1\right]\right]^T$. The above symbol consists of N samples excluding the CP. Each block is passed through the inverse discrete Fourier transform (IDFT) operation and thus becomes, $\mathbf{x} = \bar{\mathbf{F}}^*\mathbf{X}$, where $\bar{\mathbf{F}}$ is the unitary discrete Fourier Matrix whose $(n,k)^{th}$element is given by, $\bar{\mathbf{F}}(n,k) = \frac{1}{\sqrt{N}}e^{\frac{-j2\pi kn}{N}}$. Also for unitary transformation, the inverse of the matrix is equal to the complex conjugate of the matrix; resulting in $\bar{\mathbf{F}}^* = \bar{\mathbf{F}}^{-1}$.

The time domain block to be transmitted is denoted as vector such that, $\mathbf{x} = \left[x\left[-\frac{N}{2}\right], x\left[-\frac{N}{2}+1\right], \ldots\ldots x\left[\frac{N}{2}-1\right]\right]^T$; where, $x[n]$ is the n^{th} component of $\mathbf{x}$. Assuming the channel has L paths, the channel impulse response can be written in vector form as; $\mathbf{h} = [h[1], h[2], \ldots\ldots h[L]]$. It is assumed that the channel L is less than the length of the cyclic prefix L_{cp}; (i.e., $L < L_{cp}$). At the receiver, the CP is removed from the receiver and the received block of data; $\mathbf{r} = \left[r\left[-\frac{N}{2}\right], r\left[-\frac{N}{2}+1\right], \ldots\ldots r\left[\frac{N}{2}-1\right]\right]^T$ is obtained. The sampled version of the baseband equivalent model of the received signal before the I/Q imbalance is given by:

$$r[n] = x[n] \circledast h[n] + \varepsilon[n] \tag{3.30}$$

Note that, the linear convolution has been replaced by the circular convolution due to the CP extension. The matrix representation of the above equation is given by:

$$\mathbf{r} = \mathbf{h^c x} + \boldsymbol{\varepsilon} \tag{3.31}$$

where, $\mathbf{r}$ is the received signal vector denoted as, $\mathbf{r} = \left[r\left[-\frac{N}{2}\right], r\left[-\frac{N}{2}+1\right], \dots\dots r\left[\frac{N}{2}-1\right]\right]^T$ and $\overline{\mathbf{h^c}}$ is a NxN circulant matrix (the superscript c has been used to denote this) with first column equal to, $\mathbf{h} = [h[1], h[2], h[3] \dots\dots h[L],\ 0_{1xN-L}]^T$, given by

$$\overline{\mathbf{h^c}} = \begin{bmatrix} h[1] & 0_{N-L} & \cdots & 0_1 & \cdots & h[3] & h[2] \\ h[2] & h[1] & 0_{N-L} & \vdots & \vdots & \vdots & \vdots \\ \vdots & h[2] & h[1] & \vdots & \vdots & \vdots & \vdots \\ h[L_h] & \vdots & h[2] & h[1] & \vdots & \vdots & \vdots \\ 0_1 & h[L] & \vdots & h[2] & h[1] & \vdots & \vdots \\ \vdots & 0_1 & \ddots & \vdots & \ddots & \ddots & \vdots \\ 0_{N-L} & \vdots & \cdots & h[L] & \cdots & h[2] & h[1] \end{bmatrix}$$

Also, $\boldsymbol{\varepsilon}$ is the noise vector denoted as $\boldsymbol{\varepsilon} = \left[\varepsilon[1], \varepsilon[2],\ \varepsilon[3] \dots\dots \varepsilon[N]\right]^T$. After the signal goes through the I/Q imbalance in the receiver, the resultant signal's sampled version can be expressed such that:

$$\begin{aligned} y[n] = u[n] \circledast h[n] \circledast x[n] + v[n] \circledast h^*[n] \circledast x^*[n] \\ + u[n] \otimes \varepsilon[n] + v[n] \otimes \varepsilon^*[n] \end{aligned} \tag{3.32}$$

However, as the noise components do not include any CP, so they are represented by linear convolution. The received vector associated with $y[n]$ is denoted as, $\mathbf{y} = [y[1], y[2], y[3] \dots\dots y[N]]^T$. Likewise, the matrices associated with $u[n]$ and $v[n]$ are NxN circular matrices, $\overline{\mathbf{u^c}}$ and $\overline{\mathbf{v^c}}$ respectively. The matrices $\overline{\mathbf{u^c}}$ and $\overline{\mathbf{v^c}}$ can be expressed as;

$$\overline{\mathbf{u^c}} = \begin{bmatrix} u[1] & 0_{N-L_u} & \cdots & 0_1 & \cdots & u[3] & u[2] \\ u[2] & u[1] & 0_{N-L_u} & \vdots & \vdots & \vdots & \vdots \\ \vdots & u[2] & u[1] & \vdots & \vdots & \vdots & \vdots \\ u[L_u] & \vdots & u[2] & u[1] & \vdots & \vdots & \vdots \\ 0_1 & u[L_u] & \vdots & u[2] & u[1] & \vdots & \vdots \\ \vdots & 0_1 & \ddots & \vdots & \ddots & \ddots & \vdots \\ 0_{N-L_u} & \vdots & \cdots & u[L_u] & \cdots & u[2] & u[1] \end{bmatrix}$$

and

$$\overline{\mathbf{v^c}} = \begin{bmatrix} v[1] & 0_{N-L_v} & \cdots & 0_1 & \cdots & v[3] & v[2] \\ v[2] & v[1] & 0_{N-L_v} & \vdots & \vdots & \vdots & \vdots \\ \vdots & v[2] & v[1] & \vdots & \vdots & \vdots & \vdots \\ v[L_v] & \vdots & v[2] & v[1] & \vdots & \vdots & \vdots \\ 0_1 & v[L_v] & \vdots & v[2] & v[1] & \vdots & \vdots \\ \vdots & 0_1 & \ddots & \vdots & \ddots & \ddots & \vdots \\ 0_{N-L_u} & \vdots & \cdots & v[L_v] & \cdots & v[2] & v[1] \end{bmatrix}$$

The first column of $\overline{\mathbf{u^c}}$ and $\overline{\mathbf{v^c}}$ are $\mathbf{u} = [u(1), u(2) \ldots \ldots u(L_u), 0_{(1xN-L_u)}]^T$ and $\mathbf{v} = [v(1), v(2) \ldots \ldots v(L_u), 0_{(1xN-L_v)}]^T$, respectively. The number of non-zero components in $\mathbf{u}$ and $\mathbf{v}$ are L_u and L_v, correspondingly. The matrices associated with the noise terms are denoted as $\overline{\mathbf{u_n}}$ and $\overline{\mathbf{v_n}}$. However, they are not circulant matrices. They are Toeplitz matrices given as follows,

$$\overline{\mathbf{u_n}} = \begin{bmatrix} u[1] & 0_{N-L_u} & \cdots & 0_1 \\ u[2] & u[1] & 0_{N-L_u} & \vdots \\ \vdots & u[2] & u[1] & \vdots \\ u[L_u] & \vdots & u[2] & u[1] \\ 0_1 & u[L_u] & \vdots & u[2] \\ \vdots & 0_1 & \ddots & \vdots \\ 0_{N-L_{un}} & \vdots & \cdots & u[L_u] \end{bmatrix} \quad \overline{\mathbf{v_n}} = \begin{bmatrix} v[1] & 0_{N-L_v} & \cdots & 0_1 \\ v[2] & v[1] & 0_{N-L_v} & \vdots \\ \vdots & v[2] & v[1] & \vdots \\ v[L_u] & \vdots & v[2] & v[1] \\ 0_1 & v[L_v] & \vdots & v[2] \\ \vdots & 0_1 & \ddots & \vdots \\ 0_{N-L_v} & \vdots & \cdots & v[L_v] \end{bmatrix}$$

Therefore, matrix representation of the received signal in time domain is as follows,

$$\mathbf{y} = (\overline{\mathbf{u^c}})(\overline{\mathbf{h^c}})\mathbf{x} + (\overline{\mathbf{v^c}})(\overline{\mathbf{h^c}})^* \mathbf{x}^* + (\overline{\mathbf{u_n}})\,\boldsymbol{\varepsilon} + (\overline{\mathbf{v_n}})\boldsymbol{\varepsilon}^* \qquad (3.33)$$

where, $\mathbf{x}^*$ is the matrix consisting the conjugates of $\mathbf{x}$. Similarly, $\left(\overline{\mathbf{h^c}}\right)^*$ is the matrix containing the complex conjugate values of $\left(\overline{\mathbf{h^c}}\right)$. As the noise terms would not be further analysed, the total noise terms have been replaced by a vector $\boldsymbol{\varepsilon_T} = [\varepsilon_T[1], \varepsilon_T[2], \ldots \ldots \varepsilon_T[N]]$ with length N such that $\boldsymbol{\varepsilon_T} = (\overline{\mathbf{u_n}}).\,\boldsymbol{\varepsilon} + (\overline{\mathbf{v_n}}).\,\boldsymbol{\varepsilon}^*$. Similarly, equation (3.32) can be written as:

$$y[n] = u[n] \circledast h[n] \circledast x[n] + v[n] \circledast h^*[n] \circledast x^*[n] + \varepsilon_T[n] \qquad (3.34)$$

As, $(\overline{\mathbf{u^c}})$, $(\overline{\mathbf{v^c}})$, $\left(\overline{\mathbf{h^c}}\right)$ and $\left(\overline{\mathbf{h^c}}\right)^*$ are circulant matrices, they can be expressed as [5]: $(\overline{\mathbf{u^c}}) = \bar{\mathbf{F}}^*\bar{\boldsymbol{\Delta}}_\mathbf{u}\bar{\mathbf{F}}$, $(\overline{\mathbf{v^c}}) = \bar{\mathbf{F}}^*\bar{\boldsymbol{\Delta}}_\mathbf{v}\bar{\mathbf{F}}$, $\overline{\mathbf{h^c}} = \bar{\mathbf{F}}^*\bar{\boldsymbol{\Delta}}_\mathbf{h}\bar{\mathbf{F}}$ and $\left(\overline{\mathbf{h^c}}\right)^* = \bar{\mathbf{F}}^*(\bar{\boldsymbol{\Delta}}_\mathbf{h})^*\bar{\mathbf{F}}$.

Moreover, $\bar{\boldsymbol{\Delta}}_\mathbf{u}$, $\bar{\boldsymbol{\Delta}}_\mathbf{v}$, $\bar{\boldsymbol{\Delta}}_\mathbf{h}$ and $(\bar{\boldsymbol{\Delta}}_\mathbf{h})^*$ are related to the $\mathbf{u}$, $\mathbf{v}$, $\mathbf{h}$ and $\mathbf{h^*}$, respectively. They are expressed as, $\bar{\boldsymbol{\Delta}}_\mathbf{u} = diag\{\mathbf{U}\}$ and $\mathbf{U} = \bar{\mathbf{F}}\mathbf{u}$. Here $diag\{.\}$ stands for diagonal matrix operation. The elements of the diagonal matrix have been taken from the DFT of the first column of the respective circulant matrix. Also $U[k]$ is the $(k,k)^{th}$ element of, $\bar{\boldsymbol{\Delta}}_\mathbf{u}$. Similarly, $\bar{\boldsymbol{\Delta}}_\mathbf{v} = diag\{\mathbf{V}\}$, $\mathbf{V} = \bar{\mathbf{F}}\mathbf{v}$; $\bar{\boldsymbol{\Delta}}_\mathbf{h} = diag\{\mathbf{H}\}$, $\mathbf{H} = \bar{\mathbf{F}}\mathbf{h}$; **and** $(\bar{\boldsymbol{\Delta}}_\mathbf{h})^* = diag\{\mathbf{H}^\#\}$, $\mathbf{H}^\# = \bar{\mathbf{F}}\mathbf{h}^*$. As the DFT of a conjugate of a sequence returns the DFT of the original sequence in mirror frequency, $\mathbf{H}^\#$can be expressed as, $\mathbf{H}^\# = \bar{\mathbf{F}}\mathbf{h}^* = \left[H^*\left[-\frac{N}{2}\right], H^*\left[\frac{N}{2}-1\right], \ldots H^*[0] \ldots H^*\left[-\frac{N}{2}+1\right]\right]^T$. If N is even then all the frequency indexes except $H^*\left[-\frac{N}{2}\right]$ and $H^*[0]$; return the DFT of the original sequence in the mirror frequency index. Hence, equation (3.33) becomes,

$$\mathbf{y} = \bar{\mathbf{F}}^*\bar{\boldsymbol{\Delta}}_\mathbf{u}\bar{\mathbf{F}}\bar{\mathbf{F}}^*\bar{\boldsymbol{\Delta}}_\mathbf{h}\bar{\mathbf{F}}\mathbf{x} + \bar{\mathbf{F}}^*\bar{\boldsymbol{\Delta}}_\mathbf{v}\bar{\mathbf{F}}\bar{\mathbf{F}}^*(\bar{\boldsymbol{\Delta}}_\mathbf{h})^*\bar{\mathbf{F}}\mathbf{x}^* + \boldsymbol{\varepsilon_T} \qquad (3.35)$$

$$\mathbf{y} = \bar{\mathbf{F}}^*\bar{\boldsymbol{\Delta}}_\mathbf{u}\bar{\boldsymbol{\Delta}}_\mathbf{h}\bar{\mathbf{F}}\mathbf{x} + \bar{\mathbf{F}}^*\bar{\boldsymbol{\Delta}}_\mathbf{v}(\bar{\boldsymbol{\Delta}}_\mathbf{h})^*\bar{\mathbf{F}}\mathbf{x}^* + \boldsymbol{\varepsilon_T} \qquad (3.36)$$

Let, $\bar{\mathbf{F}}\mathbf{x} = \mathbf{X}$, where $\mathbf{X} = \left[X\left[-\frac{N}{2}\right], X\left[-\frac{N}{2}+1\right], \ldots \ldots X\left[\frac{N}{2}-1\right]\right]^T$, then $\bar{\mathbf{F}}.\mathbf{x}^* = \mathbf{X}^\# = \left[X^*\left[-\frac{N}{2}\right], X^*\left[\frac{N}{2}-1\right], \ldots X^*[0] \ldots X^*\left[-\frac{N}{2}+1\right]\right]^T$. As the received signal expressed in equation (3.36) now goes through the DFT operation, it can be given by:

$$\bar{\mathbf{F}}\mathbf{y} = \bar{\mathbf{F}}\bar{\mathbf{F}}^{*}\bar{\boldsymbol{\Delta}}_{\mathbf{u}}\bar{\boldsymbol{\Delta}}_{\mathbf{h}}\bar{\mathbf{F}}.\mathbf{x} + \bar{\mathbf{F}}\bar{\mathbf{F}}^{*}\bar{\boldsymbol{\Delta}}_{\mathbf{v}}(\bar{\boldsymbol{\Delta}}_{\mathbf{h}})^{*}\bar{\mathbf{F}}.\mathbf{x}^{*} + \bar{\mathbf{F}}\boldsymbol{\varepsilon}_{\mathbf{T}} \quad (3.37)$$

which results in,

$$\mathbf{Y} = \bar{\boldsymbol{\Delta}}_{\mathbf{u}}\bar{\boldsymbol{\Delta}}_{\mathbf{h}}\mathbf{X} + \bar{\boldsymbol{\Delta}}_{\mathbf{v}}(\bar{\boldsymbol{\Delta}}_{\mathbf{h}})^{*}\mathbf{X}^{\#} + \boldsymbol{\eta} \quad (3.38)$$

where, $\mathbf{Y} = \bar{\mathbf{F}}\mathbf{y}$ and $\bar{\mathbf{F}}\boldsymbol{\varepsilon}_{\mathbf{T}} = \boldsymbol{\eta}$. The resultant signal for k^{th} and $-k^{th}$frequency indices of the received signal are given by;

$$Y[k] = U[k]H[k]X[k] + V[k]H^{*}[-k]X^{*}[-k] + \eta[k] \quad (3.39)$$

$$Y[-k] = U[-k]H[-k]X[-k] + V[-k]H^{*}[k]X^{*}[k] + \eta[-k] \quad (3.40)$$

By taking the complex conjugate of equation (3.40), we obtain,

$$Y^{*}[-k] = U^{*}[-k]H^{*}[-k]X^{*}[-k] + V^{*}[-k]H[k]X[k] + \eta^{*}[-k] \quad (3.41)$$

Equations (3.39) and (3.41) can be represented in matrix form as,

$$\begin{bmatrix} Y[k] \\ Y^{*}[-k] \end{bmatrix} = \begin{bmatrix} U[k]H[k] & V[k]H^{*}[-k] \\ U^{*}[-k]H^{*}[-k] & V^{*}[-k]H[k] \end{bmatrix} \begin{bmatrix} X[k] \\ X^{*}[-k] \end{bmatrix} + \begin{bmatrix} \eta[k] \\ \eta^{*}[-k] \end{bmatrix} \quad (3.42)$$

Overall, the received signals before and after the DFT operation, which are the time domain signal and the frequency domain signal, can be briefly expressed as follows:

Time domain signal

a) Sampled version

$$y[n] = u[n] \circledast h[n] \circledast x[n] + v[n] \circledast h^{*}[n] \circledast x^{*}[n] + u[n] \otimes \varepsilon[n] + v \otimes \varepsilon^{*}[n]$$

b) Vector version

$$\mathbf{y} = (\overline{\mathbf{u^c}})(\overline{\mathbf{h^c}})\mathbf{x} + (\overline{\mathbf{v^c}})(\overline{\mathbf{h^c}})^{*}\mathbf{x}^{*} + (\overline{\mathbf{u_n}})\,\boldsymbol{\varepsilon} + (\overline{\mathbf{v_n}})\boldsymbol{\varepsilon}^{*}$$

Frequency Domain Signal

a) Sampled version

$$Y[k] = U[k]H[k]X[k] + V[k]H^{*}[-k]X^{*}[-k] + \eta[k]$$

b) Vector version

$$\mathbf{Y} = \bar{\boldsymbol{\Delta}}_{\mathbf{u}}\bar{\boldsymbol{\Delta}}_{\mathbf{h}}\mathbf{X} + \bar{\boldsymbol{\Delta}}_{\mathbf{v}}(\bar{\boldsymbol{\Delta}}_{\mathbf{h}})^{*}\mathbf{X}^{*} + \boldsymbol{\eta}$$

3.7 Effects of frequency-flat I/Q gain and phase imbalance and channel on an OFDM system

In this section, the effects of I/Q imbalance has been presented by means of the received signal constellation and SER. The signal constellation shows how the locations of the constellation points are changed due to the I/Q imbalance. Also the SER shows the effect of I/Q imbalance and channel for a wide range of AWGN variation. The I/Q imbalance has been varied to observe its effects on the received signal. However, only the effect of the frequency-flat I/Q imbalance has been shown here. When the I/Q imbalance is frequency-selective, the distortion is even more, which has been shown in the later chapters (Chapter 4 and Chapter 5). Computer simulations have been performed by MATLAB to show the effects of the I/Q imbalance and the multipath channel. The simulation set-up is shown in Figure 3-5.

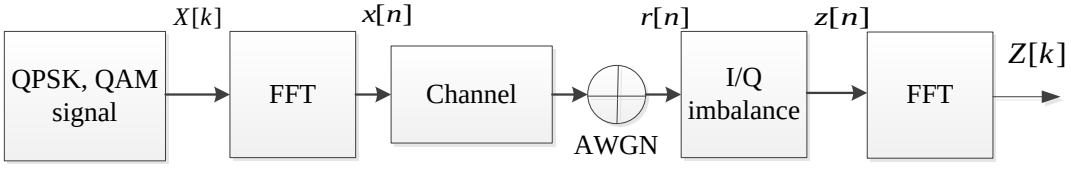

Figure 3-5 Simulation Set-up

The OFDM transmission and reception has been used by means of 64-QAM, 16-QAM and QPSK modulation. The number of subcarriers used is 1024. An I/Q gain of 20% ($g = 1.2$) and phase of 10^{o} ($\varphi=10^{o}$) have been considered for the simulation. A CP of 40 samples has been used. Finally, a nine path LTE channel has been chosen to observe

the effects of the channel and the I/Q [73]. The output of the simulation set up is just the uncompensated received signal. No compensation or equalization has been performed for the outcomes in this chapter.

3.7.1 Signal constellations

Figures 3-6, 3-7 and 3-8 represent the effects of the I/Q imbalance on the constellations of the received uncorrected/uncompensated signal, for the 64-QAM, 16-QAM and QPSK modulations, respectively. In each of these three figures, (a) represents the effect when only the gain imbalance is present, (b) shows the effect of the phase imbalance and (c) shows the combined effects of gain and phase imbalance. It has been observed that, the gain error simply appears as a non-unity scale factor in the amplitude. Phase imbalance, on the other hand, corrupts one channel with a fraction of the data pulses in the other channel.

Due to the phase imbalance the constellation plane rotates at an angle from its original location. When both of the effects are present, the signal constellation suffers from a scaling factor and a rotation, which create distortion. A similar problem is observed for the three types of modulations. However, it is obvious that the higher the modulation order, the higher the effects of the I/Q imbalance. In these figures (Figures 3-6 to 3-8), no multipath channel has been considered. The next figures, Figures 3-9 to 3-11, represent the combined effect of multipath channel and I/Q imbalance on the received signal's constellations for 64-QAM, 16-QAM and QPSK modulations, respectively. In each of these figures, a) represents the effect of only multipath channel and b) represents the combined effects of I/Q imbalance and channel.

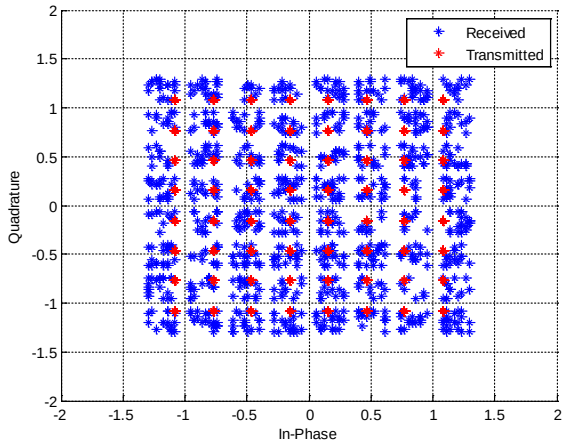

a)

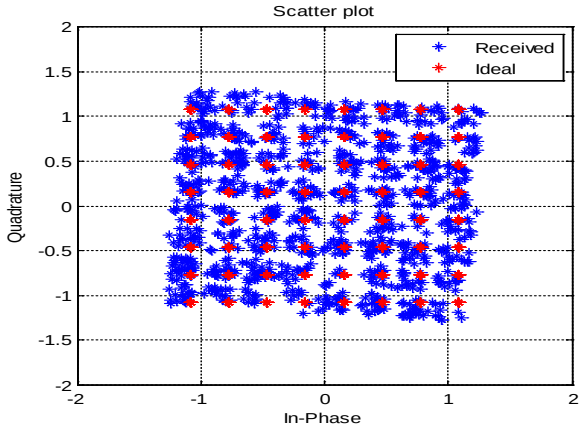

b)

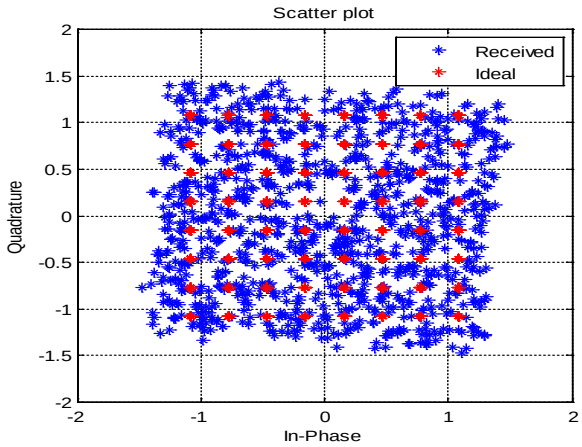

c)

Figure 3-6 Constellations of the received signal after being distorted by a) I/Q gain only, b) I/Q phase only c) I/Q gain and phase, for 64-QAM

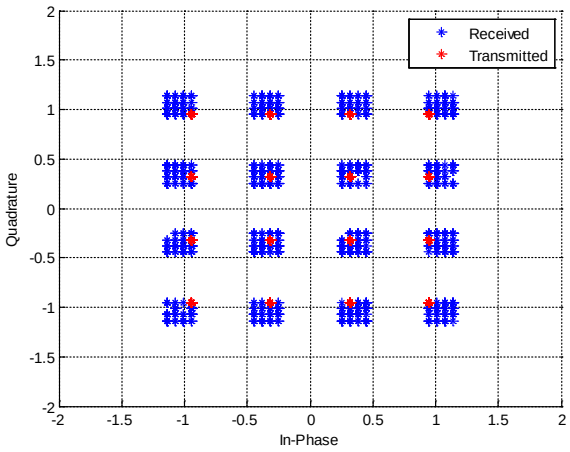

a)

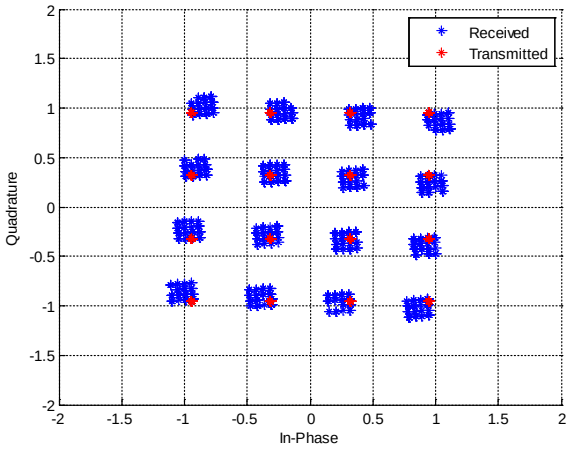

b)

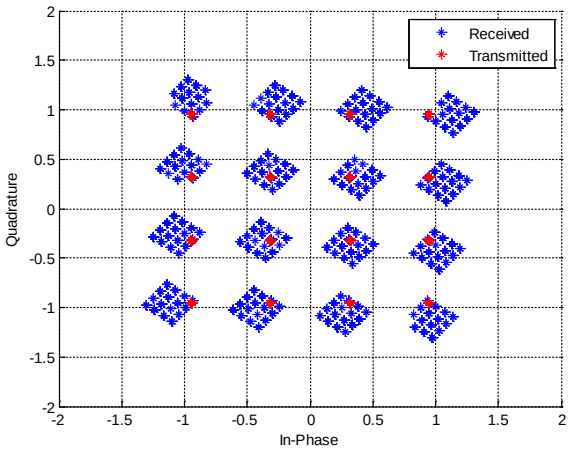

c)

Figure 3-7 Constellations of the received signal after being distorted by a) I/Q gain only, b) I/Q phase only c) I/Q gain and phase, for 16-QAM

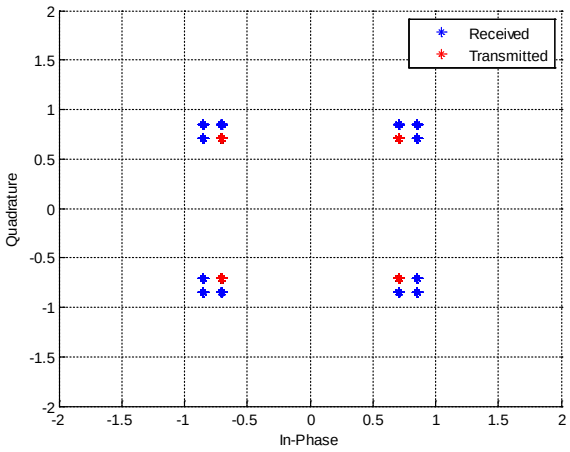

a)

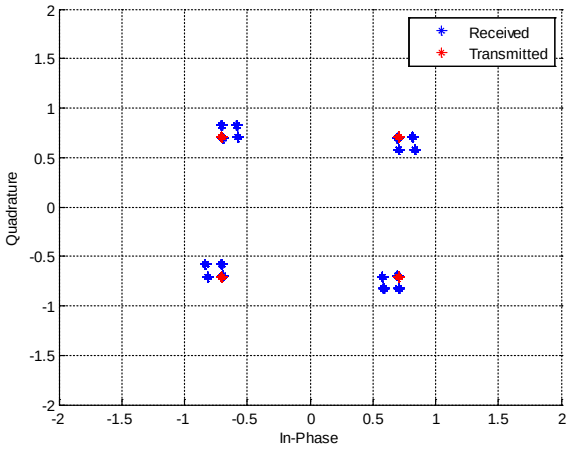

b)

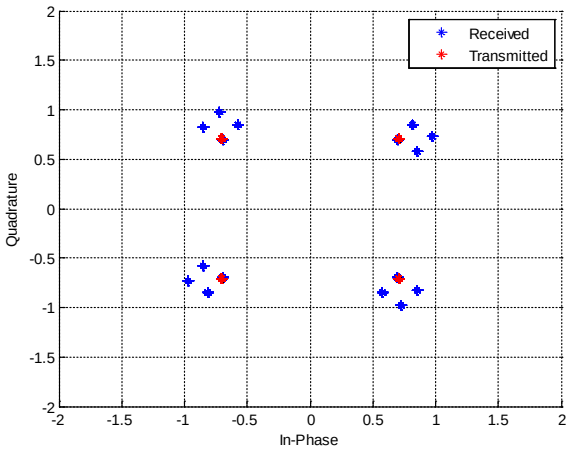

c)

Figure 3-8 Constellations of the received signal after being distorted by a) I/Q gain only, b) I/Q phase only c) I/Q gain and phase, for QPSK

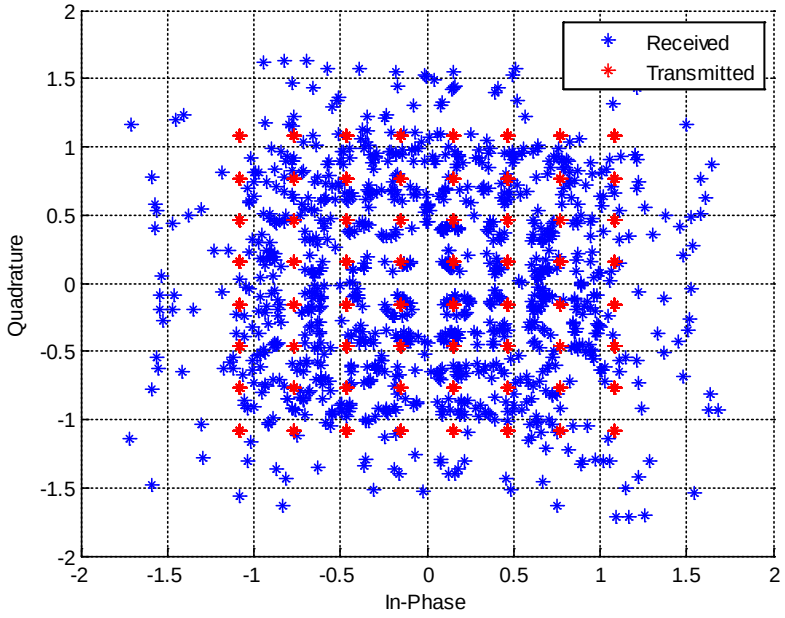

a)

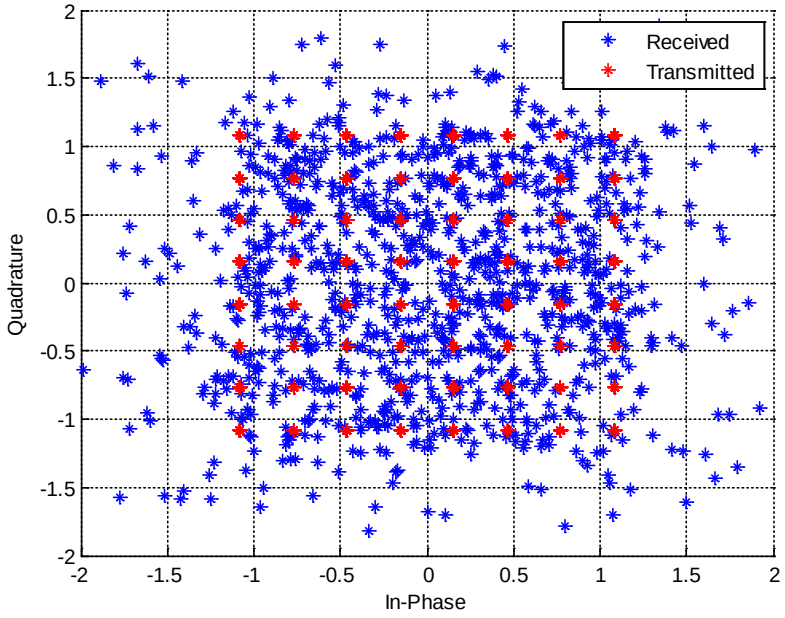

b)

Figure 3-9 Constellations of the received signal after being distorted by a) channel only, b) channel and I/Q, for 64-QAM

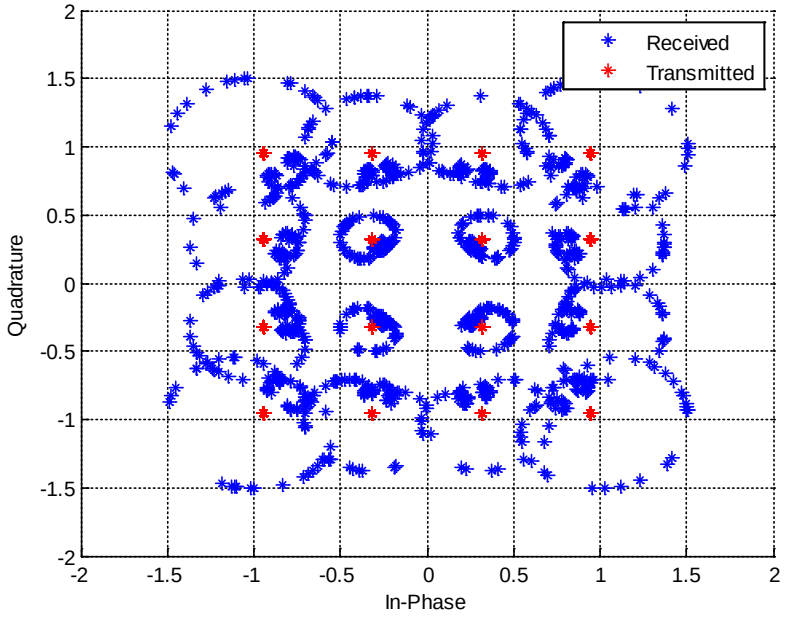

a)

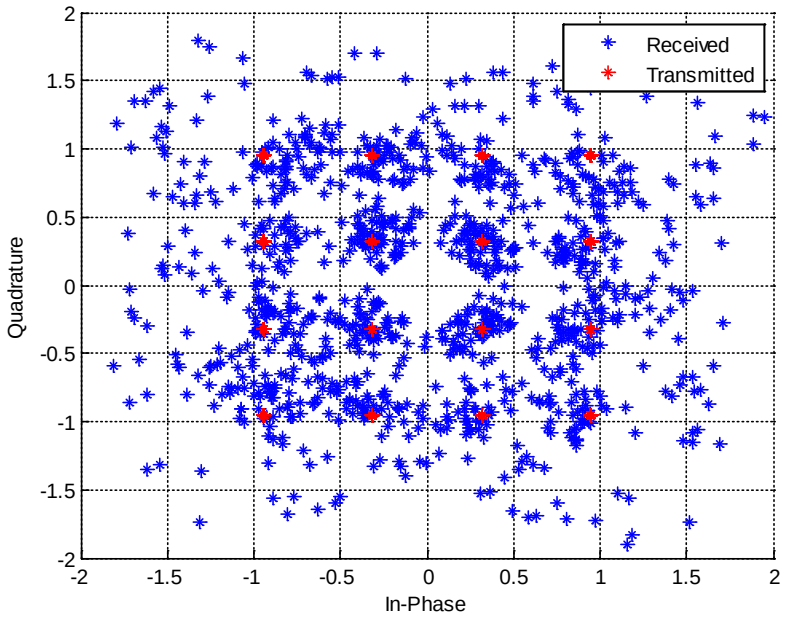

b)

Figure 3-10 Constellations of the received signal after being distorted by a) channel only, b) channel and I/Q, for 16-QAM

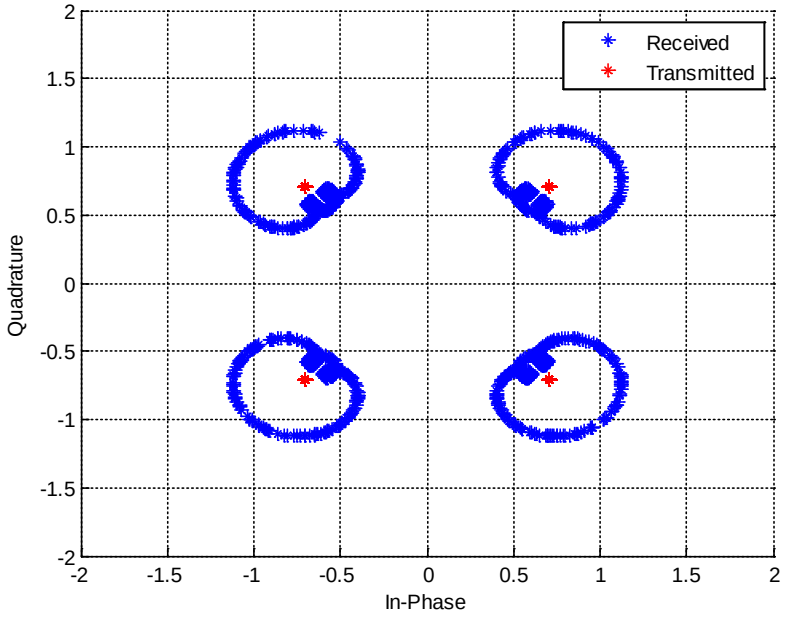

a)

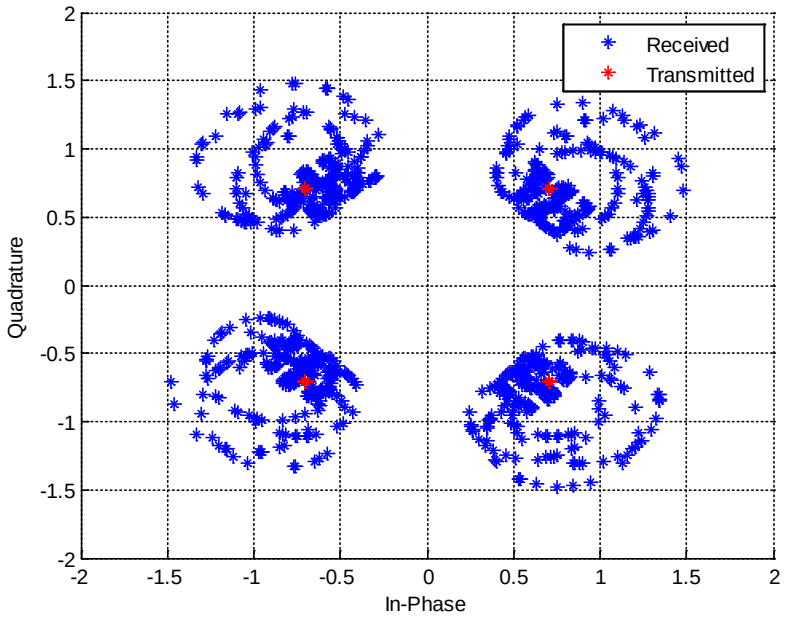

b)

Figure 3-11 Constellations of the received signal after being distorted by a) channel only, b) channel and I/Q, QPSK

Again, it has been observed that when the received signal suffers inter symbol interference (ISI) due to multipath, the location of the constellation points change. The presence of ISI scatters the constellation points from its ideal location. In addition, when the I/Q imbalance is in effect, the received signal still suffers from scattering with a further rotation. However, it is difficult to distinctly observe the effects of channel and I/Q by the means of constellations. The SER gives a much clearer picture to detect the channel and I/Q effects.

3.7.2 Symbol error rate (SER)

The effect of I/Q imbalance has been further illustrated using SER performance. Figure 3-12 and Figure 3-13 show the SER of the received signal after becoming distorted by frequency-flat I/Q imbalance, for 64-QAM and 16-QAM, respectively. For these two figures, no multipath channel has been taken into consideration. The distortion considered for these SER figures are AWGN and frequency-flat I/Q imbalance. The reason is to observe the effect of the I/Q gain and phase without any channel, under various noise conditions. The term 'Ideal' refers to when the received signal does not go through any I/Q imbalance or channel distortion. The only distortion in this case is the AWGN. The term 'I/Q gain only' refers to the SER when the received signal suffers from I/Q gain imbalance, g. The term 'I/Q phase only' refers to the SER when the received signal is distorted by the I/Q phase imbalance, φ. The term 'I/Q gain and phase' refers to the combined effect of gain, g and phase, φ on the received signal.

In Figure 3-12, it has been observed that the uncompensated received signal has a very high SER for all conditions. The curves saturate and do not change with the decrement of noise. The curves representing the effect of only I/Q gain and only I/Q phase show similar SER response. Also, as expected, the SER corresponding to the combined effect of gain and phase shows more degradation than their individual effect. As the I/Q imbalance is quite high, the uncompensated received signal saturates before 10^{-1}.

Next, Figure 3-13 represents the received uncompensated signal for a 16-QAM, modulation. As the modulation order has decreased in this case, the resultant SER curves show a much different outcome than the previous one. Here, it is observed that even for a gain imbalance of 20% the SER curves do not saturate. For an SER of 10^{-3}, the SNR is almost 3 dB higher for the received uncompensated signal than the ideal (no I/Q) condition, when only I/Q gain is in effect. Similarly, the SNR of the received uncompensated signal is almost 4 dB higher than the ideal (no I/Q) case, when only I/Q phase imbalance is present.

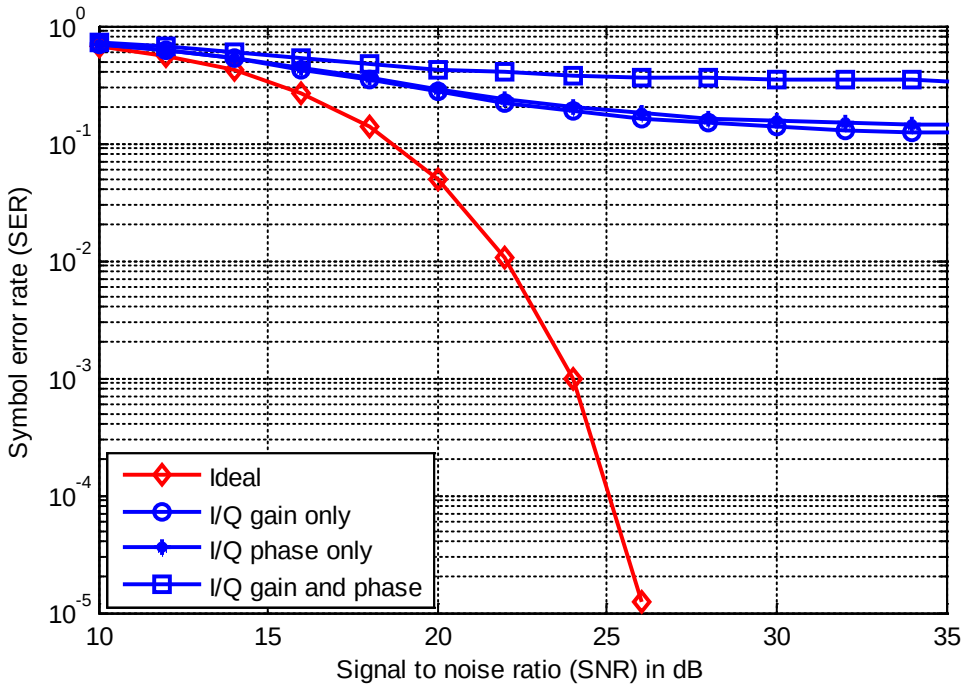

Figure 3-12 SER for uncompensated received signal for 64-QAM

It has been also observed that, for an SER 10^{-3}, the SNR degradation for the curve corresponding to the phase effect is approximately 1 dB more degraded than the curve corresponding to the gain effect. On the other hand, when both I/Q gain and phase are in effect, the SER curve shows higher values. This clearly shows that the combined effect of I/Q imbalance increases the distortion level. For the combined effect, the SNR is 18 dB higher than the ideal reference SER curve, for a specific SER of 10^{-3}.

Next, Figure 3-14 and Figure 3-15 represent the effect of several I/Q gain and phase combination on the received signal for 64-QAM and 16-QAM, respectively. It is obvious that when the I/Q gain and phase combination is low the SER will also be low. In the case of a 64-QAM modulation, for a gain imbalance of 2% and a phase imbalance of 2^o, the received uncompensated signal's SER is close to its ideal SER curve.

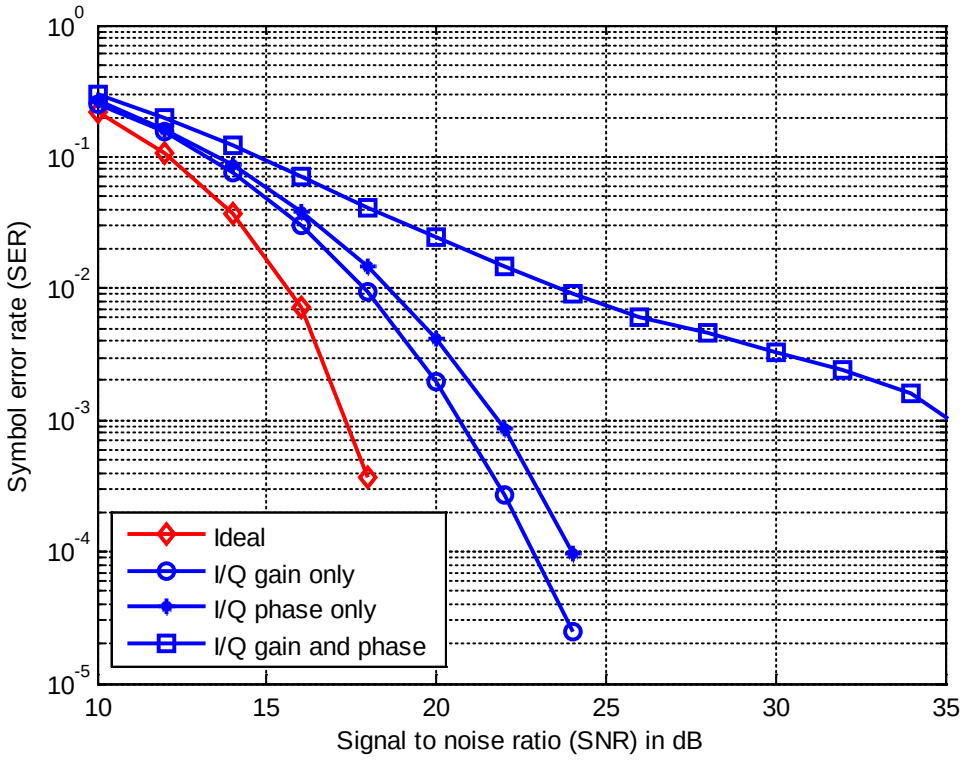

Figure 3-13 SER for uncompensated received signal for 16-QAM

The situation changes once the I/Q imbalance has been increased. To achieve an SER of 10^{-3}, at 10% gain and 2^o phase, the SNR increases approximately 7 dB more than the ideal condition. Now, keeping the gain imbalance to 10%, if the phase is increased to 5^o, the SER curves saturates at 10^{-2}. Likewise I/Q combinations that are higher than that, such as $g = 1.2$, $\varphi = 5^o$ and $g = 1.2$, $\varphi = 10^o$, provides saturated SER curves. Even without the channel, only an I/Q imbalance can affect the received signal badly. Therefore, for an I/Q case like this, correction or compensation is a necessary thing.

For a 16-QAM modulation, the SERs are a little different, as shown in Figure 3-15. For this case, the SER curves increase with the increment of I/Q imbalance. As long as the I/Q combination is less than or equal to $g = 1.1$ and $\varphi = 5^o$, for a SER of 10^{-3}, the SNR degradation is 3 dB higher than the ideal SER curve. For the rest of the two combinations of the I/Q imbalance, the SER remains high. For $g = 1.2$ and $5^o$and $g = 1.2$ and 10^o, the SNR degradation are approximately 5.5 dB and 15 dB, respectively.

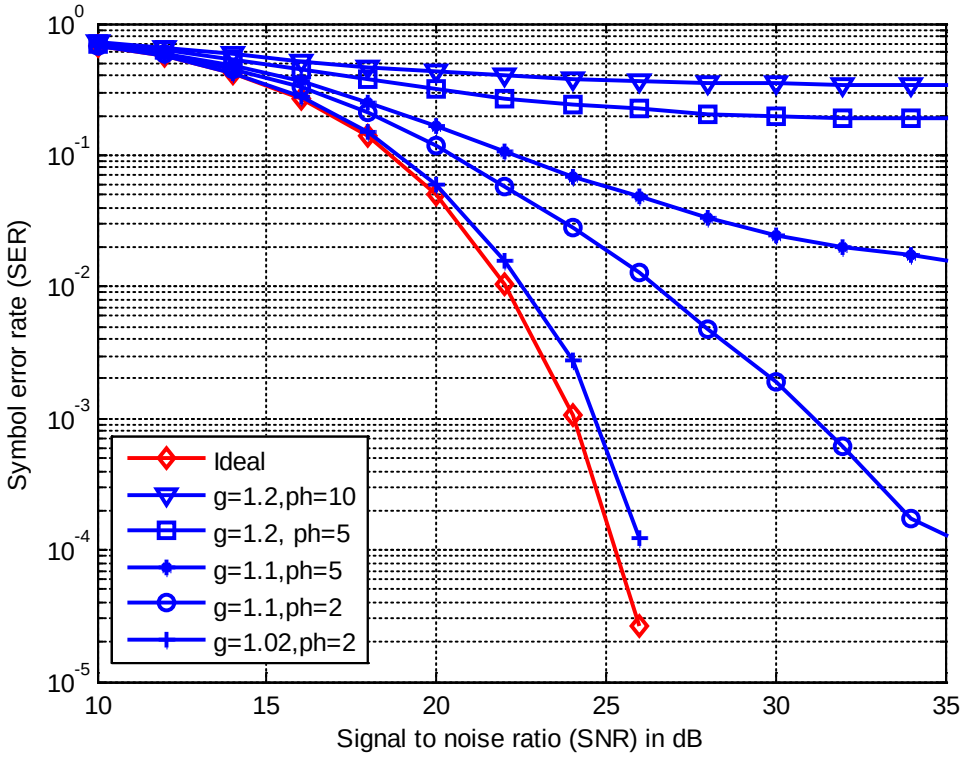

Figure 3-14 SER for uncompensated received signal distorted by different I/Q gain and phase combinations, for 64 QAM

Next, Figure 3-16 and Figure 3-17 represent the effect of the I/Q and the multipath channel, for 64-QAM and 16-QAM, respectively. The constellation corresponding to these signals have been shown in Figure 3-9 and Figure 3-10. The term 'Channel only' represents the case when the received signal has faced channel distortion only but not any I/Q imbalance.

The term 'I/Q only' represents the case when the received signal has experienced the I/Q imbalance effect only. In this case the gain and phase have been chosen as $g =$

1.2 and $\varphi = 10^o$. Furthermore the term 'Channel and I/Q' refers the case where both I/Q and channel are in effect. It has been observed that for a 64-QAM modulation, all of the SER curves become saturated and the SER values are higher than 10^{-1}.

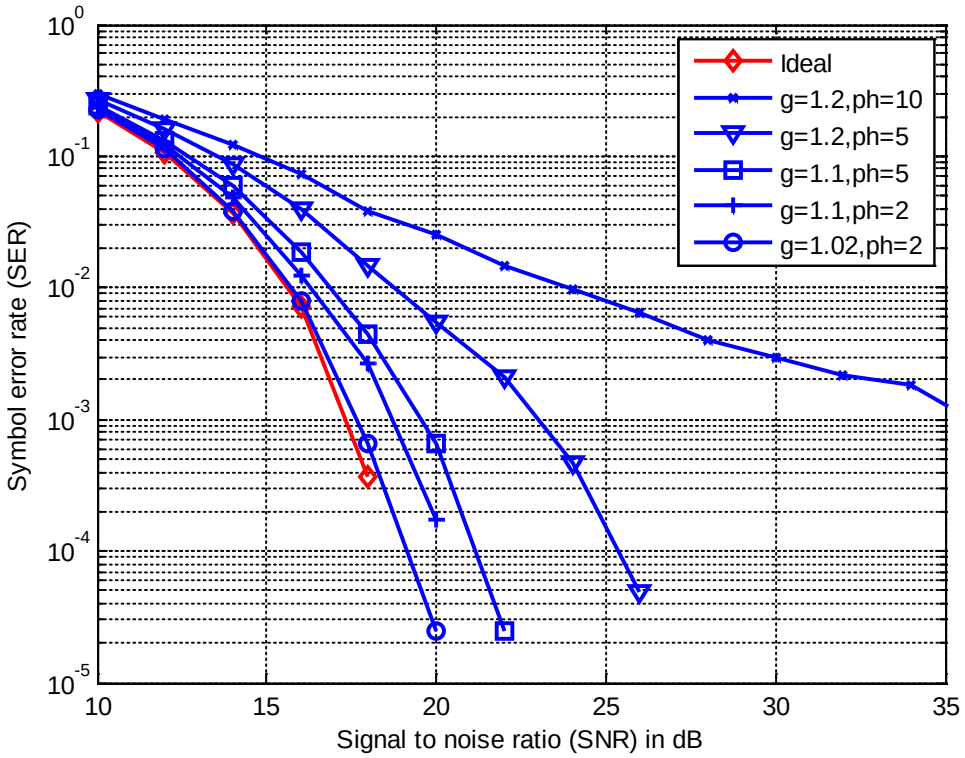

Figure 3-15 SER for uncompensated received signal distorted by different I/Q gain and phase combinations, for 16-QAM

The SER values are slightly less when only I//Q imbalance is in effect. For a 16-QAM modulation, the effect of I/Q imbalance only is much better than the effect of the channel. The combined effect of the channel and I/Q is also the worst as expected. However, even when I/Q is not present, the SER shows higher error due to the presence of the channel, especially for the higher order modulations. From the above simulation, it is clear that the I/Q imbalance can badly affect the signal and introduce a lot of distortion. Also, it has been observed that, due to the presence of a small amount of frequency-flat phase imbalance, the resultant signal can have a large amount of distortion. Therefore, it is easily understandable that the distortion would be severe when time varying and frequency-selective I/Q imbalances would be present. It is

evident that the higher the modulation order, the more sensitive it is to I/Q imbalance. Hence for the same I/Q imbalance combination, the SER for the 64-QAM modulation degrades much more than the 16-QAM. As the demand of data throughput has been markedly increased, higher order modulations are preferred to achieve an increased data rate.

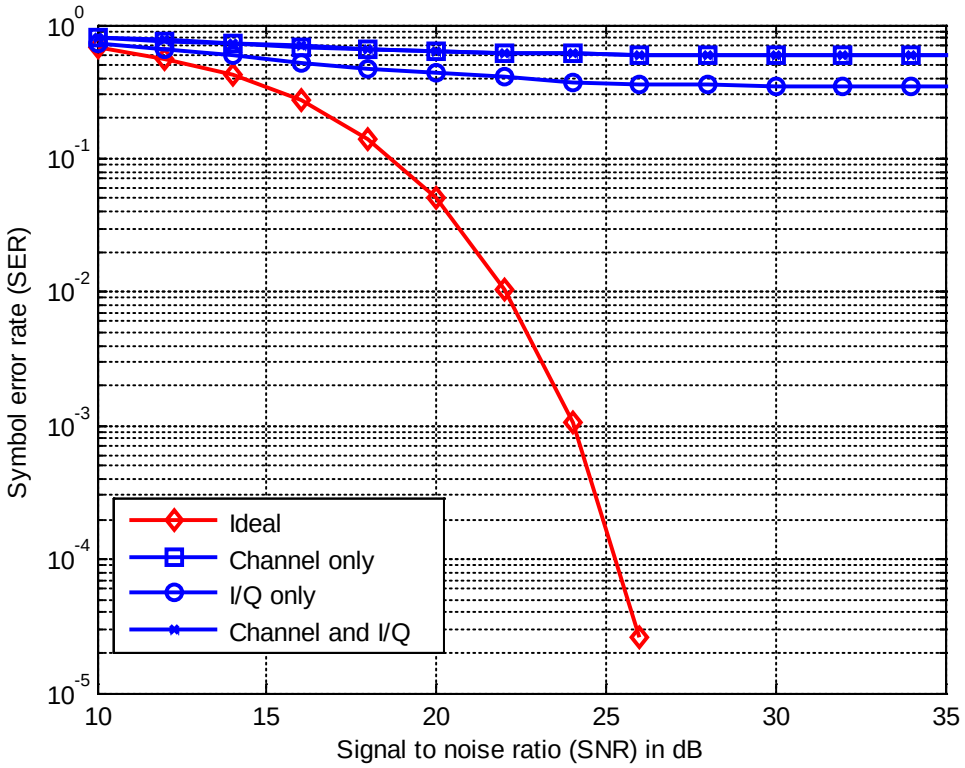

Figure 3-16 SER for uncompensated received signal distorted by I/Q and channel for 64-QAM

However, this I/Q imbalance can hinder that possibility. This is the reason compensation/ correction is necessary for I/Q imbalance. The quadrature down-conversion technique is also used in the popular superheterodyne receivers. Therefore, even the most popular superheterodyne receivers are not free from I/Q imbalance. However, as the down-conversion takes place in a low IF other than the baseband, the effects of stray reactive components are reduced for this case [16]. Therefore, even when the I/Q mismatch is present, its effect is less disturbing in the case of superheterodyne receivers than that of zero-IF receivers.

However, the DCRs have the potential for low cost and low power implementation on silicon [2]. Unlike their superheterodyne counterparts, they do not suffer from the image frequency problem. Also, channel selectivity in DCRs could be readily realized using integrated low-pass filters (LPF). They are affected by the I/Q imbalance problem, especially when higher silicon integration is desired. The key point is, however, if the I/Q imbalance can be removed from the system, the DCR architecture can be a much more popular and low cost option for the SOC application.

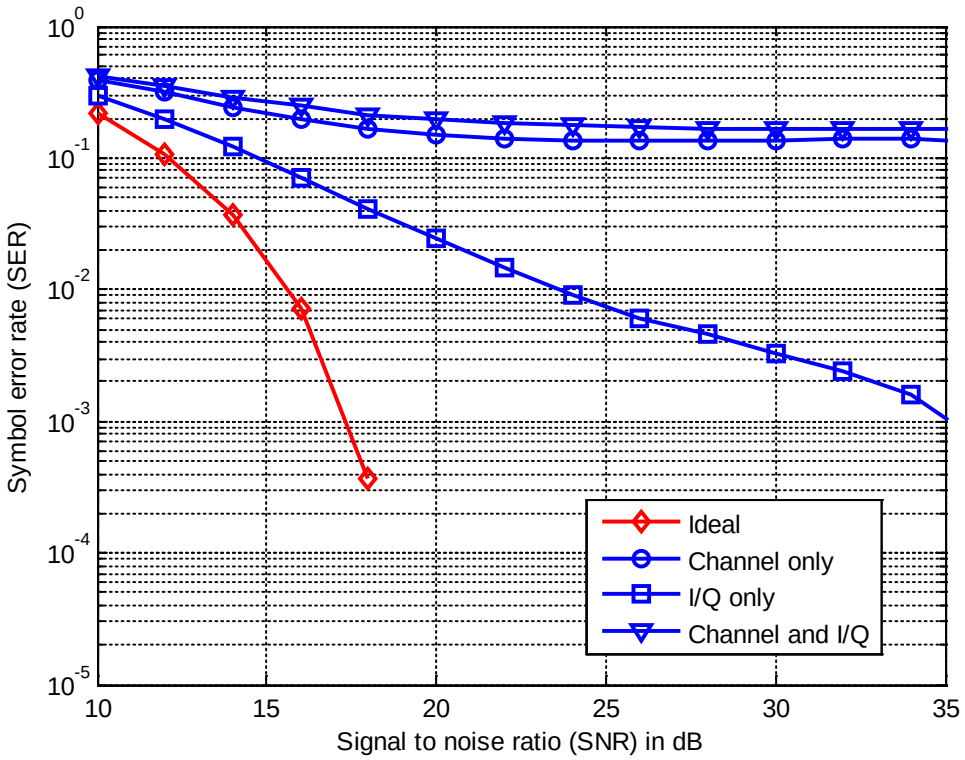

Figure 3-17 SER for uncompensated received signal distorted by I/Q and channel for 16-QAM

3.8 Summary

A general mathematical model has been presented to represent the I/Q imbalance for the single carrier modulation. The model has also been extended to explain the imbalance in the case of the OFDM signal. Finally, simulations have been performed

to demonstrate the effects of I/Q imbalance, multipath channel and their combined effects on an OFDM signal. It has been observed; that even when no channel is present, the I/Q imbalance can distort the signal quite severely. The presence of ISI makes the distortion even much worse. Furthermore, the effect of this impairment on different modulation schemes has been presented. It has been clearly shown that when I/Q is high, even for a lower order modulation the system is severely distorted. Hence a compensation/ correction scheme is very necessary in this regard. This leads to the proposition of suitable digital compensation techniques for I/Q imbalance and multipath channel in the following chapters.

CHAPTER 4

ADAPTIVE COMBINED CORRECTION AND COMPENSATION (ACCC) SCHEME FOR I/Q IMBALANCE AND MULTIPATH CHANNEL FOR OFDM RECEIVERS

4.1 Introduction

In the previous chapter, the manner in which I/Q imbalance and multipath channel parameters affect the OFDM signal has been discussed. In this chapter, a new adaptive scheme in overcoming signal distortion, caused jointly by these two impairments, has been presented for an OFDM receiver. This is a combined correction and compensation scheme. The adaptation process begins by first estimating the unknown parameters in the frequency domain with the aid of pilot tones. These estimated values are then used to calculate the nominal gain and phase. The estimated nominal gain and phase values are fed back to complete a pre-FFT correction for the next upcoming frame. These values adjust the gain and phase of the I and Q branches in such a way as to reduce the distortion caused by I/Q imbalance on the received signal. With the nominal I/Q imbalance corrected following each frame, the resulting less distorted signal can now be subjected to a simpler post compensation process to remove the effects of the multipath channel and any residue frequency dependent I/Q imbalance.

For OFDM signals, pilot symbols are often introduced to enable channel estimation for waveform equalization purposes [36]. If the same pilots can also be utilized for estimating the parameters associated with I/Q imbalance, it will result in a less

computationally complex scheme with no additional loss in data throughput. However, to our best knowledge, all of the previous works assume that the reference pilots used for the estimation of I/Q imbalance and channel are error free[2, 5, 10, 14, 15, 33, 34, 44, 48, 49, 51, 52, 54-56]. This assumption is not likely to be met in practice, particularly when severe I/Q imbalance and channel impairments are encountered in low SNR environments. As such, in our proposed method, we assume that the reference pilots used for the parameter estimation have been recovered from the received signal.

For our proposed adaptive scheme, the signal impairments caused by I/Q imbalance and multipath channel are dealt with in two steps during each cycle of operation. At first, correction of I/Q imbalance is carried out on the received signal before it is subjected to FFT. Then after FFT, the resultant signal, presumably with reduced I/Q imbalance, will enable a more accurate detection of the reference pilots. This leads to better estimations of the I/Q imbalance and channel parameters to be adopted in the next cycle of operation. At the same time, the effects of multipath propagation and remaining frequency-selective I/Q imbalance are also jointly compensated for in the frequency domain, based on the current estimated I/Q imbalance and channel parameters. In this way, the quality of the recovered signal is progressively enhanced after each iteration.

The performance of the proposed combined correction and compensation scheme operating under severe I/Q imbalance (20% gain and 10^{o} phase deviations and an IRR varying from 10 to 32 dB) in a typical urban mobile radio environment (9-path LTE extended typical urban channel model) has been studied by means of MATLAB simulation. However, only the time invariant channel has been considered for the simulation purpose. Section 4.2 gives a brief description about the values used corresponding to frequency-flat and frequency-selective I/Q imbalances. Section 4.3 presents the proposed ACCC scheme. The evaluation of the proposed scheme has been executed by simulations, which have been presented in Section 4.4. Results show that

the proposed scheme is able to perform well, even when the I/Q imbalance is high and the pilots have been detected incorrectly. Finally, Section 4.5 concludes the chapter[1].

4.2 I/Q imbalance values used

Both frequency-flat and frequency-selective I/Q imbalance have been considered in this study. The constant gain and phase are denoted as g and φ. Let $a_I[n]$ and $a_Q[n]$ denotes the impulse response of $A_I[k]$ and $A_Q[k]$, respectively. The overall I/Q imbalance is represented by $U[K]$ and $V[K]$ for I branch and Q branches, respectively. The combined effect of I/Q imbalance and channel for a specific subcarrier k can be represented as $U[k]H[k]$, $V[k]H^*[-k]$, $V^*[-k]H[k]$ and $U^*[-k]H^*[-k]$ according to equation (3.39) and equation (3.41).

For analysis, the mismatches in gain and phase that occurred in the I and Q branches of a dual-branch receiver may be modeled mathematically in various ways. For example, the gain and phase mismatches can be equally split to be present in both signal branches [1, 52]. On the other hand, in some instances, it may be more suitable to consider the entire gain and phase deviations as occurring in one branch, either the I or Q, relative to the other branch [12, 28, 66]. In our scheme, it is assumed that the entire gain imbalance is present in the I branch and the phase imbalance is on the Q branch. It follows that the complex baseband representation of the received signal, after corrupted by frequency dependent I/Q imbalance, can be written in matrix form, recalling equation (3.33):

$$\mathbf{y} = (\overline{\mathbf{u^c}})\left(\overline{\mathbf{h^c}}\right)\mathbf{x} + (\overline{\mathbf{v^c}})\left(\overline{\mathbf{h^c}}\right)^*\mathbf{x}^* + \boldsymbol{\varepsilon}_\mathbf{T} \tag{4.1}$$

The sampled version can be written as (recalling (3.34)):

[1] The contents of this chapter has been published in a conference: 9th IEEE International Symposium on Communications Systems, Networks and Digital Signal Processing *(CSNDSP 2014)*, July 2014, Manchester, UK.

$$y[n] = u[n] \circledast r[n] + v[n] \circledast r^*[n]$$

or $$y[n] = u[n] \circledast h[n] \circledast x[n] + v[n] \circledast h^*[n] \circledast x^*[n] + \varepsilon_T[n] \quad (4.2)$$

where,

$$u[n] = \frac{g a_I[n] + e^{-j\varphi} a_Q[n]}{2}$$

and

$$v[n] = \frac{g a_I[n] - e^{j\varphi} a_Q[n]}{2}$$

The expressions $A_I[k]$ and $A_Q[k]$ denotes the transfer function of $a_I[n]$ and $a_Q[n]$, respectively. The frequency domain representation of $u[n]$ and $v[n]$ can be written as,

where,

$$U[k] = \frac{g A_I[k] + e^{-j\varphi} A_Q[k]}{2} \quad (4.3)$$

and

$$V[k] = \frac{g A[k] - e^{j\varphi} A_Q[k]}{2} \quad (4.4)$$

4.2.1 Frequency-flat I/Q imbalance values used

A number of gain and phase parameters has been used in this study; they have been varied over a grid of values. As such, the gain parameter has been varied over a range of 1% to 20%. At the same time, phases ranging from 1^o to 10^o have been considered.

4.2.2 Frequency-selective I/Q imbalance

For emulating the frequency-selective I/Q imbalance, two different frequency-selective models have been chosen to verify the effectiveness of the proposed scheme. The I/Q imbalances for these models vary non-linearly with the frequency. These models are as follows:

Model 1: The frequency-selective filter for Model 1 has been set to as $A_I = 1 + 0.1z^{-1}$ and $A_Q = 1$. The model has been chosen from [1]. It has relatively small variations of gain and phase over the signal bandwidth. Frequency dependent I/Q imbalance for this model vary according to Figure 4-1 over the signal bandwidth, while the constant gain and phase has been assumed as $g = 1.2$ and $\varphi = 10^o$. The gain and phase imbalances differ approximately by ±0.8dB and $\pm 6^o$ approximately.

Model 2: The frequency-selective filter for Model 2 has been set to as $A_I = 1 + 0.2z^{-1} + 0.2z^{-2}$ and $A_Q = 1$. The gain and phase variation corresponding to this model has been shown in Figure 4-2.

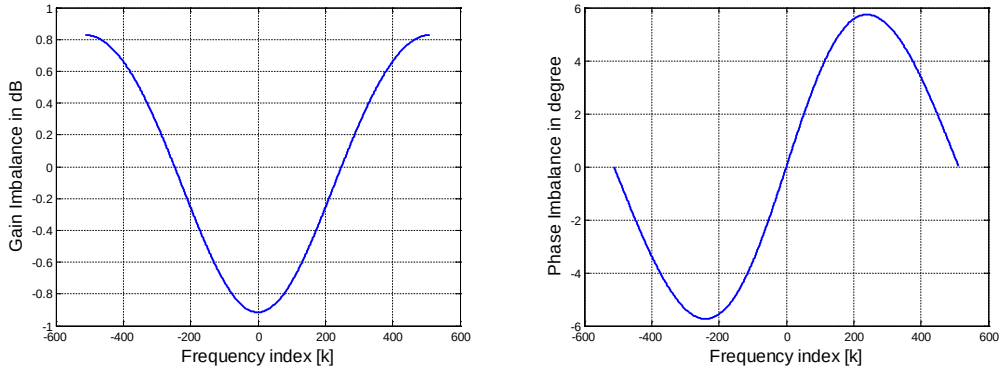

Figure 4-1 Frequency-selective I/Q imbalance for Model 1 (a) Gain imbalance = $20log_{10}\left|\frac{A_I[k]}{A_Q[k]}\right|$*, (b) Phase imbalance =*$Arg\left\{\frac{A_I[k]}{A_Q[k]}\right\}$

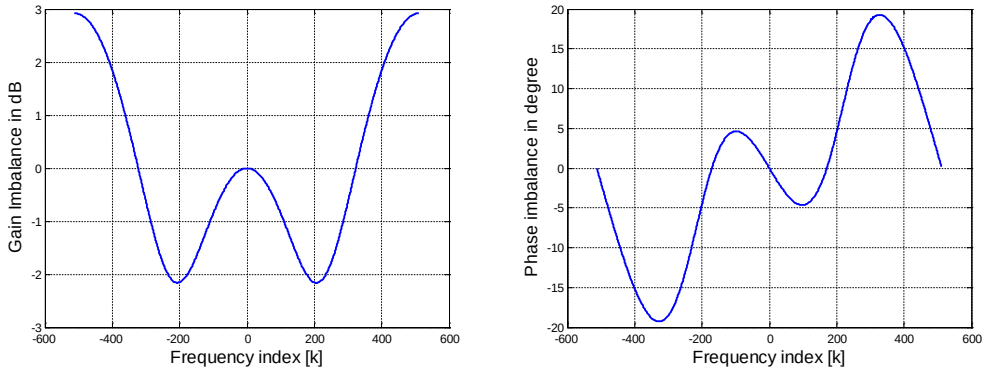

Figure 4-2 Frequency-selective I/Q imbalance for Model 2 (a) Gain imbalance = $20log_{10}\left|\frac{A_I[k]}{A_Q[k]}\right|$*, (b) Phase imbalance =*$arg\left\{\frac{A_I[k]}{A_Q[k]}\right\}$

This one has more variation compared to Model 1. The gain and phase vary ±2.5dB and ±20^{o} over the signal bandwidth.

4.3 Adaptive Combined Correction and Compensation Scheme (ACCC)

4.3.1 System model

The block diagram of the proposed ACCC scheme has been shown in Figure 4-3. The sampled version of the signal after distorted by I/Q imbalance and channel has been given in (4.2). Now, consider the special case of frequency-flat I/Q imbalance. For this case, $a_I[n] = a_Q[n] = 1$; u and v are constants, so that equation (4.2) reduces to the following:

$$y[n] = ur[n] + vr^*[n] \tag{4.5}$$

where, $u = \frac{g+e^{-j\varphi}}{2}$and $v = \frac{g-e^{j\phi}}{2}$. Under this condition, the conjugate operation is replaced by simple multiplication. By expressing equation (4.5) in terms of real and imaginary components, we obtain,

$$\begin{bmatrix} Re\{y[n]\} \\ Im\{y[n]\} \end{bmatrix} = \begin{bmatrix} g & 0 \\ -sin\varphi & cos\varphi \end{bmatrix} \begin{bmatrix} Re\{r[n]\} \\ Im\{r[n]\} \end{bmatrix} \tag{4.6}$$

Assume that the I/Q imbalance parameters, g and φ are known, then the correction can be done by performing an inverse matrix operation on equation (4.6), such that:

$$\begin{bmatrix} Re\{r[n]\} \\ Im\{r[n]\} \end{bmatrix} = \frac{1}{gcos\varphi} \begin{bmatrix} cos\varphi & 0 \\ sin\varphi & g \end{bmatrix} \begin{bmatrix} Re\{y[n]\} \\ Im\{y[n]\} \end{bmatrix} \tag{4.7}$$

This suggests that frequency-flat I/Q imbalance can be corrected in the time domain if the I/Q imbalance parameters, g and φ can somehow be estimated from the received signal $y[n]$. Let the estimated gain and phase be denoted as $\hat{g}$ and $\hat{\varphi}$, and the corrected output is $c[n]$. Now, assuming the estimated gain and phase $\hat{g}$ and $\hat{\varphi}$ are quite close to the original gain and phase g and φ, we get $c[n] \simeq r[n]$. Replacing, g with $\hat{g}$, φ with $\hat{\varphi}$ and $r[n]$ by $c[n]$, (4.7) can be expressed such that

$$\begin{bmatrix} Re\{c[n]\} \\ Im\{c[n]\} \end{bmatrix} = \frac{1}{\hat{g}cos\hat{\varphi}} \begin{bmatrix} cos\hat{\varphi} & 0 \\ sin\hat{\varphi} & \hat{g} \end{bmatrix} \begin{bmatrix} Re\{y[n]\} \\ Im\{y[n]\} \end{bmatrix} \tag{4.8}$$

Briefly, if $g = \hat{g}$ and $\varphi = \hat{\varphi}$, then, $c[n] = r[n]$. However, this is the correction of frequency-flat I/Q imbalance only. The correction of the frequency-selective I/Q imbalance becomes more complex as the gain and phase values; (i.e., g and φ); take on different values for different subcarriers.

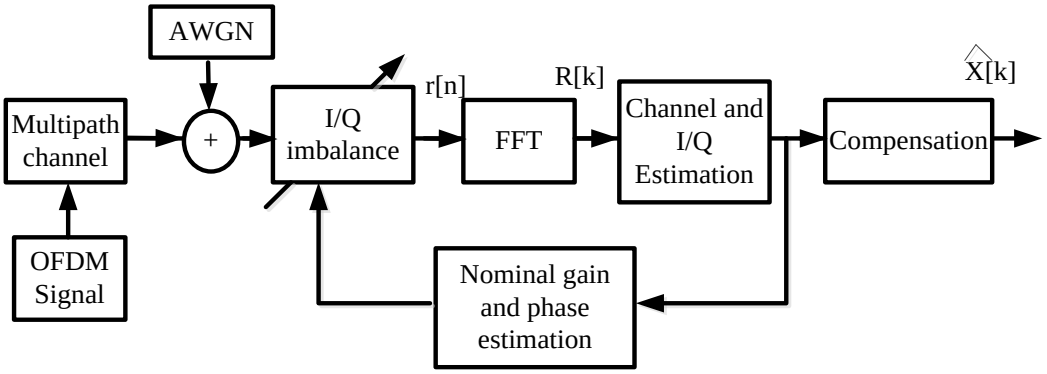

Figure 4-3 Block diagram of the ACCC scheme

In this case, the correction process will involve a convolution operation rather than the much simpler multiplication process. Therefore, the implementation complexity significantly increases. A method of compensating for such frequency-selective I/Q imbalances can be performed by means of baseband post signal processing. Using this scheme (shown in Figure 4-3), I/Q imbalance has been dealt with in two steps. First, with the aid of pilot tones, the gain and phase for each respective tone has been estimated. As for the frequency-selective I/Q imbalance case, it is expected that the

values of the estimated gain and phase; (i.e., $\hat{g}[k]$ and $\hat{\varphi}[k]$); will be different for different pilot subcarriers k.

Second, any uncorrected I/Q imbalance that remains after the time domain correction will be referred to as 'residue I/Q variations'. The residue I/Q imbalance along with the multipath channel is compensated for by means of post processing in the frequency domain.

4.3.2 Pilot pattern adopted for this proposed method

Figure 4-4 shows the diagram of the pilot/ data subcarriers. In this scheme, the total number of non-zero subcarriers in one OFDM symbol has been assumed to be N, where N is an even number. Also k is the subcarrier index relative to the centre frequency and set such that $k = [-N/2, -N/2 + 1 \ldots \ldots, 0, \ldots\ N/2 - 1]$. In addition, it is to be noted that, $k = 0$ is the centre frequency that represents the DC subcarrier (when N is even).

The pilots have been inserted along the subcarrier index k at a distance of d_p subcarriers. The arrangements ensures that the pilots will be distributed evenly about the centre subcarrier 0, which means for a pilot at subcarrier index k_p there will be another pilot carrier located at the subcarrier index – k_p. Generally, in standard OFDM systems such as IEEE 802.11a, the subcarrier indexes $k = 0$ and $k = -N/2$, carry zeroes because of implementation issues [2]. These two tones have been discarded in our simulations to avoid complexities. The total number of pilot subcarriers modelled in one OFDM symbol is $\frac{N}{d_p}$, where $\frac{N}{d_p}$ is an integer. Two successive OFDM symbols; containing these pilot subcarriers; have been referred to here as pilot symbols. They are followed by the OFDM symbols that contain only data, which have been referred as data symbols.

Each OFDM frame contains two pilot and several data symbols. According to Figure 4-4, the frequency interval d_p is 4. Later in Section 4.4, the frequency interval d_p has

been varied to observe the effectiveness of the scheme in the presence of different numbers of pilots. The same pilot pattern is repeated for the next frame after a certain time period t_p, where t_p is measured in seconds.

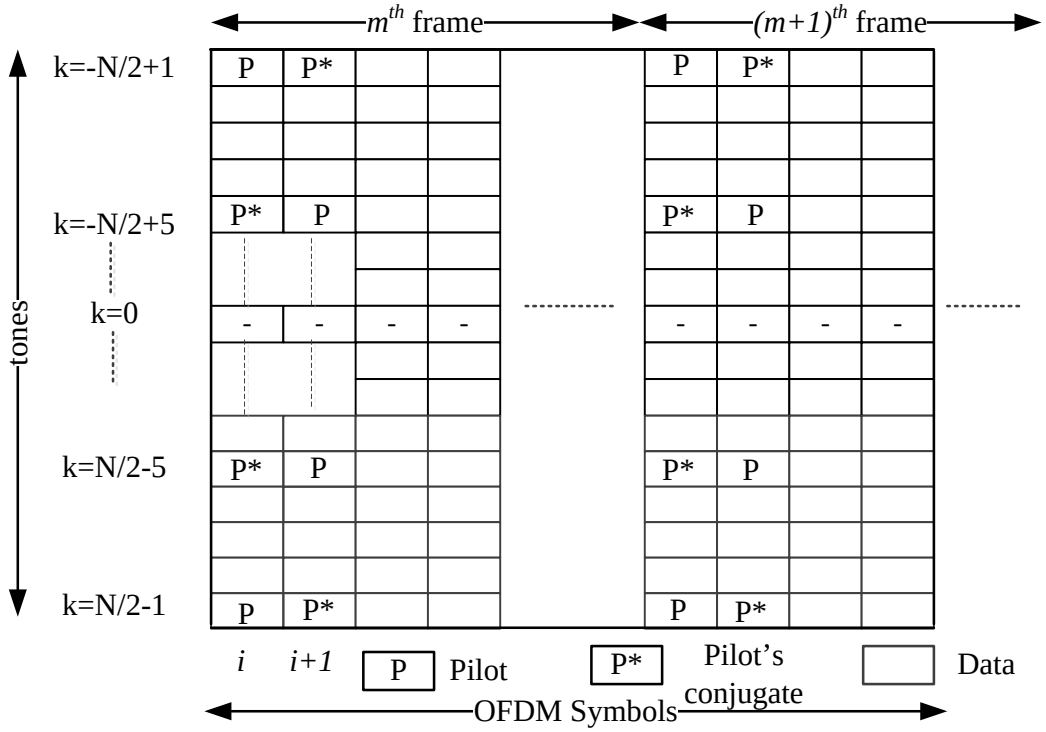

Figure 4-4 Pilot and data arrangement

The value of t_p has been chosen as 8. In the diagram the pilots are shown as P and P*. Here, P refers the pilot and P* refers the conjugate of pilot P. For m^{th} OFDM frame, the pilots for i^{th} and $(i+1)^{th}$symbol, are chosen such that $X_m^{(i)}[k_p] = X_m^{(i)}[-k_p]$, $X_m^{(i+1)}[k_p] = X_m^{(i+1)}[-k_p]$ and $X_m^{(i)}[k_p] = X_m^{(i+1)*}[k_p]$.

4.3.3 Estimation of I/Q imbalance and channel parameters

Assuming, at the beginning of the m^{th} OFDM frame, the n^{th} sample of the i^{th} received symbol $y_m^i[n]$ is expressed according to equation (4.2) as:

$$y_m^i[n] = u_m[n] \circledast r_m^i[n] + v_m[n] \circledast r_m^{*i}[n]$$

$$\text{or} \quad y_m^i[n] = u_m[n] \circledast h_m[n] \circledast x_m^i[n] + v_m[n] \circledast h_m^*[n] \circledast x_m^{*i}[n] + \varepsilon_{T,m}^i[n] \tag{4.9}$$

Here, $u_m[n]$, $v_m[n]$, $h_m[n]$ and $\varepsilon_{T,m}^i[n]$ represents $u[n]$, $v[n]$, $h[n]$ and $\varepsilon_T[n]$ in equation (4.2) for the i^{th} symbol and m^{th} frame. However, the notation for the i^{th} symbol has been omitted for $u_m[n]$, $v_m[n]$ and $h_m[n]$, assuming the channel and I/Q imbalance remain same for one OFDM frame. The expression, $y_m^i[n]$ is corrected by the nominal gain and phase, $g_{m-1}$and φ_{m-1}, estimated during the previous $(m-1)^{th}$frame. The corrected output, $c_m^i[n]$, can be obtained from (4.8) as follows;

$$\begin{bmatrix} Re\{c_m^i[n]\} \\ Im\{c_m^i[n]\} \end{bmatrix} = \begin{bmatrix} g_{m-1} & 0 \\ -sin\varphi_{m-1} & cos\varphi_{m-1} \end{bmatrix}^{-1} \begin{bmatrix} Re\{y_m^i[n]\} \\ Im\{y_m^i[n]\} \end{bmatrix} \tag{4.10}$$

$$c_m^i[n] = \check{u}_m[n] \circledast h_m[n] \circledast x_m[n] + \check{v}_m[n] \circledast h_m^*[n] + \acute{\varepsilon}_{T,m}^i[n][n] \tag{4.11}$$

In equation (4.11), $\check{u}_m[n]$, $\check{v}_m[n]$ and $\acute{\varepsilon}_{T,m}^i[n]$ represent, $u_m[n]$, $v_m[n]$, and $\varepsilon_{T,m}^i[n]$, respectively, that have been undergone I/Q imbalance correction. This forms the input of the FFT block. After the FFT on $c_m^i[n]$, the resulting frequency-domain signal can be expressed as,

$$C_m^i[k] = \check{U}_m[k]H_m[k]X_m^i[k] + \check{V}_m[k]H_m^*[-k]X_m^{*i}[-k] + \acute{\eta}_m^i[k] \tag{4.12}$$

where $\check{U}_m[k]$, $\check{V}_m[k]$, and $\acute{\eta}_m^i[k]$ represent $U[k]$, $V[k]$ and $\eta[k]$ in equation (3.39) respectively, which have experienced I/Q imbalance correction, for the i^{th} symbol and m^{th} frame. These terms will still contain some residue distortion especially the frequency-selective one. With the frequency index k replaced by its corresponding pilot location k_p, the corrected signal for the i^{th} symbol in the m^{th} frame $C_m^i[k_p]$; can be expressed as follows;

$$C_m^i[k_p] = \breve{U}_m[k_p]H_m[k_p]X_m^i[k_p] + \breve{V}_m[k_p]H_m^*[-k_p]X_m^{*i}[-k_p] + \acute{\eta}_m^i[k_p] \tag{4.13}$$

Assuming the channel and I/Q imbalance parameters remain constant between two consecutive OFDM symbols, we obtain;

$$C_m^{i+1}[k_p] = \breve{U}_m[k_p]H_m[k_p]X_m^{i+1}[k_p] + \breve{V}_m[k_p]H_m^*[-k_p]X_m^{*i}[-k_p] + \acute{\eta}_m^{i+1}[k_p] \tag{4.14}$$

Equations obtained from (4.13) and (4.14) can be re-written as:

$$\begin{bmatrix} C_m^i[k_p] \\ C_m^{i+1}[k_p] \end{bmatrix} = \begin{bmatrix} X_m^i[k_p] & X_m^{*i}[-k_p] \\ X_m^{i+1}[k_p] & X_m^{*i+1}[-k_p] \end{bmatrix} \begin{bmatrix} \breve{U}_m[k_p]H_m[k_p] \\ \breve{V}_m[k_p]H_m^*[-k_p] \end{bmatrix} + \begin{bmatrix} \acute{\eta}_m^i[k_p] \\ \acute{\eta}_m^{i+1}[k_p] \end{bmatrix} \tag{4.15}$$

Or in matrix form as;

$$\mathbf{C_p} = \overline{\mathbf{X}}_\mathbf{p}\boldsymbol{\beta}_\mathbf{p} + \boldsymbol{\eta}_\mathbf{p} \tag{4.16}$$

where, $\mathbf{C_p} = \begin{bmatrix} C_m^i[k_p] \\ C_m^{i+1}[k_p] \end{bmatrix}$, $\overline{\mathbf{X}}_\mathbf{p} = \begin{bmatrix} X_m^i[k_p] & X_m^{*i}[-k_p] \\ X_m^{i+1}[k_p] & X_m^{*i+1}[-k_p] \end{bmatrix}$, $\boldsymbol{\beta}_\mathbf{p} = \begin{bmatrix} \breve{U}_m[k_p]H_m[k_p] \\ \breve{V}_m[k_p]H_m^*[-k_p] \end{bmatrix}$,

and $\eta_p = \begin{bmatrix} \acute{\eta}_m^i[k_p] \\ \acute{\eta}_m^{i+1}[k_p] \end{bmatrix}$.

Assuming the noise to be white, with the assistance of the best linear unbiased estimator (BLUE) [5, 74], I/Q and channel parameters can be estimated as,

$$\widehat{\boldsymbol{\beta}}_\mathbf{p} = [\overline{\mathbf{X}}_\mathbf{p}]^{-\mathbf{1}}\mathbf{C_p} \tag{4.17}$$

where, $\widehat{\boldsymbol{\beta}}_\mathbf{p}$ is the estimated value of $\boldsymbol{\beta}_\mathbf{p}$ including error. Equivalently, the complex conjugate of the corrected signal for – k_p^{th} frequency index is given by;

$$\begin{bmatrix} C_m^{*i}[-k_p] \\ C_m^{*i+1}[-k_p] \end{bmatrix} = \begin{bmatrix} X_m^{*i}[-k_p] & X_m^{i}[k_p] \\ X_m^{*i+1}[-k_p] & X_m^{i+1}[p] \end{bmatrix} \begin{bmatrix} \breve{U}_m^{*}[-k_p] H_m^{*}[-k_p] \\ \breve{V}_m^{*}[-k_p] H_m[k_p] \end{bmatrix} + \begin{bmatrix} \acute{\eta}_m^{*i}[-k_p] \\ \acute{\eta}_m^{*i+1}[-k_p] \end{bmatrix} \quad (4.18)$$

denoting,

$\boldsymbol{\beta}_{\mathrm{p}}^{\mathbf{c}} = \begin{bmatrix} \breve{U}_m^{*}[-k_p] H_m^{*}[-k_p] \\ \breve{V}_m^{*}[-k_p] H_m[k_p] \end{bmatrix}$, $\overline{\mathbf{X}}_{\mathbf{p}}^{\mathbf{c}} = \begin{bmatrix} X_m^{*i}[-k_p] & X_m^{i}[k_p] \\ X_m^{*i+1}[-k_p] & X_m^{i+1}[k_p] \end{bmatrix}$, $\mathbf{C}_{\mathbf{p}}^{\mathbf{c}} = \begin{bmatrix} C_m^{*i}[-k_p] \\ C_m^{*i+1}[-k_p] \end{bmatrix}$ and $\boldsymbol{\eta}_{\mathrm{p}}^{\mathbf{c}} = \begin{bmatrix} \acute{\eta}_m^{*i}[-k_p] \\ \acute{\eta}_m^{*i+1}[-k_p] \end{bmatrix}$.

Then, equation (4.18) can be written in matrix form as;

$$\mathbf{C}_{\mathbf{p}}^{\mathbf{c}} = \overline{\mathbf{X}}_{\mathbf{p}}^{\mathbf{c}} \boldsymbol{\beta}_{\mathbf{p}}^{\mathbf{c}} + \boldsymbol{\eta}_{\mathbf{p}}^{\mathbf{c}} \quad (4.19)$$

Like equation (4.17), $\boldsymbol{\beta}_{\mathbf{p}}^{\mathbf{c}}$ can also be estimated using BLUE as;

$$\widehat{\boldsymbol{\beta}}_{\mathbf{p}}^{\mathbf{c}} = [\overline{\mathbf{X}}_{\mathbf{p}}^{\mathbf{c}}]^{-\mathbf{1}} \mathbf{C}_{\mathbf{p}}^{\mathbf{c}} \quad (4.20)$$

where, $\widehat{\boldsymbol{\beta}}_{\mathbf{p}}^{\mathbf{c}}$ is the estimate of $\boldsymbol{\beta}_{\mathbf{p}}^{\mathbf{c}}$ with noise.

4.3.4 Estimation of nominal gain and phase

In this section, the estimation process of the nominal gain and phase has been described. The received signal after the I/Q distortion, at the various pilot frequencies for the for i^{th} and $(i+1)^{th}$symbols present in the m^{th}can be expressed as;

$$\begin{bmatrix} Y_m^{i}[k_p] \\ Y_m^{i+1}[k_p] \end{bmatrix} = \begin{bmatrix} X_m^{i}[k_p] & X_m^{*i}[-k_p] \\ X_m^{i+1}[k_p] & X_m^{*i+1}[-k_p] \end{bmatrix} \begin{bmatrix} U_m[k_p] H_m[k_p] \\ V_m[k_p] H_m^{*}[-k_p] \end{bmatrix} + \begin{bmatrix} \eta_m^{i}[k_p] \\ \eta_m^{i+1}[k_p] \end{bmatrix} \quad (4.21)$$

Expressing**,**

$\mathbf{Y_p} = \begin{bmatrix} Y_m^i[k_p] \\ Y_m^{i+1}[k_p] \end{bmatrix}$, $\bar{\mathbf{X}}_\mathbf{p} = \begin{bmatrix} X_m^i[k_p] & X_m^{*i}[-k_p] \\ X_m^{i+1}[k_p] & X_m^{*i+1}[-k_p] \end{bmatrix}$, $\boldsymbol{\lambda_p} = \begin{bmatrix} U_m[k_p]H_m[k_p] \\ V_m[k_p]H_m^*[-k_p] \end{bmatrix}$,

and $\boldsymbol{\eta_p} = \begin{bmatrix} \eta_m^i[k_p] \\ \eta_m^{i+1}[k_p] \end{bmatrix}$. In the matrix form equation (4.21) can be written as;

$$\mathrm{Y_p} = \bar{\mathbf{X}}_\mathbf{p}\boldsymbol{\lambda_p} + \boldsymbol{\eta_p} \tag{4.22}$$

Now, $\boldsymbol{\lambda_p}$can be estimated from equation (4.22) as,

$$\hat{\boldsymbol{\lambda}}_\mathbf{p} = [\bar{\mathbf{X}}_\mathbf{p}]^{-\mathbf{1}}\mathrm{Y_p} \tag{4.23}$$

where, $\hat{\boldsymbol{\lambda}}_\mathbf{p}$ is the estimated version of $\boldsymbol{\lambda_p}$ containing error. Similarly, for the corresponding image pilot frequencies, we have the following;

$$\hat{\boldsymbol{\lambda}}_\mathbf{p}^\mathbf{c} = [\bar{\mathbf{X}}_\mathbf{p}^\mathbf{c}]^{-\mathbf{1}}\mathrm{Y_p^c} \tag{4.24}$$

where, $\boldsymbol{\lambda}_\mathbf{p}^\mathbf{c}$=$\begin{bmatrix} U_m^*[-k_p]H_m^*[-k_p] \\ V_m^*[-k_p]H_m[k_p] \end{bmatrix}$, $\bar{\mathbf{X}}_\mathbf{p}^\mathbf{c} = \begin{bmatrix} X_m^{*i}[-k_p] & X_m^i[k_p] \\ X_m^{*i+1}[-k_p] & X_m^{i+1}[k_p] \end{bmatrix}$ and

$\mathrm{Y_p^c} = \begin{bmatrix} Y_m^{*i}[-k_p] \\ Y_m^{*i+1}[-k_p] \end{bmatrix}$. Similarly, $\hat{\boldsymbol{\lambda}}_\mathbf{p}^\mathbf{c}$ is the estimated value of $\boldsymbol{\lambda}_\mathbf{p}^\mathbf{c}$ including error.

From equations (4.23) and (4.24), we obtain the I/Q imbalance and channel parameters for the pilot tones located at the specified subcarrier locations. Through linear interpolation shown in section 4.3.5, we could also calculate the parameter values at each of the subcarrier index k. Now, by dividing $V_m^*[-k]H_m[k]$ by $U_m[k]H_m[k]$; and $V_m[k]H_m^*[-k]$ by $U_m^*[-k]H_m^*[-k]$ and after substituting the values from (4.3) and (4.4), we obtain:

$$\frac{V_m^*[-k]}{U_m[k]} = \frac{gA_{I,m}^*[-k] - e^{-j\varphi}A_{Q,m}^*[-k]}{gA_{I,m}[k] + e^{-j\varphi}A_{Q,m}[k]} \tag{4.25}$$

and

$$\frac{V_m[k]}{U_m^*[-k]} = \frac{gA_{I,m}[k] - e^{j\varphi}A_{Q,m}[k]}{gA_{I,m}^*[-k] + e^{j\varphi}A_{Q,m}^*[-k]} \tag{4.26}$$

where, $A_{I,m}[k]$ and $A_{Q,m}[k]$ represent $A_I[k]$ and $A_Q[k]$ for the m^{th} frame. When $a_I[n]$ and $a_Q[n]$ are real, $A_{I,m}[k] = A^*_{I,m}[-k]$, and $A_{Q,m}[k] = A^*_{Q,m}[-k]$. Using these relationships, equations (4.25) and (4.26) become

$$\frac{V^*_m[-k]}{U_m[k]} = \frac{gA_{I,m}[k] - e^{-j\varphi}A_{Q,m}[k]}{gA_{I,m}[k] + e^{-j\varphi}A_{Q,m}[k]} \tag{4.27}$$

and

$$\frac{V_m[k]}{U^*_m[-k]} = \frac{gA_{I,m}[k] - e^{j\varphi}A_{Q,m}[k]}{gA_{I,m}[k] + e^{j}A_{Q,m}[k]} \tag{4.28}$$

After some algebraic manipulation, the estimated phase is obtained as follows;

$$\hat{\varphi}_e[k] = \frac{1}{2}\angle \frac{\left(1 + \frac{V^*_m[-k]}{U_m[k]}\right)\left(1 - \frac{V_m[k]}{U^*_m[-k]}\right)}{\left(1 - \frac{V^*_m[-k]}{U_m[k]}\right)\left(1 + \frac{V_m[k]}{U^*_m[-k]}\right)} \tag{4.29}$$

In addition, the estimated gain is,

$$g\frac{A_{I,m}[k]}{A_{Q,m}[k]} = e^{j\hat{\varphi}}\frac{\left(1 + \frac{V_m[k]}{U^*_m[-k]}\right)}{\left(1 - \frac{V_m[k]}{U^*_m[-k]}\right)} \tag{4.30}$$

Let,

$$\hat{g}_e[k] = g\frac{A_{I,m}[k]}{A_{Q,m}[k]} \tag{4.31}$$

The values of $\hat{g}_e[k]$ and $\hat{\varphi}_e[k]$ are averaged for all the subcarriers k to obtain a single value for gain $\acute{g}_m$ and phase $\acute{\phi}_m$ for the m^{th} OFDM frame, such that

$$\acute{g}_m = \frac{1}{N}\sum_{k=1}^{N}\hat{g}_e[k] \tag{4.32}$$

and

$$\acute{\phi}_m = \frac{1}{N}\sum_{k=1}^{N} \hat{\varphi}_e[k] \tag{4.33}$$

The newly adopted gain $\acute{g}_m$ and phase $\acute{\phi}_m$ value is then averaged with the nominal gain $\hat{g}_{m-1}$ and phase $\hat{\varphi}_{m-1}$ estimated in the previous frame i.e. $(m-1)^{th}$ frame to obtain more steady estimates and avoid drastic changes. Finally, the nominal gain $\hat{g}_m$ and phase $\hat{\varphi}_m$ are obtained as follows;

$$\hat{g}_m = \frac{\acute{g}_m + \hat{g}_{m-1}}{2} \tag{4.34}$$

$$\hat{\varphi}_m = \frac{\acute{\phi}_m + \hat{\varphi}_{m-1}}{2} \tag{4.35}$$

Finally, $\hat{g}_m$ and $\hat{\varphi}_m$ are used to correct upcoming $(m+1)^{th}$ frames.

4.3.5 Interpolation for I/Q and channel parameters

The channel and I/Q parameters for the pilot tones located at the specified subcarrier positions can be estimated using equations (4.23) and (4.24). They can be used to obtain the values at non-pilot indices through a form of linear interpolation. The linear interpolation method has been adopted from the work of [1]. If the estimates of the imbalance coefficients are available at frequency indices k_{p1} and k_{p2}, then the coefficient parameter at frequency index k, where $k_{p1} < k < k_{p2}$, can be obtained such that:

$$\begin{aligned}\breve{U}_m[k]H_m[k] = &\left(\frac{\breve{U}_m[k_{p2}]H_m[k_{p2}] - \breve{U}_m[k_{p1}]H_m[k_{p1}]}{k_{p2}-k_{p1}}\right)k \\ &+ \left(\frac{\breve{U}_m[k_{p2}]H_m[k_{p2}]k_{p2} - \breve{U}_m[k_{p1}]H_m[k_{p1}]k_{p1}}{k_{p2}-k_{p1}}\right)\end{aligned} \tag{4.36}$$

Similarly, we obtain;

$$\check{V}_m[k]H_m^*[-k]$$
$$= \left(\frac{\check{V}_m[k_{p2}]H_m^*[-k_{p2}] - \check{V}_m[k_{p1}]H_m^*[-k_{p1}]}{k_{p2} - k_{p1}}\right)k \tag{4.37}$$
$$+ \left(\frac{\check{V}_m[k_{p2}]H_m^*[-k_{p2}]k_{p2} - \check{V}_m[k_{p1}]H_m^*[-k_{p1}]k_{p1}}{k_{p2} - k_{p1}}\right)$$

The other two parameters (i.e. $\check{U}_m^*[-k_p]H_m^*[-k_p]$ and $\check{V}_m^*[-k_p]H_m[k_p]$) are obtained with the assistance of the above equations. The interpolation highly depends on the estimation of the parameters in the pilot tones. It also depends on the number of the pilot tones used. In the case where the pilot tones are detected incorrectly, this leads to incorrect interpolation increasing incorrect estimation and distortion. So the detection of pilot tones is very important in any estimation technique.

4.3.6 Correction and compensation for the data period

The gain and phase values obtained in equations (4.34) and (4.35) are stored and used to correct and compensate for the effects of I/Q imbalance and channel on all the data symbols within the said OFDM frame. For example, the d^{th} data symbol of the m^{th} frame first undergoes a time domain I/Q balance correction. Let $c_m^d[n]$ and $y_m^d[n]$ refers to the corrected signal and the received signal, respectively, for the d^{th} data symbol. The corrected signal can be expressed as follows;

$$\begin{bmatrix} Re\{c_m^d[n]\} \\ Im\{c_m^d[n]\} \end{bmatrix} = \begin{bmatrix} g_{m-1} & 0 \\ -sin\varphi_{m-1} & cos\varphi_{m-1} \end{bmatrix}^{-1} \begin{bmatrix} Re\{y_m^d[n]\} \\ Im\{y_m^d[n]\} \end{bmatrix} \tag{4.38}$$

Note that the data symbols of the m^{th} frame are also corrected by the gain and phase estimated during the $(m-1)^{th}$ frame. After that the corrected signal goes through FFT and the frequency domain signal $C_m^d[k]$ is obtained. Finally the compensated output for the d^{th} data symbol $\hat{X}_m^d[k]$ is obtained as follows;

$$\begin{bmatrix} \hat{X}_m^d[k] \\ \hat{X}_m^{*d}[-k] \end{bmatrix} = \begin{bmatrix} \breve{U}_m[k]H_m[k] & \breve{V}_m[k]H_m^*[-k] \\ \breve{V}_m^*[-k]H_m[k] & \breve{U}_m^*[-k]H_m^*[-k] \end{bmatrix}^{-1} \begin{bmatrix} C_m^d[k] \\ C_m^{*d}[-k] \end{bmatrix} \quad (4.39)$$

4.4 Evaluation of the proposed ACCC scheme

4.4.1 Simulation platform used for the evaluation of the proposed scheme

In this section the performance of the proposed scheme has been investigated through MATLAB simulation. The simulation parameters are shown in Table 4-1.

Table 4-1 Simulation Parameters

Parameters	Value
Number of Frames	40
Number of OFDM symbols in each frame	50
Number of pilot subcarriers in each symbol	16
Pilot spacing d_p	64
FFT Size	1024
Number of Symbols containing pilot tones, in each frame	2
CP size	40
Channel Type	LTE (ETU)
Number of paths	9

An OFDM system is simulated with QPSK, 16-QAM and 64-QAM modulation. For the pilot tones, only two states in the whole constellation plane have been adopted. These two states are, $\frac{7\pm7j}{\sqrt{42}}$ for 64-QAM, $\frac{3\pm3j}{\sqrt{10}}$ for 16-QAM and $\frac{1\pm1j}{\sqrt{2}}$ for QPSK, respectively. These values correspond to the constellation points associated with the highest power. As such, their estimations are less affected by the presence of noise. A wide range of frequency-flat gain and phase variation has been considered for the simulation. Also two different models, referred as Model 1 and Model 2 in section 4.2.2, has been considered to observe the proposed scheme under frequency-selective I/Q condition. An Additive white Gaussian Noise varying between 10dB to 35 dB has been adopted to show the Symbol Error Rate (SER) performances. The 9 path LTE channel for urban area has been chosen. The attenuation and delay of the multipath channel has been given in the Table 4-2.

Table 4-2 A 9 path Extended Typical Urban (ETU) LTE channel

Propagation path	Relative delay (us)	Average Power (dB)
1	0	-1
2	0.050	-1
3	0.120	-1
4	0.200	0
5	0.230	0
6	0.500	0
7	1.600	-3
8	2.300	-5
9	5.000	-7

The channel has been assumed to not vary for two consecutive OFDM symbols.

4.4.2 Pilot detection

The presence of I/Q imbalance and multipath propagation, if they remain uncorrected or uncompensated, will lead to erroneous detection of the reference pilots. However, it depends on the severity of the I/Q imbalance. Figure 4-5 (a) to (c) represent the constellations of the pilot tones for the first, second and third frames, respectively, for Model 1. Likewise, Figure 4-6(a) to (c) show the constellations for the pilot tones for the first, second and third frame respectively, for Model 2. The gain and phase values have been considered 20% and 10^{o}, correspondingly.

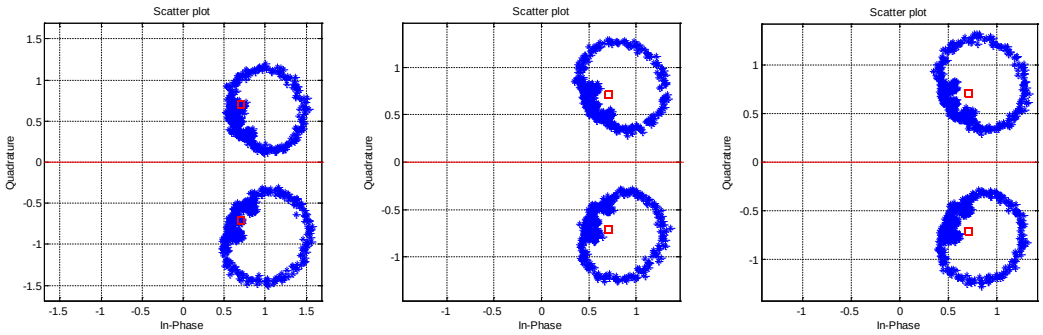

Figure 4-5 Signal constellations for the pilot tones for Model 1 for a) first frame b) second frame and c) third frame, for 30 dB SNR

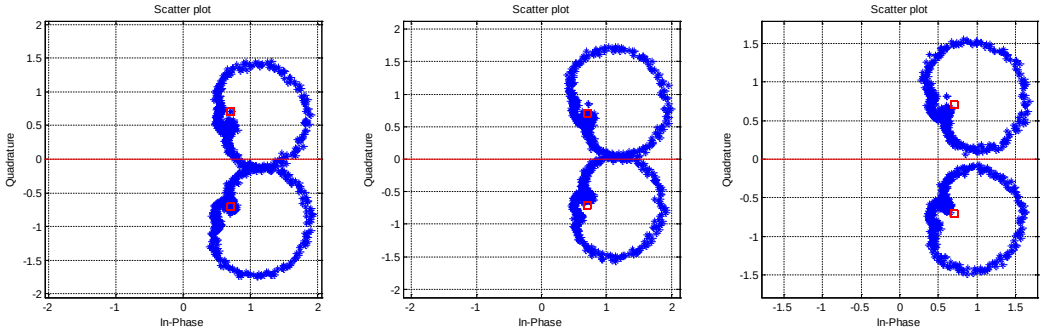

Figure 4-6 Signal constellations for the pilot tones for Model 2 for a) first frame b) second frame and c) third frame, for 30 dB SNR

The SNR for these figures are 30 dB. Since Figures 4-5 and 4-6 represent the constellations of pilot tones for 64-QAM, values, $\frac{7\pm7j}{\sqrt{42}}$, are used in a consecutive manner. These values correspond to the constellation points associated with the highest power. As such, their estimations are less affected by the presence of noise. It has been observed that for Model 1, shown in Figure 4-5, there are no overlapping pilot tones, as the frequency-selective I/Q imbalance is not severe. The pilot tones can be easily detected for this case. Therefore, this sort of I/Q imbalance does not lead to an incorrect detection of pilots. For the second and third frames, the constellation points are even further apart from each other as the correction process has been started from the beginning of the second frame. On the other hand, Model 2 shows a complete different scenario. There are several overlapping constellation points present in Figure 4-6(a) and Figure 4-6(b). For the proposed adaptive scheme, correction for I/Q imbalance begins at the second frame. It has been observed from Figure 4-6(b) that, after just one correction the constellation points tend to have much less overlapping points. The third frame shows no overlapping at all. Thus it proves that the proposed method helps the system to overcome incorrect pilot detection. In the above example, all 1024 subcarriers have been used as pilots for a better demonstration of the overlapping effect of the constellation points. However, in the rest of the simulations, only 16 pilots have been used for correction and compensation. Also, the reason for choosing a high value of SNR of 30 dB is, to show the impact of the other two distortion parameters (I/Q imbalance and channel) on the received pilot tones. Moreover, Figure 4-6 shows that even when the additive noise is very low (as SNR for AWGN is 30 dB), there is a lot of overlapping of constellation points, which will definitely lead to incorrect detection.

The next figures, Figure 4-7 and Figure 4-8 show the constellation for the same pilot tones with an SNR of 20 dB, for Model 1 and Model 2, respectively. Figure 4-7(a) to (c) represent the signal constellations obtained for the first, second and third frame respectively, for Model 1. Similarly, Figure 4-8 (a) to (c) represent the constellation of the pilot tones for the first, second and third frames, respectively for Model 2. The number of overlapping constellation points is much higher as the noise has been increased. It has been observed from Figure 4-7(a), that even when the noise is high,

the constellation points do not overlap. For Figure 4-7(b) and 4.7 (c), it has been observed that the pilot tones have become further apart from each other. This happened due to the I/Q correction. On the other hand, constellation for Model 2 shows a different outcome.

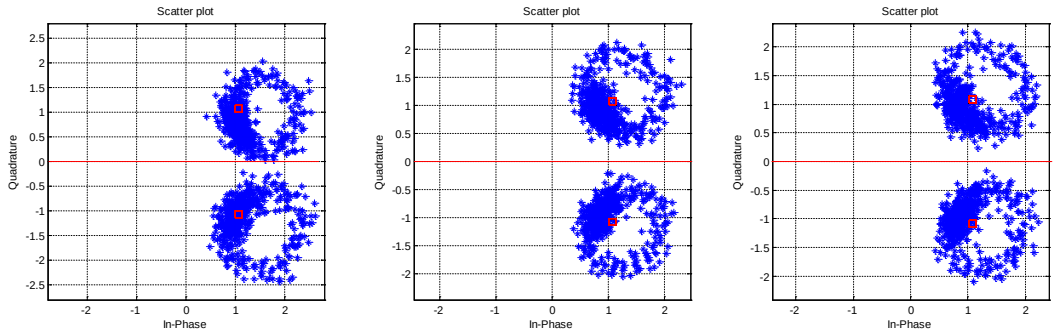

Figure 4-7 Signal constellations for the pilot tones for Model 1 for a) first frame b) second frame and c) third frame, for 20 dB SNR

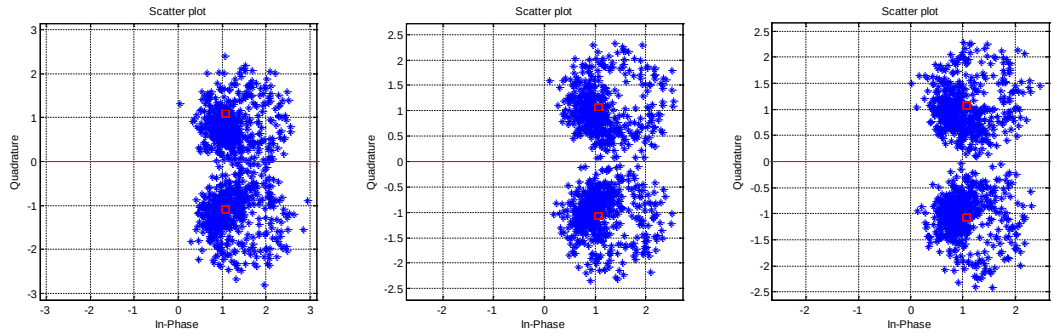

Figure 4-8 Signal constellations for the pilot tones for Model 2 for a) first frame b) second frame and c) third frame, for 20 dB SNR

As we can see from Figure 4-8 (a), there are many overlapping points. But the overlapping has decreased for Figures 4-8(b) and 4-8 (c) (corresponding to second and third frame). Another way of viewing the improvement, resulting from the correction of I/Q imbalance is to compare the number of pilots detected incorrectly in consecutive frames. Table 4-3 tabulates the percentage of pilots detected in error in the first, third, and tenth OFDM frames for several combinations of gain and phase deviations, for Model 1. These simulations have been carried out based on two values of AWGN. For

Model 1, as the variation of I/Q imbalance is not very high, the percentage of incorrectly detected pilots is almost zero (see Table 4-3).

Table 4-3 Percentage of pilots detected in error for Model 1

g	φ	Percentage (%) of pilots detected in error					
		SNR 20 dB			SNR 30 dB		
		First frame	Third frame	Tenth frame	First frame	Third frame	Tenth frame
1.02	2	0	0	0	0	0	0
1.1	2	0	0	0	0	0	0
1.1	5	0	0	0	0	0	0
1.2	5	0	0	0	0	0	0
1.2	10	0.49	0	0	0	0	0

For $g = 1.2$, and $\varphi = 10^{o}$, 0.49% of pilots have been detected erroneously, for 20 dB SNR. For the rest of the gain and phase combinations, the percentage of incorrectly detected pilots is zero. Likewise, Table 4-4 tabulates the percentage of erroneously detected pilots for Model 2.

Table 4-4 Percentage of pilots detected in error for Model 2

g	φ	Percentage (%) of pilots detected in error					
		SNR 20 dB			SNR 30 dB		
		First frame	Third frame	Tenth frame	First frame	Third frame	Tenth frame
1.02	2	1.07	0.98	0.49	0	0	0
1.1	2	2.25	0.97	0.68	0	0	0
1.1	5	3.52	0.87	1.07	0.10	0	0
1.2	5	5.47	1.17	0.98	4.69	0	0
1.2	10	8.98	1.19	0.39	8.0078	0	0

As expected, for this case, a larger percentage of pilots have been detected in error. However, the detection of pilots becomes significantly better from the beginning of the third frame. For example, with $g = 1.2$ and $\varphi = 10^{o}$, the percentage of wrongly detected pilots at an SNR of 20 dB, reduces from 8.98 % to 1.19 %, from the first to third OFDM frames. After the third frame, the percentage remains fairly steady. As we can see, with $g = 1.2$ and $\varphi = 5^{o}$, the percentage for third and tenth frames are 1.17% and 0.98%, respectively, for SNR 20 dB. For a higher SNR such as SNR 30 dB, this percentage becomes zero for third and tenth frames. It has been also observed that, due to low SNR, the number of incorrectly detected pilots become saturated, which means there will be a certain number of residue erroneous pilots. However, even with the presence of these erroneous pilots, the system still achieves a good SER which has been shown later in this chapter.

4.4.3 Estimated I/Q and channel parameters for different constant gain and phase

The I/Q and channel parameters such as $U_m[k]H_m[k]$, $V_m[k]H_m^*[-k]$, $V_m^*[-k]H_m[k]$ and $U_m^*[-k]H_m^*[-k]$, have been estimated according to equations (4.23) and (4.24). In this section, simulations have been performed to compare these estimated I/Q imbalance and channel parameters with their ideal values for different constant gain and phase combinations. The estimated values have been shown for Model 2 only. This is because, for Model 1, the pilot detection is more or less accurate for various gain and phase combinations. Therefore, the effect of the incorrect pilots would be less remarkable for Model 1. On the other hand, a significant percentage of erroneous pilots have been observed, in the case of Model 2. So the effect of these erroneous pilots on the parameter estimation can be observed using this model.

For the m^{th} frame, frequency-selective I/Q parameters can be expressed by according to equations (4.3) and (4.4) as follows;

$$U_m[k] = \frac{gA_{I,m}[k] + e^{-j\varphi}A_{Q,m}[k]}{2} \quad (4.40)$$

and

$$V_m[k] = \frac{gA_{I,m}[k] - e^{j\varphi}A_{Q,m}[k]}{2} \quad (4.41)$$

The joint effect of I/Q and channel parameter can be expressed as follows;

$$U_m[k]H_m[k] = \frac{gA_{I,m}[k]H[k] + e^{-j\varphi}A_{Q,m}[k]H[k]}{2} \quad (4.42)$$

$$V_m[k]H_m^*[-k] = \frac{gA_{I,m}[k]H^*[-k] - e^{j\varphi}A_{Q,m}[k]H^*[-k]}{2} \quad (4.43)$$

$$V_m^*[-k]H_m[k] = \frac{gA_{I,m}^*[-k]H_m[k] - e^{-j\varphi}A_{Q,m}^*[-k]H_m[k]}{2} \quad (4.44)$$

$$U_m^*[-k]H_m^*[-k] = \frac{gA_{I,m}^*[-k]H_m^*[-k] + e^{j\varphi}A_{Q,m}^*[-k]H_m^*[-k]}{2} \quad (4.45)$$

For the first frame, there are a good number of incorrectly detected pilots which leads some erroneous estimation. Table 4-5 holds the values of the estimated I/Q and channel parameters for the first frame; for different constant gain and phase combinations at an SNR of 30 dB. The term 'Est' refers the estimated values.

Table 4-5 Estimated parameters for different gain and phase combination for the first frame

g	φ	$U_m[k]H_m[k]$		$V_m[k]H_m^*[-k]$		$V_m^*[-k]H_m[k]$		$U_m^*[-k]H_m^*[-k]$	
		Ideal	Est	Ideal	Est	Ideal	Est	Ideal	Est
1.02	2.0	1.06-0.64i	1.07-0.63i	0.04-0.23i	0.05-0.23i	0.05-0.19i	.06-0.19i	1.07-0.60i	1.09-0.63i
1.1	2	1.10-0.67i	1.11-0.68i	0.08-0.26i	0.09-0.26i	0.09-0.23i	0.10-0.24i	1.11-0.64i	1.11-0.65i
1.1	5	1.09-0.70i	1.81+0.38i	0.07-0.29i	-0.98+0.41i	0.11-0.20i	0.29-0.08i	1.12-0.61i	1.06-0.45i
1.2	5	1.14-0.74i	1.91+0.39i	0.13-0.33i	-1.04+0.42i	0.16-0.24i	0.41-0.06i	1.17-0.65i	0.99-0.41i
1.2	10	1.12-0.78i	1.95+0.29i	0.11-0.37i	-1.00+0.46i	.18-0.20i	0.41+0.00i	1.18-0.60i	0.98-0.40i

The estimated values are different for each tone. However, here values for one tone have been tabulated just to show the effectiveness of the proposed scheme. The value of k in Table 4-5 has been chosen as 110. For this, when the gain and phase combination is quite severe, such as when $g = 1.1$ and $\varphi = 5^{o}$ or $g = 1.2$ and $\varphi = 10^{o}$, the estimated and the ideal parameters show a lot of differences. Whereas, when the I/Q gain and phase combination is small, such as when $g = 1.02$ and $\varphi = 2^{o}$, the difference between the ideal and the estimated parameter becomes low, or we can say the estimated values become close to the ideal values. The next table, Table 4-6 shows the values for the third frame when the nominal gain and phase has been estimated and the pilot detection has been performed.

Table 4-6 Estimated parameters for different gain and phase combination for the third frame

g	φ	$U_m[k]H_m[k]$		$V_m[k]H_m^*[-k]$		$V_m^*[-k]H_m[k]$		$U_m^*[-k]H_m^*[-k]$	
0	0	Ideal	Est	Ideal	Est	Ideal	Est	Ideal	Est
1.02	2.0	1.05-0.67i	1.05-0.66i	0.03-0.26i	0.05-0.25i	0.07-0.17i	0.07-0.16i	1.08-0.58i	1.09-0.58i
1.1	2	1.11-0.68i	1.09-0.69i	0.08-0.26i	0.07-0.25i	0.09-0.23i	0.09-0.23i	1.1 - 0.64i	1.09 - 0.62i
1.1	5	1.09 - 0.70i	1.091 - 0.68i	0.07 - 0.29i	0.07 - 0.29i	0.11 - 0.20i	0.12 - 0.19i	1.12 - 0.62i	1.14 - 0.62i
1.2	5	1.15 - 0.74i	1.12 - 0.72i	0.13 - 0.33i	0.15 - 0.33i	0.16 - 0.24i	0.17 -0.22i	1.17 - 0.65i	1.2 - 0.64i
1.2	10	1.12 - 0.78i	1.10 - 0.77i	0.11-0.37i	0.09 - 0.35i	0.19 - 0.20i	0.17 - 0.21i	1.19 - 0.61i	1.20 - 0.59i

This illustrates that, as some corrections have been done for this case, even when the gain and phase values are high, the estimated parameters are quite similar to the ideal parameters.

4.4.4 Estimated I/Q and channel parameters for different variable I/Q models

In this section, the estimated and ideal values for I/Q and channel parameters have been shown for both of the models. In the previous section, values corresponding to one tone have been presented in Table 4-5 and Table 4-6. Now, the effect of the incorrect pilot tones on the estimated values has been further illustrated by plotting them for the whole frequency spectrum.

Figure 4-9 shows the estimated and ideal values for Model 1 for $g = 1.2$ and $\varphi = 10^{o}$ for the first frame, for an SNR of 30 dB. Figure 4-10 shows the same results for the third frame. For both frames, the ideal and the estimated value do not show a lot of differences. The reason is that, for Model 1, the frequency-selective I/Q variation is low.

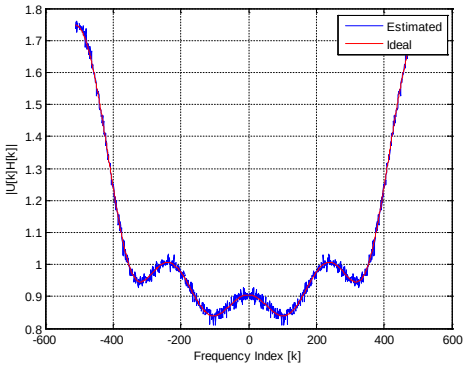

a)

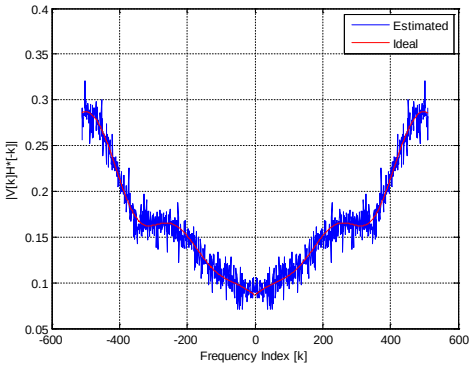

b)

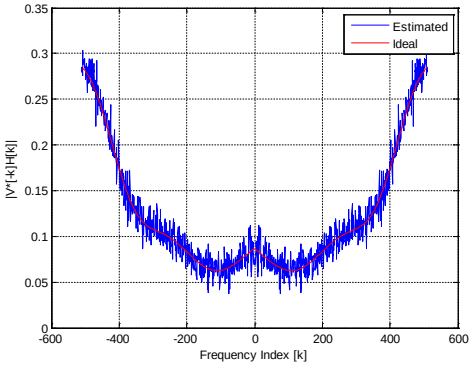

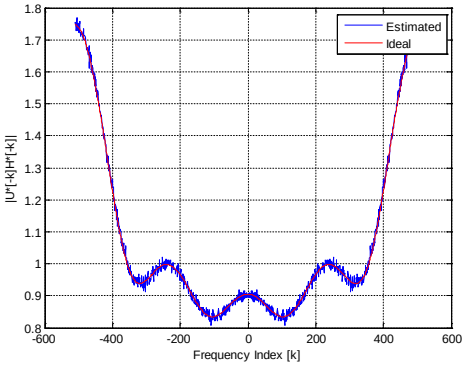

c) d)

Figure 4-9 Estimated I/Q and channel parameters for Model 1 for first frame

Similarly, in Figure 4-11, the estimated and ideal values corresponding to Model 2, for $g = 1.2$ and $\varphi = 10^{o}$ have been shown, for the first frame. Figure 4-12 shows the same parameters for the third frame after some corrections have been performed. Unlike the Model 1, this time Model 2 shows different result for first and third frames.

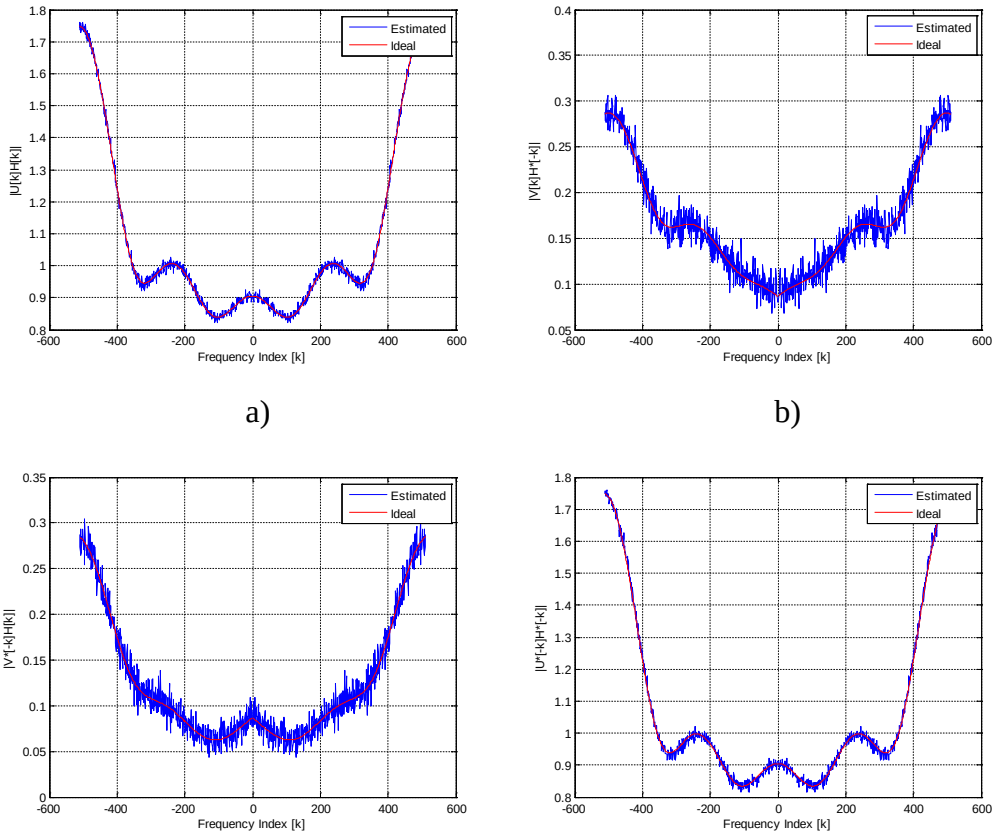

a) b)

c) d)

Figure 4-10 Estimated I/Q and channel parameters for Model 1 for third frame

From Figure 4-11, it has been observed that estimated values for some of the subcarrier indices are quite different from its ideal values. In Figure 4-11, for subcarrier indexes $k = 350$ to $k = 450$ and $k = -350$ to $k = -450$, the estimated values have been changed drastically. This occurs due to the incorrect pilot detection. The incorrect pilots lead to the incorrect estimation and interpolation which is responsible for this

distortion. As for the first frame, there has been no correction performed, the number of incorrectly detected pilot is quite high. However, the situation is expected to change for the consecutive frames after correction has been performed.

Figure 4-12 shows the estimated I/Q and channel parameters for the third frame, corresponding to Model 2. For Figure 4-12, the estimated and ideal values are close to each other and show very fewer differences: Because the system now uses a feedback correction process so that the next available frame can be corrected before the pilot extraction.

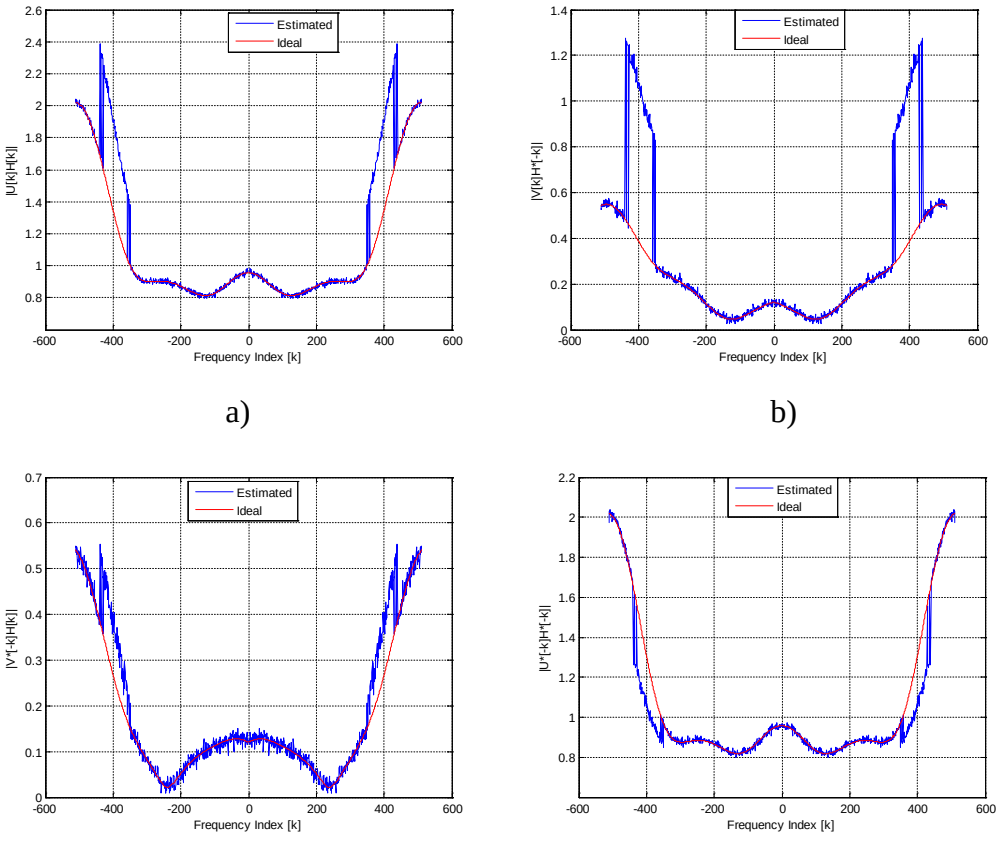

Figure 4-11 Estimated I/Q and channel parameters for Model 2 for first frame

The extracted pilots get more and more accurate in each consecutive frame. Thus the estimation values also get better for each consecutive frame. In addition, for Figure 4-12, no drastic differences between the estimated and ideal values have been observed.

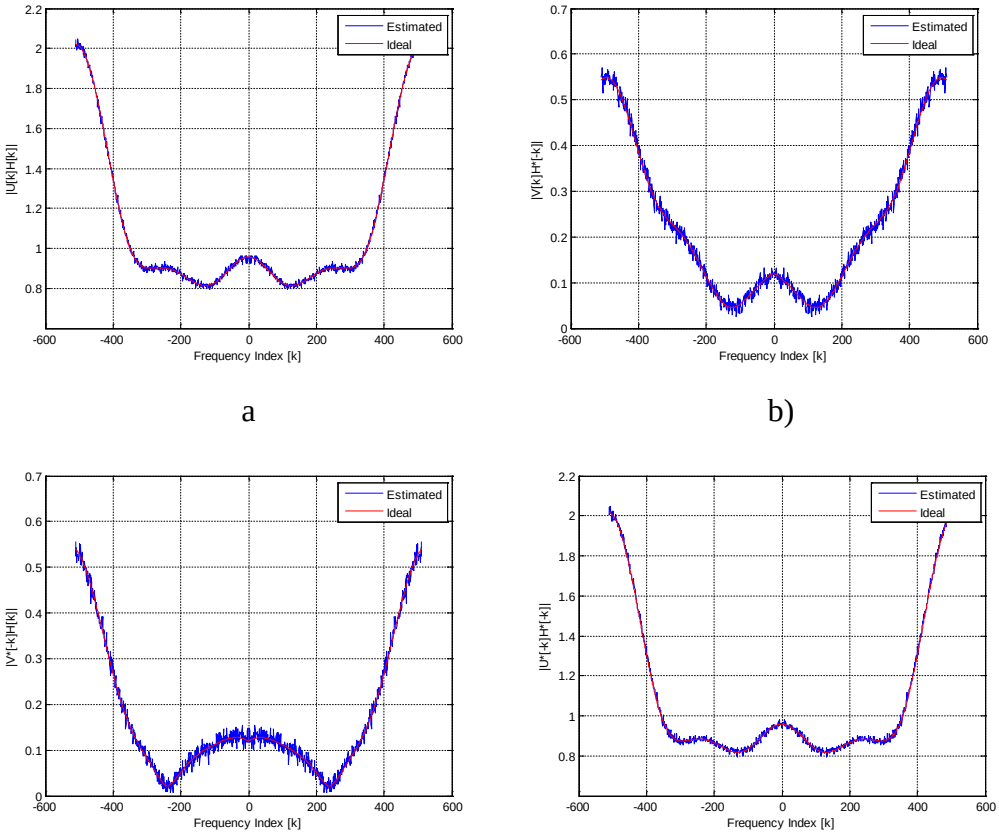

Figure 4-12 Estimated I/Q and channel parameters for Model 2 for third frame

4.4.5 Estimated nominal gain and phase

Figures 4-13(a) and (b) show the estimated nominal values of gain and phase imbalance, respectively, for Model 1. Similarly, Figures 4-14(a) and (b) show the estimated nominal values of gain and phase imbalance, respectively, for Model 2. These have been obtained for up to 15 frames with an SNR of 20 dB and 30 dB for. For Model 1, the estimated value reaches close to its ideal value just after first frame.

For Model 2, the estimated results are a little different. In this case, it takes at least four frames before the estimated nominal gain and phase reaches close to its ideal value.

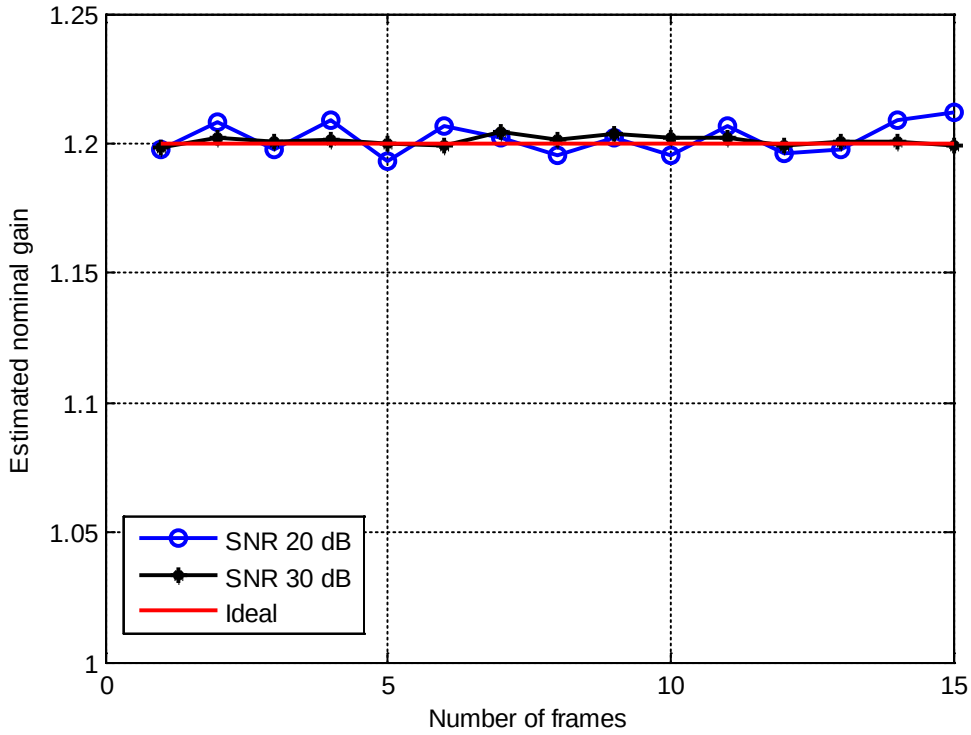

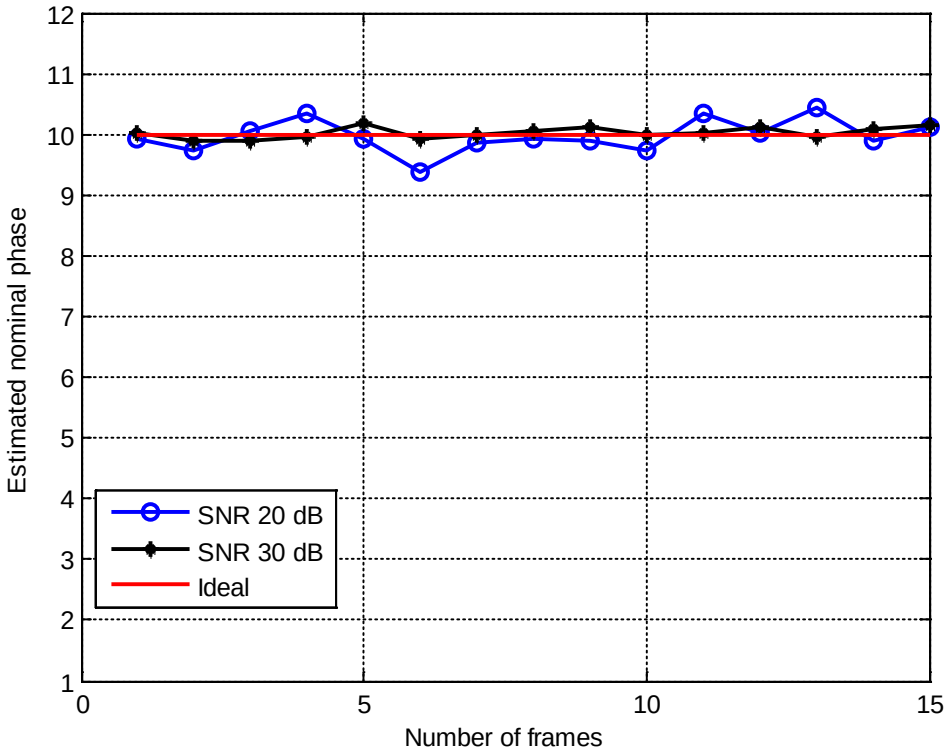

Figure 4-13 Estimated a) Nominal gain and b) Nominal phase for Model 1 for different number of frames

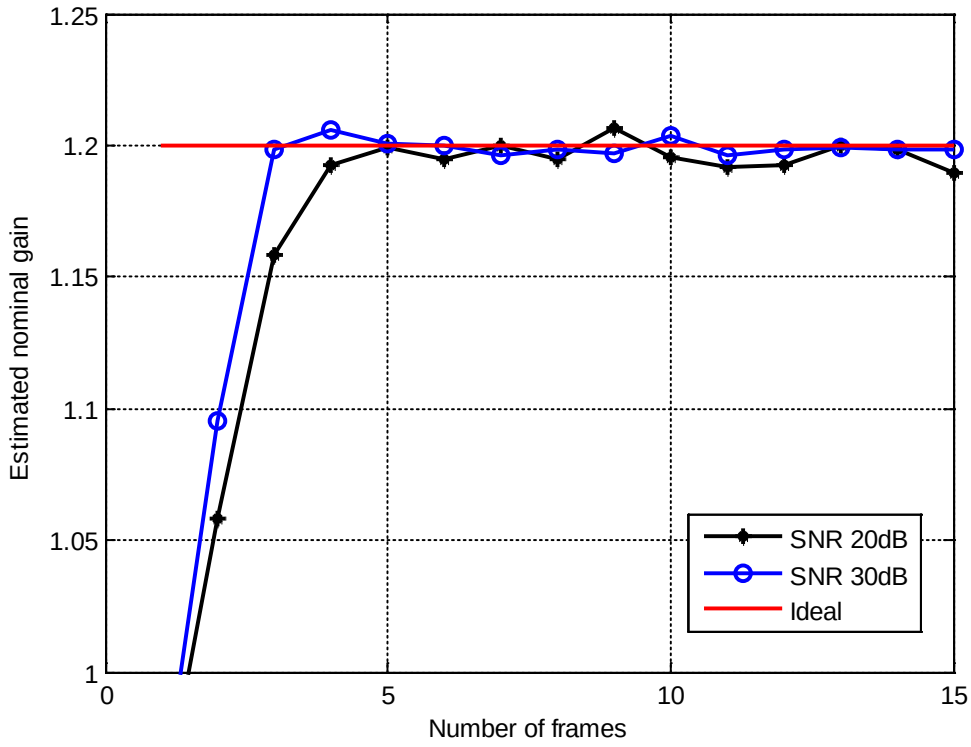

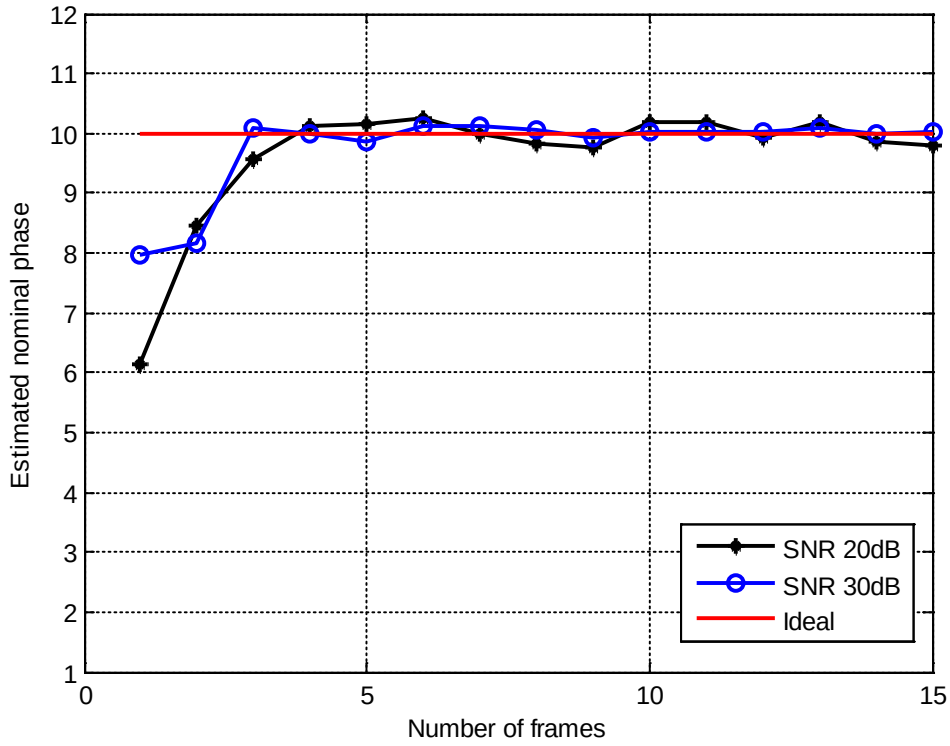

Figure 4-14 Estimated a) nominal gain and b) nominal phase for Model 2 for different number of frames

Again, if the frequency-flat gain and phase i.e. g and φ are less, then the estimated nominal gain and phase would require less frames to reach the expected values. For both cases, SNR 20 dB shows more degradation than SNR 30 dB, as expected. Table 4-7 shows the estimated nominal gain and phase for different values of constant I/Q imbalance, at an SNR of 20 dB. From the table, it can be clearly seen that for Model 1; the estimated gain and phase values approach the ideal value from the first frame. Even for a large value of I/Q imbalance, such as $g = 1.2$ and $\varphi = 10^{o}$, the estimated $\hat{g}$ and $\hat{\varphi}$ are 1.18 and 10.09^{o} , for the first frame. However, in the case of Model 2, for an I/Q imbalance with $g = 1.2$ and $\varphi = 10^{o}$, the estimated $\hat{g}$ and $\hat{\varphi}$ corresponding to the first frame are 0.98 and 6.31^{o} , which are far different from the ideal g and φ. After third frame the estimated $\hat{g}$ and $\hat{\varphi}$ becomes close to the ideal g and φ.

Table 4-7 Nominal gain and phase for different frequency-flat gain and phase

Ideal g	Ideal φ	Estimated g and φ for Model 1						Estimated g and φ for Model 2					
		First frame		Third frame		Tenth frame		First frame		Third frame		Tenth frame	
		g	φ	g	φ	g	φ	g	φ	g	φ	g	φ
1.02	2	1.02	2.04	1.03	1.92	1.02	2.02	1.03	1.90	1.01	2.25	1.02	1.90
1.1	2	1.10	1.85	1.10	1.65	1.10	2.15	1.07	1.78	1.09	1.84	1.10	2.16
1.1	5	1.10	5.57	1.10	5.11	1.10	5.05	1.03	4.08	1.08	4.74	1.10	5.37
1.2	5	1.19	5.30	1.21	5.12	1.20	5.02	1.05	1.86	1.17	5.00	1.19	4.94
1.2	10	1.18	10.09	1.22	10.20	1.20	10.22	0.98	6.31	1.19	9.36	1.20	9.69

4.4.6 Signal constellations

In this section, the signal constellations have been presented to show the outcome after the correction and compensation have been performed. The frequency-flat gain and phase have been chosen as $g = 1.2$ and $\varphi = 10^{o}$ for the signal constellations shown in Figures 4-15 to 4-20. The legend 'Ideal' refers to the signal constellations obtained without any I/Q imbalance, channel and AWGN. Likewise, the legend 'Received'

refers to the received signal constellations. Figure 4-15 (a) to (c) show the constellations of the data symbols in the OFDM data frames, for 64-QAM signals for Model 1. Figure 4-15 (a) shows the uncompensated data signal. Figure 4-15(b) and Figure 4-15(c) represent the data signal after having been corrected and compensated for I/Q imbalance and channel effects, corresponding to the first frame and third frame, respectively. Similarly, Figure 4-16 (a)-(c) show the constellations for 16-QAM, for Model 1. Figure 4-16(a) represent the uncompensated signal. In the same way, Figure 4-16(b) and Figure 4-16(c) represent the signal for first and third frame, respectively, after being corrected and compensated by the proposed ACCC scheme. Figure 4-17(a)-(c) represent the uncompensated signal, the corrected/compensated signal for the first frame, the corrected/compensated signal for the third frame, respectively for Model 1, for QPSK signal. The reason for showing 3 types of modulation scheme is to observe the I/Q imbalance and the proposed scheme's effect on different modulation scenario. It is evident that higher order modulation is much more sensitive to I/Q imbalance.

From Figures 4-15 to 4-17, it has been observed that the corrected and compensated signal's constellations for all the modulation schemes show significant improvement compared to the uncompensated signal's constellations. For Model 1, the constellations obtained for the first frame (Figure 4-15 (b), Figure 4-16 (b), and Figure 4-17 (b)) hardly show any difference compared to the constellations obtained for the third frame (Figure 4-15 (c), Figure 4-16 (c) and Figure 4-17 (c)).

The constellations for Model 2 have been presented in Figure 4-18 to Figure 4-20 for 64-QAM, 16-QAM and QPSK, respectively. Figure 4-18(a) to (c) show the signal constellations for the uncompensated signal, corrected/compensated signal for the first frame and corrected/compensated signal for the third frame, respectively, for the 64-QAM modulations. Similarly, Figure 4-19(a) to (c) represent constellations of uncompensated signal, corrected/compensated signal for the first frame and corrected/compensated for the third frame, respectively, for the 16-QAM modulations. Figure 4-20 (a) to (c) show the same constellations for the QPSK modulation.

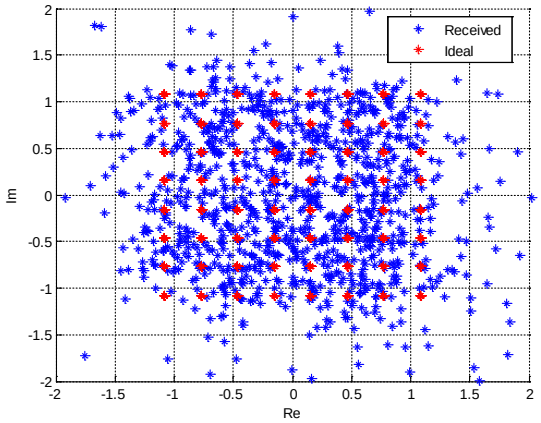

a)

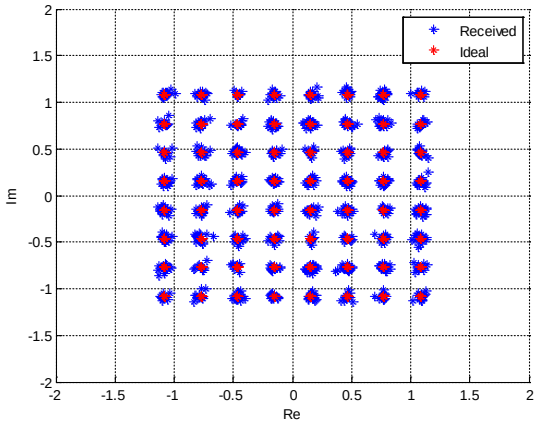

b)

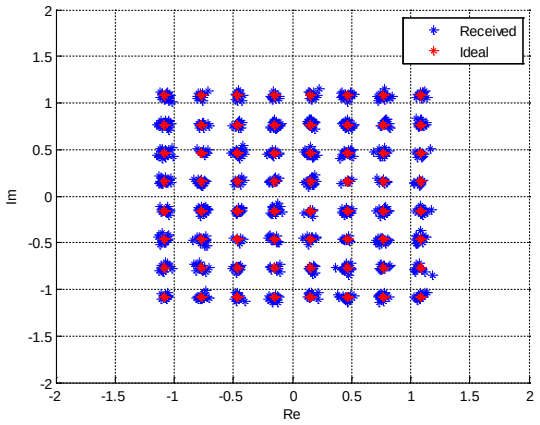

c)

Figure 4-15 Constellations for 64-QAM signal for Model 1 for a) uncompensated b) first frame and c) third frame

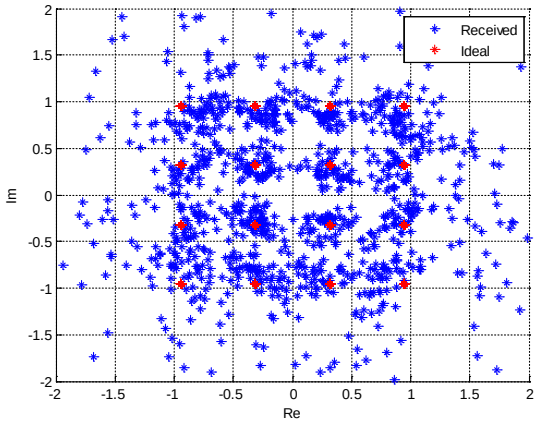

a)

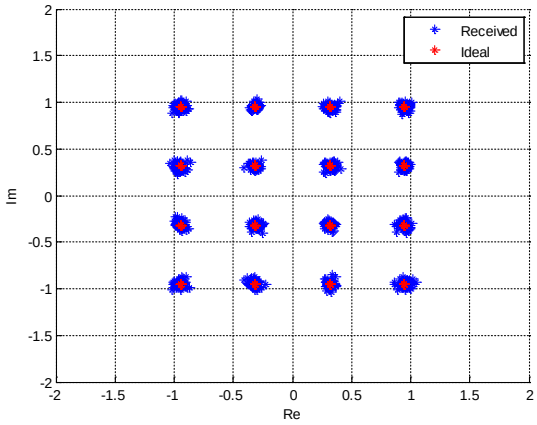

b)

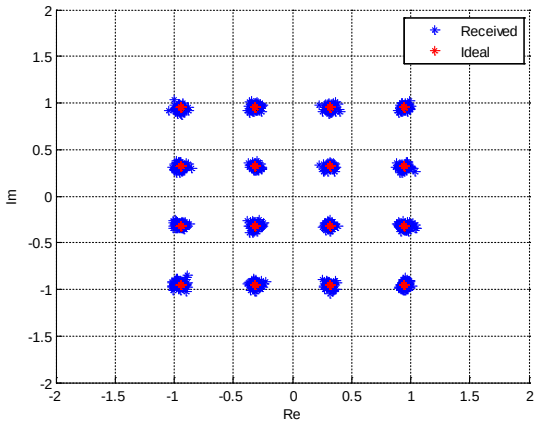

c)

Figure 4-16 Constellations for 16-QAM signal for Model 1 for a) uncompensated b) first frame and c) third frame

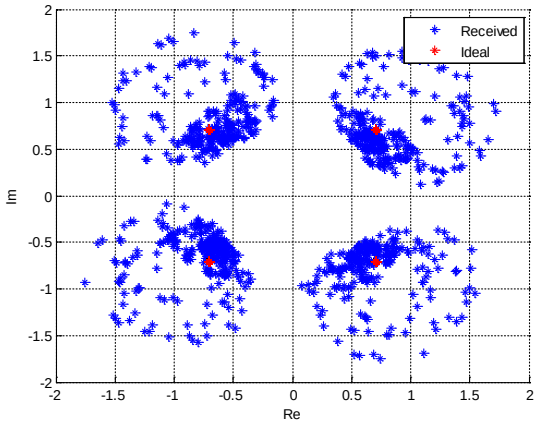

a)

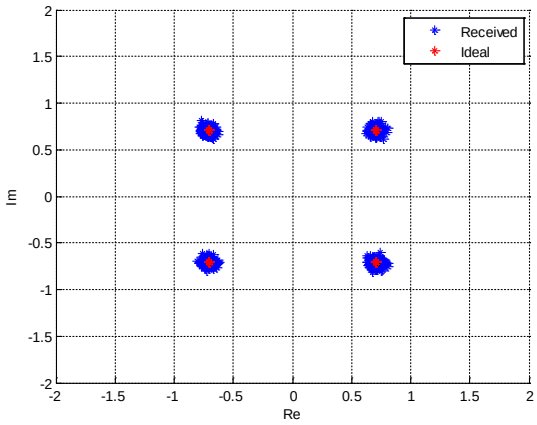

b)

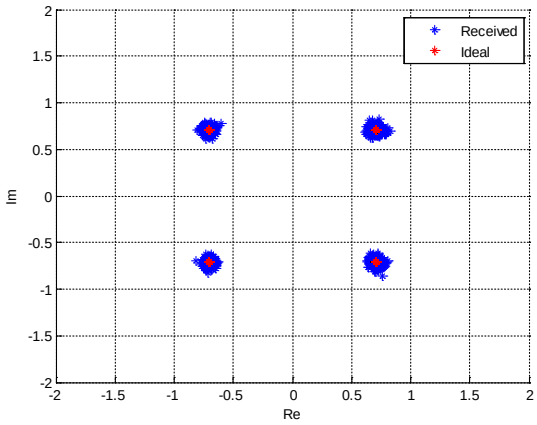

c)

Figure 4-17 Constellations for QPSK signal for Model 1 for a) uncompensated b) first frame and c) third frame

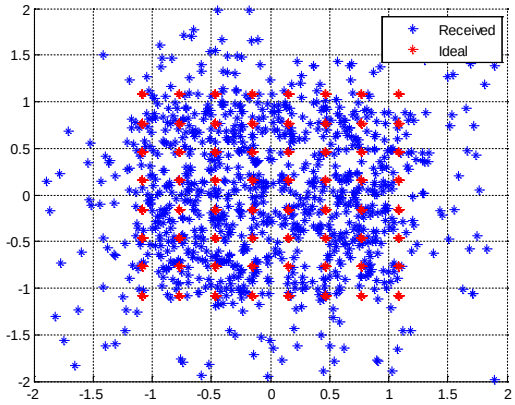

a)

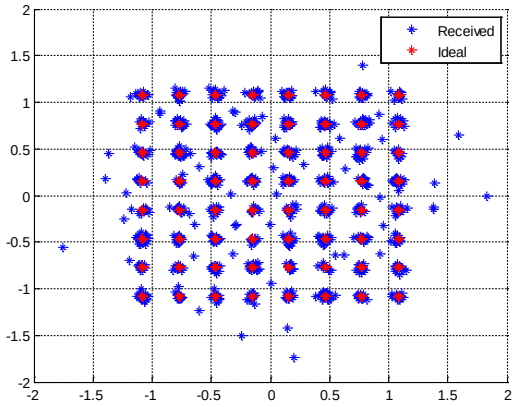

b)

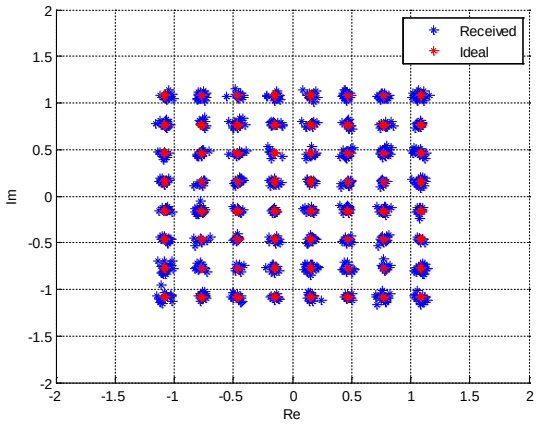

c)

Figure 4-18 Constellations for 64-QAM signal for Model 2 for a) uncompensated b) first frame and c) third frame

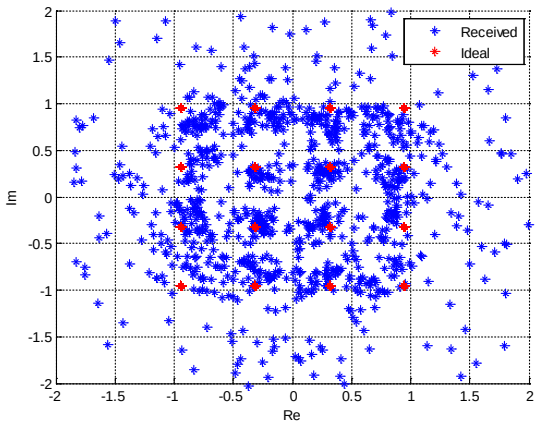

a)

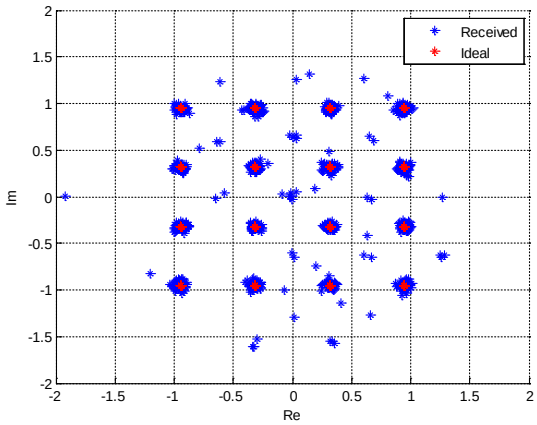

b)

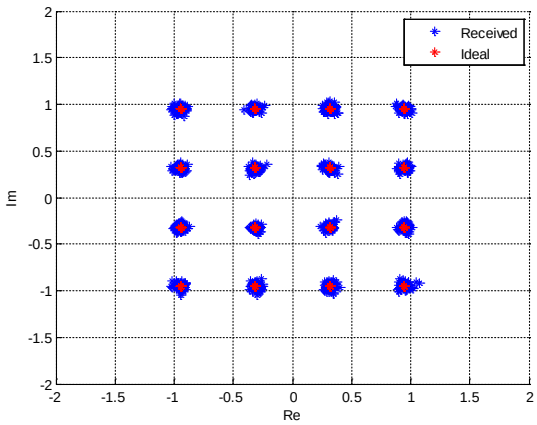

c)

Figure 4-19 Constellations for 16-QAM signal for Model 2 for a) uncompensated b) first frame and c) third frame

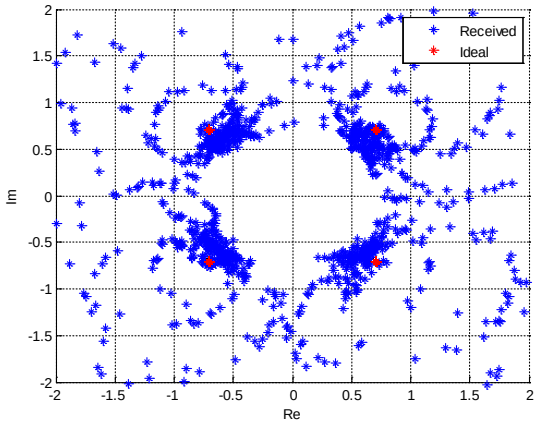

a)

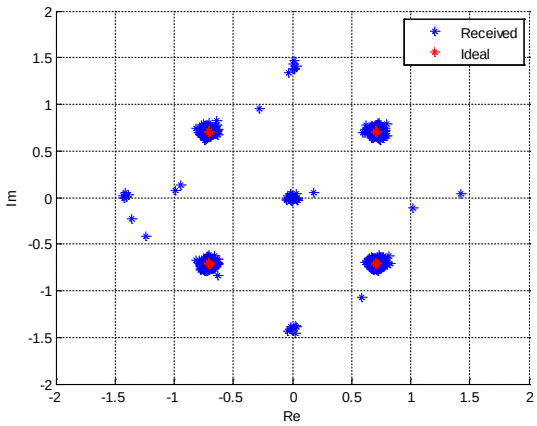

b)

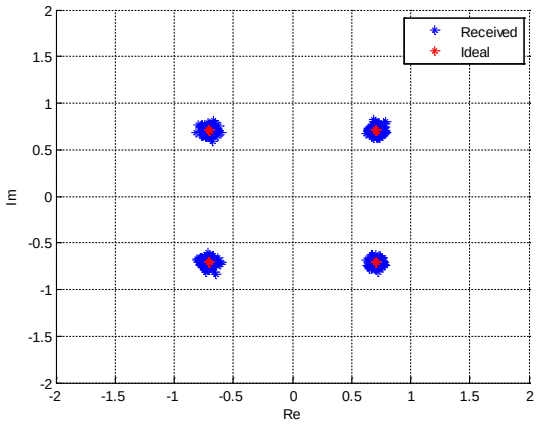

c)

Figure 4-20 Constellations for QPSK signal for Model 2 for a) uncompensated b) first frame and c) third frame

Constellations obtained for Model 2 are different than those of Model 1. For Model 2, for each modulation scenario (even lower order modulations like QPSK), the outputs obtained for the third frame (shown in Figure 4-18 (c), Figure 4-19 (c) and Figure 4-20 (c)) are significantly improved compared to those of the first frame (shown in Figure 4-18 (b), Figure 4-19 (b) and Figure 4-20 (b)). Also, it has been observed, that for Model 2, the constellations have some scattered points for the first frame, which have been reduced significantly for the third frame.

4.4.7 Error vector magnitude (EVM)

The effectiveness of the proposed adaptive correction/compensation method is further illustrated by the resulting values of error vector magnitude (EVM). The EVM is a quantitative measure used to specify the variance of the constellation cluster relative to the ideal constellation points. In this way, the effectiveness of a given scheme in correcting/compensating for the uncompensated received signal could be specified by a numerical value of EVM. Also it determines how close the estimated signal is to the original signal. The EVM corresponds to the ratio of the variance of the constellation cluster of $\hat{x}[n]$ to that of the constellation points of the ideal signal $x[n]$, as presented in the work of [75];

$$EVM = \left\{ \frac{\sum_{n=1}^{N_s} |x[n] - \hat{x}[n]|^2}{\sum_{n=1}^{N_s} |x[n]|^2} \right\} \tag{4.46}$$

here, N_s is the number of points used in the calculation of the EVM. The EVM values for Models 1 and 2 have been presented in Figure 4-21 and 4-22, respectively for 64-QAM.

The curves in Figure 4-21, labelled as ‘Frame 1’, ‘Frame 2’, ‘Frame 3’ and ‘Frame 10’, correspond to the EVM values obtained in the first, second, third and tenth frames, respectively, with the proposed ACCC scheme operating under different SNR. Furthermore, as a reference for performance comparison, the EVM values associated

with the condition of no I/Q imbalance and channel are plotted in curves labelled as 'Ideal'. Similarly, EVM values associated with the condition when no correction or compensation has been done is labelled as 'Uncompensated' in Figure 4-21.As expected, the EVM values for all the cases considered tend to decrease with increase in SNR.

It has been observed from Figure 4-21 that, the EVM values obtained in the first, second, third and tenth frames with the proposed adaptive scheme closely approach those of the 'Ideal' condition. As the frequency-selective I/Q is not very severe in case of Model 1, the output shows better result from the first frame. The second, third and the next consecutive frames show almost the same results after the correction and compensation has been performed.

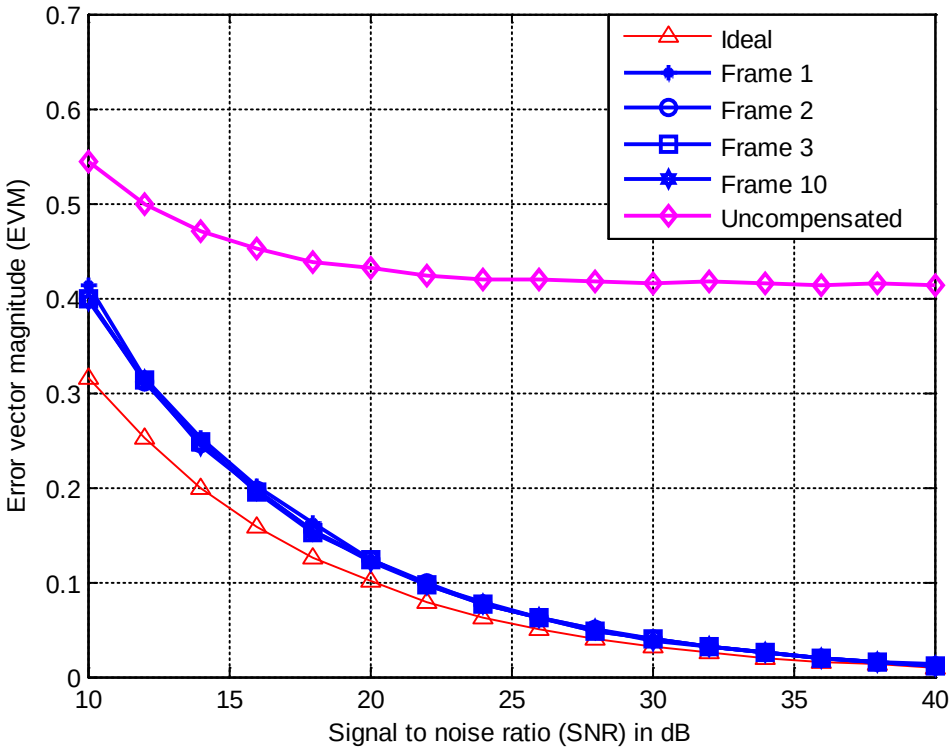

Figure 4-21 EVM for different OFDM frames for Model 1

On the other hand, the EVM values obtained for Model 2, which have been shown in Figure 4-22, are different than Figure 4-21. In Figure 4-22 the same labels have been

used for presenting the outputs of different OFDM frames. For this case, the first frame with the proposed scheme shows high EVM values. Now this is to be expected prior to the correction of the I/Q imbalance in the proposed scheme, which is only carried out starting from the second frame.

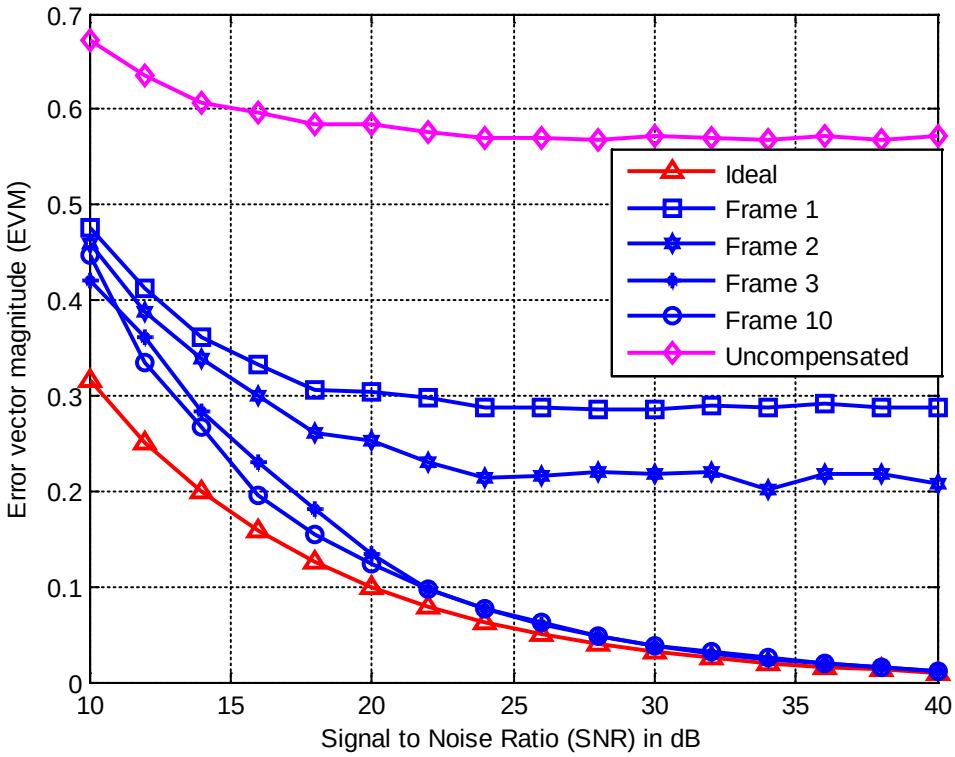

Figure 4-22 EVM for different OFDM frames for Model 2

However, the first frame still has much less error than the 'Uncompensated' case but much more error is observed than the 'Ideal' case. The second frame shows much improvement by having less than the first frame. From the third frame, it has even less error and gets close to the ideal case. The same results continue for the next consecutive frames. Therefore, the tenth frame's output is quite close to the ideal value as well.

4.4.8 Average Symbol error rate (SER) performance

In this section, the proposed method has been illustrated by average SER. Figures 4-23 and 4-24 show the average SERs, achieved for Models 1 and 2, respectively for 64-QAM. The same labels used in Figures 4-21 and 4-22, have been used for Figure 4-23 and 4-24. Overall, 1,000,000 symbols have been used to calculate the SER. Since the SER and EVM are closely related for a given modulation type, the response of SER under the operating conditions considered in Figure 4-23 has been observed to be very similar to the response of the EVM curve depicted in Figure 4-21.

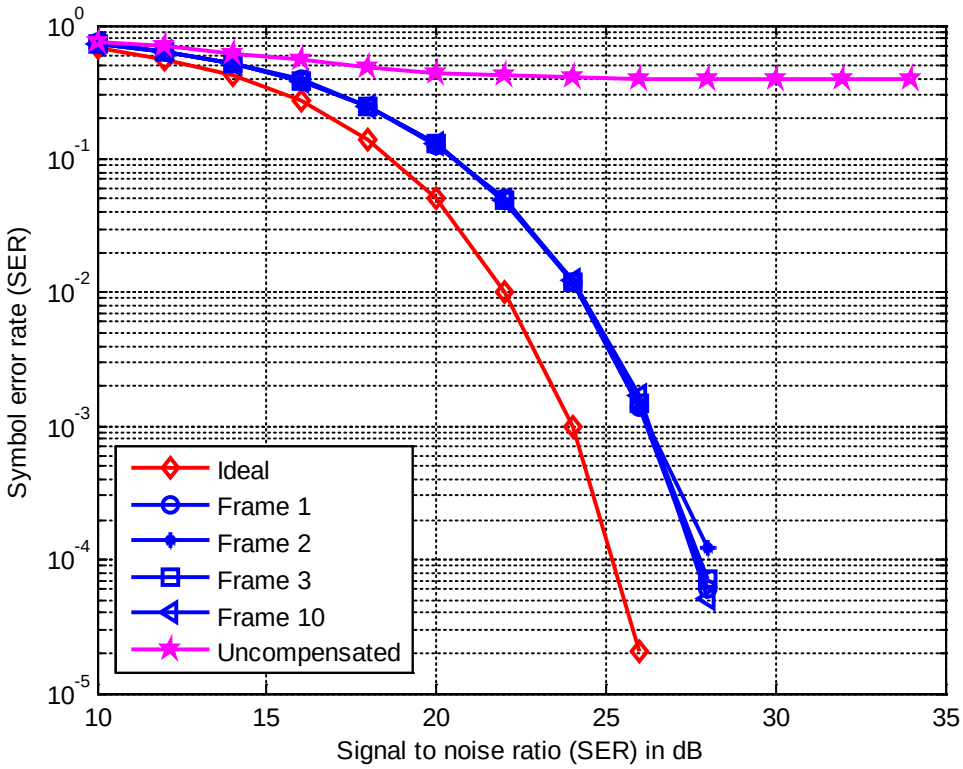

Figure 4-23 SER for different OFDM frames for Model 1

From Figure 4-23, it has been observed that for Model 1, the SER obtained for the first, second, third and tenth frames are quite similar to each other and they are also close to the 'Ideal' condition. For an SER of 10^{-3}, the SNR degradation of the corrected/compensated signal is 2 dB from the ideal SER curve.

The Figure 4-24 represents the SER obtained for the first, second, third, and tenth frames for the Model 2. From the below figure it has been observed that, the first frame shows the most degraded performance, as no correction has been done for this case. The second frame shows a little improvement. On the other hand, the SER has improved significantly for the third frame. The degradation in SER for Frames 3 and 10 achieved with the proposed scheme is approximately 2 dB when compared with the ideal case for a specific SER of 10^{-3}.

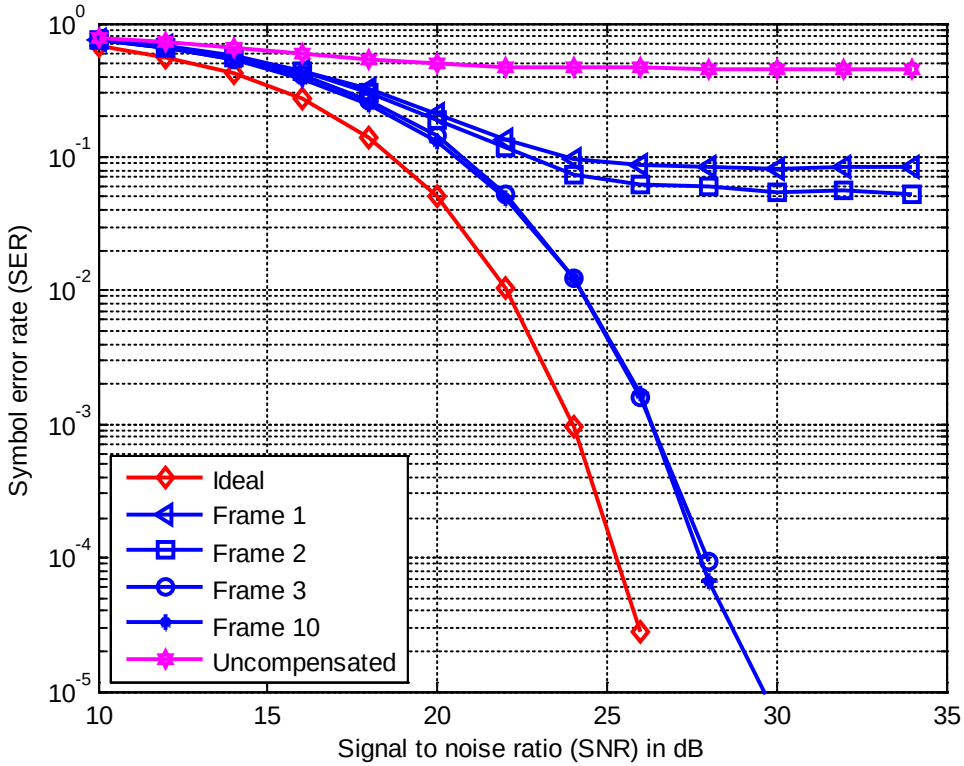

Figure 4-24 SER for different OFDM frames for Model 2

Next, Figure 4-25 shows the SER for different frequency-flat gain and phase imbalances for the tenth frame for Model 2. The reason for choosing only Model 2 is because it has got more severe I/Q imbalance than Model 1. Therefore, the effectiveness of the proposed scheme for different frequency-flat I/Q imbalance would be much more significant in case of Model 2. The tenth frame has been chosen because the system

needs few frames before it can work its best. The gain imbalance has been chosen to be between 1% to 20% and the phase has been chosen to be between 1° to 10°.

From Figure 4-25, it has been observed that the SER performance is similar for different values of gain and phase. This implies that, the proposed scheme is capable of correcting/compensating for I/Q imbalance for a wide range. With the proposed ACCC scheme, the SNR degradation remains 2 dB, at the specified SER of 10^{-3}, in the presence of different combination of frequency-flat gain and phase.

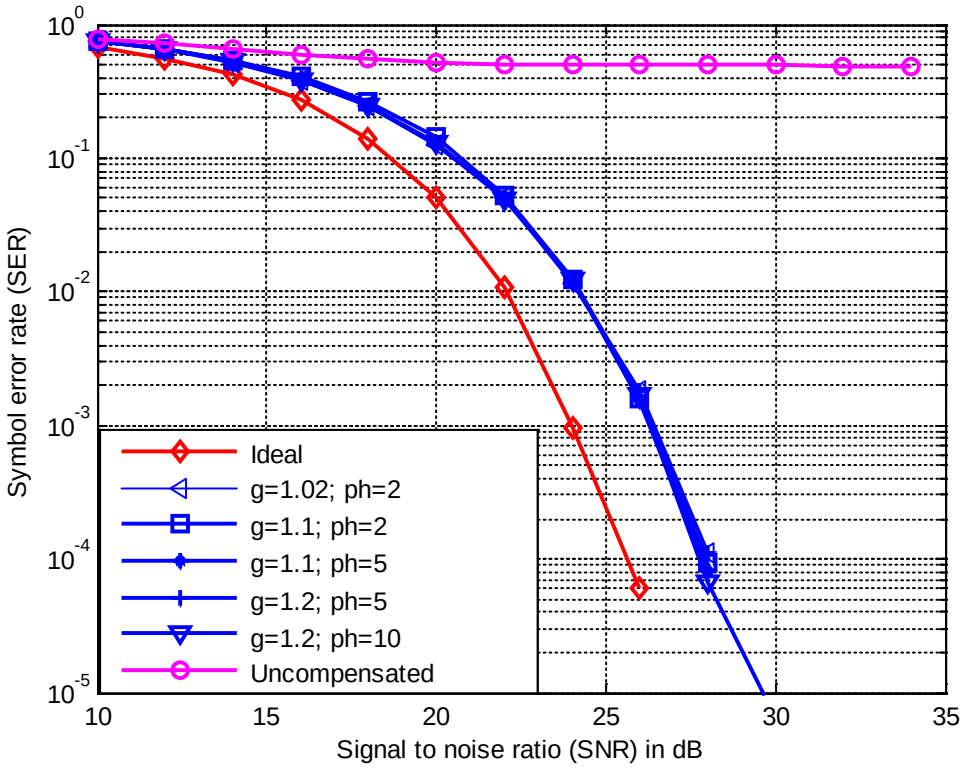

Figure 4-25 SER for different frequency-flat gain and phase combination for tenth frame for Model 2

The SER performance has also been studied based on the use of different number of reference pilot tones. The results are depicted in Figure 4-26. Also in this case, the SER performance for the tenth frame has been presented. The output of the proposed ACCC scheme performs very well even with the use of only 16 pilots. In the case when only 8 pilots have been used, the SER curve saturates before 10^{-1}. The reason for this higher

level of error is the frequency sampling is not enough to perform the linear interpolation.

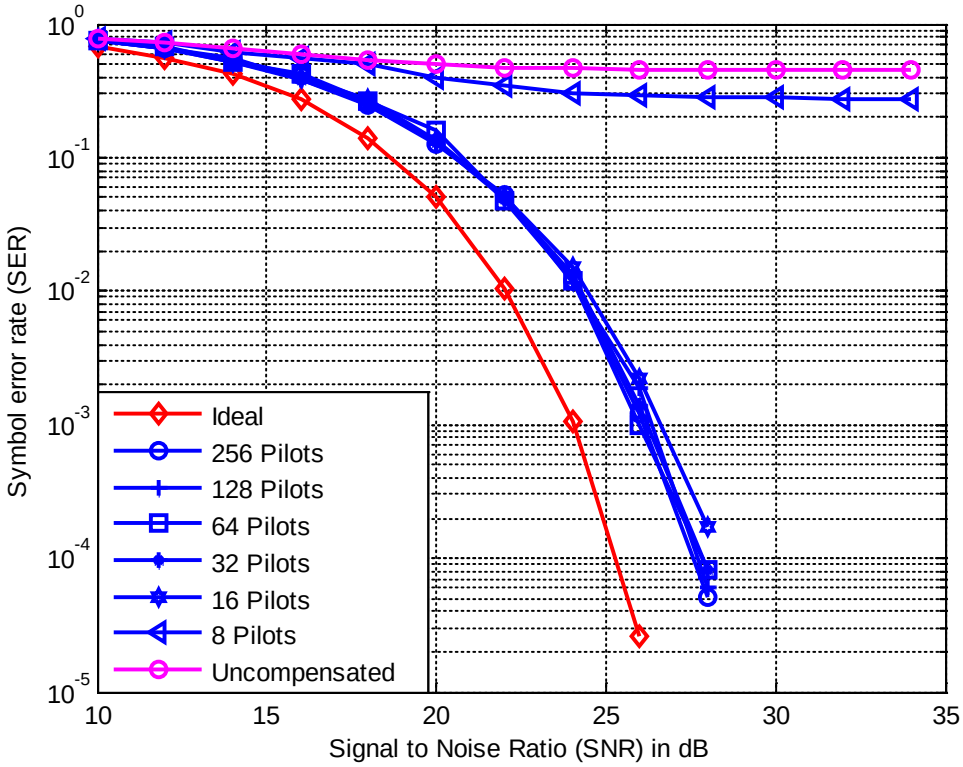

Figure 4-26 SER for different numbers of pilots for tenth frame for Model 2

4.4.9 Evaluation of the proposed scheme for different channel scenario

The proposed scheme has been examined under various channel conditions. The probability of obtaining incorrectly detected pilot subcarriers; depends not only on the value of the I/Q imbalance, but also on the channel properties. All the simulations results shown above have been done for a 9 path LTE channel an ETU scenario. The percentage of the incorrectly detected pilots reduces if the channel property is different. For applications, such as DVB-T, a two path Ricean fading channel can be assumed appropriate [1]. If the multi-path fading channel is assumed to be Ricean, the output $y[n]$ will be related to the input $x[n]$, such that [1]:

$$y[n] = \frac{\sqrt{p_o}x[n] + \sum_{l=1}^{L-1}\sqrt{p_l}e^{-j\varphi_l}x[n-\tau_l]}{\sqrt{\sum_{l=0}^{L-1}p_l}} \tag{4.47}$$

where p_o and p_l are the received powers of the line-of–sight (LOS) path and the l^{th}path, respectively; $e^{-j\varphi_l}$ denotes the phase shift of the l^{th} path and τ_l is the delay of the l^{th}path relative to the LOS path. Also L is the total number of propagation paths. The Ricean factor can be stated as,

$$K = 10log\left(\frac{p_0}{\sum_{l=1}^{L-1}p_l}\right) \tag{4.48}$$

In the DVB-T standard (ETSI 2001), a Ricean factor of 10 dB is considered typical [1]. The pilot detection is more accurate for a channel like this compared to the ETU channel. It depends on the delay between the LOS path and the second path. Figure 4-27 shows the constellation of pilot tones for 64-QAM signal, for a Ricean channel with a K factor 10 dB, for three different delays, for the first Frame, for Model 2. Sampling time has been denoted by T_s. Delays considered for Figure 4-27 (a) to (c) are T_s, $7T_s$ and $14T_s$, respectively.

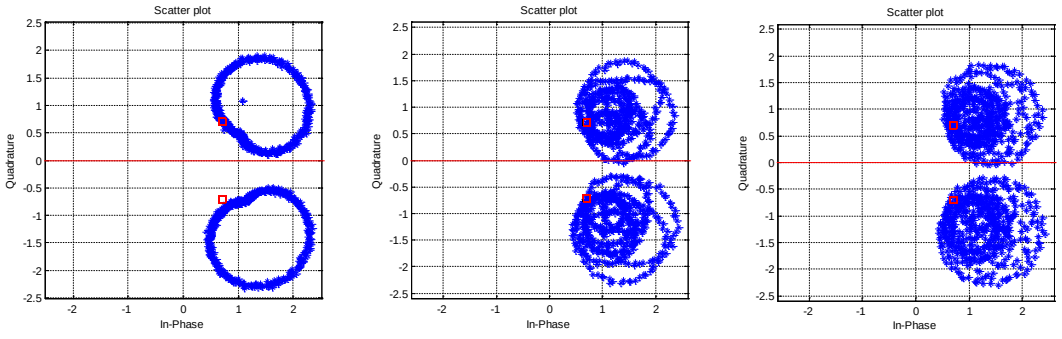

Figure 4-27 Signal constellation of pilot tones, for Ricean channel for delays of a) 1Ts b) 7Ts and c) 14Ts

As the delay increases, the channel become more frequency-selective. It can be observed that the number of overlapping points is much less for Figure 4-27 (a), which

corresponds to a delay of T_s. On the other hand, a delay like $14T_s$, the pilots have many overlapping constellation points that lead to incorrect detection.

Figure 4-28 shows comparative SERs of first and tenth frame for Ricean and ETU channel. For the ETU, the first Frame shows a significant amount of error. But for the tenth frame, the SNR is just 2 dB higher than the ideal SNR, at an SER of 10^{-3}. For the Ricean channel, the second path has a delay of 1Ts. In the case of the Ricean channel, for first frame, SNR is just approximately 3 dB higher than the ideal case at an SER of 10^{-3}. For the tenth frame, a further improvement of 1 dB has been observed.

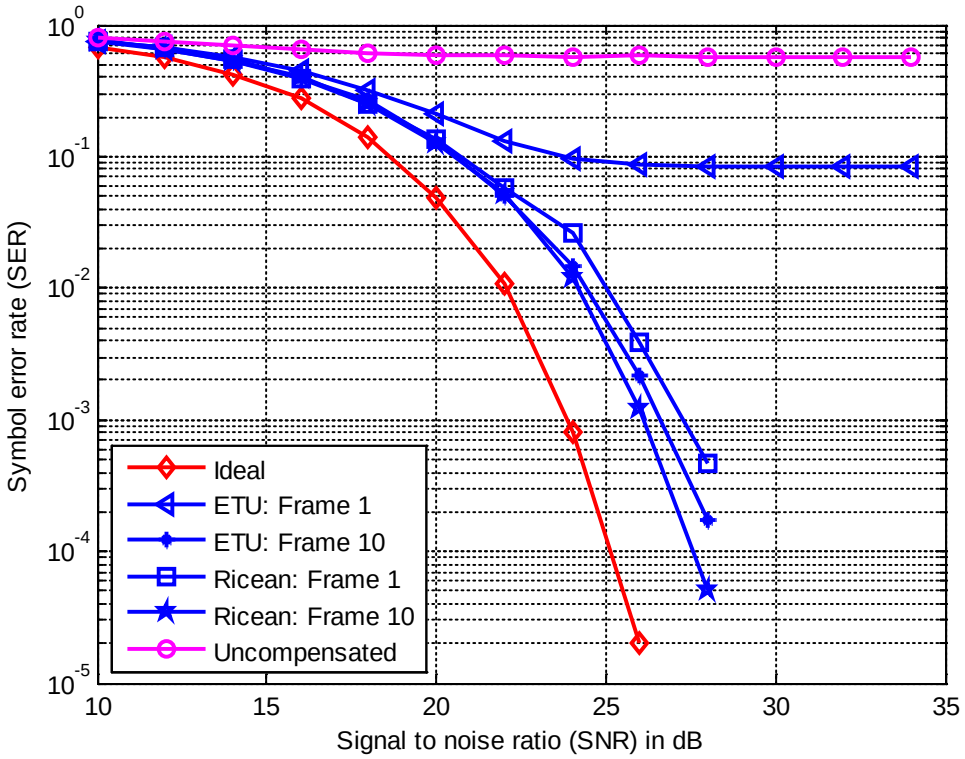

Figure 4-28 SER for ETU and Ricean channel for first and tenth frames for Model 2

Therefore, for the Ricean channel the output shows better performance from the very beginning, i.e. even for the first frame. However, the situation is different when the Ricean channel becomes highly frequency-selective. As the relative delay increases, to a delay of $7T_s$ or a delay of $14T_s$; the SNR degradation increases. Figure 4-29 shows the SER for the first frame for different delays. For delays up to $3T_s$, the first frame

shows good performance. The SNR degradation for the first frame is within a 3 dB range. On the other hand, for delays like $7T_s$ and $14T_s$ the degradation is significant. The label 'ETU' in Figure 4-29 stands for the performance of the first frame in ETU channel. The Ricean channel with a delay of 7Ts and 14Ts results in less SER than the ETU channel. However, the compensation achieved for the first frame is not enough to achieve an acceptable SER. Next, the output SER for these channels has been shown; after the correction and compensation have been done for a few frames.

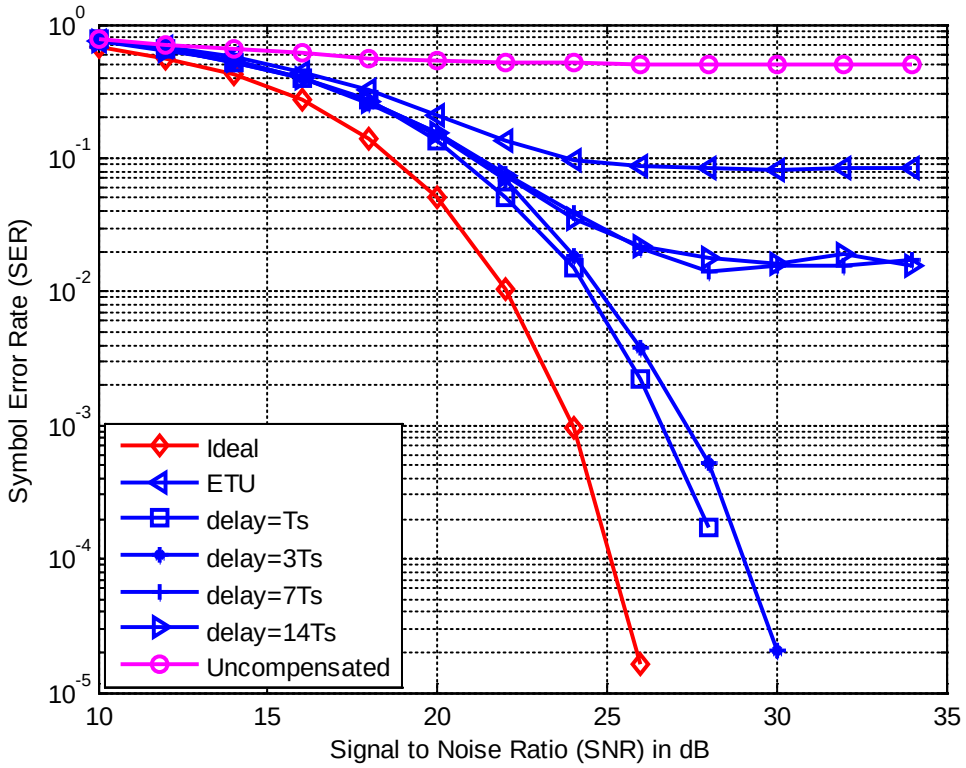

Figure 4-29 SER for ETU and Ricean channel for first frame, corresponding to different delays

The SER performance for the tenth frame for the same channels (as shown in Figure 4-29); has been shown in Figure 4-30. It can clearly be seen that for all delays, the tenth frame demonstrates a good performance. The SNR degradation for T_s, $3T_s$, $7T_s$ and $14T_s$ is approximately 2 dB, at an SER of 10^{-3}. This proves that the ACCC scheme is suitable for a DVB-T channel scenario as well.

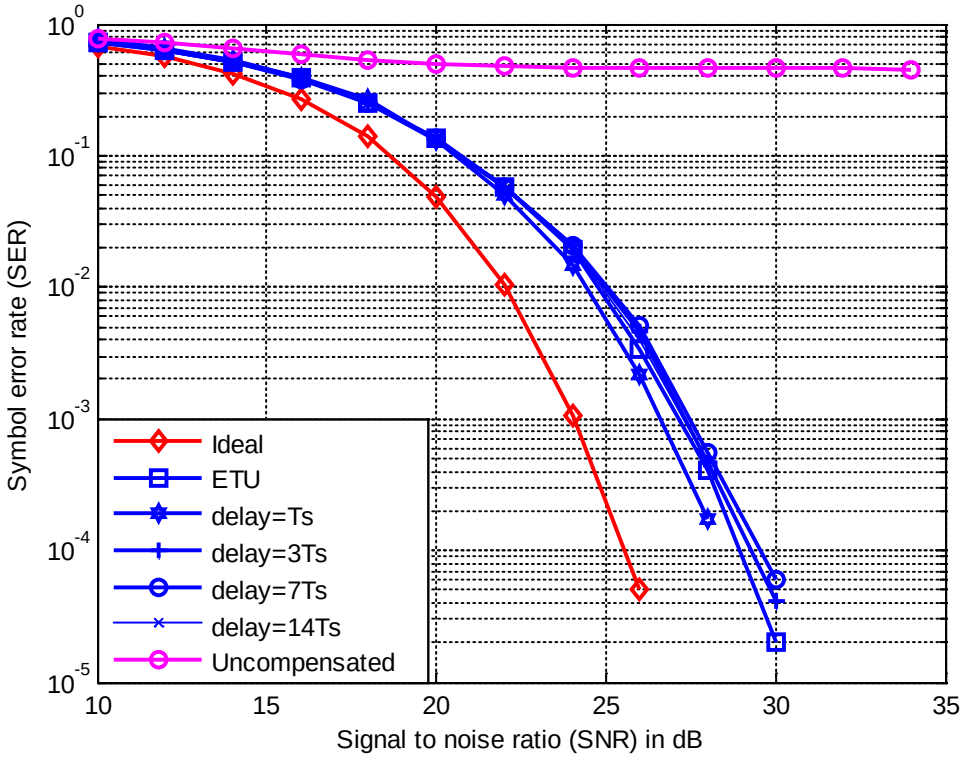

Figure 4-30 SER for ETU and Ricean channel for tenth frame, corresponding to different delays

4.4.10 Evaluation of the proposed scheme for frequency-flat I/Q imbalance

This section describes the effect of the proposed method in the case when the I/Q imbalance is frequency-flat. For the frequency-flat case, the convolution of the signal with the I/Q parameters $u[n]$ and $v[n]$ will be replaced by multiplication in equation (4.2). Moreover, the frequency-selective I/Q imbalance parameters for the I and Q branches, $a_I[n]$ and $a_Q[n]$, respectively, becomes 1. Therefore, for the frequency-flat case, equation (4.2) can be re-written as:

$$y[n] = uh[n] \circledast x[n] + vh^*[n] \circledast x^*[n] \qquad (4.49)$$
$$+u\,\varepsilon[n] + v\varepsilon^*[n]$$

Now, u and v are defined as;

$$u = \frac{g + e^{-j\varphi}}{2}$$
$$v = \frac{g - e^{j\varphi}}{2}$$

Recalling equations (3.15) and (3.16) and using the discrete notations, we obtain:

$$Re\{z[n]\} = z_I[n] = gr_I[n] \text{ and} \tag{4.50}$$

$$Im\{z[n]\} = z_Q[n] = cos\varphi\, r_Q[n] - sin\,\varphi\, r_I[n] \tag{4.51}$$

Also recalling equations (3.17) and (3.18) and replacing linear convolution by circular convolution, we obtain:

$$Re\{y[n]\} = y_I[n] = z_I[n] \circledast a_I[n] \tag{4.52}$$

$$Im\{y[n]\} = y_Q[n] = z_Q[n] \circledast a_Q[n] \tag{4.53}$$

As $a_I[n] = a_Q[n] = 1$, thus we have:

$$y_I[n] = z_I[n] = gr_I[n] \tag{4.54}$$

$$y_Q[n] = z_Q[n] = cos\varphi\, r_Q[n] - sin\,\varphi\, r_I[n] \tag{4.55}$$

After the FFT, the received frequency domain signal at the various pilot frequencies for the $i^{th}$and $(i+1)^{th}$symbols in the m^{th} frame can be expressed according to equation (4.21) as:

$$\begin{bmatrix} Y_m^i[k_p] \\ Y_m^{i+1}[k_p] \end{bmatrix} = \begin{bmatrix} X_m^i[k_p] & X_m^{*i}[-k_p] \\ X_m^{i+1}[k_p] & X_m^{*i+1}[-k_p] \end{bmatrix} \begin{bmatrix} U_m H_m[k_p] \\ V_m H_m^*[-k_p] \end{bmatrix} + \begin{bmatrix} \eta_m^i[k_p] & \eta_m^{*i}[-k_p] \\ \eta_m^{i+1}[k_p] & \eta_m^{*i+1}[-k_p] \end{bmatrix} \tag{4.56}$$

And

$$\begin{bmatrix} Y_m^{*i}[-k_p] \\ Y_m^{*i+1}[-k_p] \end{bmatrix} = \begin{bmatrix} X_m^{*i}[-k_p] & X_m^{i}[k_p] \\ X_m^{*i+1}[-k_p] & X_m^{i+1}[k_p] \end{bmatrix} \begin{bmatrix} U_m^* H_m^*[-k_p] \\ V_m^* H_m[k_p] \end{bmatrix} + \begin{bmatrix} \eta_m^{*i}[-k_p] & \eta_m^{i}[k_p] \\ \eta_m^{*i+1}[-k_p] & \eta_m^{i+1}[k_p] \end{bmatrix} \tag{4.57}$$

Therefore with the help of the received signal and the pilot tones, the I/Q and channel parameters $U_m H_m[k_p]$, $V_m H_m^*[-k_p]$, $U_m^* H_m^*[-k_p]$ and $V_m^* H_m[k_p]$ have been estimated. Then by dividing $V_m H_m^*[-k_p]$ by $U_m^* H_m^*[-k_p]$, and $V_m^* H_m[k_p]$ by $U_m H_m[k_p]$, we obtain,

$$\frac{V_m^*}{U_m} = \frac{g - e^{-j\varphi}}{g + e^{-j\varphi}} \tag{4.58}$$

and

$$\frac{V_m}{U_m^*} = \frac{g - e^{j\varphi}}{g + e^{j\varphi}} \tag{4.59}$$

Now, by elaboration, the frequency-flat gain and phase can be calculated as;

$$\hat{\varphi}_e = \frac{1}{2} \angle \frac{\left(1 + \frac{V_m^*}{U_m}\right)\left(1 - \frac{V_m}{U_m^*}\right)}{\left(1 - \frac{V_m^*}{U_m}\right)\left(1 + \frac{V_m}{U_m^*}\right)} \tag{4.60}$$

In addition, the estimated gain is as follows:

$$\hat{g}_e = e^{j\hat{\varphi}_e} \frac{\left(1 + \frac{V_m}{U_m^*}\right)}{\left(1 - \frac{V_m}{U_m^*}\right)} \tag{4.61}$$

Due to the noise, the estimated values of the gain and phase will be different for each tone. Thus it is more appropriate to denote these as $\hat{g}_e[k]$ and $\hat{\varphi}_e[k]$. The values of $\hat{g}_e[k]$ and $\hat{\varphi}_e[k]$ are averaged for all subcarriers k to obtain a single value for gain $\acute{g}_m$ and phase $\acute{\phi}_m$ for the m^{th} OFDM frame, such that:

$$\acute{g}_m = \frac{1}{N}\sum_{k=1}^{N} \hat{g}_e[k] \text{ and } \acute{\varphi}_m = \frac{1}{N}\sum_{k=1}^{N} \hat{\varphi}_e[k] \tag{4.62}$$

Finally, the newly adopted gain $\acute{g}_m$and phase $\acute{\varphi}_m$ value is then averaged according to equations (4.34) and (4.35) to obtain the nominal gain and phase for the m^{th} frame denoted as, $\hat{g}_m$ and $\hat{\varphi}_m$. The $(m+1)^{th}$ frame has been corrected by the gain and phase obtained in the m^{th}frame. Subsequently, by using the values of $\hat{g}_m$ and $\hat{\varphi}_m$, the corrected $(m+1)^{th}$ frame can be obtained as in (4.8):

$$\begin{bmatrix} Re\{c_{m+1}^{i}[n]\} \\ Im\{c_{m+1}^{i}[n]\} \end{bmatrix} = \frac{1}{\hat{g}_m cos\hat{\varphi}_m} \begin{bmatrix} cos\hat{\varphi}_m & 0 \\ sin\hat{\varphi}_m & \hat{g}_m \end{bmatrix} \begin{bmatrix} Re\{y_{m+1}^{i}[n]\} \\ Im\{y_{m+1}^{i}[n]\} \end{bmatrix} \tag{4.63}$$

or

$$\begin{bmatrix} Re\{c_{m+1}^{i}[n]\} \\ Im\{c_{m+1}^{i}[n]\} \end{bmatrix} = \frac{1}{\hat{g}_m cos\hat{\varphi}_m} \begin{bmatrix} cos\hat{\varphi}_m & 0 \\ sin\hat{\varphi}_m & \hat{g}_m \end{bmatrix} \begin{bmatrix} gRe\{r_{m+1}^{i}[n]\} \\ cos\varphi Im\{r_{m+1}^{i}[n]\} - sin\,\varphi\, Re\{r_{m+1}^{i}[n]\} \end{bmatrix} \tag{4.64}$$

Assuming the estimated values, $\hat{g}_m \simeq g$ and $\hat{\varphi}_m \simeq \varphi$. Then we obtain,

$$Re\{c_{m+1}^{i}[n]\} \simeq Re\{r_{m+1}^{i}[n]\} \tag{4.65}$$

and

$$Im\{c_{m+1}^{i}[n]\} \simeq Im\{r_{m+1}^{i}[n]\} \tag{4.66}$$

Thus we attain,

$$c_{m+1}^{i}[n] \simeq r_{m+1}^{i}[n] \simeq h_m[n] \circledast x_{m+1}^{i}[n] + \acute{\varepsilon}_T[n] \tag{4.67}$$

After the FFT, the corrected output before the compensation becomes,

$$C_m^i[k] = H_m[k]X_m^i[k] + \acute{\eta}_m^i[k] \tag{4.68}$$

Thus, the corrected signal has only channel imperfection. The I/Q has been removed during the correction stage and the compensator will work as an equalizer. Finally, the compensated output is achieved using BLUE as follows;

$$X_m^i[k] = H_m[k]^{-1} C_m^i[k] \tag{4.69}$$

4.5 Summary

In this chapter, a novel combined I/Q imbalance correction and compensation technique that makes use of a specific pilot pattern has been presented. The scheme has been investigated for two different frequency-selective I/Q models. It has been observed that when the I/Q model is not severe as in the case of Model 1, the scheme tends to perform properly from the very beginning (i.e. from the first frame). However for Model 2, the output of the first frame is distorted. The distortion has been removed after few consecutive frames. Also the scheme has been tested under a range of frequency-flat gain and phase conditions. The compensated output is similar for a wide range of I/Q imbalance. It means the scheme is capable of removing a wide range of I/Q imbalances. Moreover, two different sorts of channels have been considered. One is a nine path ETU channel and another one is a two path Ricean channel. The scheme works for both of the channel conditions. Again, when the Ricean channel is very frequency-selective, it takes two to three OFDM frames to provide a low level SER. It has been shown that even severe I/Q imbalances can be corrected and compensated for by this scheme using just 16 pilots, which is 1.56% of the total subcarriers in one OFDM symbol. The proposed ACCC scheme can also be applied to remove I/Q imbalance and channel effect from the single carrier frequency domain equalization (SC-FDE) (details in Appendix A).

CHAPTER 5

PERFORMANCE COMPARISON FOR DIFFERENT CORRECTION AND COMPENSATION SCHEMES

5.1 Introduction

In this chapter, the performances of different I/Q imbalance compensation/correction schemes have been compared with the proposed ACCC method. Three different compensation/correction schemes have been considered for the comparison. They are the joint compensation scheme [14], the decoupled/separate compensation scheme [15] and the adaptive LMS compensation scheme [2]. Section 5.2 to 5.4 describes these three compensation schemes. All of these compensation techniques have used pilot tones as references.

However, it has been assumed that the pilots have been detected correctly. In this chapter, how these methods perform when the detected pilots are extracted from the received signal and distorted by I/Q imbalance has been demonstrated. Also, these methods have been tested with a wide range of frequency-flat and frequency-selective I/Q imbalance combinations and then compared with the proposed ACCC scheme. Moreover, these methods have been tested under different numbers of pilot subcarriers to observe their robustness.

5.2 The joint compensation scheme

In the joint compensation scheme [14], the effect of I/Q imbalance on the orthogonal frequency division multiple access-uplink (OFDMA-UL) system has been considered. The received signal with I/Q distortion parameters and channel has been mathematically formulated. The signal model is then used to equalize the channel and compensate for the I/Q parameters from the system. However, they have proposed two methods for two different channel scenarios. One method is where it is assumed that the bandwidth of two symbols containing the pilot subcarriers is less than the coherence bandwidth of the channel. In the other method, it is assumed that the time duration between two symbols containing pilot subcarriers is less than the coherence time of the channel. For this chapter, we have only compared the latter case, as the first one is not suitable for frequency-selective channels. In this paper, the OFDMA-UL frame has been divided into several tiles. Each tile has a dimension of three symbols by four subcarriers/tones. The pilot tones are situated one symbol and two subcarriers apart. The OFDM frame structure described here is similar to the structure shown in Figure 4-4. The only difference is that for the proposed ACCC structure, the pilots are situated in the first two consecutive symbols. Now recalling the equations (3.39) and (3.41) for the received signal where both I/Q and channel parameters are present, we obtain,

$$Y[k] = U[k]H[k]X[k] + V[k]H^*[-k]X^*[-k] + \eta[k] \text{ and} \tag{5.1}$$

$$Y^*[-k] = U^*[-k]H^*[-k]X^*[-k] + V^*[-k][k]H[k]X[k] + \eta^*[-k] \tag{5.2}$$

The received signal after the I/Q distortion, at the various pilot subcarriers k_p for the i^{th} symbols in the m^{th} frame can be expressed in matrix form as,

$$\begin{bmatrix} Y_m^i[k_p] \\ Y_m^{*i}[-k_p] \end{bmatrix} = \begin{bmatrix} U_m[k_p]H_m[k_p] & V_m[k_p]H_m^*[-k_p] \\ V_m^*[-k_p]H_m[k_p] & U_m^*[-k_p]H_m^*[-k_p] \end{bmatrix} \begin{bmatrix} X_m^i[k_p] \\ X_m^{*i}[-k_p] \end{bmatrix} + \begin{bmatrix} \eta_m^i[k_p] \\ [\eta_m^{*i}[-k_p]] \end{bmatrix} \tag{5.3}$$

$$\begin{bmatrix} Y_m^i[k_p] \\ Y_m^{*i}[-k_p] \end{bmatrix} = \bar{\mathbf{Z}} \begin{bmatrix} X_m^i[k_p] \\ X_m^{*i}[-k_p] \end{bmatrix} + \begin{bmatrix} \eta_m^i[k_p] \\ [\eta_m^{*i}[-k_p]] \end{bmatrix} \tag{5.4}$$

where, $\bar{\mathbf{Z}} = \begin{bmatrix} U_m[k_p]H_m[k_p] & V_m[k_p]H_m^*[-k_p] \\ V_m^*[-k_p]H_m[k_p] & U_m^*[-k_p]H_m^*[-k_p] \end{bmatrix}$.

According to the tile structure presented in the work of [14], the pilots present are the i^{th} and $(i+2)^{th}$ symbols. Assuming the channel and I/Q parameters are not varying between the i^{th} and $(i+2)^{th}$ symbols, the received signal for these symbols in the m^{th} frame can be expressed as:

$$\begin{bmatrix} Y_m^i[k_p] \\ Y_m^{i+2}[k_p] \end{bmatrix} = \begin{bmatrix} X_m^i[k_p] & X_m^{*i}[-k_p] \\ X_m^{i+2}[k_p] & X_m^{*i+2}[-k_p] \end{bmatrix} \begin{bmatrix} U_m[k_p]H_m[k_p] \\ V_m[k_p]H_m^*[-k_p] \end{bmatrix} + \begin{bmatrix} \eta_m^i[k_p] \\ \eta_m^{i+2}[k_p] \end{bmatrix} \tag{5.5}$$

Similarly we can obtain,

$$\begin{bmatrix} Y_m^{*i}[-k_p] \\ Y_m^{*(i+2)}[-k_p] \end{bmatrix} = \begin{bmatrix} X_m^{*i}[-k_p] & X_m^i[k_p] \\ X_m^{*(i+2)}[-k_p] & X_m^{i+2}[k_p] \end{bmatrix} \begin{bmatrix} U_m^*[-k_p]H_m^*[-k_p] \\ V_m^*[-k_p]H_m[k_p] \end{bmatrix} + \begin{bmatrix} \eta_m^{*i}[-k_p] \\ \eta_m^{*(i+2)}[-k_p] \end{bmatrix} \tag{5.6}$$

Now the I/Q and channel parameters can be estimated according to the BLUE method as follows:

$$\begin{bmatrix} U_m[k_p]\widehat{H_m}[k_p] \\ V_m[k_p]H_m^*[-k_p] \end{bmatrix} \simeq \begin{bmatrix} X_m^i[k_p] & X_m^{*i}[-k_p] \\ X_m^{i+2}[k_p] & X_m^{*i+2}[-k_p] \end{bmatrix}^{-1} \begin{bmatrix} Y_m^i[k_p] \\ Y_m^{(i+2)}[k_p] \end{bmatrix} \tag{5.7}$$

and

$$\begin{bmatrix} U_m^*[-k_p]\widehat{H_m^*[-k_p]} \\ V_m^*[-k_p]H_m[k_p] \end{bmatrix} \simeq \begin{bmatrix} X_m^{*i}[-k_p] & X_m^i[k_p] \\ X_m^{*(i+2)}[-k_p] & X_m^{i+2}[k_p] \end{bmatrix}^{-1} \begin{bmatrix} Y_m^{*i}[-k_p] \\ Y_m^{*(i+2)}[-k_p] \end{bmatrix} \quad (5.8)$$

The '$\widehat{\ }$' sign denotes the estimate of the unknown parameters. After the four unknown parameters $U_m[k_p]H_m[k_p]$, $V_m[k_p]H_m^*[-k_p]$, $U_m^*[-k_p]H_m^*[-k_p]$, and $V_m^*[-k_p]H_m[k_p]$ in equation (5.3) have been estimated, the transmit signal can be estimated by an inverse matrix operation of equation (5.4), such that:

$$\begin{bmatrix} X_m^i[k_p] \\ X_m^{*i}[-k_p] \end{bmatrix} \simeq [\mathbf{Z}]^{-1} \begin{bmatrix} Y_m^i[k_p] \\ Y_m^i[-k_p] \end{bmatrix} \quad (5.9)$$

If the estimates of the imbalance coefficients are available at frequency indices k_{p1} and k_{p2}, then the coefficient parameter at frequency index k, where $k_{p1} < k < k_{p2}$, has been obtained by the linear interpolation as expressed in equations (4.36) and (4.37). The distance between two consecutive pilots i.e. between $k_{p1}$and k_{p2} is 2, according to this method. However later in this chapter this distance have been varied to observe the effectiveness of the scheme. The joint compensation scheme is similar to the ACCC except the correction part for the frequency-flat I/Q imbalance.

5.3 The separate/de-coupled compensation scheme

Another popular scheme for compensating for the I/Q imbalance is the separate/decoupled compensation technique. We have compared the separate compensation scheme described in the work of [15]. In this scheme, the I/Q imbalance and the channel have been compensated separately. As the I/Q imbalances vary much less frequently than the channel, the compensation of these two impairments has been performed successively. The compensation has been done in reversed order in appearance (i.e., received signal's I/Q imbalance first, then the channel's). According to the authors, the noise has also been altered by the I/Q imbalance. They have expressed this as follows:

$$\begin{bmatrix} Y_m^i[k_p] \\ Y_m^i[-k_p] \end{bmatrix} = \begin{bmatrix} U_m[k_p]H_m[k_p] & V_m[k_p]H_m^*[-k_p] \\ V_m^*[-k_p]H_m[k_p] & U_m^*[-k_p]H_m^*[-k_p] \end{bmatrix} \begin{bmatrix} X_m^i[k_p] \\ X_m^{*i}[-k_p] \end{bmatrix} + \begin{bmatrix} U_m[k_p] & V_m[k_p] \\ V_m^*[-k_p] & U_m^*[-k_p] \end{bmatrix} \begin{bmatrix} \eta_m^i[k_p] \\ [\eta_m^{*i}[-k_p]] \end{bmatrix} \quad (5.10)$$

According to this scheme, the unknown parameter matrix $\bar{\mathbf{Z}}$, can be separated as a multiplication of two matrices, $\bar{\mathbf{Z}}_\mathbf{s}$ and $\bar{\mathbf{H}}_\mathbf{s}$, where $\bar{\mathbf{Z}}_\mathbf{s}$ contains I/Q parameters and $\bar{\mathbf{H}}_\mathbf{s}$ contains channel parameters, such that:

$$\bar{\mathbf{Z}} = \begin{bmatrix} U_m[k_p] & V_m[k_p] \\ V_m^*[-k_p] & U_m^*[-k_p] \end{bmatrix} \begin{bmatrix} H_m[k_p] & 0 \\ 0 & H_m^*[-k_p] \end{bmatrix} = \bar{\mathbf{Z}}_\mathbf{s}\bar{\mathbf{H}}_\mathbf{s} \quad (5.11)$$

So equation (5.10) can be written as:

$$\begin{bmatrix} Y_m^i[k_p] \\ Y_m^i[-k_p] \end{bmatrix} = \bar{\mathbf{Z}}_\mathbf{s}\bar{\mathbf{H}}_\mathbf{s} \begin{bmatrix} X_m^i[k_p] \\ X_m^{*i}[-k_p] \end{bmatrix} + \bar{\mathbf{Z}}_\mathbf{s} \begin{bmatrix} \eta_m^i[k_p] \\ [\eta_m^{*i}[-k_p]] \end{bmatrix} \quad (5.12)$$

According to the authors [15], if $\bar{\mathbf{Z}}_\mathbf{s}$ can be accurately estimated, then the I/Q imbalance can be removed from the received signal presented in equation (5.12) by multiplying the equation by $[\bar{\mathbf{Z}}_\mathbf{s}]^{-\mathbf{1}}$. Therefore, it becomes:

$$[\bar{\mathbf{Z}}_\mathbf{s}]^{-\mathbf{1}} \begin{bmatrix} Y_m^i[k_p] \\ Y_m^i[-k_p] \end{bmatrix} = \bar{\mathbf{H}}_\mathbf{s} \begin{bmatrix} X_m^i[k_p] \\ X_m^{*i}[-k_p] \end{bmatrix} + \begin{bmatrix} \eta_m^i[k_p] \\ [\eta_m^{*i}[-k_p]] \end{bmatrix} \quad (5.13)$$

In equation (5.12), it has been shown that the transmit signal matrix and the noise matrix are multiplied by the same I/Q parameter matrix $\bar{\mathbf{Z}}_\mathbf{s}$, which is not quite right, as recalling (3.33), we get:

$$\mathbf{y} = (\overline{\mathbf{u^c}}).(\overline{\mathbf{h^c}}).\mathbf{x} + (\overline{\mathbf{v^c}}).(\overline{\mathbf{h^c}})^*.\mathbf{x}^* + (\overline{\mathbf{u_n}}).\boldsymbol{\varepsilon} + (\overline{\mathbf{v_n}}).\boldsymbol{\varepsilon}^* \quad (5.14)$$

As we can see, the I/Q parameter multiplied to the desired and image signals (i.e., $\overline{\mathbf{u^c}}$ and $\overline{\mathbf{v^c}}$) are different from the I/Q parameters multiplied to the noise and noise image, (i.e., $\overline{\mathbf{u_n}}$ and $\overline{\mathbf{v_n}}$) because the noise does not have a CP. Therefore, while the desired and image signals are multiplied by the circular matrices, the noise and its image are multiplied by a Toeplitz matrix. Even if the I/Q parameters are estimated accurately, the I/Q imbalance in the noise cannot be eliminated according to equation (5.13) as stated in the work of [15]. On the other hand, according to our evaluation in equation (3.42), if the received signal is multiplied by $[\bar{\mathbf{Z}}_\mathbf{s}]^{-\mathbf{1}}$, the resultant signal becomes:

$$[\mathbf{Z_s}]^{-\mathbf{1}}\begin{bmatrix} Y_m^i[k_p] \\ Y_m^i[-k_p] \end{bmatrix} = \begin{bmatrix} X_m^i[k_p] \\ X_m^{*i}[-k_p] \end{bmatrix} + [\mathbf{Z_s}]^{-\mathbf{1}}\begin{bmatrix} \eta_m^i[k_p] \\ [\eta_m^{*i}[-k_p]] \end{bmatrix} \tag{5.15}$$

The parameters in $[\mathbf{Z_s}]^{-\mathbf{1}}$ have been estimated using pilot tones. Two consecutive OFDM symbols have been used as pilots. The unknown parameters have been estimated according to equations (5.7) and (5.8) (similar to the joint compensation scheme). In this scheme the i^{th} and $(i+1)^{th}$symbols have been considered for I/Q and channel estimation purposes, assuming that I/Q and channel parameters are constant during these two symbol durations. Also, a specific number of pilots have been used in k_p indices and then the parameters for all the indices k have been obtained by interpolation.

After the estimation of the parameters in $[\mathbf{Z_s}]$, an I/Q compensator coefficient has been obtained. The I/Q compensator coefficients have been denoted by $\widehat{W}_k$, which is obtained as follows:

$$\widehat{W}_k = -\frac{V_m[k]H^*[-k]}{U_m^*[-k]H^*[-k]} = -\frac{V_m[k]}{U_m^*[-k]} \tag{5.16}$$

and

$$\widehat{W}_{-k} = -\left(\frac{V_m^*[-k]H[k]}{U_m[k]H[k]}\right)^* = -\frac{V_m[-k]}{U_m^*[k]} \tag{5.17}$$

Then, an adaptive image cancellation method is adopted to remove the I/Q imbalance from the signal. The signal (after removing the I/Q imbalance) is denoted by $Y_{c,m}[k]$. The subscript c references the fact that the signal has been compensated for, and m refers to the m^{th} frame. The compensated signal $Y_{c,m}[k]$ has been obtained from the received signal as:

$$Y_{c,m}[k] = Y_m[k] + \widehat{W}_k Y_m^*[-k] \tag{5.18}$$

Now, inputting the value of $Y_m[k]$ and $Y_m^*[-k]$ according to equations (5.1) and (5.2), respectively, in equation (5.18) we obtain:

$$\begin{aligned} Y_{c,m}[k] = (U_m[k] + \widehat{W}_k V_m^*[-k])H_m[k]X_m[k] \\ +(V_m[k] + \widehat{W}_k U_m^*[-k])H_m^*[-k]X_m^*[-k] + \eta_m[k] \end{aligned} \tag{5.19}$$

To eliminate the I/Q imbalance, $V_m[k] + \widehat{W}_k U_m^*[k] = 0$, or $V_m[k] = -\widehat{W}_k U_m^*[k]$; for the subcarrier index k, this yields the ideal compensator coefficients:

$$\widehat{W}_k = -\frac{V_m[k]]}{U_m^*[-k]} \tag{5.20}$$

Substituting this ideal value of $\widehat{W}_k$ into equation (5.19), the compensated signal becomes:

$$Y_{c,m}[k] = \left(U_m[k] - \frac{V_m[k]V_m^*[-k]}{U_m^*[-k]}\right)H_m[k]X_m[k] + \eta_m[k] \tag{5.21}$$

Assuming $V_m[k] \ll U_m[k]$ and $U_m[k] \simeq 1$, the above equation can be written as follows:

$$Y_{c,m}[k] = U_m[k]H_m[k]X_m[k] + \eta[k] \tag{5.22}$$

Thus, the image signal is removed from the desired signal and then the signal is left with some linear distortion $U_m[k]H_m[k]$, which is then compensated for in the equalization stage.

Finally, the equalized signal $\hat{X}_m^i[k]$ for i^{th} symbol of the m^{th} frame can be estimated using BLUE as follows:

$$\hat{X}_m^i[k] = \frac{Y_{c,m}^i[k]}{U_m^i[k]H_m^i[k]} \tag{5.23}$$

Least square (LS) and weighted least square (WLS) estimation techniques have been presented in the work of [15] to smooth the values of $\widehat{W}_k$. However, in this scheme, the WLS-based method shows little difference compared to the uncompensated method, when the SNR is over 25 dB. When the SNR is lower than this value, there is little difference between the compensated and uncompensated signal. This is why, in our comparison, we have not applied the WLS smoothing function. Only the raw estimates of the $\widehat{W}_k$ have been considered.

5.4 The adaptive LMS compensation scheme

In the work of [2], an adaptive equalization technique has been adopted to compensate for the channel and I/Q parameters. Let the equalized signal be $\hat{X}_m^i[k]$. In addition, the equalization coefficients are denoted as $\boldsymbol{w}_k$ and $\boldsymbol{w}_{N-k+2}$. The value of k for this method is 0 to $N/2$. The equalization coefficients are expressed as follows:

$$\boldsymbol{w}_k = [w_1[k] \quad w_2[k]] \tag{5.24}$$

$$\boldsymbol{w}_{N-k+2} = [w_3[k] \quad w_4[k]] \tag{5.25}$$

The adaptive equalization has been done as follows:

$$\hat{X}[k] = \boldsymbol{w}_k \begin{bmatrix} Y[k] \\ Y^*[N-k+2] \end{bmatrix} \text{ and} \tag{5.26}$$

$$\hat{X}^*[N-k+2] = \boldsymbol{w}_{N-k+2} \begin{bmatrix} Y[k] \\ Y^*[N-k+2] \end{bmatrix} \tag{5.27}$$

The equalization coefficients are updated according to the LMS algorithm. Let $\boldsymbol{w}_{k,m}^{i}$ stand for the equalization coefficient for the m^{th} frame for the i^{th} symbol. In other words, i is also the time index that represents iterations. Therefore, the equalized OFDM signal for the k_p^{th} pilot tone in the i^{th} symbol block for the m^{th} frame is expressed as follows:

$$\hat{X}_m^i[k_p] = \boldsymbol{w}_{k_p,m}^i \begin{bmatrix} Y_m^i[k_p] \\ Y_m^{*i}[N-k_p+2] \end{bmatrix} \tag{5.28}$$

$$\hat{X}_m^{*i}[N-k_p+2] = \boldsymbol{w}_{k_p,m}^i \begin{bmatrix} Y_m^i[k_p] \\ Y_m^{*i}[N-k_p+2] \end{bmatrix} \tag{5.29}$$

The equalization coefficients are updated according to the LMS rule as follows:

$$\boldsymbol{w}_{k_p,m}^{i+1} = \boldsymbol{w}_{k_p,m}^i + \mu \left(\begin{bmatrix} Y_m^i[k_p] \\ Y_m^{*i}[N-k_p+2] \end{bmatrix} \right)^* e_m^i[k] \tag{5.30}$$

$$\boldsymbol{w}_{N-k_p+2,m}^{i+1} = \boldsymbol{w}_{k_p,m}^i + \mu \left(\begin{bmatrix} Y_m^i[k_p] \\ Y_m^{*i}[N-k_p+2] \end{bmatrix} \right)^* e_m^i[N-k_p+2] \tag{5.31}$$

where μ is the LMS adaptation step size, and $e_m^i[k]$ is the error for the i^{th} symbol/iteration. The error is updated as follows:

$$e_m^i[k_p] = X_m^i[k_p] - \boldsymbol{w}_{k_p,m}^i \begin{bmatrix} Y_m^i[k_p] \\ Y_m^{*i}[N-k_p+2] \end{bmatrix} \text{ and} \tag{5.32}$$

$$e_m^i[N-k_p+2] = X_m^{*i}[N-k_p+2] - \boldsymbol{w}_{N-k_p+2,m}^i \begin{bmatrix} Y_m^i[k_p] \\ Y_m^{*i}[N-k_p+2] \end{bmatrix} \tag{5.33}$$

where $X_m^i[k_p]$ is the pilot for k_p^{th} tone. As LMS is a slow adaptive method, usually the adaptive coefficient values take a lot of symbols before converging. This is why the authors have initialized the equalization coefficients $\boldsymbol{w}_{k,m}^i$ with known channel parameters

$$\boldsymbol{w}_{k_p,m}^{0} = [G_k \quad 0] \text{ and} \tag{5.34}$$

$$\boldsymbol{w}_{N-k_p+2,m}^{0} = [0 \quad G_k\ ] \tag{5.35}$$

where,

$$G_k = \frac{\sum_{i=1}^{ntr} X_{m,k_p}^{*i} Y_{m,k_p}^{i}}{\sum_{i=1}^{ntr} X_{m,k_p}^{*i} X_{m,k_p}^{i}} \tag{5.36}$$

5.5 Performance comparison of different schemes

The above three schemes (i.e., joint compensation, decoupled compensation, and adaptive LMS compensation schemes) have been compared with each other and also with the proposed ACCC scheme (described in Chapter 4). The simulation parameters are described in Section 4.4.1. The methods have been applied on OFDM signals having a 64-QAM modulation. For the adaptive LMS method, the adaptation step size μ has been chosen 0.1, as a typical measure. A nine-path LTE channel for the ETU condition has been chosen, and AWGN varying from 10 dB to 35 dB has been taken into consideration for the simulation. A variety of frequency-flat I/Q ranging from $g = 1.02$, $\varphi = 2^{\text{o}}$ to $g = 1.2$, $\varphi = 10^{\text{o}}$ have been chosen. For frequency-selective I/Q, both Model 1 and Model 2, described in Chapter 4 has been taken into consideration. The above methods have been observed by signal constellation, EVM, and SER. The signal constellation shows a visual presentation of the received signal's constellations. It shows whether a method is capable enough to remove distortions. At the same time, the EVM shows how these methods work for an extensive range of AWGN. The ideal EVM of the received signal is obtained when no I/Q imbalance and channel distortion is present. For a lower value of SNR, the EVM is expected to be higher. With the increment of the SNR the EVM should decrease and become close to the ideal EVM value. Similarly, with the increment of the SNR the SER should also decease for the received signal compensated for by the methods stated above. Thus, the effectiveness of all these methods can be observed for different SNR levels for different I/Q and channel conditions.

Several conditions have been considered for the comparison among all the schemes stated above. These conditions are as follows:

- Different frequency-flat I/Q,
- Two different models of frequency-selective I/Q, Model 1 and 2,
- Different IRR levels,
- Different numbers of pilot subcarriers used.

Previously, in all the schemes (except the proposed ACCC scheme) the pilots were assumed to have been detected perfectly. But in this chapter, the simulations for all the methods have been performed by extracting the pilots from the received signal. Model 1 has a low variation of I/Q. It gives fewer falsely detected pilots. Thus, almost all of the methods work well for Model 1. On the other hand, as in Model 2, the I/Q variation is higher and the number of falsely detected pilots is higher. This results in incorrect parameter estimation that leads to distortion, causing higher EVM and SER.

5.5.1 Performance comparison under different frequency-selective I/Q imbalance

- ***Signal Constellations***

In this section, the methods have been compared using signal constellations. Figure 5-1 (a) to (f) show the constellations of the (a) uncompensated signal, (b) compensated signal obtained by the decoupled compensation, (c) compensated signal obtained by joint compensation, (d) compensated signal obtained by the adaptive LMS compensation, (e) compensated signal for the first frame, obtained by the proposed ACCC and (f) compensated signal for the third frame obtained by the proposed ACCC scheme. Also, the outputs shown in Figure 5-1 have been achieved for Model 1 for the 64-QAM modulation. The frequency-flat gain and phase has been chosen as $g = 1.2$ and $\varphi = 10^{o}$. The AWGN has been chosen to have a 30 dB SNR in this case. The reason for choosing a high SNR is to show the distortion related by the channel and I/Q only.

The frequency-flat gain and phase and the AWGN remain unchanged for Figure 5-2, Figure 5-3, and Figure 5-4.

From Figure 5-1 (a) and (b), it has been observed that the constellations are scattered from the original location due to the I/Q and channel distortion. From Figure 5-1 (b), it has been observed that even after the compensation a significant amount of distortion remains in the system, which has been reflected later in the EVM and SER results. The distortion observed in constellations of the joint compensation, adaptive LMS compensation, and ACCC schemes are much less than that of the decoupled compensation scheme. Model 1 has lower frequency-selective I/Q imbalance variation. That is why almost all the methods except the decoupled one are capable of mitigating I/Q and channel. The constellations of the joint compensation and the adaptive compensation in Figure 5-1 (b) and (d), respectively, show very similar results. Likewise, the proposed ACCC compensation shows similar results for the first and the third frames shown in Figure 5-1 (e) to (f). The proposed method gets better in consecutive frames. However, when the I/Q variation is as small as in Model 1, it shows good results even from the very first frame.

Figure 5-2 shows the constellations for these schemes for a lower order modulation QPSK for Model 1. The effect of I/Q and channel distortion depends on the modulation order. The higher the modulation order, the higher the I/Q and channel distortion. The objective is to see how these methods perform in the case of a lower order modulation. Figure 5-2 (a) shows the uncompensated signal, which is much more detectable compared to 5-1 (a). Also, the received signal obtained after it has been compensated for by decoupled compensation scheme shown in Figure 5-2 (b) is also detectable and shows improved constellations over those shown in Figure 5-1 (b). The joint compensation and the adaptive LMS compensation shown in the Figure 5-2 (c) and (d) shows the similar results. Similarly, it has been observed that the constellations of the received signal after compensation by the proposed ACCC method for the first and for the third frames are also similar.

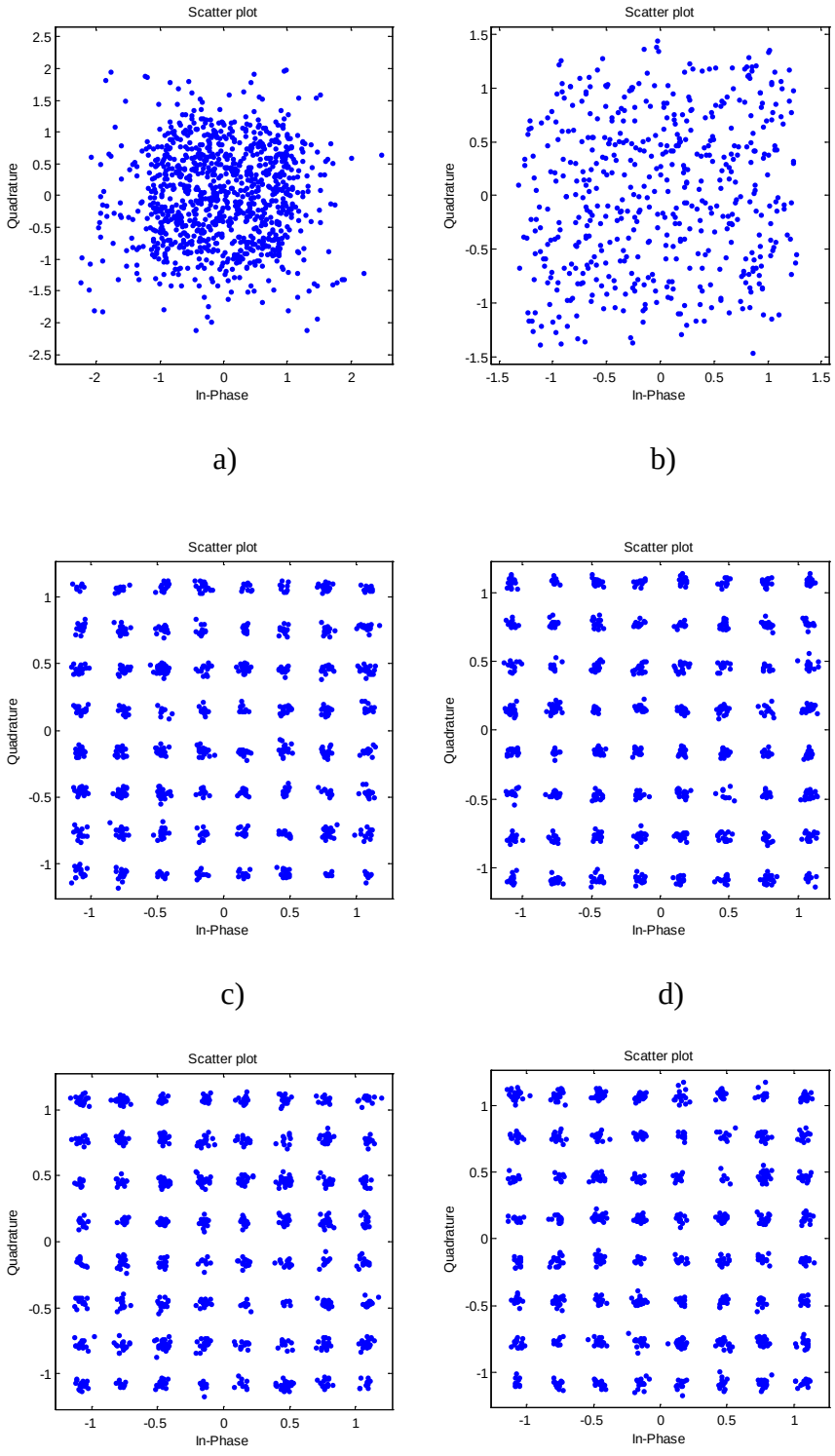

Figure 5-1 Constellations of a) Uncompensated b) Decoupled compensation c) Joint compensation d) adaptive LMS compensation e) ACCC Frame 1 f) ACCC Frame 3, for 64-QAM, for Model 1

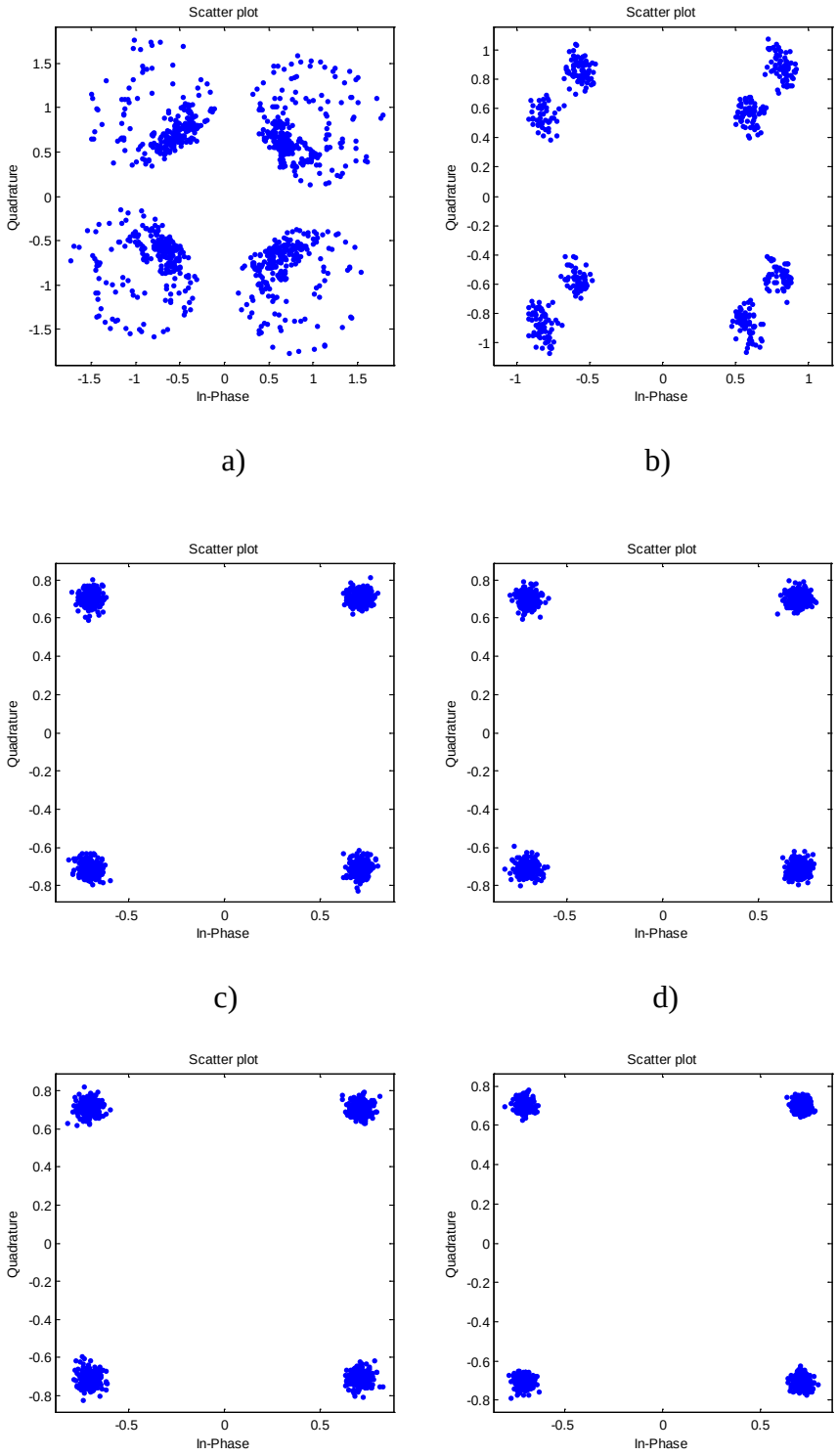

Figure 5-2 Constellations of a) Uncompensated b) Decoupled compensation c) Joint compensation d) Adaptive LMS compensation e) ACCC Frame 1 f) ACCC Frame 3, for QPSK, for Model 1

Figures 5-3 (a) to (f) show the constellations of the (a) uncompensated signal, (b) compensated signal for the decoupled compensation, (c) compensated signal for the joint compensation method, (d) compensated signal for the adaptive compensation method, (e) compensated signal of the first frame obtained by ACCC, and (f) compensated signal of the third frame obtained by ACCC. Also, in this figure, the modulation order is 64-QAM and the frequency-selective I/Q variation has been considered as Model 2. The constellation obtained for Model 2 is significantly different than that obtained for Model 1. Figure 5-3 (b) shows the signal constellation for the decoupled compensation. Like 5-1 (b), this one also shows a high level of distortion.

The constellation points are scattered all over in the X-Y plane. On the other hand, for the case of joint and adaptive LMS compensation schemes, less scattered points compared with the decoupled scheme have been observed. As the I/Q is higher, the incorrectly detected pilots are also higher for this case. These incorrectly detected pilots give incorrect estimations that result in distorted output. Figure 5-3 (e) shows the constellation for the proposed method for the first frame. As it can be seen, even the proposed method shows a lot of distortion for the first frame. However, as the consecutive frames arrive, it starts to deliver better results after the second or third frame. Figure 5-3 (f) shows the constellation for the third frame. This one shows the least scattered constellation points. Although the I/Q variation is higher, the proposed method is capable of mitigating the effects and demonstrates the least distortion.

Figures 5-4 (a) to (f) show the received signal constellation for the compensation schemes shown in Figure 5-3 for QPSK. The uncompensated QPSK signal for Model 2 in Figure 5-4 (a) is much more distorted than Model 1 shown in Figure 5-2 (a). Figures 5-4 (b) to (e) illustrate the constellation corresponding to the joint compensation, adaptive LMS compensation, and proposed ACCC compensation scheme for first frame, respectively. These three constellation plots show many scattered points. But the compensated signal for the proposed method obtained for the third frame shown in Figure 5-4 (f) shows the best results.

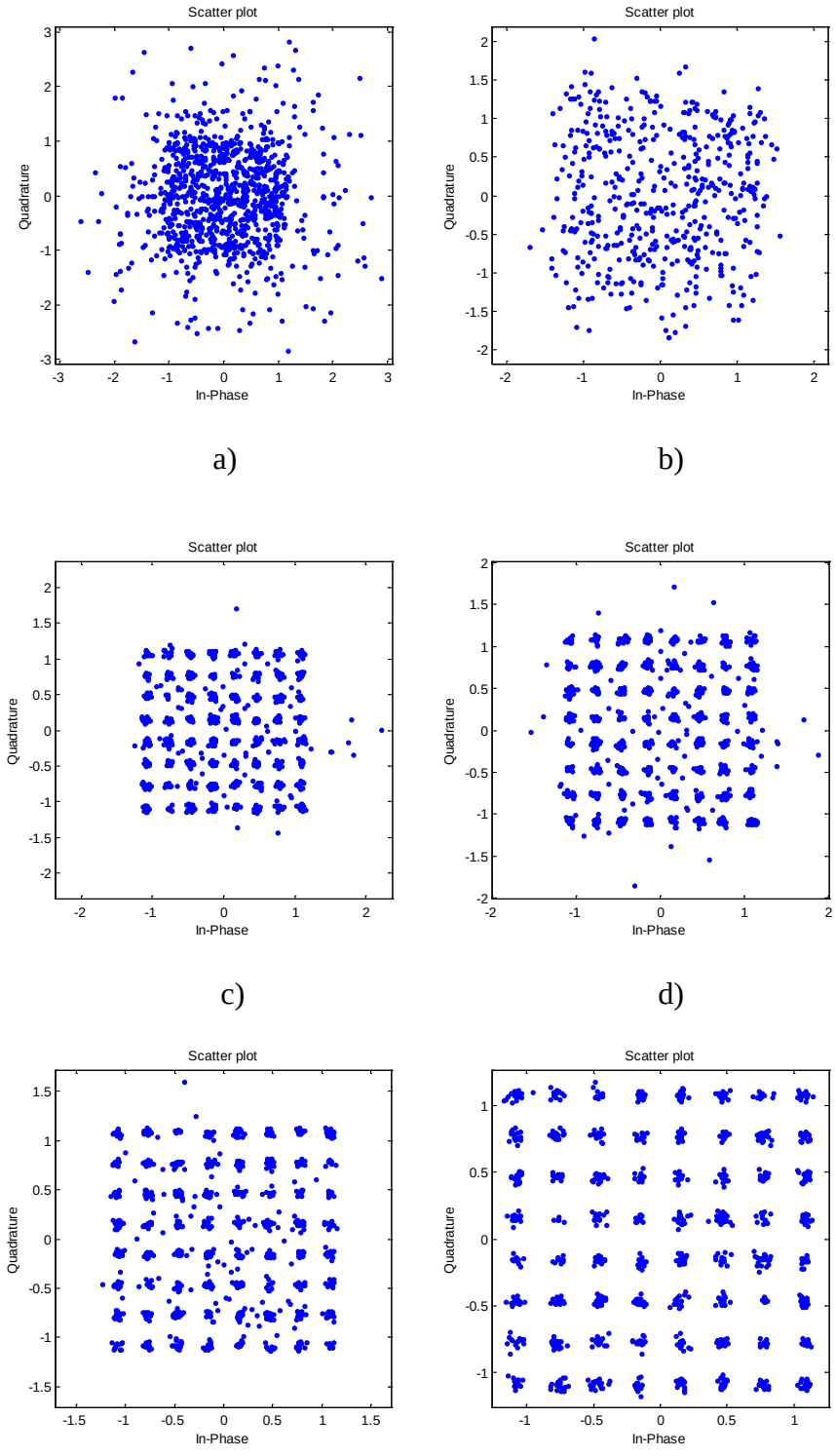

Figure 5-3 Constellations of a) Uncompensated b) Decoupled compensation c) Joint compensation d) Adaptive LMS compensation e) ACCC Frame 1 f) ACCC Frame 3 ,for 64-QAM, for Model 2

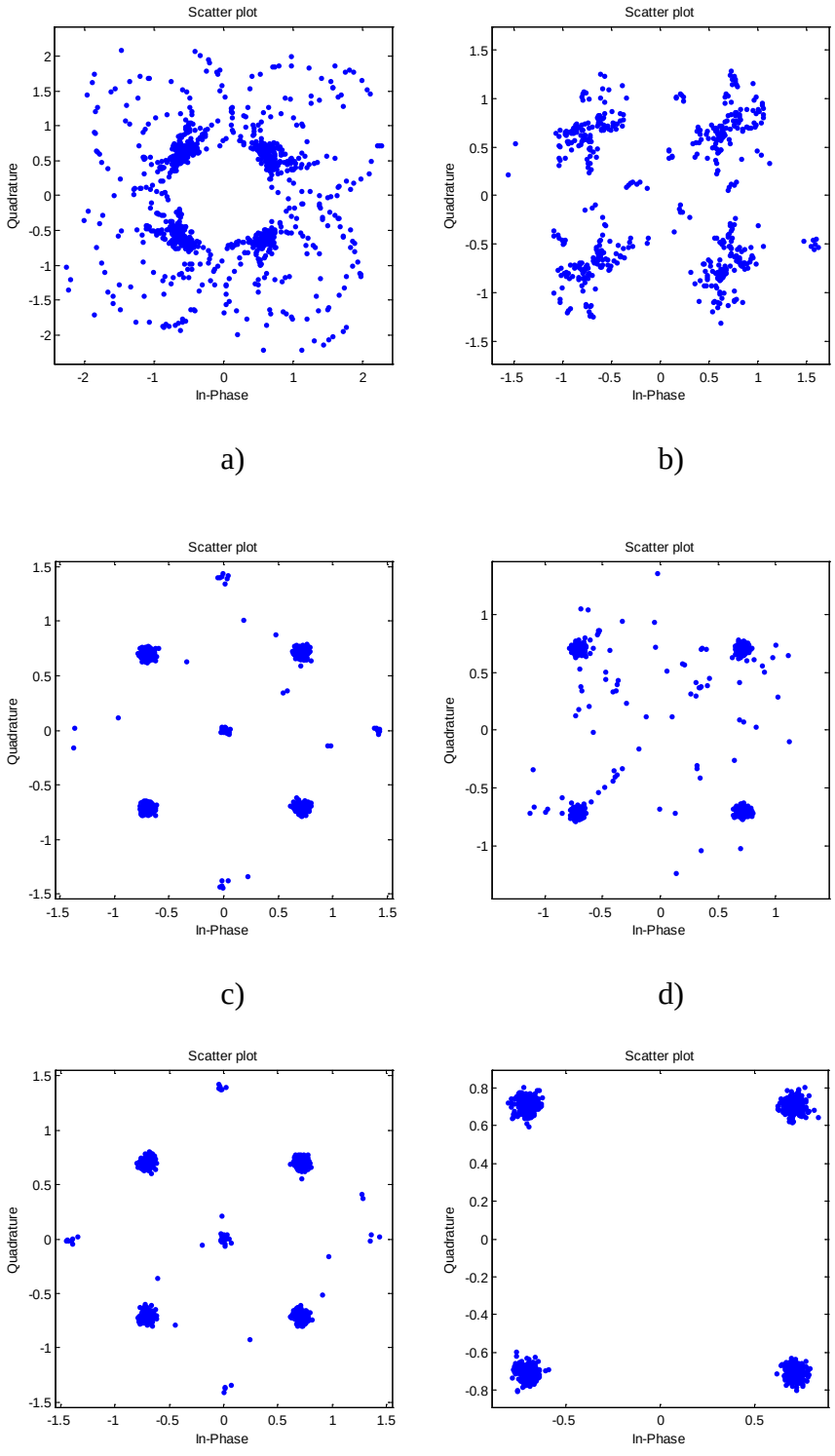

Figure 5-4 Constellations of a) Uncompensated b) Decoupled compensation c) Joint compensation d) Adaptive LMS compensation e) ACCC Frame 1 f) ACCC Frame 3, for QPSK, for Model 2

However, it is difficult to distinguish and compare the performance of the compensation schemes by observing the constellations. In the next section, EVM and the average SER have been shown for comparing these schemes.

- ***Error vector magnitude (EVM) for different schemes***

In this section the EVM structure for these methods have been shown for different compensation schemes. It should be noted that the EVM and SER performances have been shown for a 64-QAM modulation scheme only. Figure 5-5 shows the EVM curves for the compensation schemes stated above.

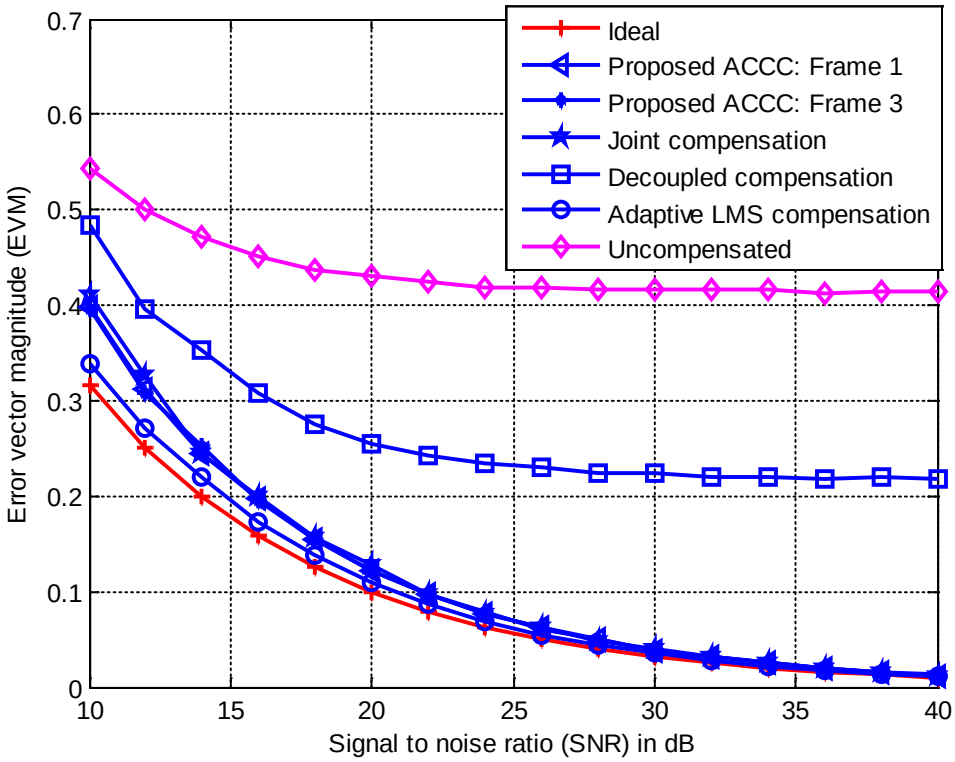

Figure 5-5 EVM for different I/Q imbalance compensation schemes, for Model 1, for 64-QAM

The legend 'Uncompensated' refers to the received signal that has not gone through any correction/compensation. The term 'Ideal' refers the ideal case where the received signal does not have any I/Q or channel distortion. The only distortion for the ideal case is the AWGN. The terms 'joint compensation', 'adaptive LMS compensation', and 'decoupled compensation' refer to the output received signal that has gone through

I/Q and channel mitigation by joint compensation, adaptive LMS compensation, and decoupled compensation, respectively. Moreover, the term ‘proposed ACCC: Frame 1’ and ‘proposed ACCC: Frame 3’ refer to the received signal corresponding to the first and third frames, respectively, after compensation and correction by the ACCC scheme. Also, in Figure 5-5, the frequency-selective I/Q has been chosen as Model 1. As in this model, the frequency-selective I/Q imbalance is not severe, and the EVM of all the schemes are close to the ‘Ideal’ condition, except the decoupled compensation scheme. The decoupled compensation scheme shows the highest EVM with a value of 0.23 for an SNR of 25 dB.

On the other hand, a different result has been observed in the case of Model 2, where the I/Q imbalance is high. The EVM performance for Model 2 has been shown in Figure 5-6. In this case, only the proposed ACCC scheme obtained for the third frame is close enough to the ideal condition.

The rest of the schemes produce large EVM. The adaptive compensation scheme shows the second best results after the ACCC scheme. The joint and decoupled methods show a large EVM. Even the proposed method shows higher EVM for the first frame. However, with time, performance increases by combining the pre-FFT correction and post-FFT compensation. Finally, by the end of the third frame, it achieves the lowest EVM of 0.08 for an SNR of 25 dB. Similar performance has been observed in the case of ‘Joint compensation’ and ‘Proposed ACCC: Frame 1’. For all compensation schemes, pilot subcarriers have been retrieved from the received signal rather than assuming that all pilots are perfectly detected. Therefore, if one pilot gets incorrectly detected it generates several incorrect interpolated values that leads to incorrect estimation. Thus, the incorrectly estimated pilots may be serious in cases like this. However, for the proposed method, a pre-FFT correction is performed before the pilot detection. Thus, as the correction progresses, the probability of obtaining incorrectly estimated pilots become less and less. Also, from Figure 5-6 it can be observed that the adaptive compensation technique starts to show slightly better results for low SNR. As the SNR progresses to more than 12 dB, the EVM corresponding to the ACCC becomes the least.

For the adaptive compensation scheme, at least 60 OFDM symbols containing pilot tones are required. The pilot tones can be placed in an equidistant space, and the parameters for the non-pilot indices are obtained by linear interpolation. Also a minimum number of 16 pilots are required for each symbol to make the system functional. Therefore, in one frame a minimum number of 60 x 16 is required (i.e., 960 pilot subcarriers).

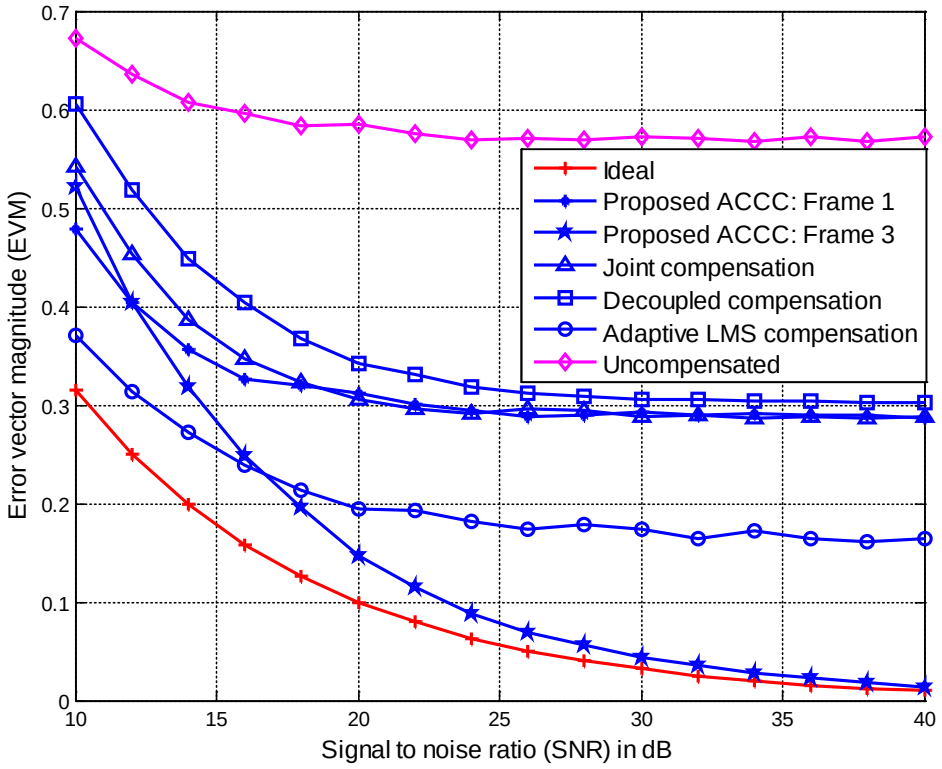

Figure 5-6 EVM for different I/Q imbalance compensation schemes, for Model 2, for 64-QAM

Whereas in the case of the ACCC scheme, only two OFDM symbols, each containing 16 symbols (i.e., 32 pilot subcarriers), are enough to mitigate the distortion and provide the same results. That means the ACCC scheme requires 30 times fewer pilot subcarriers than the adaptive scheme to obtain the same results. Again, when the I/Q is high, the adaptive LMS scheme saturates at an EVM of 0.3. Therefore, in the data throughput perspective, the proposed method requires fewer pilot subcarriers and is capable of I/Q mitigation even when the I/Q variation is high such as in Model 2.

- ***Symbol error rate (SER) for different schemes***

The effectiveness of the compensation schemes is further studied using the SER performance. The SER performance demonstrates a similar outcome as the EVM performance. Figure 5-7 shows the comparative SER of the received signal after compensation by joint compensation, adaptive LMS compensation, decoupled compensation, and the proposed compensation methods for Model 1.

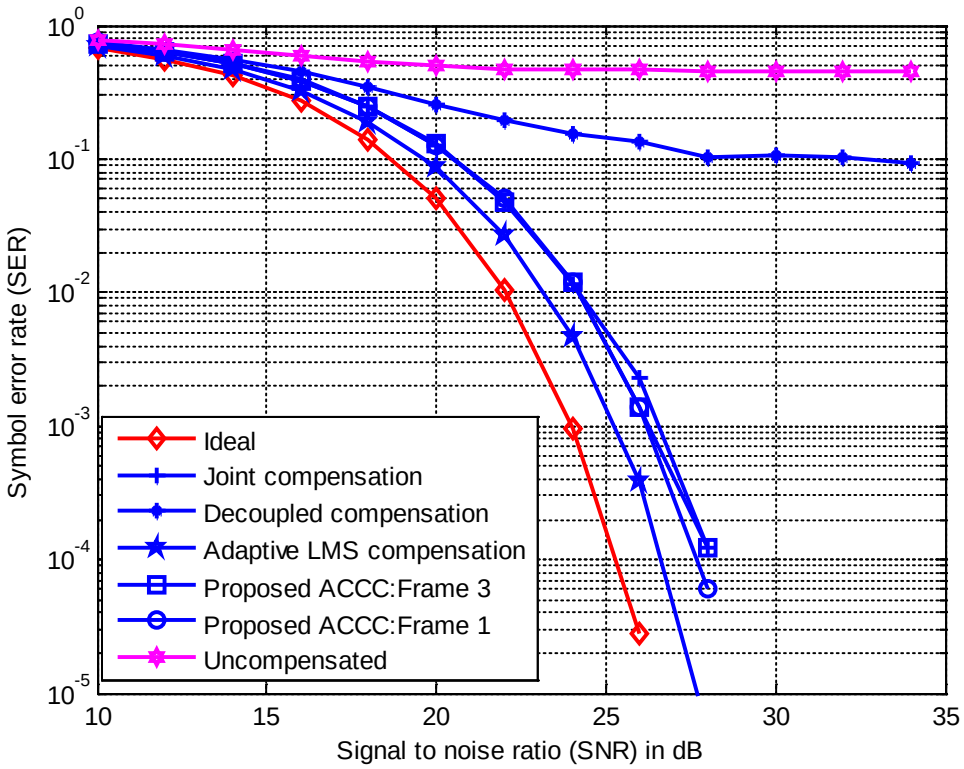

Figure 5-7 SER for different I/Q imbalance compensation schemes, for Model 1, for 64-QAM

The first and third frames of the proposed compensation method have been presented as well. The legends are similar to those in Figure 5-5. Figure 5-7 contains all the results for the 64-QAM modulations. The SER performance is similar to the EVM performance shown in Figure 5-5 for Model 1. It has been observed that the decoupled scheme shows the highest SER of 10^{-1} at an SNR of 30 dB. All the other schemes show good performances. The SER for the proposed method for the first and the third frames is almost equal. The joint compensation also coincides with them. The adaptive

compensation shows better results than the joint and the proposed compensation schemes. For an SER of 10^{-3}, the SNR corresponding to the adaptive LMS compensation is 1 dB degraded compared to the 'Ideal' SER with no I/Q and channel. For the ACCC scheme, the SNR is 2 dB degraded compared to the ideal SER at a specific SER of 10^{-3}. Therefore, the adaptive LMS scheme achieves 1 dB less degradation than the ACCC scheme. Following, Figure 5-8 portrays the SER performance for all compensation schemes for Model 2 for the 64-QAM modulations.

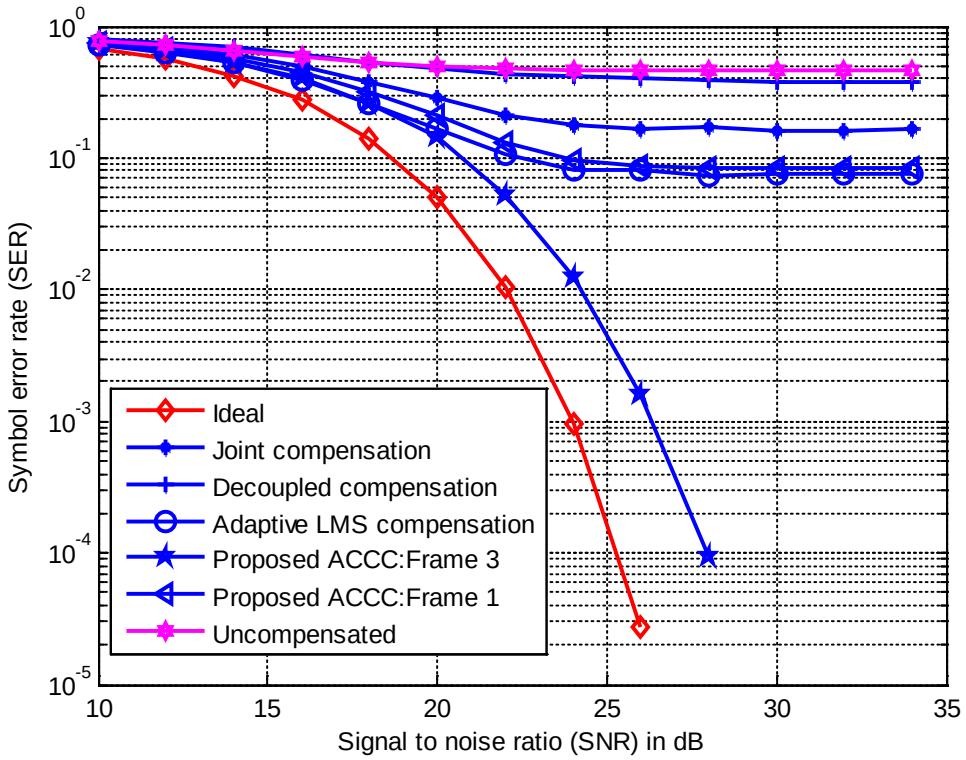

Figure 5-8 SER for different I/Q imbalance compensation schemes, for Model 2, for 64-QAM

In this case, only the graph representing the 'Proposed ACCC: Frame 3' performs close to the 'Ideal' condition. For the rest, the SER curves saturate at/before 10^{-1}. The decoupled compensation scheme shows the highest SER. The joint compensation shows better performance than the decoupled one, yet is far from the acceptable range. After, the proposed ACCC method's first frame obtains a SER that is lower than the joint compensation scheme. The SER corresponding to the adaptive LMS

compensation scheme is slightly better than that of the first frame of the proposed ACCC scheme. But the third frame of the ACCC scheme shows huge improvement, and the output SNR is 2 dB degraded compared to the ideal curve for an SER of 10^{-3}.

5.5.2 Performance comparison under various frequency-flat gain and phase

Next, the schemes have been studied for different frequency-flat gain and phase imbalances. Figure 5-9 shows the SER of the received signal compensated for by the decoupled and joint compensation methods. The frequency-flat gain and phase have been varied and the frequency-selective gain and phase have been chosen as Model 1. The legend '$g = 1.2$; ph $= 10$: decoupled' refers the received output signal after compensation by the decoupled compensation scheme for a frequency-flat gain and phase of $g = 1.2$ and $\varphi = 10^{o}$. The terms 'g' and 'ph' in the legends in Figure 5-9 refer to the gain and phase imbalance values. Similarly, the legend '$g = 1.2$; ph $= 10$: joint' refers to the SER of the received signal after compensation by the joint compensation scheme in the presence of a frequency-flat gain of $g = 1.2$ and phase of $\varphi = 10^{o}$.

From Figure 5-9, it has been observed that even when the gain and phase imbalance is as low as $g = 1.02$ and $\varphi = 2^{o}$ the SNR corresponding to the decoupled compensation is still almost 10 dB degraded compared to the ideal SER curve, for a specific SER of 10^{-2}. However, for this combination of gain and phase, the SER curve has not been saturated with the increment of SNR. As the g and φ are increased, the SER of the decoupled compensation method increases as well. For the highest gain and phase combination, which is $g = 1.2$ and $\varphi = 10^{o}$, the SER curve saturates before 10^{-1}, and it remains far from the ideal (no I/Q and channel condition).

On the other hand, the joint compensation scheme shows good results. The SER curve is almost same for all gain and phase combinations for the joint compensation scheme. Moreover, the resultant SER is close to the ideal SER curve. Thus, it is observed that even the frequency-flat I/Q has been increased, while the joint compensation's

performance remains unchanged. Also, if the frequency-selective gain and phase is not very high, then the joint compensation technique is capable of mitigation of I/Q and channel. The SNR degradation is 2 dB compared to the ideal SER curve, for a specific SER of 10^{-3}, whereas the decoupled compensation works only when both frequency-flat and frequency-selective I/Q is low.

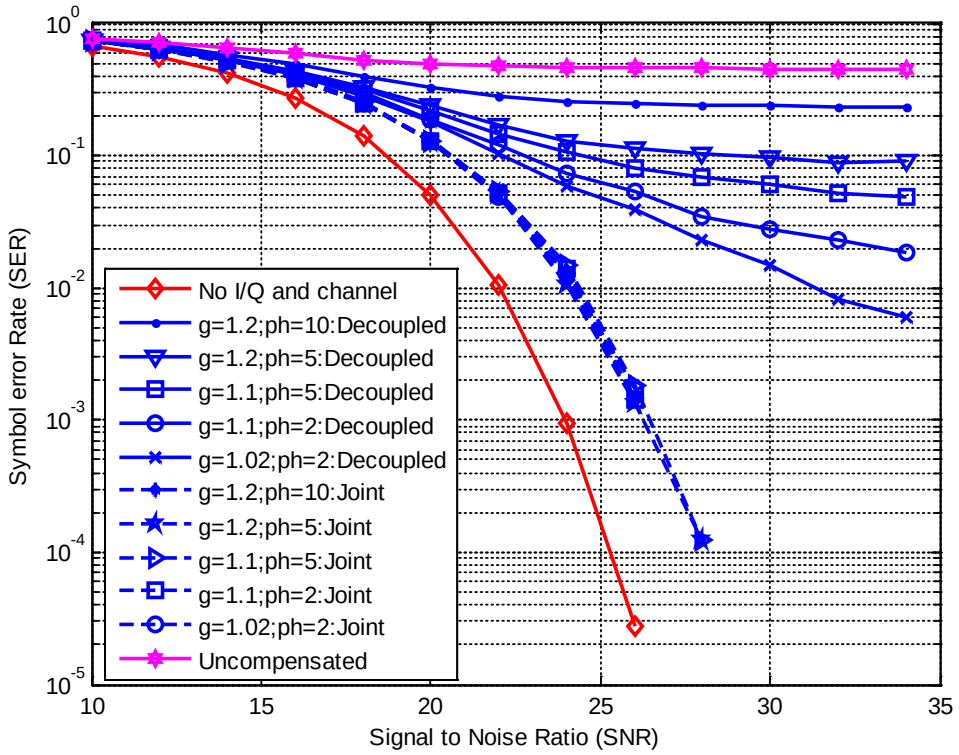

Figure 5-9 SER for different frequency-flat gain and phase for Model 1, for joint and decoupled compensation schemes

Even for the low I/Q, the SER achieved is higher than the ideal values. The SERs for the decoupled and the joint compensation schemes for Model 2 have been presented in Figure 5-10. It has been observed that for the decoupled compensation, the SER curves for all combinations of gains and phases have saturated before 10^{-1}. Also, they are close to the SER of the uncompensated signal. The SER curve for a lower gain and phase, such as $g = 1.02$ and $\varphi = 2^o$, shows slightly better results than the SER curve with a higher gain and phase combination, such as $g = 1.2$ and $\varphi = 10^o$. For joint compensation, the SER is close to the ideal for the lower combination of gain and

phase, such as $g = 1.02$ and $\varphi = 2^o$; $g = 1.1$ and $\varphi = 2^o$. Any gain and phase combination higher than this results in higher SER. The SER corresponding to $g = 1.1$ and $\varphi = 5^o$ is almost 10 dB degraded compared to the ideal curve, for an SER of 10^{-2}. For $g = 1.2$ and $\varphi = 5^o$, the SER curve becomes saturated at 10^{-1}. For the highest frequency-flat I/Q combination, $g = 1.2$ and $\varphi = 10^o$, the SER curve becomes similar to the curve of the uncompensated signal.

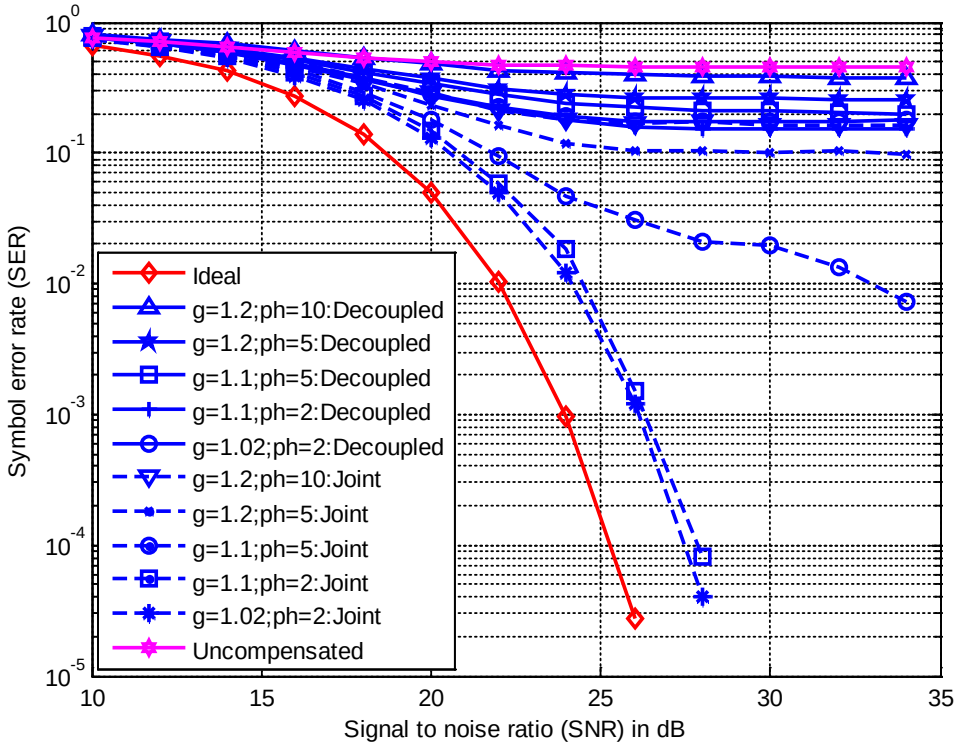

Figure 5-10 SER for different frequency-flat gain and phase for Model 2, for joint and decoupled Compensation schemes

Figure 5-11 presents the SER curves obtained after compensation by the adaptive LMS compensation and proposed ACCC schemes for different combinations of frequency-flat gain and phase for Model 1. Similarly, Figure 5-12 presents SER corresponding to the adaptive LMS and ACCC scheme for Model 2. For the ACCC scheme, the SER has been obtained for the third frame.

In Figure 5-11, both of the adaptive compensation and ACCC schemes show good results. The SER curves for both methods stay close to the ideal condition for all I/Q gain and phase combinations. The adaptive curves show a slightly better result. For an SER of 10^{-3}, the SNR for the adaptive scheme is approximately 1 dB less degraded compared to the proposed ACCC method. The legend '$g = 1.2;\ \mathrm{ph} = 10$: adaptive' refers to the received output signal after compensation by the adaptive LMS compensation scheme for a frequency-flat gain and phase of $g = 1.2$ and $\varphi = 10^{o}$.

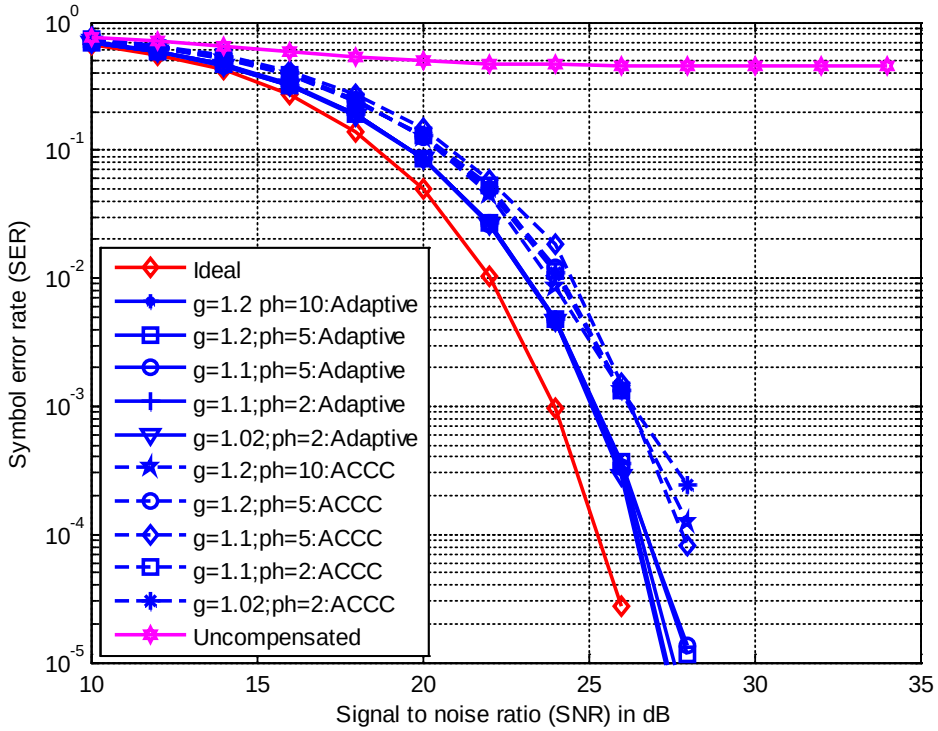

Figure 5-11 SER for different frequency-flat gain and phase for Model 1, for adaptive LMS and proposed ACCC schemes.

For Figure 5-12, the adaptive LMS scheme does not able to compensate when the frequency-flat gain and phase is as high such as $g = 1.2, \varphi = 10^{o}$ and g= $1.2, \varphi = 5^{o}$. On the other hand, the proposed method remains unchanged for all the combination of g and φ.

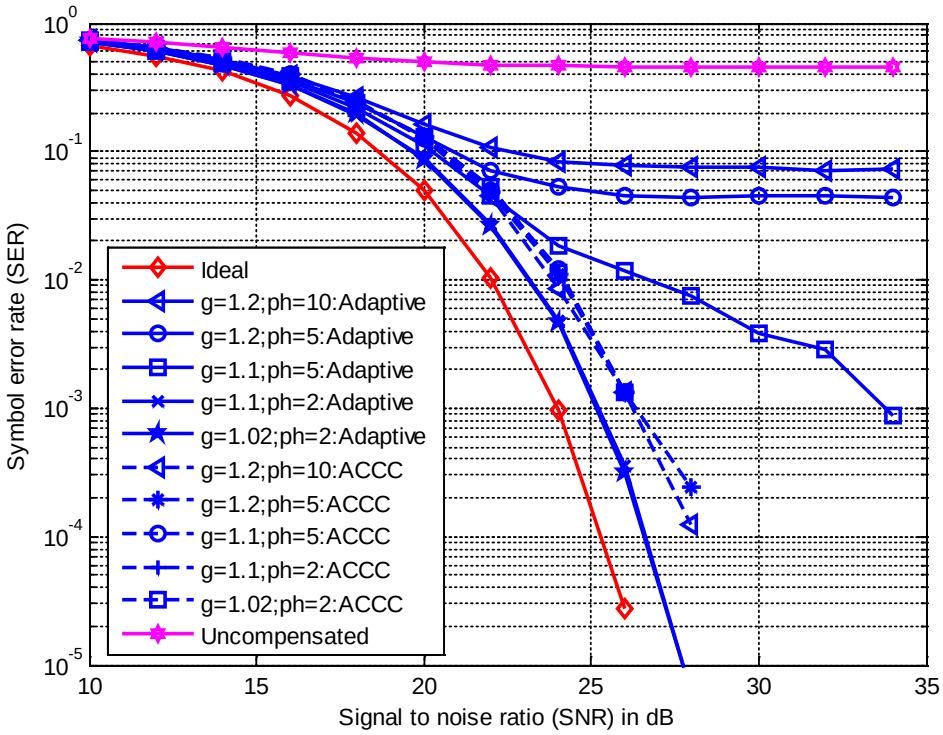

Figure 5-12 SER for different frequency-flat gain and phase for Model 2, for adaptive LMS and proposed ACCC schemes.

However, it has been observed, when $g = 1.02$ and $\varphi = 2^o$, the adaptive LMS method shows better result than the ACCC method. But the ACCC remains consistent for all the combinations of frequency-flat I/Q imbalance.

5.5.3 Performance comparison under different IRR level

In this section, the all the schemes stated above have been compared for different IRR levels. Three different levels of IRR have been chosen, which correspond to low I/Q, typical/moderate I/Q, and high I/Q. These are stated below:

- ***Low I/Q:***

For the low I/Q, the frequency-flat gain and phase have been chosen as $g = 1.02$ and $\varphi = 2^o$, and frequency-selective gain and phase have been chosen as Model 1. The IRR varies from 23 to 30 dB with an average value of 25.93 dB. The IRR for this has

been shown in Figure 5-13. The SER performance of the compensation schemes with low I/Q value has been shown in Figure 5-14. It has been observed from the SER performance that the adaptive LMS compensation performs the best.

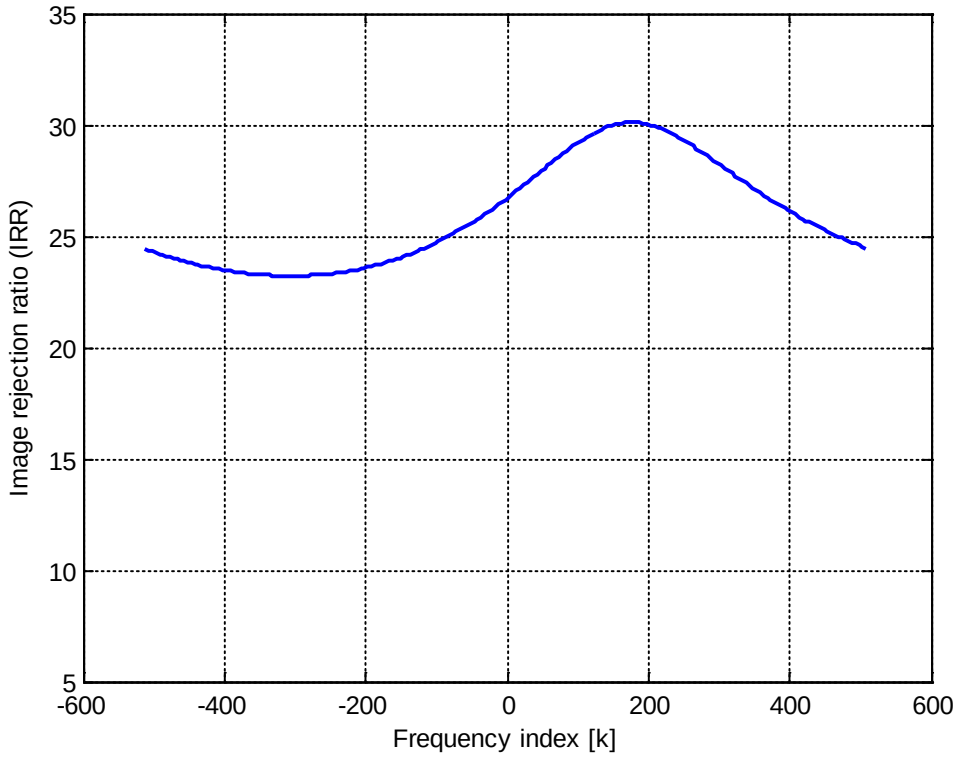

Figure 5-13 IRR corresponding to low I/Q

The SNR of the proposed ACCC and joint compensation methods are just 1.5 dB more degraded than the adaptive LMS method for an SER of 10^{-3}. For an SER of 10^{-3}, the SNR corresponding to the decoupled compensation scheme is almost 10 dB more degraded than the ideal SER curve.

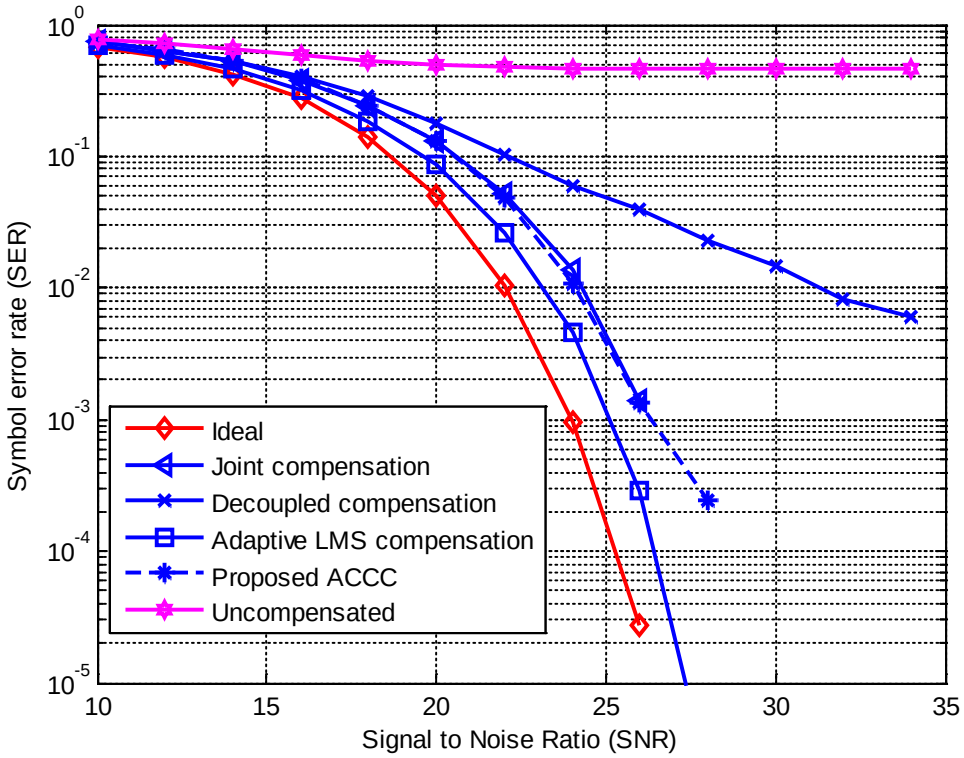

Figure 5-14 SER performance under low I/Q

- ***Moderate I/Q:***

For the moderate I/Q, the frequency-flat gain and phase have been chosen as $g = 1.2$ and $\varphi = 10^{o}$, and frequency-selective I/Q has been chosen as Model 2. The variation of IRR over the signal bandwidth is 10 to 32 dB with an average IRR of 17.1 dB. The IRR corresponding to the moderate I/Q has been shown in Figure 5-15.

The SERs obtained by means of different compensation schemes for this I/Q level have been shown in Figure 5-16.

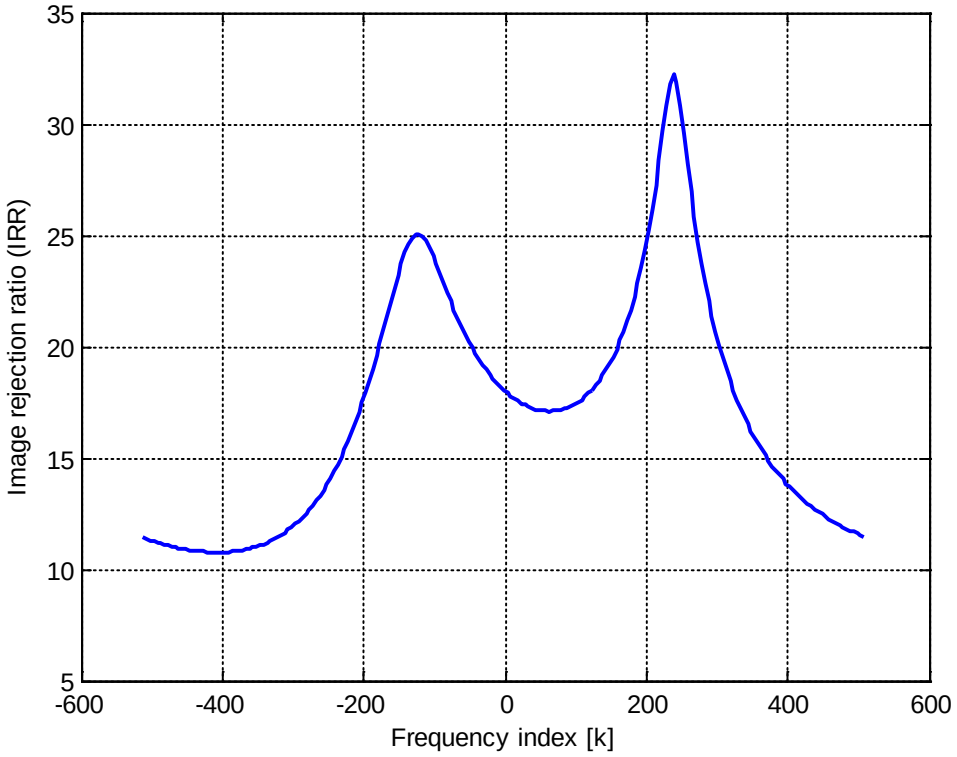

Figure 5-15 IRR corresponding to moderate I/Q

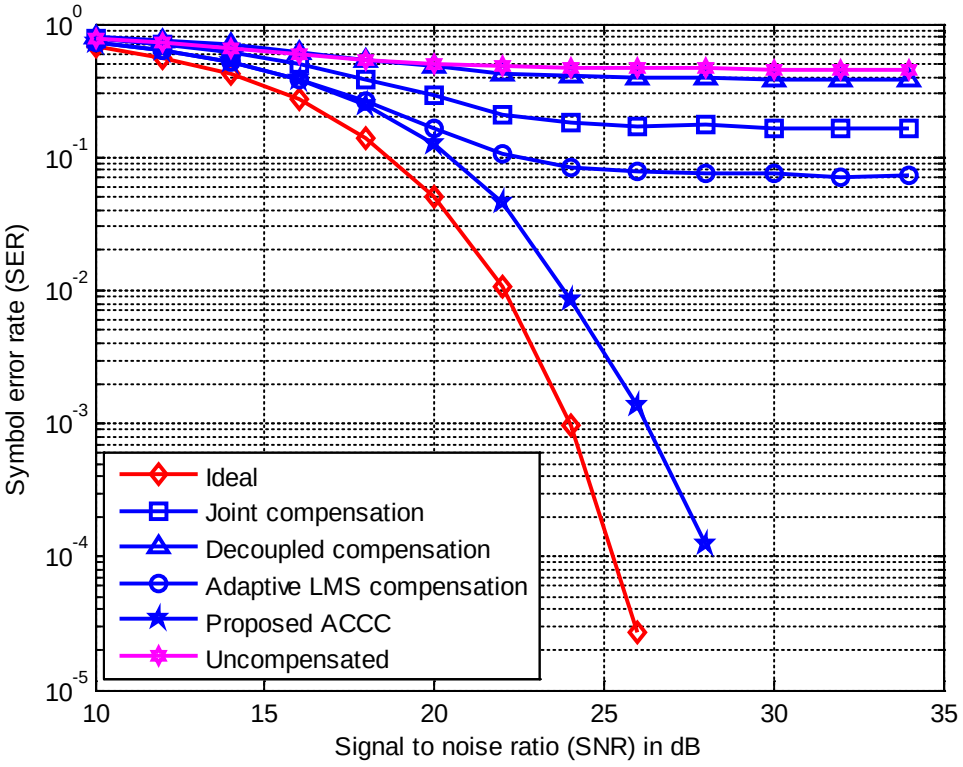

Figure 5-16 SER performance under moderate I/Q

The SER corresponding to the ACCC scheme has been taken for the third OFDM frame. From the SER performance under moderate I/Q, it has been shown that none of the schemes except the proposed ACCC could achieve an acceptable SER result. The SNR for the ACCC scheme is 2 dB higher than the ideal SER for an SER of 10^{-3}. The SER curves corresponding to the rest of the schemes have saturated before 10^{-1}. The adaptive LMS scheme shows slightly better result than the SER corresponding to the joint and decoupled compensations.

- ***High I/Q***:

For the high I/Q level, the frequency-flat gain and phase have been chosen to be $g = 1.7$ and $\varphi = 30^{o}$, and frequency-selective I/Q has been chosen as Model 2. The variation of IRR over the signal bandwidth is 5 to 12 dB and the average IRR is 8.6 dB. The IRR has been shown in Figure 5-17, and the SER performance has been shown in Figure 5-18.

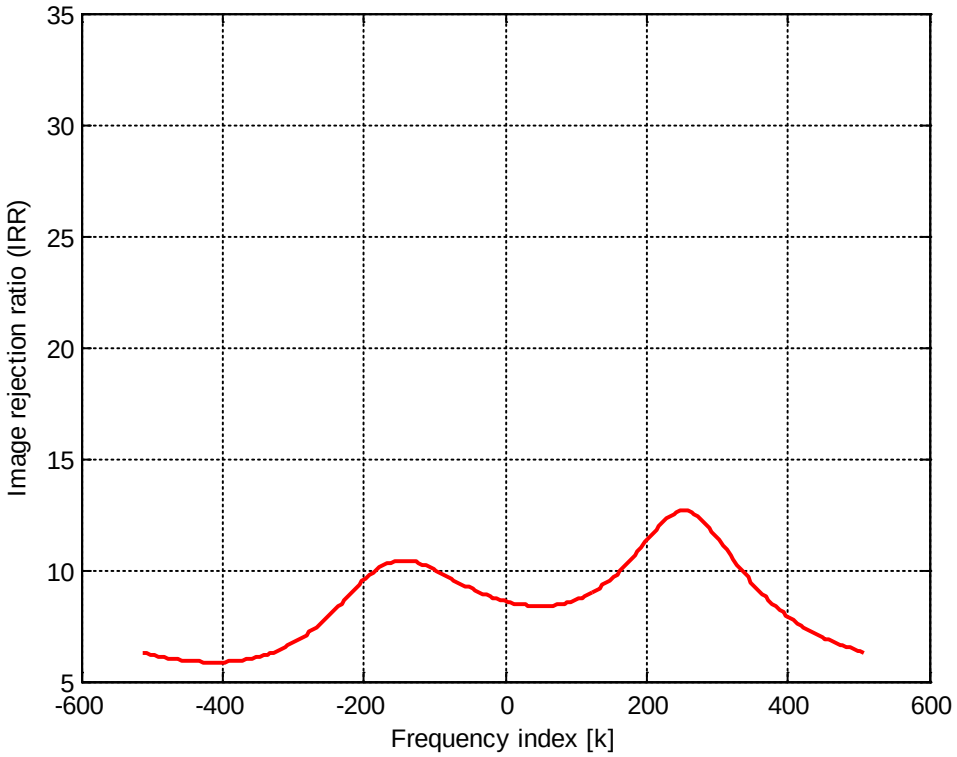

Figure 5-17 IRR corresponding to high I/Q

Again, it has been observed that only the proposed ACCC method is capable of achieving the lowest SER of 10^{-4} for 30 dB SNR. The SER curves corresponding to the other schemes have an SER value higher than 10^{-1}. The SER of the adaptive LMS scheme shows a slightly better result than the joint and decoupled compensation methods.

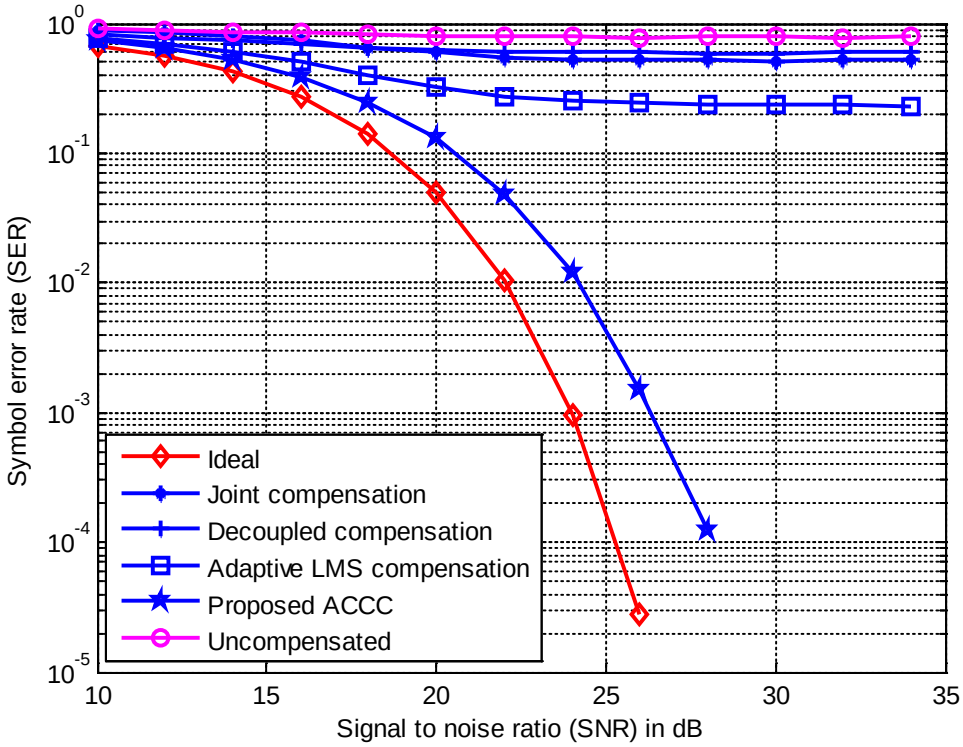

Figure 5-18 SER performance under high I/Q

By observing the SER for Figure 5-14, Figure 5-16, and 5-18, it has been observed that almost all of the schemes are capable of mitigating the I/Q and channel for low I/Q conditions. The reason for the decoupled method to give significantly higher error is because the I/Q parameters considered in this thesis are very high compared to the I/Q imbalance considered in [15]. The basis of the scheme in [15] is established on the assumption of $V_m[k] \ll U_m[k]$ and $U_m[k] \simeq 1$, which is not valid when I/Q is very high. The adaptive LMS performs the best in this case. However, for moderate and high I/Q conditions, the ACCC scheme outperforms all other schemes.

5.5.4 Performance comparison under different number of pilots

Figure 5-19 to Figure 5-22 present the SER in presence of different numbers of pilots for joint compensation, decoupled compensation, adaptive LMS compensation, and the ACCC scheme, respectively. Only Model 1 has been considered for this case. Also the frequency-flat gain and phase for these figures are chosen as $g = 1.2$ and $\varphi = 10^o$. The reason for choosing Model 1 is that when the frequency-flat I/Q is high and Model 2 is in effect, none of the schemes except the ACCC is capable of mitigating the I/Q and channel. Even if a large number of pilots are used, the result does not change at all. Model 1 has been considered so that the minimum number of pilots required for each scheme can be observed.

In Figure 5-19, the SER obtained for the joint compensation scheme for different numbers of pilots has been presented. The joint compensation scheme performs consistently for different numbers of pilots. The minimum number of pilots for getting an acceptable SER is 16. Less pilots create distortion and result in high SER. If 8 pilot subcarriers are used, then the SER becomes high and saturates before 10^{-2}.

Figure 5-20 represents the SER for the decoupled compensation method. As the decoupled compensation method fails to mitigate when $g = 1.2$ and $\varphi = 10^o$ even in Model 1, no matter how many pilots are used the results would always be the same. For different numbers of pilots, it illustrates almost the same results. All the curves are close to the curve of the uncompensated signal.

Figure 5-21 represents the SER for the received signal obtained after compensation by the adaptive LMS compensation scheme. It shows almost the same results as the joint compensation method shown in Figure 5-19. The SERs are quite consistent for up to 16 pilots. Pilots less than that create distortions. Figure 5-22 represents the SER for the third frame of the received signal compensated for by the ACCC scheme.

The ACCC scheme is also capable of mitigating the I/Q and channel with the presence of a minimum of 16 pilots. While using eight pilots, high distortion has resulted, and high SER has been observed.

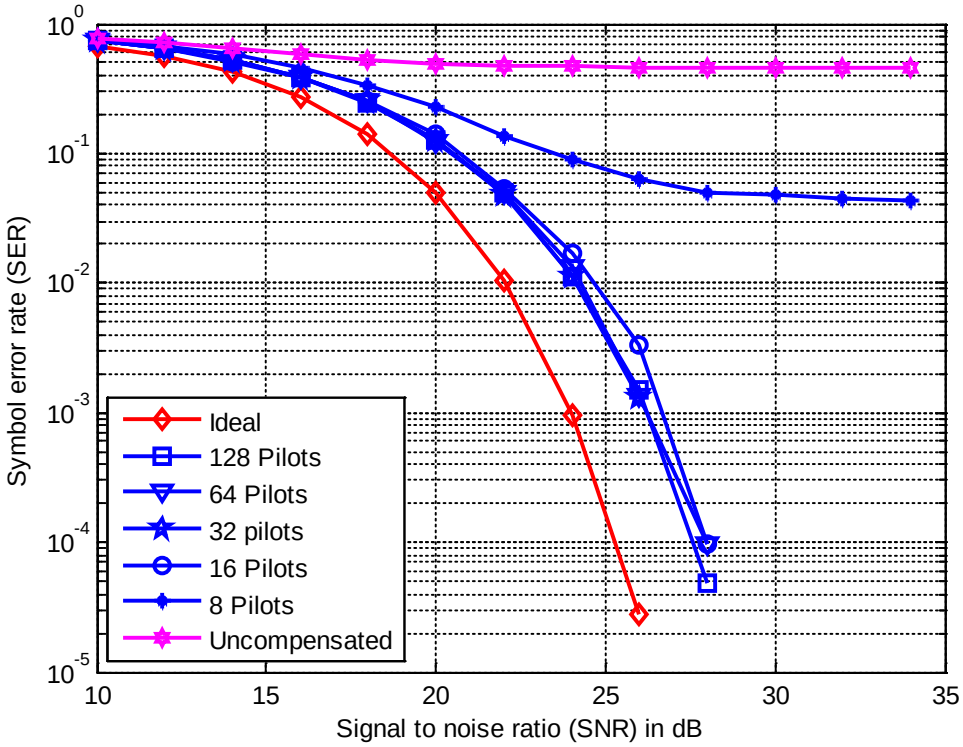

Figure 5-19 SER for different pilots for Model 1 for the joint compensation scheme

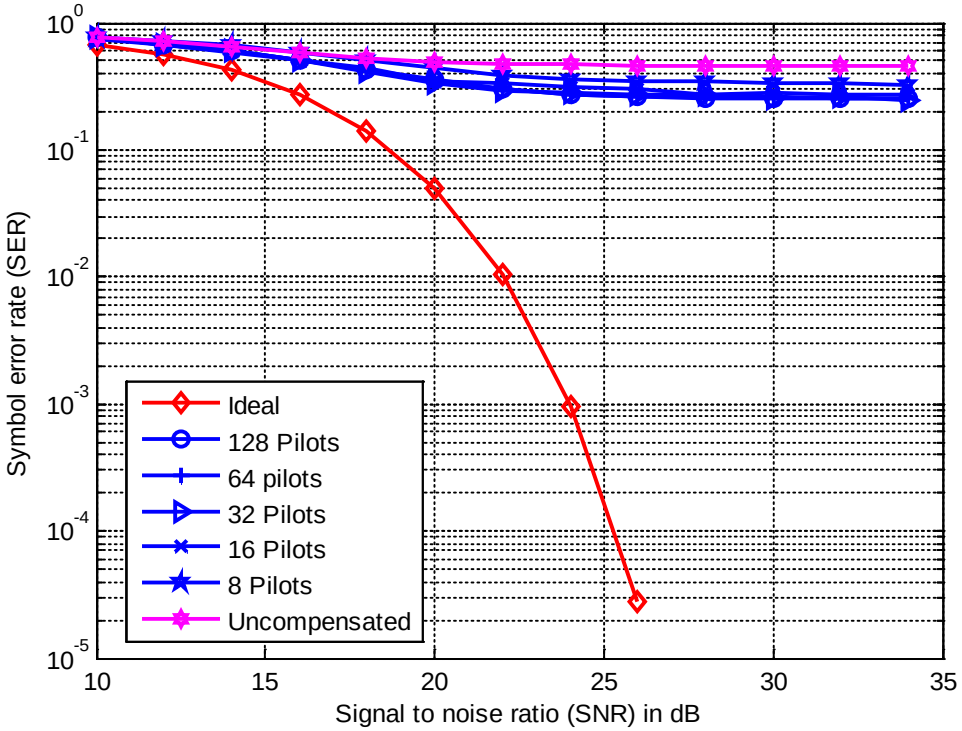

Figure 5-20 SER for different pilots for Model 1 for the decoupled compensation scheme

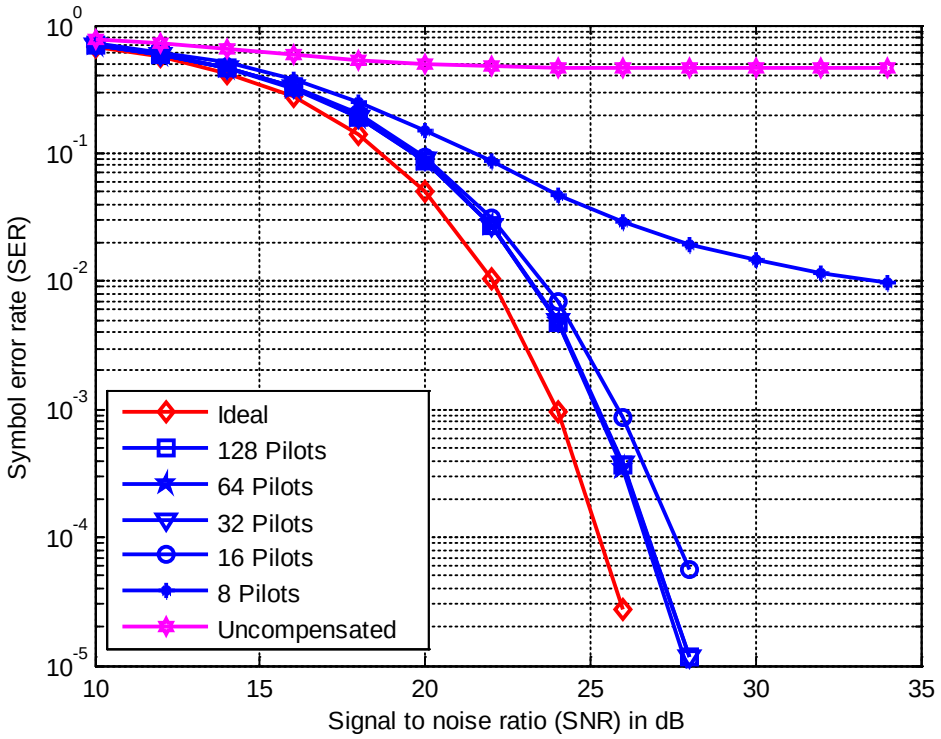

Figure 5-21 SER for different pilots for Model 1 for the adaptive LMS compensation scheme

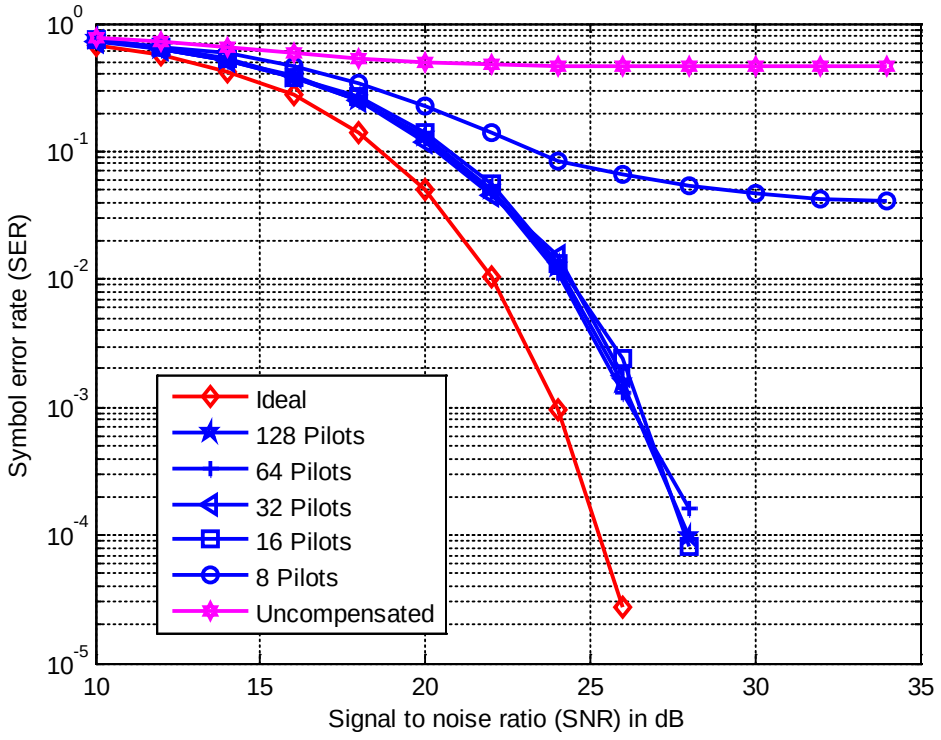

Figure 5-22 SER for different pilots for Model 1 for the proposed ACCC scheme

The SERs shown in Figure 5-19 to Figure 5-22 show that all of the methods stated above need at least 16 pilots in order to be functional. As for Model 1, the chances of obtaining an incorrect pilot tone are rare, so even 16 pilots are enough to complete the estimation and interpolation. In the case where the pilots are detected incorrectly, the estimation and the interpolation results will be erroneous.

5.6 Summary

A performance comparison of three different I/Q imbalance and channel compensation schemes has been studied. These schemes have been compared with the ACCC scheme under several conditions to observe the robustness of the proposed scheme. The proposed method works consistently under different conditions when many other compensation schemes provide distorted outputs. Also, the proposed method provides the best results even in the presence of high I/Q combinations.

CHAPTER 6

CORRECTION AND COMPENSATION OF I/Q IMBALANCE FOR SINGLE CARRIER MODULATIONS

6.1 Introduction

This chapter presents compensation and correction schemes for I/Q imbalance and channel in the case of single carrier modulation. Two compensation/correction methods have been adopted; method 1 is the time domain correction and method 2 is the frequency domain compensation. Both of these methods use the same technique to estimate the unknown channel and I/Q parameters. For the time domain correction method, an adaptive approach, which involves first correcting for the I/Q imbalance before the signal is compensated for due to the effect of a multipath channel, has been proposed. Estimations of the I/Q imbalance and channel parameters are carried out with the aid of a common reference signal. The system uses a feedback technique to send the estimated gain and phase imbalances to complete the correction process before equalizing the channel. If the I/Q imbalance can be corrected before equalization, the equalizer will perform better and converge much quickly. Briefly, this technique involves correcting the I/Q imbalance parameters and equalizing the channel afterwards

On the other hand, in the case of the frequency domain compensation method, a technique is adopted incorporating adaptive estimation and compensation to mitigate the combined effects of I/Q imbalance and multipath channel on the received signal.

Estimation of the channel and I/Q imbalance parameters is performed in the time domain using a training sequence similar to the time domain method. Based on the estimated I/Q imbalance and channel parameters, a joint compensation for the I/Q and the channel are performed in the frequency domain. In this chapter, only frequency-flat I/Q imbalance has been considered.

6.2 I/Q imbalance for the single carrier modulation

The general model of I/Q imbalance has been described in Section 3.4. Recalling equation (3.25), the received signal in the time domain suffering in I/Q imbalance and channel can be expressed as follows:

$$y[n] = u[n] \otimes h[n] \otimes x[n] + v[n] \otimes h^*[n] \otimes x^*[n] + u[n] \otimes \varepsilon[n] + v[n] \otimes \varepsilon^*[n] \quad (6.1)$$

where,

$$u[n] = \frac{g a_I[n] + e^{-j\varphi} a_Q[n]}{2}$$

and

$$v[n] = \frac{g a_I[n] - e^{j\varphi} a_Q[n]}{2}$$

The propagation paths are denoted as l where, $l = 1,2,3 \ldots\ldots L$, and L corresponds to the total number of propagation paths. In the case of the frequency-flat I/Q imbalance, $a_I[n] = a_Q[n] = 1$, thus the I/Q parameters $u[n]$ and $v[n]$ will be replaced by u and v, which are given as:

$$u = \frac{g + e^{-j\varphi}}{2} \quad (6.2)$$

and

$$v = \frac{g - e^{j\varphi}}{2}. \quad (6.3)$$

Thus equation (6.1) can be written for the frequency-flat case as:

$$y[n] = uh[n] \otimes x[n] + vh^*[n] \otimes x^*[n] + u\,\varepsilon[n] + v\varepsilon^*[n] \tag{6.4}$$

or

$$y[n] = u\sum_{l=1}^{L} h[l]x[n-l+1] + v\sum_{l=1}^{L} h^*[l]x^*[n-l+1] + u\,\varepsilon[n] + v\,\varepsilon^*[n] \tag{6.5}$$

Substituting the values of u and v in equation (6.4), we obtain,

$$\begin{aligned} y[n] = {} & \tfrac{1}{2}g\{(h[n] \otimes x[n] + \varepsilon[n]) + (h[n] \otimes x[n])^* + \varepsilon^*[n]\} \\ & + \frac{1}{2}cos\varphi\{(h[n] \otimes x[n] + \varepsilon[n]) - (h[n] \otimes x[n] + \varepsilon[n])^*)\} \\ & - \tfrac{1}{2}jsin\varphi\{(h[n] \otimes x[n] + \varepsilon[n]) + (h[n] \otimes x[n] + \varepsilon[n])^*\} \end{aligned} \tag{6.6}$$

Substituting $r[n] = h[n] \otimes x[n] + \varepsilon[n]$, we get,

$$\begin{aligned} y[n] = {} & \frac{1}{2}\{g(r[n] + r^*[n])\} + \frac{1}{2}\{cos\varphi(r[n] \\ & - r^*[n])\} - \tfrac{1}{2}\{jsin\varphi(r[n] + r^*[n])\} \end{aligned} \tag{6.7}$$

Expressing $y[n]$ in equation (6.6) in terms of its real component, $y_I[n]$, and imaginary component, $y_Q[n]$, we obtain:

$$y_I[n] = gr_I[n] \tag{6.8}$$

and

$$y_Q[n] = cos\,\varphi\, r_Q[n] - sin\,\varphi\, r_I[n] \tag{6.9}$$

Equations (6.8) and (6.9) can be written in matrix form as:

$$\begin{bmatrix} y_I[n] \\ y_Q[n] \end{bmatrix} = \begin{bmatrix} g & 0 \\ -sin\,\varphi & cos\,\varphi \end{bmatrix} \begin{bmatrix} r_I[n] \\ r_Q[n] \end{bmatrix} \quad (6.10)$$

In this case, if the I/Q imbalance parameters, g and φ are known, then the received signal $r[n]$ can be found by performing an inverse matrix operation on equation (6.10), so that

$$\begin{bmatrix} \hat{r}_I[n] \\ \hat{r}_Q[n] \end{bmatrix} = \frac{1}{gcos(\varphi)} \begin{bmatrix} cos\varphi & 0 \\ sin\,\varphi & g \end{bmatrix} \begin{bmatrix} y_I[n] \\ y_Q[n] \end{bmatrix} \quad (6.11)$$

Equation (6.11) offers us a method of recovering the original received signal, $r[n]$, from the I/Q imbalance corrupted signal $y[n]$. It is shown in the next section that the values of I/Q imbalance parameters, g and φ, required for equation (6.11) can be estimated from the I/Q imbalance corrupted signal $y[n]$.

6.3 Method 1: An Adaptive time domain estimation and correction method

This section presents the adaptive time domain method for I/Q and channel mitigation[2]. In this method, both I/Q imbalance and multipath channel parameters have been estimated in the time domain according to the functional block diagram of Figure 6-1. Its operation is based on the transmit data being arranged in a frame structure as shown in Figure 6-2. In this case, each data frame begins with a pre-specified sequence, referred to here as the reference signal, and followed by information data. The same reference signal is used in estimating both the I/Q imbalance and channel parameters. The simulation setup used for this method has been presented in Figure 6-3.

[2] The contents of this section has been published in a conference: IEEE Australian Communications Theory Workshop *(AUSCTW 2014)*, February 2014, Sydney, Australia.

Each frame contains training symbols followed by data symbols. Let $n = 1,2,3 \ldots . \acute{N}$ represent the indices of symbol and $\acute{N}$ is the total number of symbols in each frame. Now, let us assume that the received signal is synchronized with the transmit signal, and the reference signal has been correctly detected.

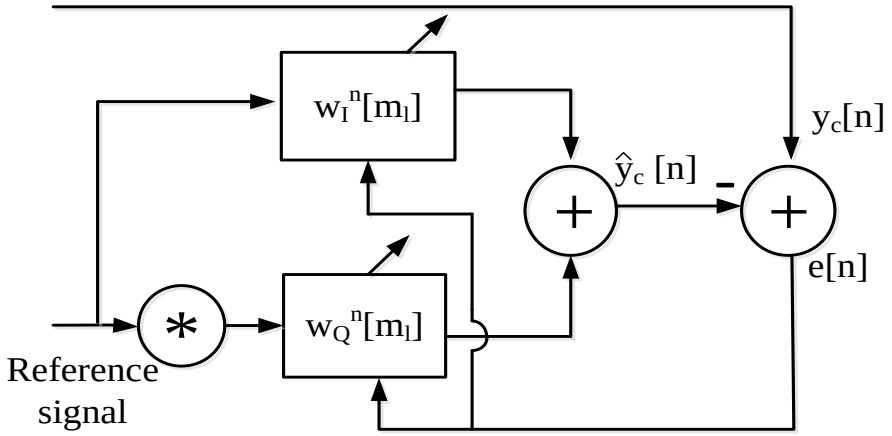

Figure 6-1 Adaptive estimations of I/Q imbalance and channel parameters with an In-phase and Quadrature filter network.

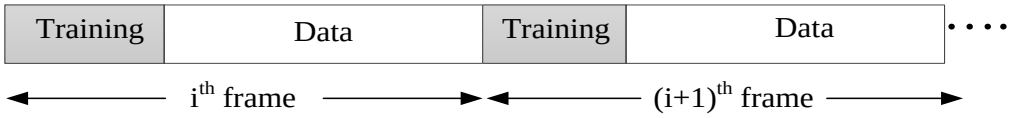

Figure 6-2 A frame structure that incorporates a preamble for the reference training signal in each frame

The I/Q imbalance corrupted signal, $y[n]$, first undergoes correction according to equation (6.11) based on the gain and phase values estimated in the previous frame. Let $y_c[n]$ denote the corrected version of $y[n]$. After that, the reference data sequence is detected from $y_c[n]$, and then used in conjunction with the filter weights $w_I^n[m_l]$ and $w_Q^n[m_l]$ to reproduce an estimated version, $\hat{y}_c[n]$, of the corrected signal corresponding to this reference. Here, $m_l = 1,2,3 \ldots . . M_l$, and M_l corresponds to the total number of filter taps used. Moreover, as the iteration process progresses, the

weights $w_I^n[m_l]$ and $w_Q^n[m_l]$ are updated based on the error signal $[n]$, which is the difference between $y_c[n]$ and $\hat{y}_c[n]$. Based on $w_I^n[m_l]$ and $w_Q^n[m_l]$, we are able to calculate $\hat{y}_c[n]$, yielding

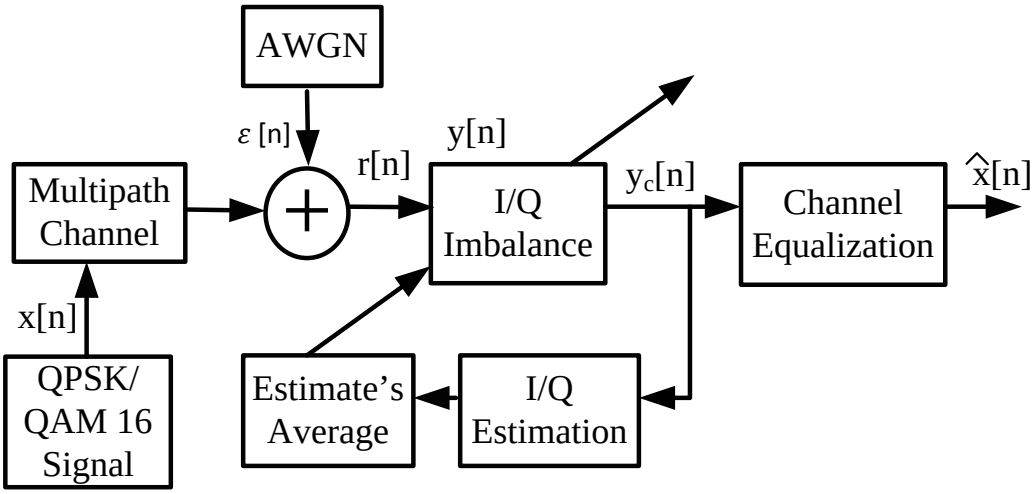

Figure 6-3 Simulation setup for the time domain correction method

$$\hat{y}_c[n] = \sum_{m_l=1}^{M_l} w_I^n[m_l]x[n-m_l+1] + \sum_{m_l=1}^{M_l} w_Q^n[m_l]x^*[n-m_l+1] \tag{6.12}$$

Here, $x[n-m_l+1]$ represents the reference signal. The tap weights are updated according to the LMS algorithm with a step size μ, such that:

$$e[n] = y_c[n] - \hat{y}_c[n] \tag{6.13}$$

$$w_I^{n+1}[m_l] = w_I^n[m_l] + \mu e[n]x^*[n-m_l+1] \tag{6.14}$$

$$w_Q^{n+1}[m_l] = w_Q^n[m_l] + \mu e[n]x[n-m_l+1] \tag{6.15}$$

Also, the estimates of the channel and I/Q imbalance coefficients $w_I[m_l]$ and $w_Q[m_l]$ can be expressed as,

$$\sum_{m_l=1}^{M_l} w_I[m_l] \approx u \sum_{l=1}^{L} h[l] \tag{6.16}$$

and

$$\sum_{m_l=1}^{M_l} w_Q[m_l] \approx v \sum_{l=1}^{L} h^*[l] \tag{6.17}$$

Now, taking the conjugate of equation (6.17) and dividing it by equation (6.16) we obtain,

$$\frac{v^*}{u} \approx \frac{\sum_{m_l=1}^{M_l} {w_Q}^*[m_l]}{\sum_{m_l=1}^{M_l} w_I[m_l]} \tag{6.18}$$

Similarly, dividing equation (6.17) by the conjugate of equation (6.16), we obtain,

$$\frac{v}{u^*} \approx \frac{\sum_{m_l=1}^{M_l} w_Q[m_l]}{\sum_{m_l=1}^{M_l} {w_I}^*[m_l]} \tag{6.19}$$

Now, inputting values of u and v from equations (6.2) and (6.3) into equations (6.18) and (6.19), then performing algebraic manipulation, the gain g and phase φ can be estimated as:

$$\acute{\varphi} = \frac{1}{2} \angle \frac{(1 - \frac{v}{u^*})(1 + \frac{v^*}{u})}{(1 - \frac{v^*}{u})(1 + \frac{v}{u^*})} \tag{6.20}$$

and

$$\acute{g} = \left| e^{j\acute{\varphi}} \frac{\left(1 + \frac{v}{u^*}\right)}{\left(1 - \frac{v}{u^*}\right)} \right| \tag{6.21}$$

where, $\acute{g}$ and $\acute{\varphi}$ denotes the estimates of gain g and phase φ, respectively. For the reference signal corresponding to the i^{th} frame, these estimated values ($\acute{g}$ and $\acute{\varphi}$) have been denoted as $\acute{g}_i$ and $\acute{\varphi}_i$. These estimated values have been averaged with the values obtained for the $(i-1)^{th}$ frame, such that

$$\hat{g}_i = \frac{\acute{g}_i + \hat{g}_{i-1}}{2} \tag{6.22}$$

$$\hat{\varphi}_i = \frac{\acute{\varphi}_i + \hat{\varphi}_{i-1}}{2} \tag{6.23}$$

The moving average in equations (6.22) and (6.23) has been calculated to avoid any drastic changes of gain and phase estimates. At the start of the estimation process, we set $\hat{g}_0 = 1$ and $\hat{\varphi}_0 = 0$. Finally, these estimated values, $\hat{g}_i$ and $\hat{\varphi}_i$, are used for correcting I/Q imbalance in the data of the i^{th} frame. Furthermore, $\hat{g}_i$ and $\hat{\varphi}_i$ are used to correct the I/Q imbalance in the reference signal of the upcoming $(i+1)^{th}$ frame. Consequently, the channel impulse response, $\hat{h}_i[m]$, for the i^{th} frame can be estimated from the following:

$$\hat{h}_i[m_l] = \frac{w_{I,i}[m_l]}{u_i} \tag{6.24}$$

where $w_{I,i}[m_l]$ is the filter weight $w_I[m_l]$ obtained for the i^{th} frame. Finally, the equalized output for the i^{th} data frame is obtained by de-convolving the I/Q imbalance corrected signal $y_{c,i}[n]$ ($y_{c,i}[n]$ is the corrected signal $y_c[n]$ for i^{th} frame) with the estimated channel impulse response, $\hat{h}_i[m_l]$, such that

$$\hat{x}_i[n] = y_{c,i}[n] \circledast^{-1} \hat{h}_i[n] \tag{6.25}$$

where $\circledast^{-1}$ stands for de-convolution.

6.3.1 Simulation results for time domain correction method

- ***Simulation platform***

The various parameters adopted for the simulation are tabulated in Table 6-1.

Table 6-1 Simulation Condition

Transmitter	Modulation type	QPSK, 16-QAM, 64-QAM
	Modulation type for the reference signal	QPSK
	Number of frames per run	50
	No. of symbols per frame	1000
	No. of reference symbols per frame	80
	Samples/symbol	16
	Symbol Period T_s	2 us
Channel	Channel type	GSM channel
	Signal-to-noise ratio SNR	20 or 30 dB
Receiver	Adaptation step size, μ	0.08
	Number of filter taps M_l	6
	Adaptation method	Least mean square (LMS)

The proposed adaptive scheme has been studied using MATLAB simulation based on the block diagram shown in Figure 6-3. For the simulations, it has been assumed that the I/Q imbalance is frequency-flat with gain and phase deviations of $g = 1.2$ and $\varphi = 10^{\circ}$, respectively. The channel represents a typical UHF urban environment with 6 propagation paths [76].The relative delays and normalized average powers of the individual paths are as given in Table 6-2.

The filters $w_I[m_l]$ and $w_Q[m_l]$ have 6 taps, and are initialized with all their coefficients set to zero. The reference signal has been modulated as QPSK. A lower order

modulation scheme is adopted for the reference signal to allow it to be detected more reliably.

Table 6-2 Channel Parameters

Propagation path	**Relative delay (us)**	**Relative delay (T_s)**	**Average Power (dB)**
1	0	0.00 T_s	-3.0
2	0.2	0.10 T_s	0.0
3	0.5	0.25 T_s	-2.0
4	1.6	0.80 T_s	-6.0
5	2.3	1.15 T_s	-8.0
6	5.0	2.50 T_s	-10.0

- ***Mean squared error (MSE)***

In this section, the mean squared error (MSE) has been used to evaluate how well the gain and phase imbalance can be estimated in presence of global system for mobile communications (GSM) channel and AWGN. The squared error has been adopted in a vector defined as $\mathbf{e_{sq}}$ which can be expressed as,

$$\mathbf{e_{sq}} = [|e[1]|^2, |e[2]|^2, \dots \dots |e[N_t]|^2] \tag{6.26}$$

where the elements in $\mathbf{e_{sq}}$ has been denoted by $e[n_t]$, which has been calculated by means of equation (6.13), where $n_t = 1,2,3 \dots \dots N_t$. Also N_t is defined as the total number of training symbols or iterations that have been used to determine the mean squared error. The simulations need to be run for several times to obtain average values of the squared errors. Let, $\mathbf{e_{sq}^p}$ denotes a row vector containing the squared errors for the p^{th} run, same as defined in equation (6.26). For a total number of P runs, these row vectors form a PxN_t matrix denoted as, $\bar{\mathbf{E}}_{\mathbf{sq}}$, in where $\mathbf{e_{sq}^p}$ represents the p^{th} row. Thus the MSE can be obtained as,

$$MSE(n_t) = \frac{1}{P}\sum_{p=1}^{P} \bar{\mathbf{E}}_{sq}(p, n_t) \tag{6.27}$$

Equation (6.27) provides the MSE, denoted as $MSE(n_t)$ for a specific iteration n_t. Therefore, for a total of N_t iterations, the **MSE** vector can be obtained by:

$$\mathbf{MSE} = [MSE(1), MSE(2) \ldots \ldots MSE(N_t)] \tag{6.28}$$

The mean squared error values obtained from equation (6.28) for the proposed time domain correction method have been shown in Figure 6-4, for 64-QAM[3].

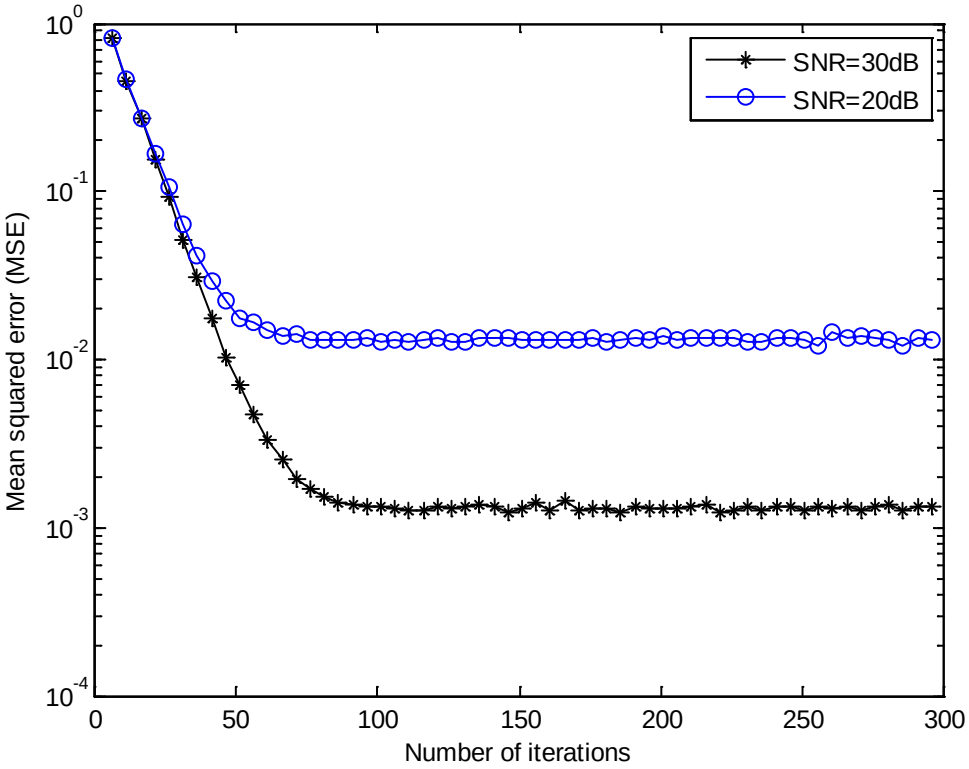

Figure 6-4 MSE for different SNR level for 64-QAM

For simulation purpose, a total number of one thousand runs have been performed ($P = 1000$) for averaging. Also, 300 iterations have been completed ($N_t = 300$) to

[3] The reference signal has been used to obtain the MSE values. As the reference signal is modulated as QPSK, the MSE output obtained for 64-QAM and 16-QAM will be same.

show the convergence of the MSE curve. The legends 'SNR=20 dB' and 'SNR=30 dB' represent the MSE curves obtained for different level of SNR. For an SNR of 30 dB, the MSE takes at least 80 iterations to converge. On the other hand for 20 dB SNR, the curve converges after 64 iterations. As expected the residue error in the case of 20 dB SNR is much higher than that of the 30 dB SNR.

Figure 6-5 shows the MSE obtained for different step sizes. The legend 'step size' refers the MSE obtained for a particular step size μ. The MSE values have been obtained for 30 dB SNR. The small step size of μ=0.02, gives the lowest MSE values. However it takes more than 200 iterations to converge.

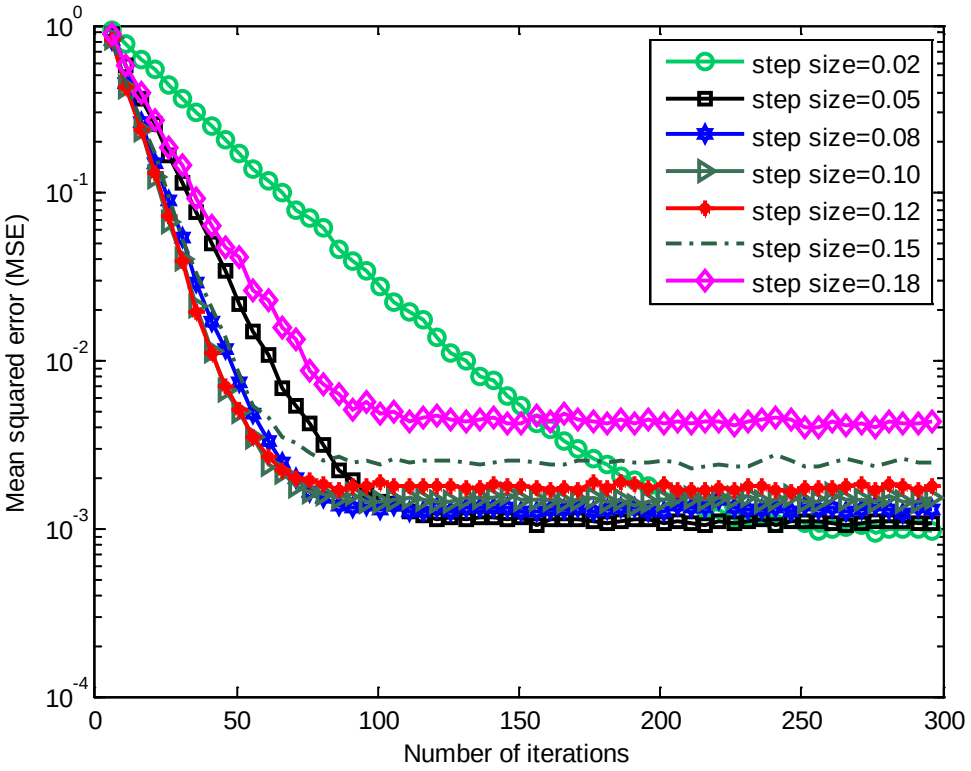

Figure 6-5 MSE for different step size μ, for 64-QAM

On the other hand, if a larger value of step size, such as μ=0.18 is adopted, the MSE curve converges before 100 iterations but the residue error is quite high. The residue error for this step size is $4.3x10^{-3}$. For the rest of the simulations, the step size has been chosen as μ=0.08. For this step size, the MSE curve converges before 80 iteration.

Also the lowest error obtained for this step size is, $1.3x10^{-3}$. For the MSE plot shown in Figure 6-4 and Figure 6-5, 300 iterations have been carried out. However, for all the simulations, 80 iterations have been used for estimation purpose. The reason for taking 300 iterations for the MSE plot is to show the convergence speed and residue error for different step size.

- ***Estimated gain and phase***

The estimated values of the gain and phase deviations (obtained by equations (6.22) and (6.23), respectively) for a run of 20 consecutive frames have been presented in Figures 6-6 and 6-7, respectively. Here, the data has been modulated with 64-QAM. It has been observed that the estimations of both the gain and phase deviations converge in less than 10 frames. However, a larger variation in the estimated gain and phase values is observed for the lower SNR of 20 dB.

Figures 6-8 and 6-9 show the estimated nominal gain and phase, respectively, for the 16-QAM signals. The variation of the estimated values is slightly less compared to the 64-QAM signals. It is because the I/Q and channel effect are more significant and therefore cause more distortion for higher order modulations. Again, the estimated values approach the ideal values after approximately 5 frames.

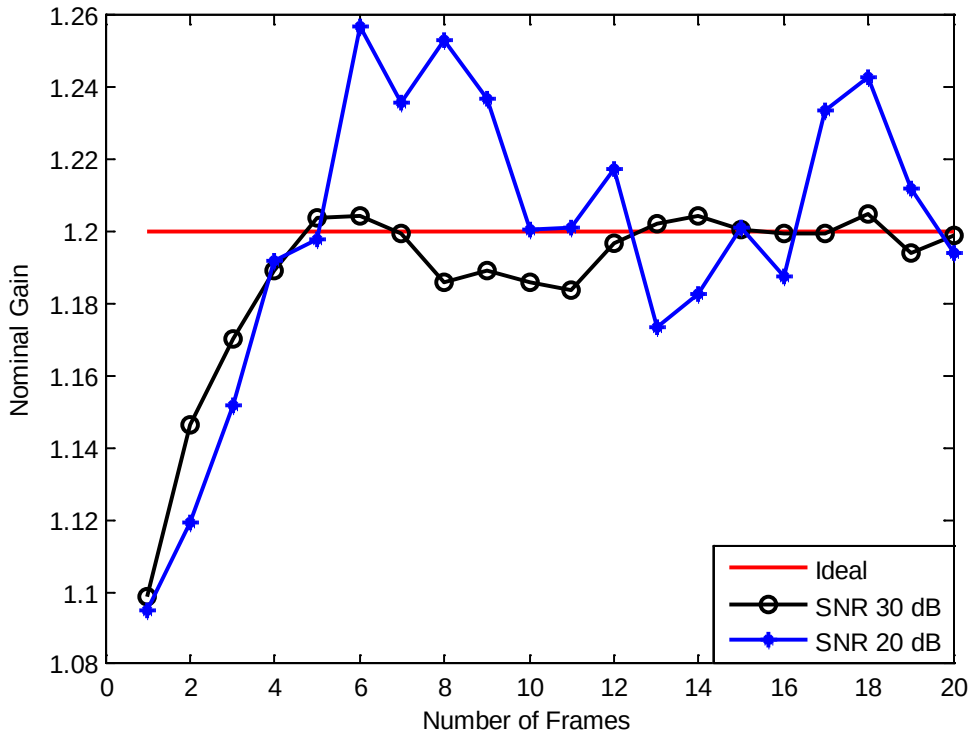

Figure 6-6 Estimated nominal gain for 64-QAM

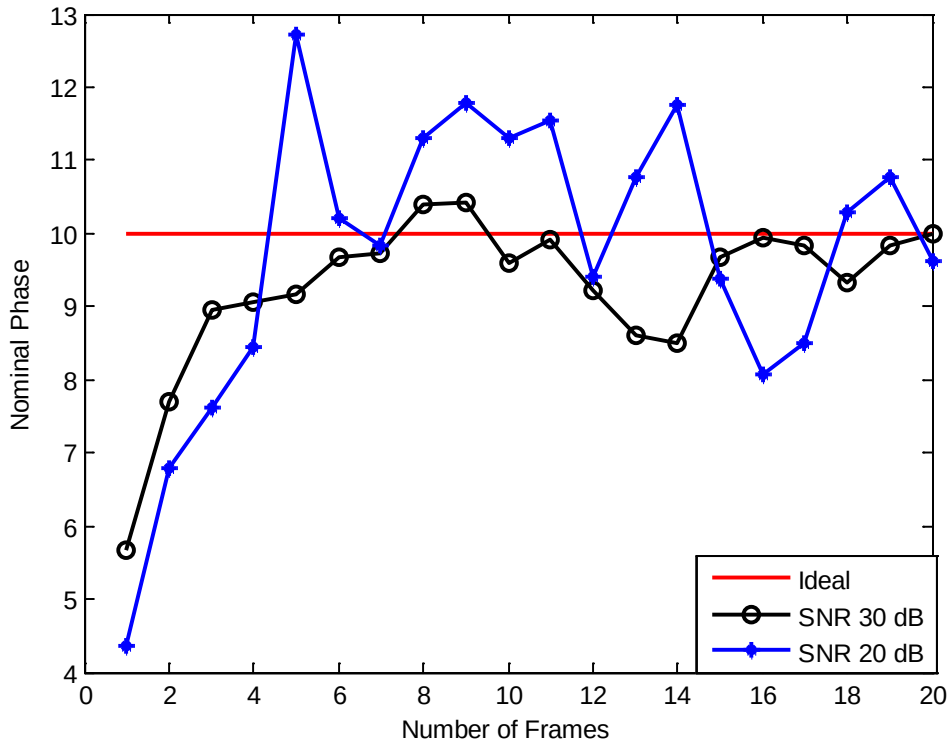

Figure 6-7 Estimated nominal phase for 64-QAM

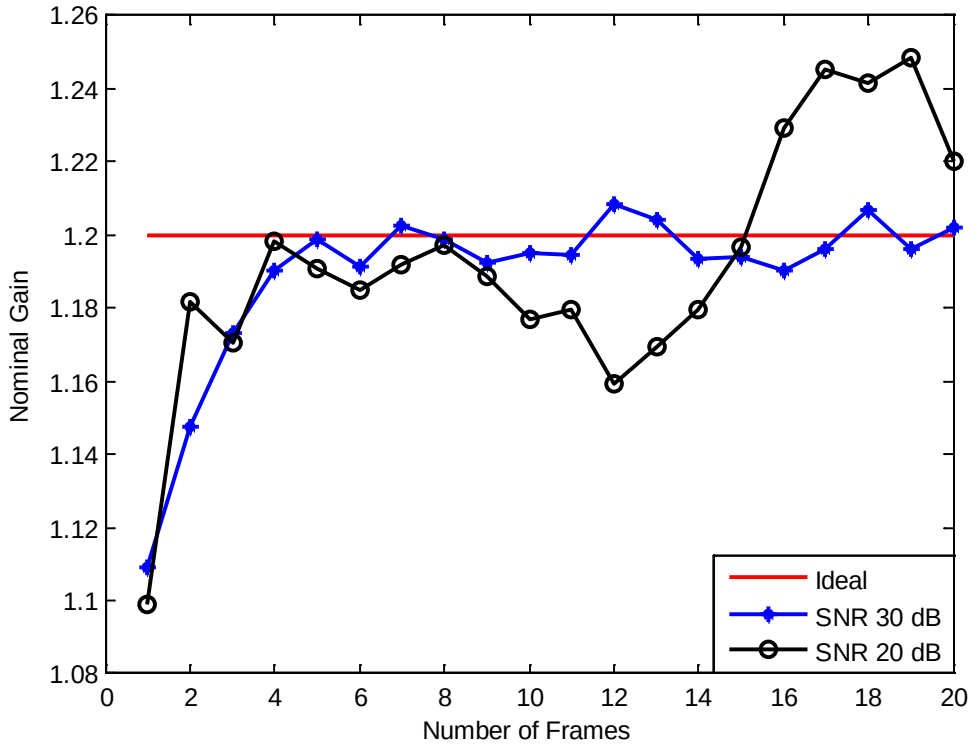

Figure 6-8 Estimated nominal gain for16-QAM

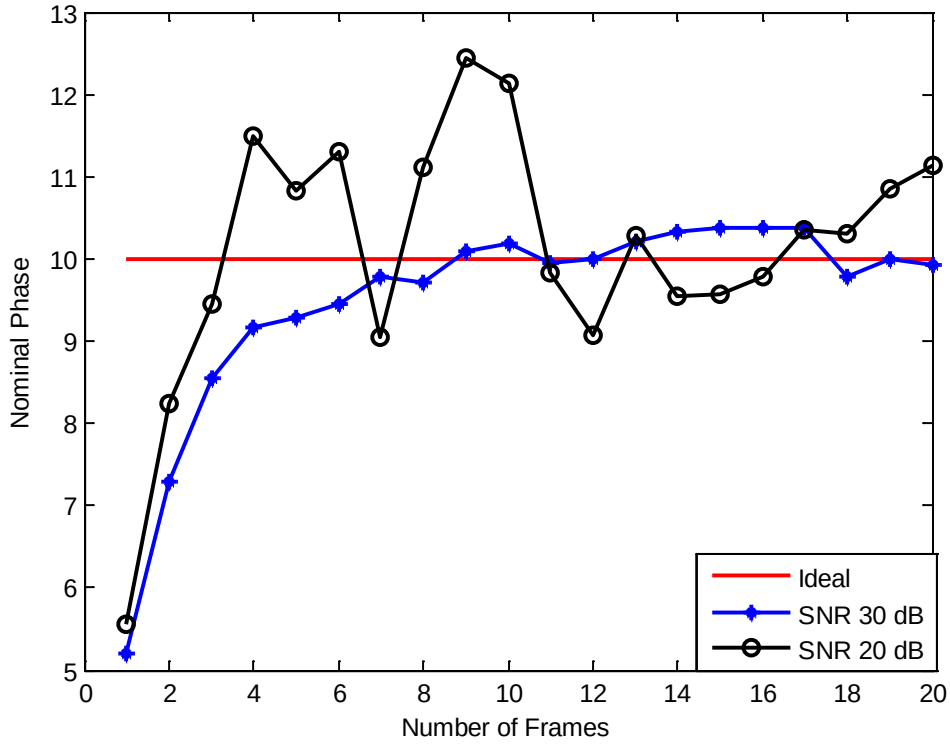

Figure 6-9 Estimated nominal phase for 16-QAM

- ***Signal Constellations***

The constant gain and phase imbalance has been chosen for the constellation presentation as 20% and 10^{o}, respectively. The constellations of the uncorrected and the corrected signal has been presented for 64-QAM, 16-QAM and QPSK. For the corrected signal, the constellations have been taken for the fifth frame after the system has been converged and the estimated gain and phase has reached fairly close to its original values.

In Figure 6-10 and Figure 6-11, the constellations representing the uncorrected and corrected signal for 64-QAM modulation have been illustrated, respectively. Figure 6-12 and Figure 6-13 presents the constellations of the received uncorrected signal and the corrected signal, respectively for 16-QAM modulations. Similarly, Figures 6-14 and 6-15 represent the constellation of the received uncorrected and corrected signals, respectively, for QPSK modulation. The legend, 'Ideal' refers to the transmit signal and the legend 'Received' refers to the received signal.

From Figure 6-10, it can be seen that the individual states in the signal constellation for the uncorrected signal are spread out due to the presence of the I/Q imbalance and channel effect. After the time domain estimation and correction have been performed, the constellations obtained for the fifth frame have been presented in Figure 6-11. The corrected signal's constellation shows much improvement compared to the uncorrected one.

Similarly, from Figure 6-12 it has been observed that the uncorrected signal obtained for 16-QAM appears similar to the uncorrected signal obtained for the 64-QAM signals shown in Figure 6-10. However, the corrected signal shown in Figure 6-13 shows much improvement.

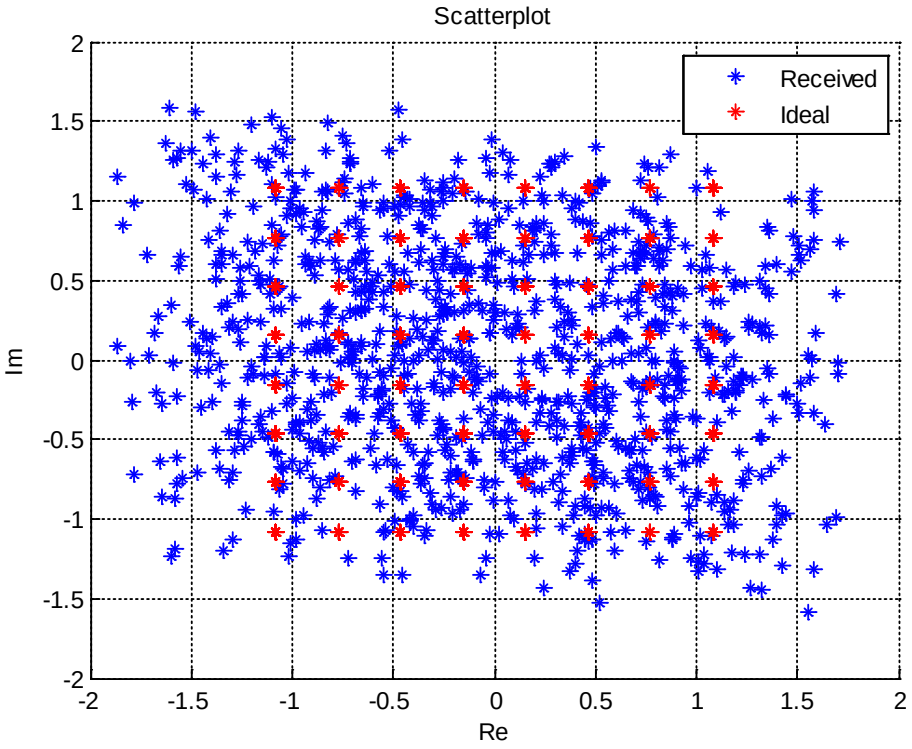

Figure 6-10 Constellation of the uncorrected signal, for 64-QAM

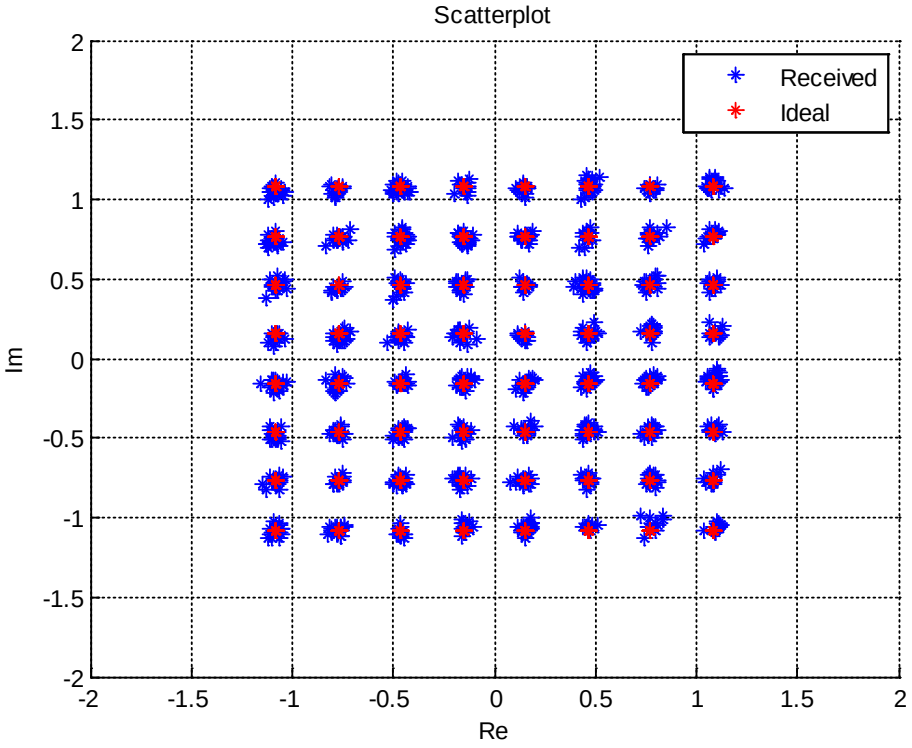

Figure 6-11 Constellation of the received signal after being corrected by the time domain correction method, for 64-QAM

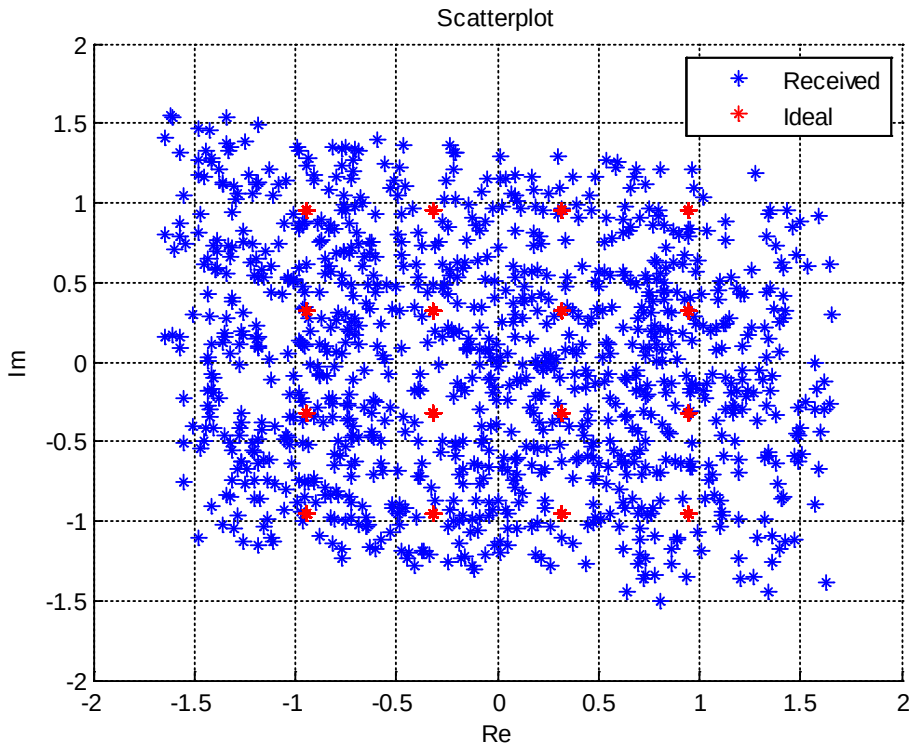

Figure 6-12 Constellation of the uncorrected signal, for 16-QAM

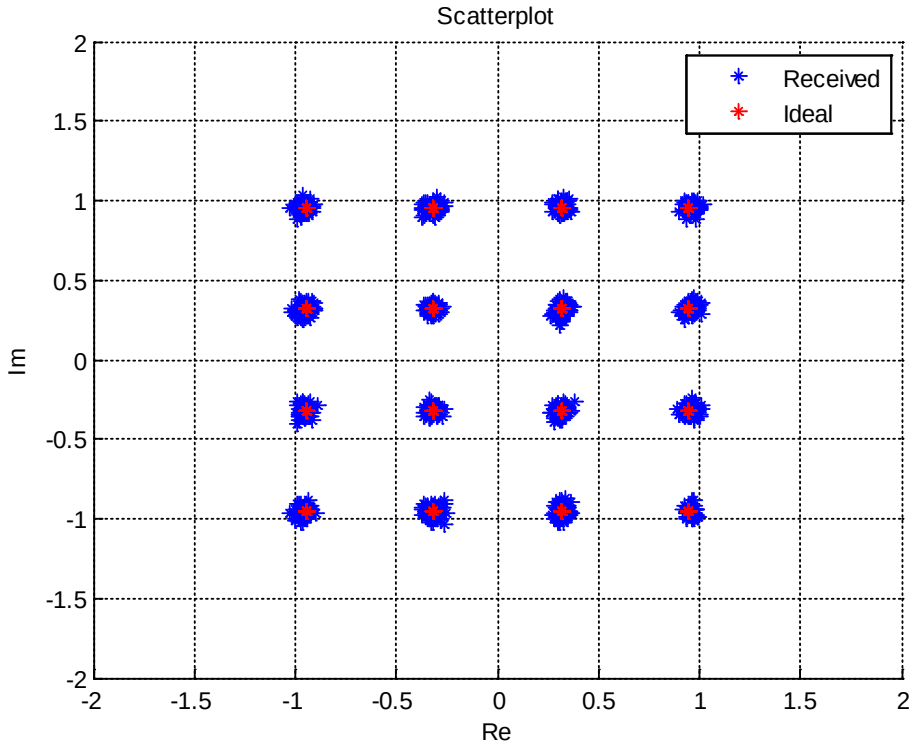

Figure 6-13 Constellation of the received signal after being corrected by the time domain correction method, for 16-QAM

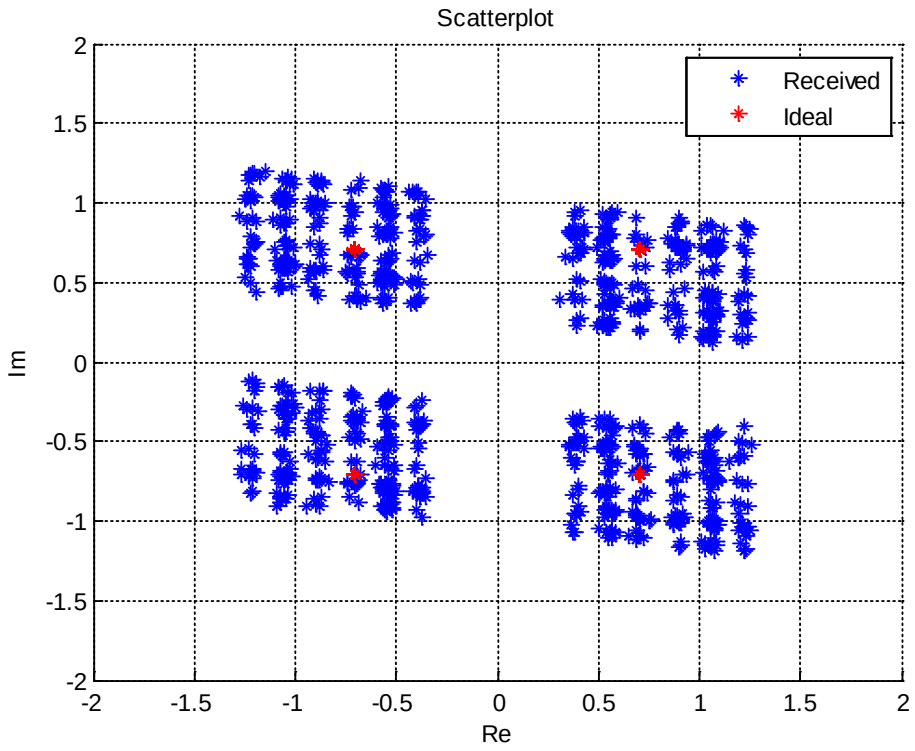

Figure 6-14 Constellation of the uncorrected signal, for QPSK

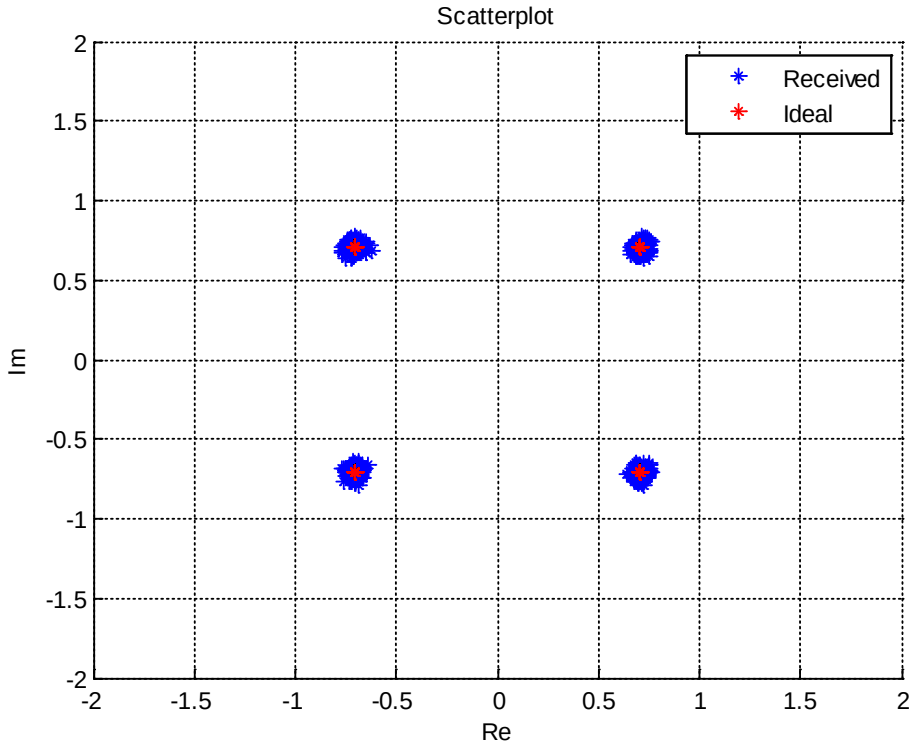

Figure 6-15 Constellation of the received signal after being corrected by the time domain correction method, for QPSK

Next, from Figure 6-14 it has been observed that even for a lower order modulation, such as QPSK, the I/Q imbalance has a bad effect, as it can be seen from the plot of the uncorrected signal that the constellation points have been rotated from the original location. Figure 6-15 shows the corrected QPSK signal with fewer distortions.

- ***Error vector magnitude (EVM)***

As discussed in Chapter 4, the EVM can be used for obtaining a quantitative measure of the constellation points obtained after the time domain correction. In this section, the EVM for the proposed time domain correction technique has been obtained. The EVMs are observed for different frames to perceive the performance of the scheme with the progress of consecutive frames. Furthermore, the EVMs for different gain and phase combinations have been presented. Figure 6-16 represents the EVM of the received 64-QAM signals after correction by the proposed time domain correction method for different frames. Similarly, Figure 6-17 shows the EVMs representing different frames of the received 16-QAM signals after correction. The gain and phase have been chosen as $g = 1.2$ and $\varphi = 10^{o}$ for these two cases.

The legends ‘Frame 1’, ‘Frame 2,’, ‘Frame 3’, ‘Frame 4’, ‘Frame 5’ and ‘Frame 10’ refers the first, second, third, fourth, fifth and the tenth frame, respectively. The term ‘Ideal’ refers when the received signal hasn’t been gone through any I/Q imbalance or channel distortion. The only distortion for the ‘Ideal’ case is the AWGN. Similarly, the term ‘Uncorrected’ refers when the received signal has been distorted by I/Q imbalance, channel and noise but has not gone through any kind of correction or equalization.

As the system is an adaptive one, it gets better with the number of frames. From the nominal gain and phase figures shown in Figures 6-6 and 6-7, it is observed that it takes at least four to five frames for the system to estimate the values of gain and phase for 64-QAM modulations. That is why the EVM is higher for the earlier frames, whereas it is lower for the latter frames, as the I/Q imbalance has been corrected by the end of fourth or fifth frames.

It has been also observed from Figure 6-16 that the EVM is the highest for the first frame, as expected. The EVM value corresponding to the first frame, for 25 dB SNR is 0.2. After the fifth frame the system estimates the gain and phase quite accurately. So, the EVM corresponding to the fifth frame has decreased quite significantly compared to the EVM for the first frame.

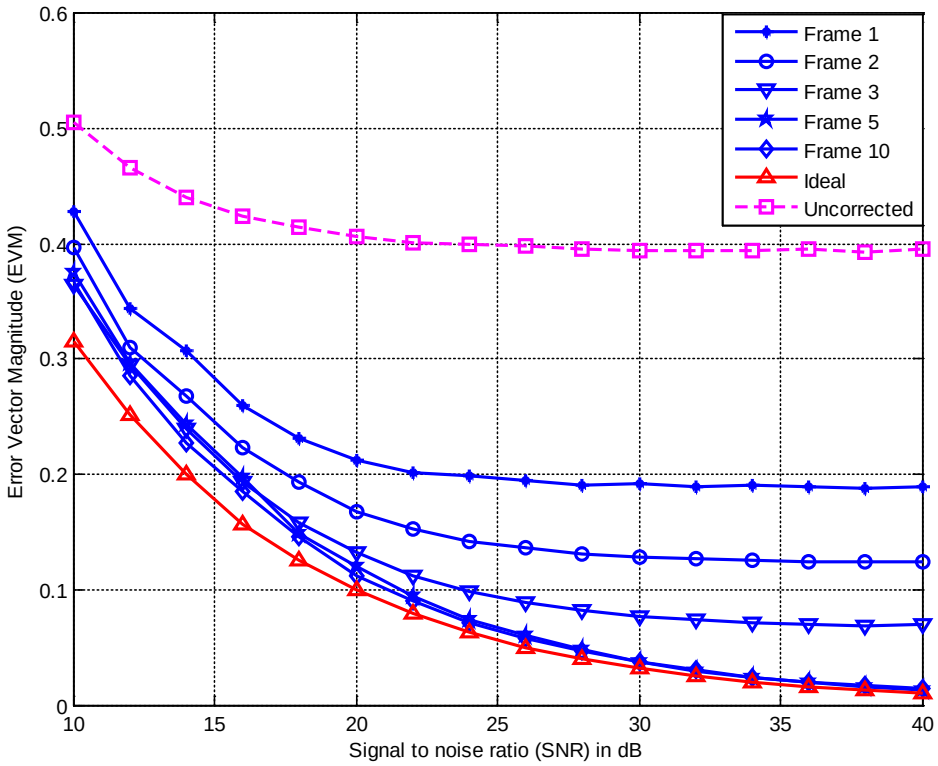

Figure 6-16 EVM for different frames of the received signal corrected by the time domain correction method, for 64-QAM

The value for fifth frame at an SNR of 25 dB is 0.07. After the fifth frame, the EVM curve saturates and remains almost equal to the 'Ideal' EVM curve for an SNR higher than 20 dB. The EVM for the fifth and tenth frame shows similar results. Next, EVM corresponding to different frames have been shown for 16-QAM modulations in Figure 6-17. Here, the EVM curve corresponding to the first frame shows the highest EVM values. However, it gets better for the upcoming consecutive frames. For Figure 6-17, the EVMs of the fifth and the tenth frames do not show difference at all, unlike EVMs for 64-QAM signal shown in Figure 6-16. Thus it can be observed, that for 16-

QAM, the system gets saturated after fifth consecutive frames and remain steady after that. Also these are quite close to the 'Ideal' EVM curve after 20dB SNR. So from the above figures it has been observed that after the tenth frame, the EVM becomes the lowest. In this case, the gain and phase has been kept steady and the effect of the correction scheme on different frame has been observed.

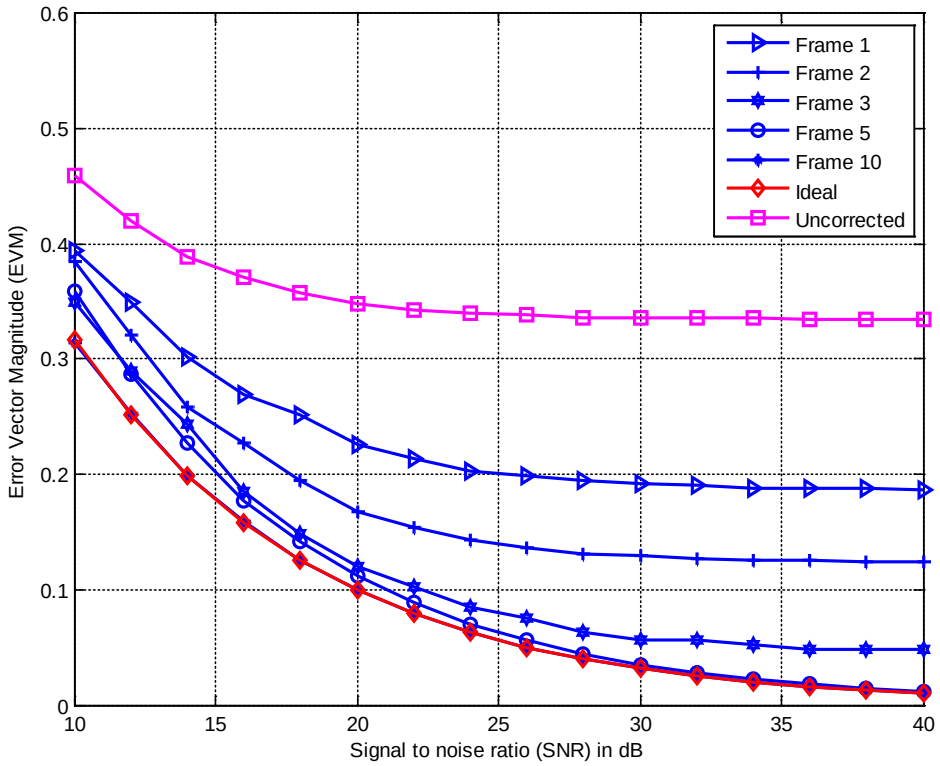

Figure 6-17 EVM for different frames of the received signal corrected by the time domain correction method, for 16-QAM

For the next two figures, different combinations of gain and phase values have been tested to observe the performance of the proposed time domain correction scheme. For this, the output has been obtained for fifth frame specifically, after the system has converged properly. Figure 6-18 shows the EVMs for different frequency-flat I/Q gain and phase combination for 64-QAM modulation. The term '$g = \mathrm{a}, \mathrm{ph} = \mathrm{b}$' refers to the value of g and φ are a and b^{o}, respectively. Gain imbalance has been varied from 2% to 20%, and phase imbalance has been varied from 2^{o} to 10^{o}. The EVMs for

different gain and phase show quite similar response. This means the method is capable of mitigating a wide variety of I/Q imbalance.

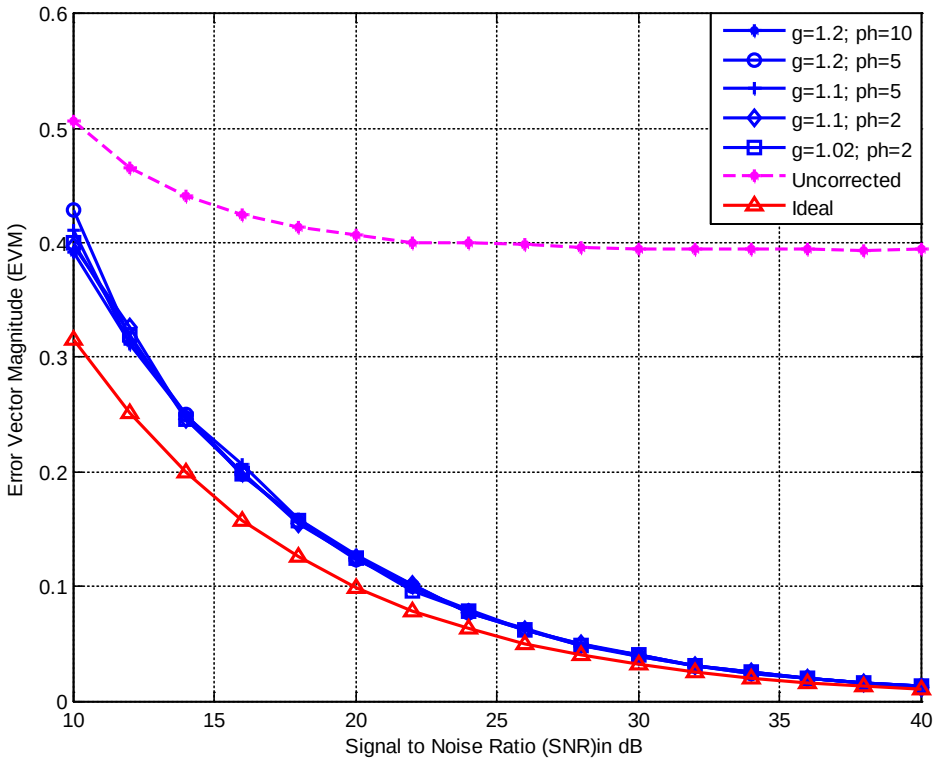

Figure 6-18 EVM for different gain and phase after being corrected by the time domain correction method, for 64-QAM

Figure 6-19 presents the EVM for different gain and phase combinations for 16-QAM modulations. The EVM curves are similar to those shown in Figure 6-18. The EVMs corresponding to the lowest I/Q gain and phase combinations of $g = 1.02$ and $\varphi = 2^o$ show hardly any differences from the highest I/Q gain and phase combinations of $g = 1.2$ and $\varphi = 10^o$. This proves the proposed scheme is suitable for a wide range of I/Q gain and phase. Also, the EVM for 64-QAM shown in Figure 6-18 is similar to the EVM of the received signal obtained for 16-QAM shown in Figure 6-19, which means the performance of the scheme is similar for both of the modulation techniques.

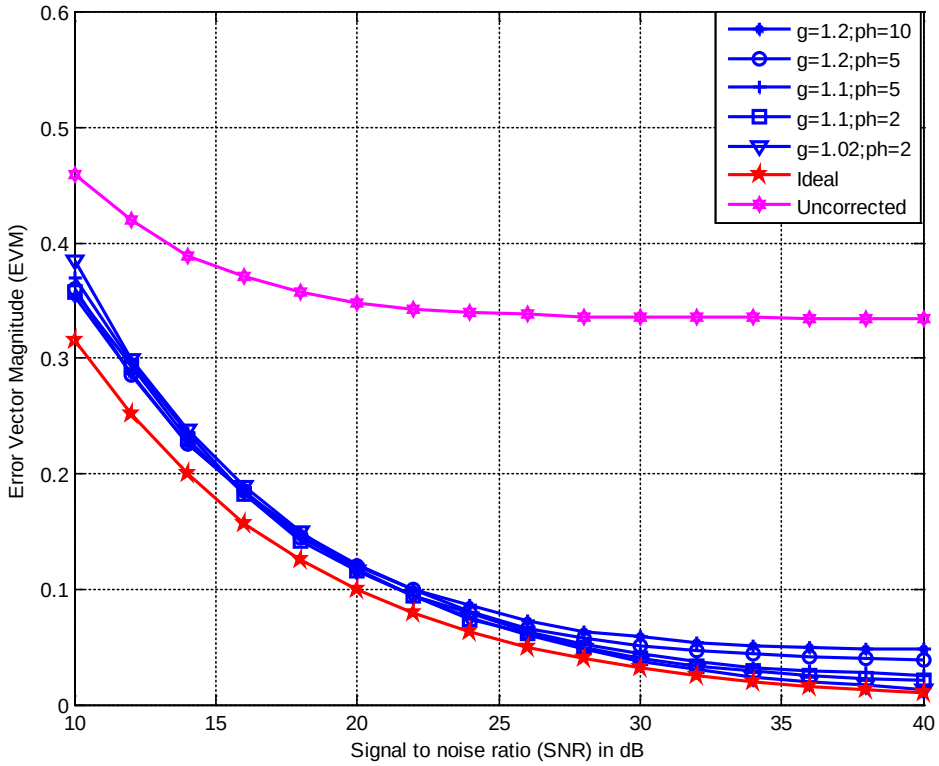

Figure 6-19 EVM for different gain and phase after being corrected by the time domain correction method, for 16-QAM

- ***Symbol error rate (SER)***

The effectiveness of the time domain correction scheme has been further illustrated by the average SER achieved. The SERs obtained for different frames of the received 64-QAM signals after correction by the time domain correction method have been shown in Figure 6-20. The I/Q gain and phase have been chosen as $g = 1.2$ and $\varphi = 10^o$ for obtaining this SER. Like the EVM curves, in this figure, the reference SER has been obtained without any I/Q imbalance and channel imperfection. It has been denoted as 'Ideal'. Also 'Frame 1', 'Frame 2', 'Frame 3', 'Frame 4', 'Frame 5' and 'Frame 10' refers to the SER of the received corrected signal obtained for the first, second, third, fourth, fifth and tenth frames (as in Figure 6-16 and 6-17). Similarly, Figure 6-21 shows the SER for different frames for 16-QAM modulations after the correction has been applied. The legends used in Figure 6-20 have also been used in Figure 6-21. Figure 6-20 shows similar results as the EVMs shown in Figure 6-17. In Figure 6-20,

it has been observed that the received signal shows the highest SER for the first frame. As for first frame, the estimated I/Q gain and phase are quite different from its original gain and phase, and the SER corresponding to this frame are quite high.

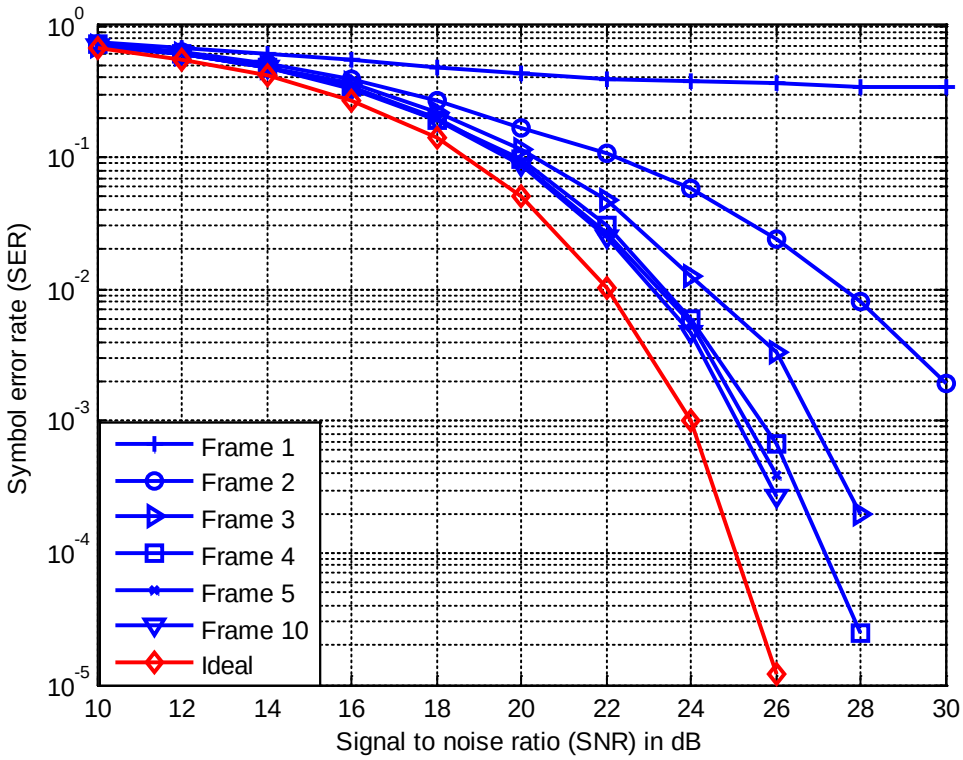

Figure 6-20 SER for different frames of the received signal corrected by the time domain correction method, for 64-QAM

It saturates before 10^{-1} and does not get better even when the SNR is as high as 30 dB. The SERs corresponding to the second and third frame are also quite high compared to the reference SER. As the system adapts the I/Q parameters for the upcoming frames, the SER response improves with time. That is why, the SER response for the Frame 3 and Frame 4 show significant improvement than that of Frame 1. After the fifth frame, the SER responses for all upcoming frames become similar. To achieve SERs of 10^{-3}, the SNR of the corrected signal for the fifth frame is just 1 dB higher than the 'ideal' (where there are no I/Q and channel conditions). The SERs of the fifth and tenth frames show almost similar outcomes.

Figure 6-21 shows the SER for different frames obtained for 16-QAM modulation. Even for 16-QAM modulation, the SER for the first frame is quite high. The SNR of first frame for an SER of 10^{-3} is almost 7 dB higher than the reference 'Ideal' curve. From the second frame the SER tends to reduce significantly. The SERs obtained for the third, fourth, fifth and tenth frames are quite similar to each other and for an SER of 10^{-3}, the SNR corresponding to these frames are approximately just 1 dB higher than the ideal reference curve.

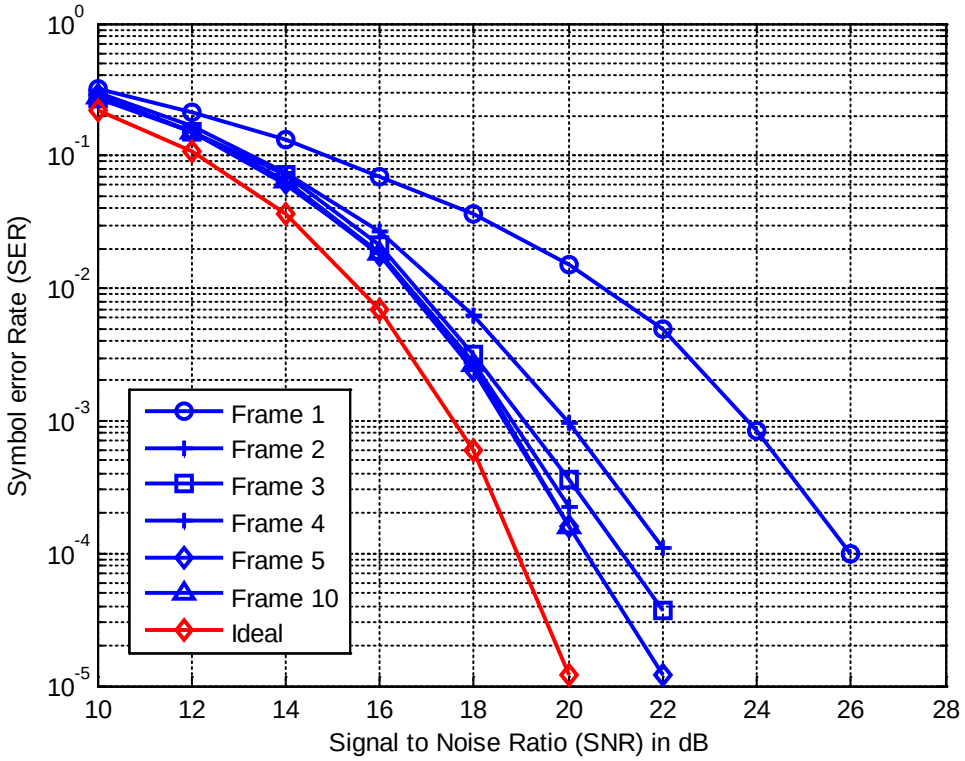

Figure 6-21 SER for different frames of the received signal corrected by the time domain correction method, for 16-QAM

Figure 6-22 shows the SER for different I/Q gain and phase combinations. Like the EVM response shown in Figures 6-18 and 6-19, the SER response is also similar for a variety of gain and phase combinations. Figure 6-22 presents the SER curves for 16-QAM and 64-QAM concisely. The results have been obtained for the fifth frame after the system has adapted the gain and phase imbalances. For all combinations of gain and phase, the SER curves show similar results. This means the system works the same

for high and low I/Q gain and phase combinations. For SERs of 10^{-3}, the SNR of the output for the received signal is around 1 dB higher than that of the ideal signal for a 64-QAM modulation. For the 16-QAM modulations, this difference is also around 1dB.

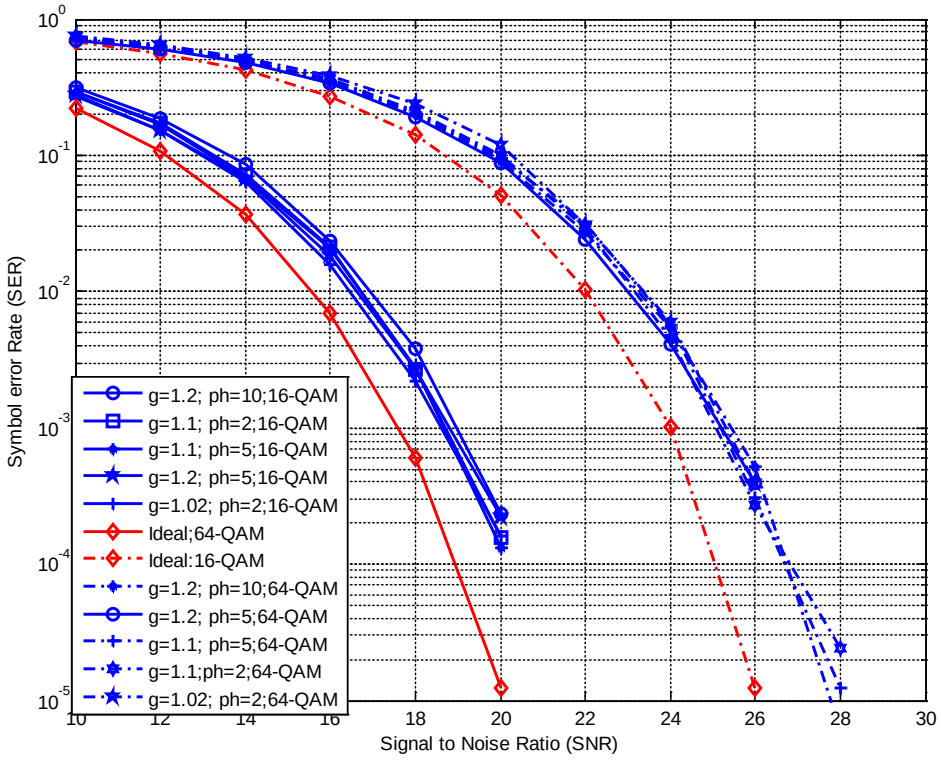

Figure 6-22 SER for different gain and phase combinations after being corrected by the time domain correction method, for 64-QAM and 16-QAM

6.4 Method 2: A frequency domain compensation method by adding CP

In this section, a frequency domain compensation scheme has been presented in order to mitigate I/Q and channel effect for 64-QAM and 16-QAM signals[4]. In this technique, the estimation of the unknown I/Q and channel parameters has also been obtained in the time domain. But the compensation takes place in the frequency

[4] The contents of this section have been published in a conference: 19th IEEE Asia Pacific Conference on Communications *(APCC 2013)*, October 2013, Bali, Indonesia.

domain. For the parameter estimation, the two-way filter network shown in Figure 6-1 has been used in this case as well. In addition, the symbols have been divided into frames. A training sequence has been inserted followed by the desired data sequence during transmission for each frame, as shown in Figure 6-2.

The difference of this method from the previous method is that there is no feedback correction technique involved. The channel and I/Q parameters have been estimated jointly in the time domain. Afterwards, the frequency representation of these estimated parameters have been used to compensate for the distorted signal in the frequency domain. A block diagram for the proposed compensation scheme is shown in Figure 6-23.

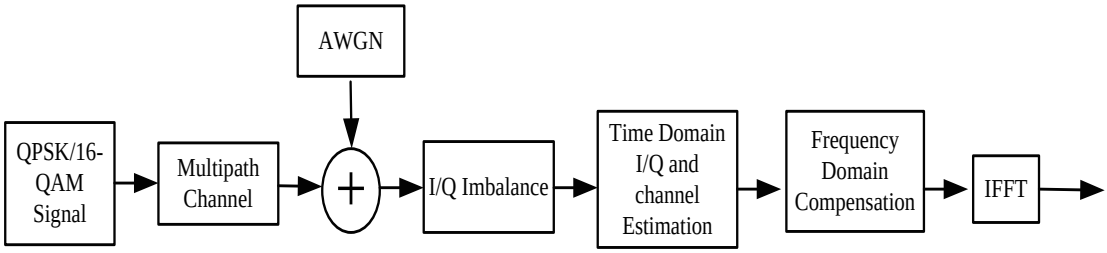

Figure 6-23 Simulation set-up for the frequency domain compensation method

In the receiver, the training sequence is extracted and utilized to reproduce the transmitted signal, which has been used as reference signal, in order to estimate the channel and I/Q imbalance coefficients denoted as $uh[n]$ and $vh^*[n]$. The LMS adaptation technique has been adopted to do the estimation. In the frequency domain, the FFT of these unknown parameters (denoted as $uH[K]$ and $vH^*[-k]$) are obtained, which is used to compensate the received signal by means of post processing. For this method to work, a CP is added in front of the training signal before the transmission.

Due to the CP, the estimation of the adaptive filter coefficients, such as $w_I$and w_Q, have been slightly different than the previous method. The transmitted symbol can be written in vector form as, $\mathbf{x} = \left[x\left[-\frac{\acute{N}}{2}\right], x\left[-\frac{\acute{N}}{2}+1\right], \ldots\ldots x\left[\frac{\acute{N}}{2}\right]\right]^T$. The above symbol

consists of $\acute{N}$ samples excluding the CP. As the CP is added, the linear convolution in (6.4) have been replaced by the circular convolution and written as follows:

$$y[n] = uh[n] \circledast x[n] + vh^*[n] \circledast x^*[n] + u\varepsilon[n] + v\varepsilon^*[n] \qquad (6.29)$$

Recalling (3.27), the received signal can be written in matrix form as,

$$\mathbf{y} = u\left(\overline{\mathbf{h^c}}\right).\mathbf{x} + v\left(\overline{\mathbf{h^c}}\right)^*.\mathbf{x}^* + u\,\boldsymbol{\varepsilon} + v\boldsymbol{\varepsilon}^* \qquad (6.30)$$

With the reference signal $x[n]$ acting as inputs to the I and Q filters, $w_I[n]$and $w_Q[n]$ respectively, an estimated output, $\hat{y}[n]$, is generated (during the training period, the reference signal has been denoted as $x[n]$. It has been assumed that the transmitted reference signal has been detected accurately and synchronized with the received signal). The obtained output $\hat{y}[n]$ is then compared with the received signal, $y[n]$, to produce an error signal, $e[n]$, which updates the filter coefficients, $w_I[n]$ and $w_Q[n]$. Upon convergence of the I and Q filters, the values of $w_I[n]$ and $w_Q[n]$ become estimates of, $uh[n]$, $vh^*[n]$, in the output signal $y[n]$ as given in (6.29).
The estimated output signal $\hat{y}[n]$ is then given by:

$$\hat{y}[n] = w_I[n] \circledast x[n] + w_Q[n] \circledast x^*[n] \qquad (6.31)$$

The noise term has been avoided in equation (6.31) for simplicity. However, in presence of noise, the estimated received signal $\hat{y}[n]$, will be much different from $y[n]$. Let, $\acute{M}$ corresponds to the number of filter taps used; μ is the step size and n is the iteration number. Let $\acute{m}_l = n - \acute{m}_l + 1$. The estimated received signal for the n^{th} iteration can be written as

$$\hat{y}[n] = \begin{cases} \sum_{\acute{m}_l=1}^{\acute{M}_l} w_I^n[\acute{m}_l]x\left[\acute{\acute{m}}_l\right] + \sum_{\acute{m}_l=1}^{\acute{M}_l} w_Q^n[\acute{m}_l]x^*\left[\acute{\acute{m}}_l\right] & \acute{\acute{m}}_l > 0 \\ \sum_{\acute{m}_l=1}^{\acute{M}_l} w_I^n[\acute{m}_l]x\left[N + \acute{\acute{m}}_l\right] + \sum_{\acute{m}_l=1}^{\acute{M}_l} w_Q^n[\acute{m}_l]x^*\left[N + \acute{\acute{m}}_l\right] & \acute{\acute{m}}_l \leq 0 \end{cases} \quad (6.32)$$

The error signal $e[n]$ is updated according to,

$$e[n] = y[n] - \hat{y}[n] \quad (6.33)$$

$$w_I^{n+1}[\acute{m}_l] = \begin{cases} w_I^n[\acute{m}_l] + \mu e[n]x^*[\acute{\acute{m}}_l] & \acute{\acute{m}}_l > 0 \\ . & \\ w_I^n[\acute{m}_l] + \mu e[n]x^*[N + \acute{\acute{m}}_l] & \acute{\acute{m}}_l \leq 0 \end{cases} \quad (6.34)$$

and

$$w_Q^{n+1}[\acute{m}_l] = \begin{cases} w_Q^n[\acute{m}_l] + \mu e[n]x[\acute{\acute{m}}_l] & \acute{\acute{m}}_l > 0 \\ . & \\ w_Q^n[\acute{m}_l] + \mu e[n]x[N + \acute{\acute{m}}_l] & \acute{\acute{m}}_l \leq 0 \end{cases} \quad (6.35)$$

Expressing, $\mathbf{w_I} = [w_I(1), w_I(2) \dots \dots w_I(\acute{M}_l), 0_{(1x\acute{N}-\acute{M}_l)}]^T$ and $\mathbf{w_Q} = [w_Q(1), w_Q(2) \dots \dots w_Q(\acute{M}_l), 0_{(1x\acute{N}-\acute{M}_l)}]^T$. These have been initialized as $[\mathbf{w_I}]^1 = [\mathbf{w_Q}]^1 = 0$. After the final estimation, the received signal in equation (6.32) can be expressed in matrix form as,

$$\hat{\mathbf{y}} = (\bar{\mathbf{w}}_\mathbf{I}^\mathbf{c}).\mathbf{x} + \left(\bar{\mathbf{w}}_\mathbf{Q}^\mathbf{c}\right)^*.\mathbf{x}^* \quad (6.36)$$

where, $\bar{\mathbf{w}}_\mathbf{I}^\mathbf{c}$ and $\bar{\mathbf{w}}_\mathbf{Q}^\mathbf{c}$ are the (NxN) circulant matrices which have been obtained after the final iteration. They are expressed as,

$$\bar{\mathbf{w}}_{\mathbf{I}}^{\mathbf{c}} = \begin{bmatrix} w_I[1] & 0_{N-\acute{M}_l} & \cdots & 0_1 & \cdots & w_I[3] & w_I[2] \\ w_I[2] & w_I[1] & 0_{N-\acute{M}_l} & \vdots & \vdots & \vdots & \vdots \\ \vdots & w_I[2] & w_I[1] & \vdots & \vdots & \vdots & \vdots \\ w_I[\acute{M}_l] & \vdots & w_I[2] & w_I[1] & \vdots & \vdots & \vdots \\ 0_1 & w_I[\acute{M}_l] & \vdots & w_I[2] & w_I[1] & \vdots & \vdots \\ \vdots & 0_1 & \ddots & \vdots & \ddots & \ddots & \vdots \\ 0_{N-\acute{M}_l} & \vdots & \cdots & w_I[\acute{M}_l] & \cdots & w_I[2] & w_I[1] \end{bmatrix}$$

and,

$$\bar{\mathbf{w}}_{\mathbf{Q}}^{\mathbf{c}} = \begin{bmatrix} w_Q[1] & 0_{N-\acute{M}_l} & \cdots & 0_1 & \cdots & w_Q[3] & w_Q[2] \\ w_Q[2] & w_Q[1] & 0_{N-\acute{M}_l} & \vdots & \vdots & \vdots & \vdots \\ \vdots & w_Q[2] & w_Q[1] & \vdots & \vdots & \vdots & \vdots \\ w_Q[\acute{M}_l] & \vdots & w_Q[2] & w_Q[1] & \vdots & \vdots & \vdots \\ 0_1 & w_Q[\acute{M}_l] & \vdots & w_Q[2] & w_Q[1] & \vdots & \vdots \\ \vdots & 0_1 & \ddots & \vdots & \ddots & \ddots & \vdots \\ 0_{N-\acute{M}_l} & \vdots & \cdots & w_Q[\acute{M}_l] & \cdots & w_Q[2] & w_Q[1] \end{bmatrix}$$

The first column of $\bar{\mathbf{w}}_{\mathbf{I}}^{\mathbf{c}}$and $\bar{\mathbf{w}}_{\mathbf{Q}}^{\mathbf{c}}$ are $\mathbf{w_I}$ and $\mathbf{w_Q}$, respectively. $\bar{\mathbf{w}}_{\mathbf{I}}^{\mathbf{c}}$, and $\bar{\mathbf{w}}_{\mathbf{Q}}^{\mathbf{c}}$ can be expressed as $\bar{\mathbf{w}}_{\mathbf{I}}^{\mathbf{c}} = \bar{\mathbf{F}}^{*}\bar{\boldsymbol{\Delta}}_{\mathbf{w_I}}\bar{\mathbf{F}}$ and $\bar{\mathbf{w}}_{\mathbf{Q}}^{\mathbf{c}} = \bar{\mathbf{F}}^{*}\bar{\boldsymbol{\Delta}}_{\mathbf{w_Q}}\bar{\mathbf{F}}$. Here, $\bar{\boldsymbol{\Delta}}_{\mathbf{w_I}}$ and $\bar{\boldsymbol{\Delta}}_{\mathbf{w_Q}}$ are related to the $\mathbf{w_I}$ and $\mathbf{w_Q}$, respectively. They are expressed as, $\bar{\boldsymbol{\Delta}}_{\boldsymbol{w_I}} = diag\{\mathbf{W_I}\}$ where $\mathbf{W_I} = \bar{\mathbf{F}}\mathbf{w_I}$. Also, $\bar{\boldsymbol{\Delta}}_{\boldsymbol{w_Q}} = \boldsymbol{diag}\{\mathbf{W_Q}\}$ where $\mathbf{W_Q} = \bar{\mathbf{F}}\mathbf{w_Q}$, where $diag\{.\}$ stands for diagonal matrix operation. The elements of the diagonal matrix have been taken from the DFT of the first column of the respective circulant matrix. Substitution using, $\bar{\mathbf{w}}_{\mathbf{I}}^{\mathbf{c}} = \bar{\mathbf{F}}^{*}\bar{\boldsymbol{\Delta}}_{\boldsymbol{w_I}}\bar{\mathbf{F}}$ and $\bar{\mathbf{w}}_{\boldsymbol{Q}}^{\mathbf{c}} = \bar{\mathbf{F}}^{*}\bar{\boldsymbol{\Delta}}_{\mathbf{w_Q}}\bar{\mathbf{F}}$, equation (6.36) results in,

$$\hat{\mathbf{y}} = \bar{\mathbf{F}}^{*}\bar{\boldsymbol{\Delta}}_{\boldsymbol{w_I}}\bar{\mathbf{F}}.\mathbf{x} + \bar{\mathbf{F}}^{*}\bar{\boldsymbol{\Delta}}_{\boldsymbol{w_Q}}\bar{\mathbf{F}}.\mathbf{x}^{*} \qquad (6.37)$$

as, $\bar{\mathbf{F}}.\mathbf{x} = \mathbf{X}$, where $\mathbf{X} = \left[X\left[-\frac{N}{2}\right], X\left[-\frac{N}{2}+1\right], \ldots \ldots X\left[\frac{N}{2}-1\right]\right]^{T}$. $\bar{\mathbf{F}}.\mathbf{x}^{*} = \boldsymbol{X}^{\#} = \left[X^{*}\left[-\frac{N}{2}\right], X^{*}\left[\frac{N}{2}-1\right], \ldots X^{*}[0] \ldots X^{*}\left[-\frac{N}{2}+1\right]\right]^{T}$, the received signal after the DFT operation can be given by,

$$\bar{\mathbf{F}}\hat{\mathbf{y}} = \bar{\mathbf{F}}\bar{\mathbf{F}}^{*}\bar{\boldsymbol{\Delta}}_{\boldsymbol{w_I}}\bar{\mathbf{F}}.\mathbf{x} + \bar{\mathbf{F}}\bar{\mathbf{F}}^{*}\bar{\boldsymbol{\Delta}}_{\boldsymbol{w_Q}}\bar{\mathbf{F}}.\mathbf{x}^{*} \qquad (6.38)$$

thus, $$\widehat{\mathbf{Y}} = \overline{\boldsymbol{\Delta}}_{\boldsymbol{w_I}}\mathbf{X} + \overline{\boldsymbol{\Delta}}_{\boldsymbol{w_Q}}\mathbf{X}^{*} \quad (6.39)$$

where, $\widehat{\mathbf{Y}} = \bar{\mathbf{F}}\mathbf{y}$. The resultant signal for k^{th} frequency index of the received signal is given by,

$$\hat{Y}[k] = W_I[k]X[k] + W_Q[k]X^*[-k] \quad (6.40)$$

where, $W_I[k]$ and $W_Q[k]$ are the $(k,k)^{th}$ element of the diagonal matrix $\overline{\boldsymbol{\Delta}}_{\boldsymbol{w_I}}$ and $\overline{\boldsymbol{\Delta}}_{\boldsymbol{w_Q}}$, respectively. Also, $W_I[k]$ and $W_Q[k]$ are the estimates of $uH[k]$ and $vH^*[-k]$ respectively. In case of no I/Q imbalance situation, $W_Q[k]$ =0 and $W_I[k] = H[k]$. Due to the I/Q imbalance, not only the $H[k]$ itself, but also $H^*[-k]$, affect the received signal. Therefore estimating and equalizing only for $H[k]$ is not adequate to get an accepted level of SER.

Similarly, the conjugate of the received signal in $[-k]^{th}$frequency index is given as:

$$\hat{Y}^*[-k] = W_I^*[-k]X^*[-k] + W_Q^*[-k]X[k] \quad (6.41)$$

These two equations can be written in matrix form as,

$$\begin{bmatrix} \hat{Y}[k] \\ \hat{Y}^*[-k] \end{bmatrix} = \begin{bmatrix} W_I[k] & W_Q[k] \\ W_Q{}^*[-k] & W_I{}^*[-k] \end{bmatrix} \begin{bmatrix} X[k] \\ X^*[-k] \end{bmatrix} \quad (6.42)$$

Therefore, $X[k]$ and $X^*[-k]$ can be estimated as,

$$\begin{bmatrix} \hat{X}[k] \\ \hat{X}^*[-k] \end{bmatrix} = \begin{bmatrix} W_I[k] & W_Q[k] \\ W_Q{}^*[-k] & W_I{}^*[-k] \end{bmatrix}^{-1} \begin{bmatrix} \hat{Y}[k] \\ \hat{Y}[-k] \end{bmatrix} \quad (6.43)$$

The elements of the inverse matrix given in equation (6.43) will be finite, under the condition that $W_I[k] * W_I{}^*[-k] \neq W_Q[k] * W_Q{}^*[-k]$. By means of the inverse fast

Fourier transform (IFFT) of $\widehat{\mathbf{X}} = \left[\hat{X}\left[-\frac{N}{2}\right], \hat{X}\left[-\frac{N}{2}+1\right], \ldots \ldots \hat{X}\left[\frac{N}{2}-1\right]\right]^T$, we obtain the compensated signal $\hat{\mathbf{x}}$, such that:

$$\hat{\mathbf{x}} = \bar{\mathbf{F}}^* \widehat{\mathbf{X}} \tag{6.44}$$

thus,

$$\hat{\mathbf{x}} = \left[\hat{x}\left[-\frac{N}{2}\right], \hat{x}\left[-\frac{N}{2}+1\right], \ldots \ldots \hat{x}\left[\frac{N}{2}-1\right]\right]^T \tag{6.45}$$

6.4.1 Simulation results for the frequency domain compensation

In this section, the performance of the proposed compensation scheme has been evaluated through MATLAB simulations. The same simulation parameters given in Tables 6-1 and 6-2 have been used in this case as well. The gain and phase imbalances have been considered to be g = 1.2 and φ = 10º, respectively. The reference signal has been coded as QPSK.

- ***Mean squared error (MSE)***

Figure 6-24 shows the MSE for this scheme. The MSE converges before 70 iterations. Moreover, the MSE has been obtained for a gain of 20% and a phase of 10º. The MSE has been shown for two different SNR levels. For the SNR of 20 dB, the MSE converges at 60 iterations, but the residue error is high. After 60 iterations, the MSE value for 20 dB of SNR is $1.5x10^{-2}$. On the other hand, for SNR of 30 dB, it has taken 70 iterations to converge and the residue error is $1.5x10^{-3}$ for this case, which is much lower than the previous case.

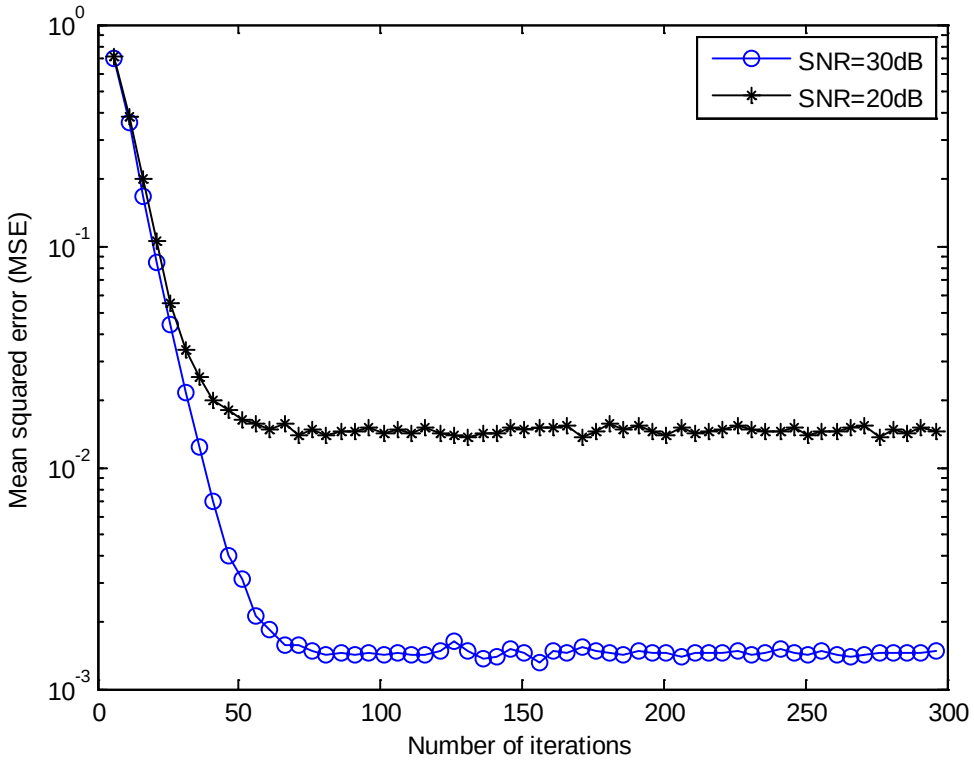

Figure 6-24 MSE for different SNR levels

- ***Signal constellations***

For an I/Q gain and phase combination of $g = 1.2$ and $\varphi = 10^{o}$, the received signal's constellations have been presented in this section. Constellations of 64-QAM, 16-QAM, and QPSK have been illustrated for uncompensated and compensated cases. The SNR has been chosen as 30 dB for this simulation. In Figure 6-25, the constellation of the received signal without any compensation, has been presented for 64-QAM signal. Figure 6-26 shows the received signal after compensation by the proposed frequency domain compensation scheme. Comparing these two constellations, it is clear that the compensated signal shows more improvement than the uncompensated one. Similarly, Figures 6-27 and 6-28 present the uncompensated and compensated received signal for the 16-QAM modulation.

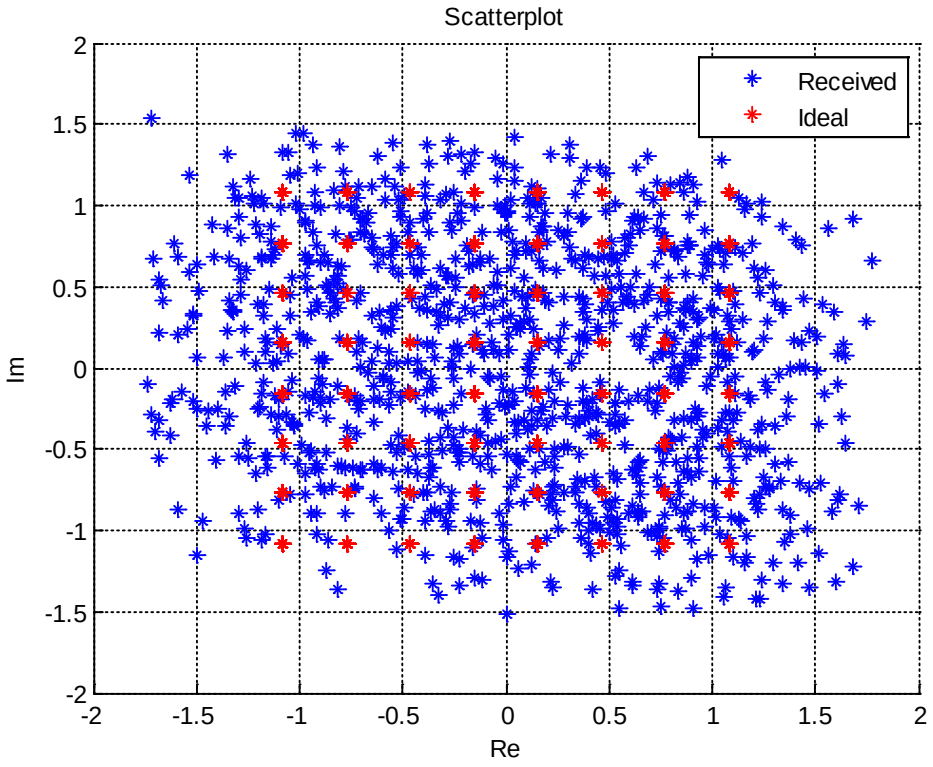

Figure 6-25 Constellation of the uncompensated signal, for 64-QAM

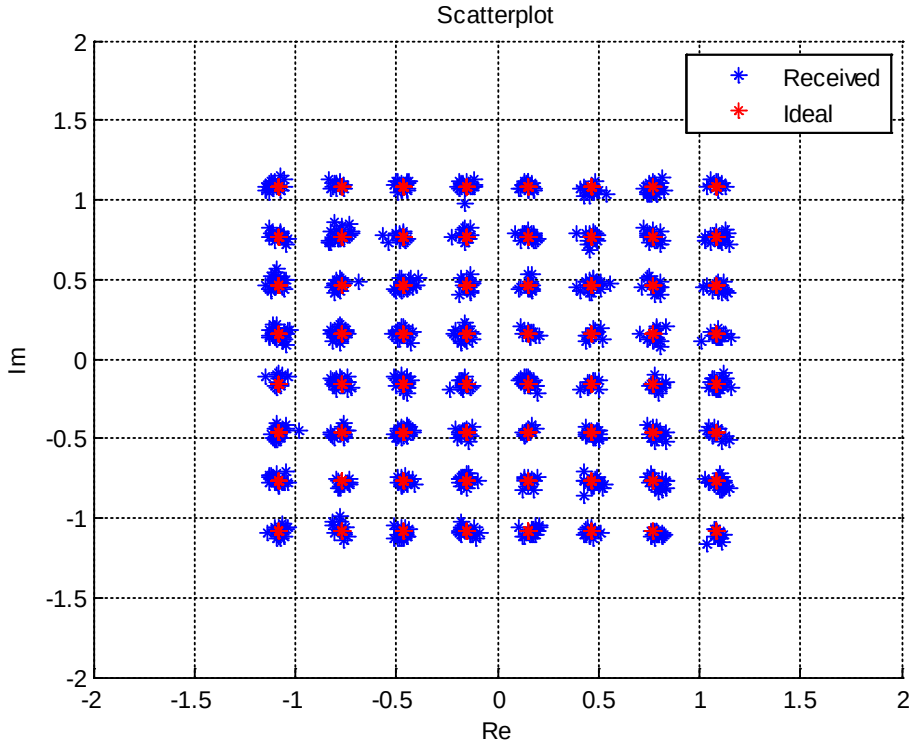

Figure 6-26 Constellation of the received signal after being compensated by the frequency domain compensation method, for 64-QAM

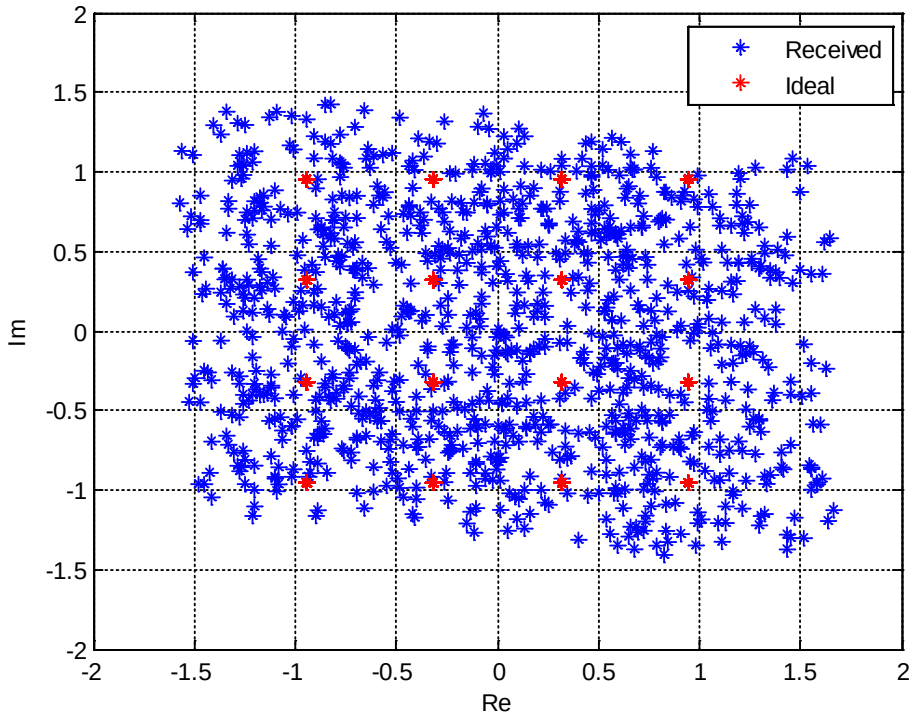

Figure 6-27 Constellation of the uncompensated signal, for 16-QAM

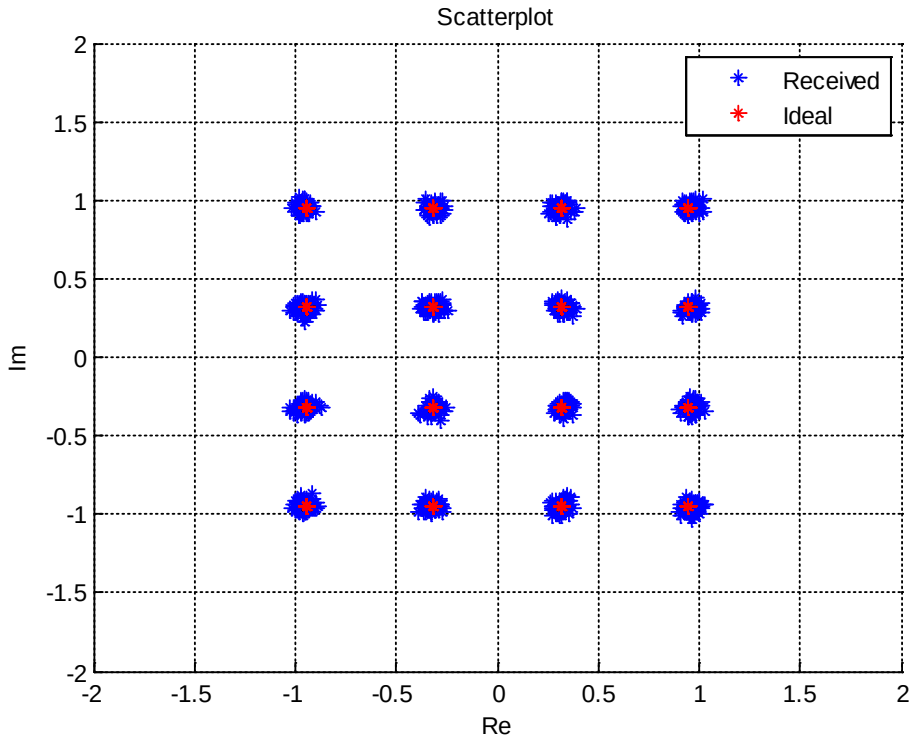

Figure 6-28 Constellation of the received signal after being compensated by the frequency domain compensation method, for 16-QAM

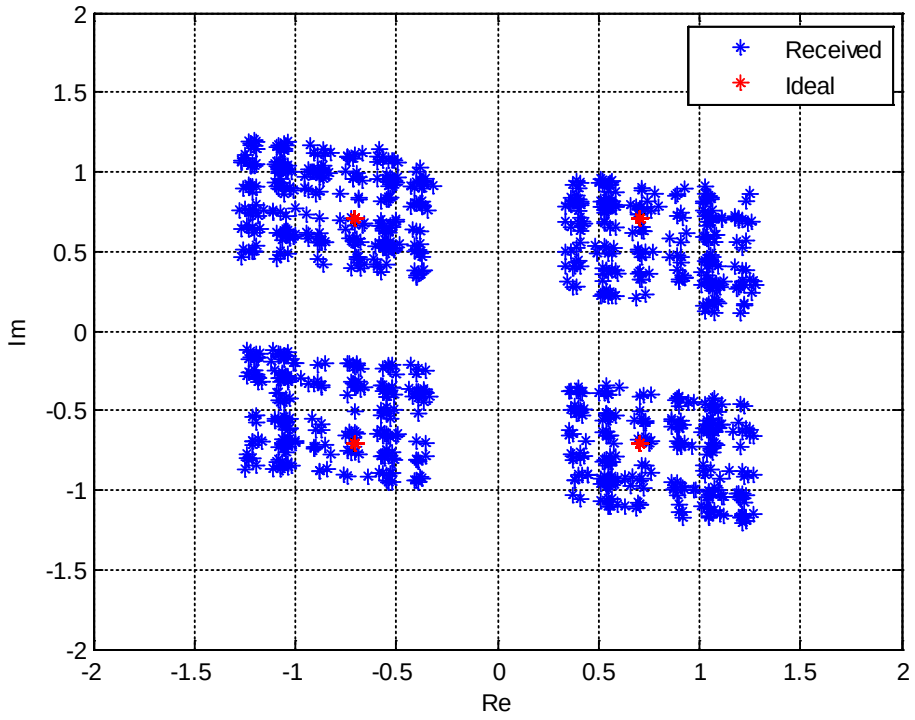

Figure 6-29 Constellation of the uncompensated signal, for QPSK

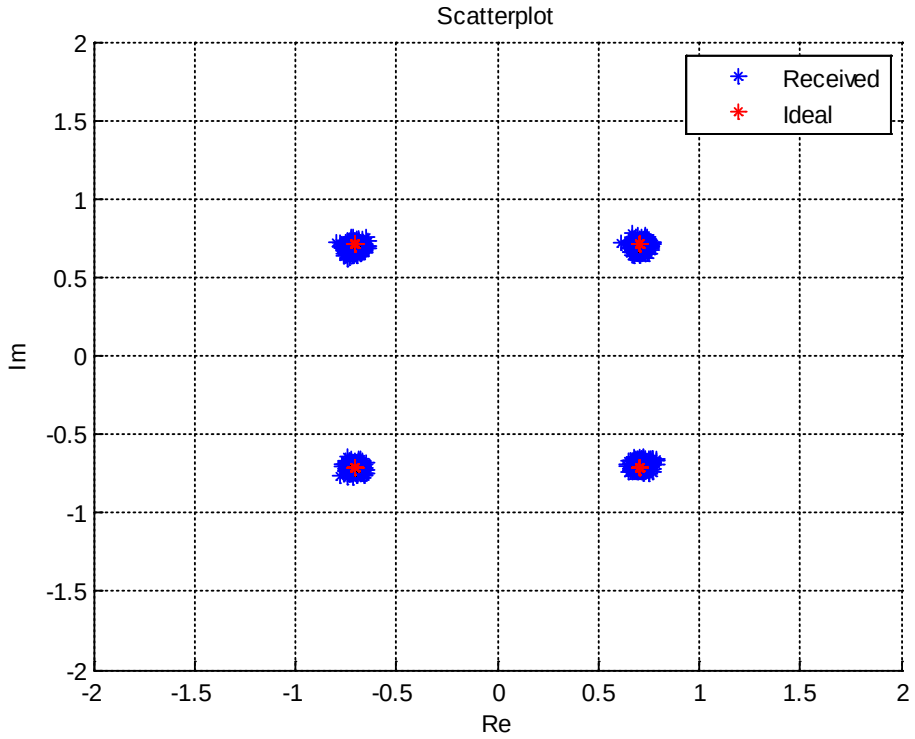

Figure 6-30 Constellation of the received signal after being compensated by the frequency domain compensation method, for QPSK

The uncompensated signal of 16-QAM is also quite similar to the uncompensated 64-QAM signal. However, the compensated signal demonstrates much improvement. Also, in Figures 6-29 and 6-30, the constellation of the uncompensated and compensated signal for the QPSK modulation has been presented. For all the modulation types stated above, the compensated output has been enhanced significantly compared to the uncompensated signal.

- ***Error vector magnitude (EVM)***

In this section, the scheme has been further illustrated in terms of the EVM. The EVMs have been taken for different gain and phase combinations for 64-QAM and 16-QAM modulations. The EVM corresponding to 64-QAM has been shown in Figure 6-31.

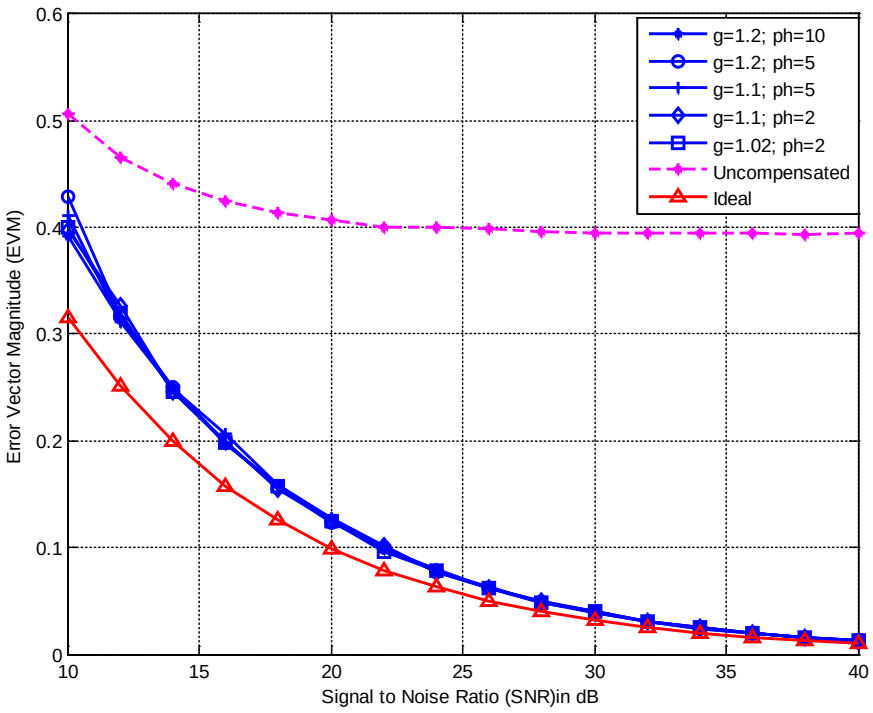

Figure 6-31 EVM for different gain and phase combinations after compensation by the frequency domain compensation technique for 64-QAM.

The term 'g' and 'ph' in the legend refer the gain and phase deviation. Also, the term 'uncompensated' refers to the received signal before experiencing any I/Q and channel

compensation. The legend 'ideal' refers to the case when the received signal has not undergone any I/Q or channel distortion. It has been observed that the EVM curves are similar to each other and close to the ideal (no I/Q and channel condition) for a variety of I/Q gain and phase combinations. In Figure 6-32, the EVM curves have been shown for the 16-QAM signal. Here also, the EVM curves for the received signal are equal to each other and close to the ideal condition.

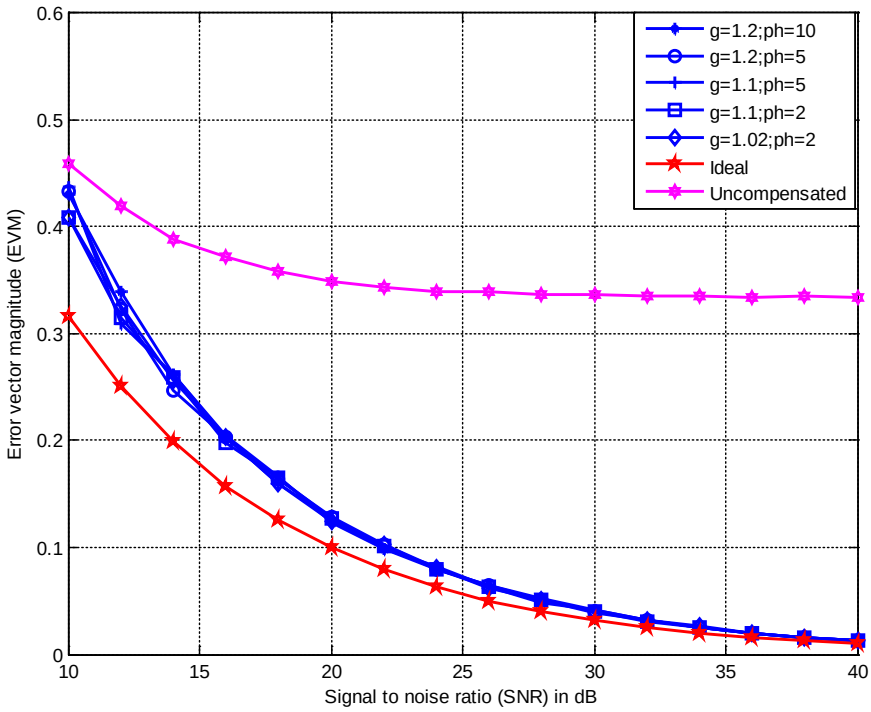

Figure 6-32 EVM for different gain and phase combinations after compensation by the frequency domain compensation technique for 16-QAM.

- ***Symbol error rate (SER)***

For the same gain and phase combination, the SERs have also been obtained for 64-QAM and 16-QAM modulations. The SER results after the received signal has been compensated for by the proposed method have been shown in Figure 6-33 for different I/Q imbalance combinations.

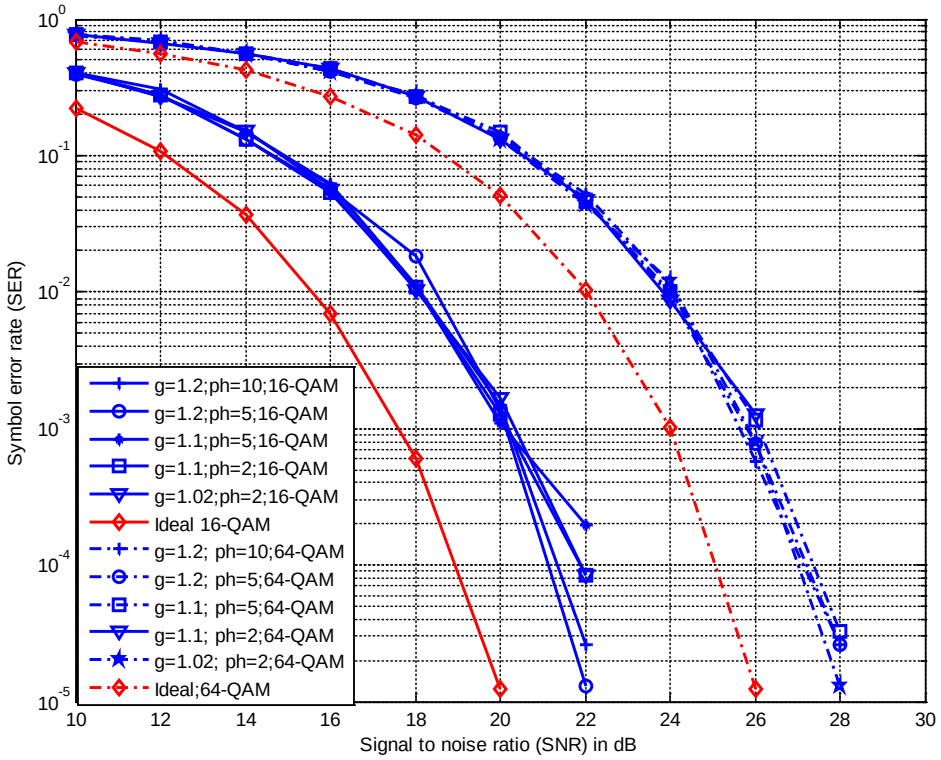

Figure 6-33 SER for different gain and phase combinations after being compensated by the frequency domain compensation technique, for 64-QAM and 16-QAM

The term 'g=1.2, ph=10: 16-QAM' references that the value of g and φ are 1.2 and 10^{o}, respectively, and the modulation technique is 16-QAM. It has been observed from the SER performance that the SERs for different gain and phase combinations are almost same. Also, for the 16-QAM modulation, the SNR for the received compensated signal is 2.5 dB higher than the ideal condition for a specific SER of 10^{-3}. For 64-QAM with SERs of 10^{-3}, the SNR is 2 dB higher than the ideal curve.

6.5 Comparison of time domain correction and frequency domain compensation schemes

Both of the time domain correction and the frequency domain compensation schemes are capable of mitigating the I/Q imbalance and channel in the case of single carrier

modulation. However, they both have some advantages and drawbacks. A comparison between the outputs of these two proposed methods has been shown in terms of EVM and SER. For the time domain case, as the signal gets better for successive frames, the output of the fifth frame has been taken for calculating the EVM and SER. On the other hand, for the frequency domain case, the output starts to perform well from the very first frame; therefore, for this case, the first frame has been taken for calculating the EVM and SER. Figures 6-34 and 6-35 present the EVM of the received signal for 64-QAM and 16-QAM, respectively, after compensation by both methods (i.e., the time domain correction and the frequency domain compensation).

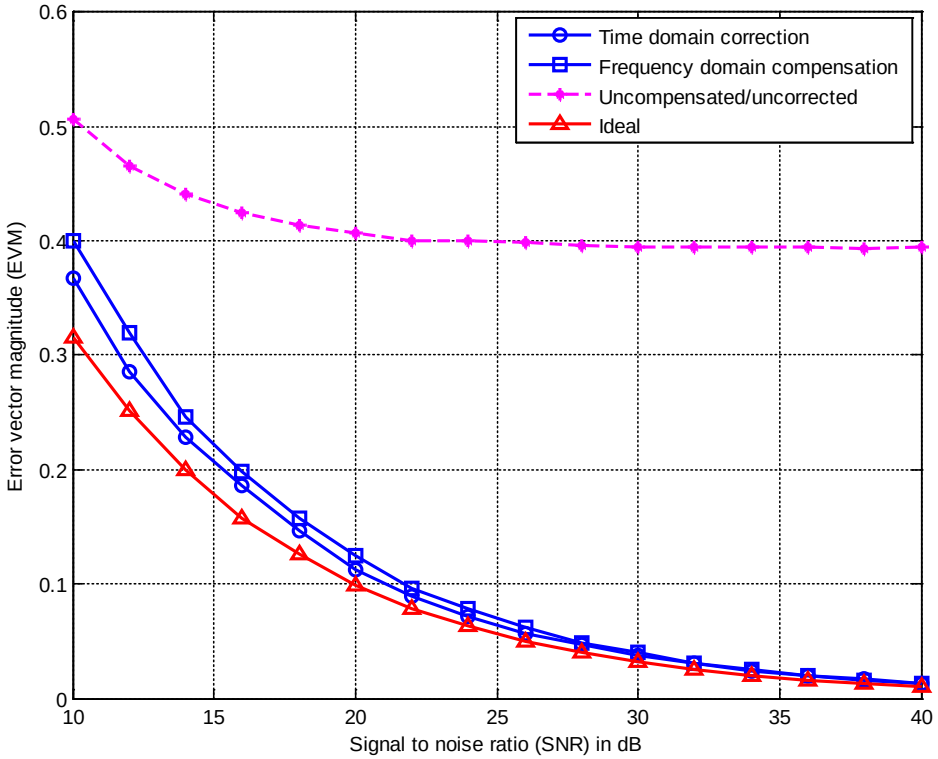

Figure 6-34 EVM representation for the time domain correction and frequency domain compensation, for 64-QAM

The term ‘time domain correction’ and ‘frequency domain compensation’ refer to the received signal after correction/compensation by the time domain correction method and the frequency domain compensation method, respectively. In Figure 6-34, it can be observed that the EVM corresponding to the received signal obtained by the time

domain correction method shows slightly lower values than the EVM obtained for the frequency domain compensation. However, the difference is only visible for an SNR lower than 20 dB. Similarly, in the case of the EVM shown in Figure 6-35 for the 16-QAM modulation, the time domain correction scheme has less error value than the frequency domain compensation scheme when the noise is more than 20 dB. For an SNR less than 20 dB, the frequency domain compensation scheme shows less error.

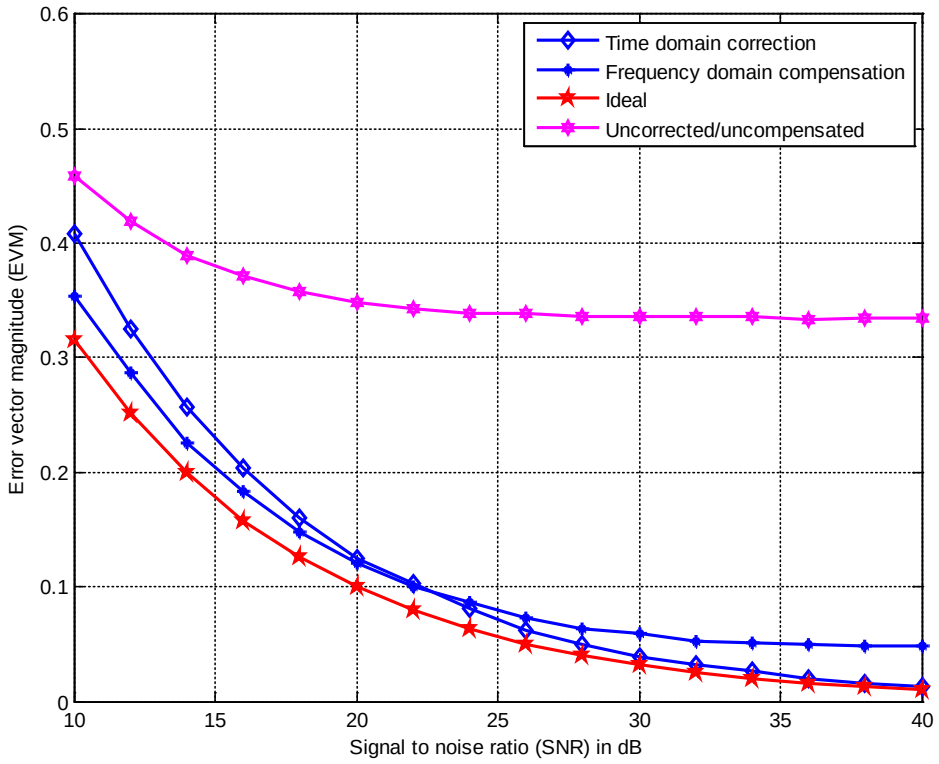

Figure 6-35 EVM representation for the time domain correction and frequency domain compensation, for 16-QAM

The difference is more realizable in the case of the SER. In Figure 6-36, the SERs corresponding to these two methods have been shown. Also, the same figure contains the SERs corresponding to 64-QAM and 16-QAM. By means of the SER curves, it has been observed that for both of the modulations (64-QAM and 16-QAM), the time domain correction scheme performs better than the frequency domain compensation scheme.

For 16-QAM, for SERs of 10^{-3}, the SNR for the time domain correction method is 1.2 dB higher than the ideal (no I/Q and channel) condition, whereas for the same SER, the SNR for the frequency domain compensation scheme is approximately 2.2 dB higher than the ideal SER curve. Thus, the SNR corresponding to the frequency domain scheme is 1 dB higher than the time domain scheme.

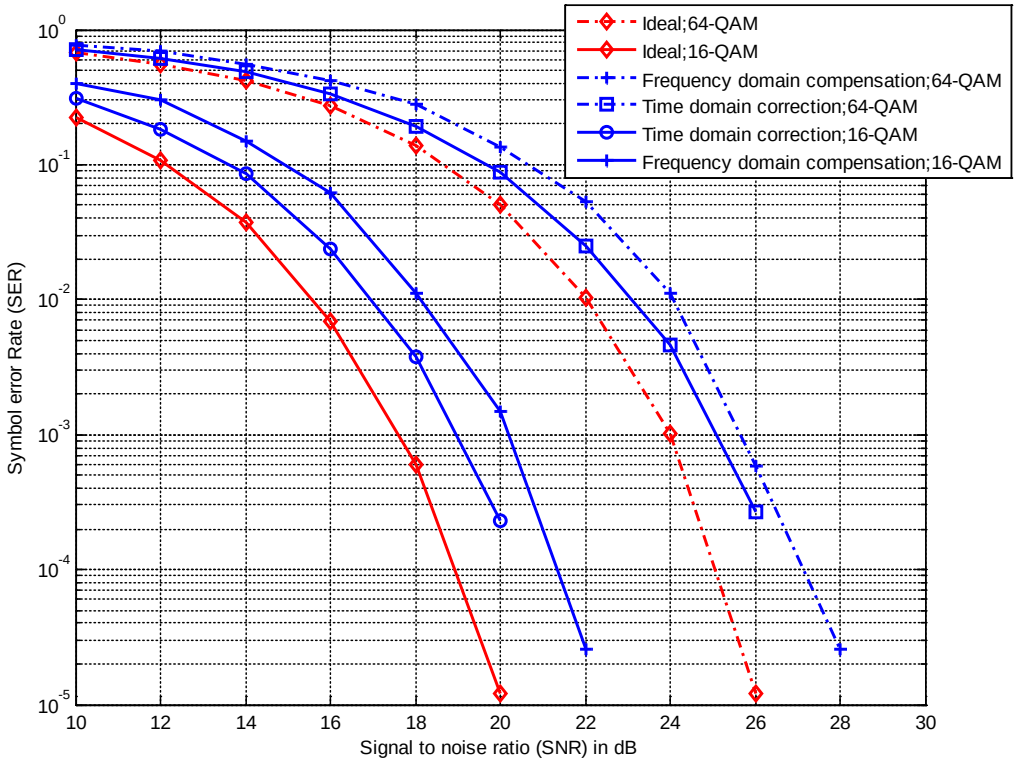

Figure 6-36 SER representation for the time domain correction and frequency domain compensation

For the 64-QAM modulation for SERs of 10^{-3}, the SNR corresponding to the time domain scheme is approximately 1 dB higher than the ideal SER curve. Similarly, for the same SER, the SNR for the frequency domain compensation is approximately 1.8 dB higher than the ideal curve. Therefore, for 64-QAM SNR degradation is 0.8 dB more in the case of the frequency domain compensation scheme than the time domain correction scheme.

From the EVM and SER, it can be observed that the time domain correction method shows slightly better results than the frequency domain compensation scheme. When the I/Q varies slowly, the gain and phase imbalance values obtained for several frames can be averaged, and more steady estimates of the imbalance values can be achieved. In cases when the channel changes more frequently than the I/Q, these estimated I/Q values can be held for several frames while only updating the channel. This reduces computational burden. Also, if the I/Q can be estimated and corrected prior to the channel equalization, the equalizer would converge more quickly. Moreover, prior correction of I/Q parameters would help when extracting the training sequences from the received signal, which means the chances of getting faulty training symbols decrease for each consecutive frame. However, the time domain correction scheme requires at least five to ten frames to get a close approximate value of the imbalance gain and phase. Also, this method would not be suitable for frequency-selective I/Q variation.

On the other hand, the frequency domain scheme does not have to wait for these frames. It can perform well from the very first frame. But the channel and I/Q needs to be updated in every single frame. Additionally, the training needs to be perfectly synchronized with the received signal, as there is no option for a prior correction. Moreover, this method requires an extra CP in order to be functional. However, this method can be made useful for frequency–selective I/Q by increasing the number of filter taps. Depending on the I/Q characteristics (i.e., whether the I/Q is frequency-selective, or time variant) any one of the methods can be chosen.

Both of these methods use the two-way filter network shown in Figure 6-1. Instead of using the two-way filter network, parallel correction and equalization can also be performed using a conventional equalizer. However, the system then requires a lot of time to converge (details in Appendix A).

6.6 Summary

In this chapter, a time domain estimation and correction technique and a frequency domain compensation technique have been presented. Both of the methods are capable of mitigating the I/Q and channel for a single carrier modulation technique. The frequency domain method can also be used for the case of single carrier frequency domain equalization (SC-FDE). Simulation results show that the EVM of the corrected or compensated output can be made as low as the ideal EVM. In addition, the SER representations show that, to achieve an SER of 10^{-3}, the SNR of the corrected and compensated signal is around 1 dB more degraded than the ideal case.

CHAPTER 7
CONCLUSION AND FUTURE WORKS

7.1 Conclusion

Superheterodyne receivers require high quality off-chip bandpass filters for image rejection and channel selectivity. That makes them unsuitable for monolithic integration. Also, conventional low-IF receivers require very large image rejection levels. The required image rejection level can be up to 70 dB [1]. Therefore, they require very precise matching of I and Q signal paths. On the other hand, direct conversion or zero-IF receivers are suitable for monolithic integration. A problem with the DCRs (compared to their superheterodyne counterparts) is that the baseband signal is severely affected by the mismatches of gain and phase in the I and Q branches. Moreover, this distortion is likely to increase in the future when higher silicon integration and higher carrier frequencies will be required [2]. Therefore, the main goal of this research has been mitigating this I/Q imbalance and channel distortion for DCRs. In this regard, robust schemes to correct and compensate for the I/Q imbalance and multipath channel intended for both OFDM and single carrier modulations have been developed.

The main conclusions of this research are presented as follows:

Some well-known receiver architecture as the DCRs and superheterodyne receivers with their advantages and drawbacks have been presented in Chapter 2. A brief discussion regarding the establishment of the I/Q mismatch, the reasons involved for

the development of the I/Q imbalance, and the significance of its adverse consequences on the received signal have also been discussed in this chapter. Mathematical representations for the baseband and the bandpass signal with multipath channel effect have been presented. A general mathematical model of I/Q imbalance on single carrier modulation has been presented. The I/Q model has been extended for the OFDM signal. Finally, the individual effects of frequency-flat I/Q gain and phase on the received signal have been shown by means of Matlab simulations. The simulation results show that only the presence of a frequency-flat phase imbalance of 10^{o} can increase the SER significantly. Therefore, it is evident that the signal condition would be much worse when the received signal suffers by ISI due to the multipath channel and both gain and phase imbalances are present. Thus a correction of this I/Q gain and phase mismatch or a compensation for the I/Q and channel are necessary in order to obtain an acceptable SER. This chapter discusses the necessity of I/Q imbalance correction and compensation as well.

Chapter 3 includes an up-to-date literature review in the field of I/Q imbalance and multipath channel. The discussion includes the correction and compensation schemes in both the digital and analogue domains. In the digital domain, there are many correction/compensation schemes present for the single carrier and multicarrier modulations. There are a wide variety of parameters and conditions on which the performance of these schemes depend. Also, different schemes are suitable for different application areas, such as DVB-T, LTE, WiMax, Wi-Fi, etc.

In Chapter 4, a novel adaptive combined correction and compensation scheme (ACCC) has been proposed for OFDM modulation. The scheme uses a fixed pilot pattern to estimate the I/Q and channel parameters. From the estimated parameters, the frequency-flat gain and phase (called the nominal gain and phase) have been estimated. These gain and phase values are fed back to make a correction to the upcoming OFDM frame. At the same time, the current frame goes through the compensator where the remaining frequency-selective I/Q imbalance (residue I/Q) and the channel effect are mitigated. The scheme requires at least three to five frames to complete the estimation correctly. After approximately five OFDM frames, the estimated parameters become

close to the actual value. In addition, unlike some other well-known methods, in this scheme the pilot tones are retrieved from the received signal. Among the retrieved pilots, a good percentage of the pilots have been detected incorrectly due to the I/Q imbalance and channel. These incorrectly estimated pilots lead to an incorrect estimation of the I/Q parameters. However, in this scheme the upcoming frames get corrected before the pilot extraction. Thus, some portion of the I/Q imbalance is eliminated before the pilot extraction. As the estimation and correction improve for consecutive frames, the extraction of pilots also improves for the following frames. After approximately five OFDM frames, the percentage of incorrectly detected pilots can be reduced to 0.1% from 10%. Different numbers of pilots have been used to obtain the minimum number of pilots the scheme requires to stay functional. It has been found that the scheme can work perfectly by making use of less than 2% of the subcarriers as pilot tones. Moreover, the scheme is suitable for high frequency-selective I/Q imbalances.

A special pilot pattern has been used for estimation. Only two states having the highest power have been used as pilots from the entire constellation. This assures good estimation in the presence of noise. Also, using only two states reduces the chance of detecting incorrect pilot tones. The system has been evaluated in the presence of different frequency-flat I/Q gain and phase combinations. The frequency-flat gain has been chosen to be from 2% to 20%. Similarly, the frequency-flat phase has been chosen to be from 2^{o} to 10^{o}. The lesser the value of gain and phase, the earlier it results in an accurate estimation. The ACCC scheme is capable of mitigating the I/Q imbalance and channel for this wide range of frequency-flat gain and phase. The resultant output is almost the same for all combinations of gain and phase imbalance. Moreover, two different frequency-selective I/Q imbalance models have been used. In Section 4.4.4, the estimation of I/Q and channel parameters have been presented for the first and third frames for these two models. Model 1 has a very low variation of I/Q, so from the very first frame the estimations are quite accurate. On the other hand, due to the high variation in Model 2, the estimation becomes accurate after at least three frames.

In Section 4.4.9, the system has been assessed for different channel scenarios. Two channel models have been considered, one is a nine-path LTE channel for ETU and the other one is a two-path Ricean channel. The maximum delay spread of the Ricean channel has been changed to see the effect on the received signal for two models of frequency-selective I/Q imbalance for different frames. The proposed ACCC scheme mitigates the channel and I/Q imbalance for different channel scenarios as well.

Chapter 5 is basically a comparison and performance analysis of the proposed ACCC scheme with some of the well-known schemes existing in literature. Three compensation methods suitable for the OFDM have been chosen for the comparison. These methods have been tested under several conditions, such as different numbers of pilots, different frequency-flat and frequency-selective I/Q imbalances, different channel scenarios, etc. Moreover, in all the schemes, the detected pilot tones have been retrieved from the received signal. This means the extracted pilots have error. The goal was to observe how these schemes work in the case when all the detected pilots have not been chosen perfectly. All the schemes seem to work well when the I/Q variation is lower. For Model 1, the adaptive compensation scheme works better than the proposed ACCC scheme. However, for a higher variation of the I/Q imbalance, only the ACCC scheme works well even when pilots are incorrectly detected.

Chapter 6 presents two methods to mitigate the I/Q and channel for the single carrier modulation. Both of these methods use time domain estimation of I/Q and channel parameters using a two-way filter network. After the estimation, one method uses a feedback based time domain correction. On the other hand, the other method uses frequency domain compensation by utilizing the estimated parameters. For both of the methods, iterative LMS schemes have been used to obtain the channel and the I/Q parameters. Both of the methods use training signals for parameter estimation. The time domain correction method has been described in Section 6.3.

The gain and phase associated are estimated and sent back to complete the correction for the upcoming frame. Meanwhile, the signal passes through the equalizer to mitigate the channel effect. For the upcoming consecutive frames, the system obtains more

accurate estimates for the gain and phase values. This leads to much better equalization resulting in better output as well. Thus, the system performance improves with the number of the following frames. Similar to the ACCC scheme, this scheme is also able to obtain a close approximate estimation after almost five successive frames. It has been shown in Section 6.3.1.3 that the gain and phase approach the ideal values after five frames for different order modulation, such as 64-QAM and 16-QAM. The SER performance shows that the system improves with the consecutive frames. Also, it is evident from the SER response that the resultant output is similar for different frequency-selective I/Q gain and phase combinations. On the other hand, the frequency domain compensation method, presented in Section 6.4, does not use any feedback. Instead, it is a joint compensation method for both the I/Q and channel. The difference is that after the parameters have been estimated in the time domain, the values have been converted to the frequency domain. The channel and I/Q compensation in the frequency domain is less computationally complex. A CP has been added before the start of each frame before transmission. On the receiver side, frequency domain compensation has been performed to mitigate both the I/Q imbalance and channel effect simultaneously. The effectiveness of the proposed frequency domain compensation scheme, in order to correct a combination of I/Q imbalance and multipath channel, has been demonstrated in Section 6.4.1. The SER performance of the proposed frequency domain compensation scheme operating with various I/Q gain and phase has been presented in Section 6.4.1.4. It has been shown that an acceptable SER can be achieved for all values of I/Q imbalance and multipath channel.

These two methods have been compared with the assistance of SER in Section 6.5. The time domain method shows slightly better results than the frequency domain correction method. The frequency domain method would be suitable for single carrier frequency domain estimation known as SC-FDE (Appendix A).

7.2 Future work

The next stage of the research will focus on the hardware implementation of the proposed signal processing architecture. For this reason, the following topics need to be considered in greater detail.

The application area of the I/Q imbalance correction/compensation described in Chapter 4 is mainly the DCRs. However, the DCRs suffer from another well-known distortion known as the DC offset. The effect of DC offsets on the operation of the proposed scheme must be determined. The I/Q imbalance has been chosen as frequency-flat for the methods described in Chapter 6. In addition, the training signal has been assumed to be perfectly detected for these methods. Also, it has been assumed that the training signal has been synchronized perfectly. These issues will be taken into consideration in the future before the hardware implementation.

APPENDIX A

PROPOSED ACCC FOR SC-FDE

The ACCC scheme can be applied for single carrier frequency domain equalization. The block diagram shown in Figure A-1, presents the ACCC scheme on SC-FDE. The scheme can be divided into three steps. The steps are, 1) Pre-FFT correction, 2) Nominal gain and phase estimation and 3) Frequency domain compensation.

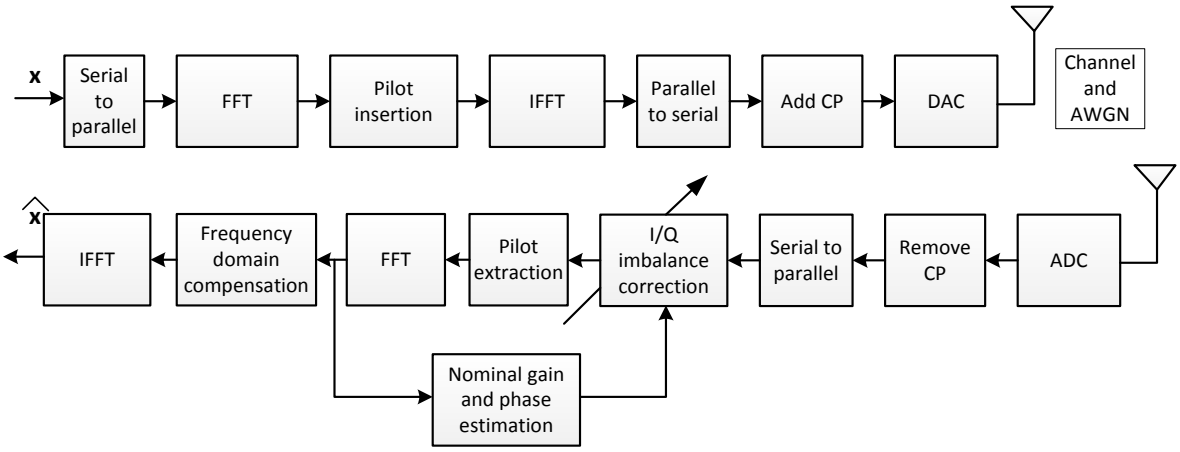

Figure A-1 Block diagram of the ACCC scheme on SC-FDE

Step 1: Pre-FFT Correction

The pilots have been inserted after the FFT has been performed in the transmitter side. The pilot pattern shown in Figure can be used for this case. At the receiver side, before the FFT, the time domain sampled version of the received signal including the I/Q imbalance and channel has been given below. At the beginning of the m^{th} frame, the n^{th} sample of the i^{th} received symbol $y_m^i[n]$ is expressed as according to (4.2),

$$y_m^i[n] = u_m[n] \circledast r_m^i[n] + v_m[n] \circledast r_m^{*i}[n]$$

$$\text{or} \quad y_m^i[n] = u_m[n] \circledast h_m[n] \circledast x_m^i[n] + v_m[n] \circledast h_m^*[n] \circledast x_m^{*i}[n] + \varepsilon_{T,m}^i[n] \tag{A.1}$$

Here, $u_m[n]$, $v_m[n]$, $h_m[n]$ and $\varepsilon_{T,m}^i[n]$ represents $u[n]$, $v[n]$, $h[n]$ and $\varepsilon_T[n]$ in (4.2) for the i^{th} symbol and m^{th} frame. However, the notation for the i^{th} symbol has been omitted for $u_m[n]$, $v_m[n]$ and $h_m[n]$, assuming the channel and I/Q imbalance remain same for one frame.

$y_m^i[n]$ is corrected by the nominal gain and phase, $g_{m-1}$and φ_{m-1}, estimated during the previous $(m-1)^{th}$frame. The corrected output, $c_m^i[n]$, can be obtained from (4.6) as,

$$\begin{bmatrix} Re\{c_m^i[n]\} \\ Im\{c_m^i[n]\} \end{bmatrix} = \begin{bmatrix} g_{m-1} & 0 \\ -sin\varphi_{m-1} & cos\varphi_{m-1} \end{bmatrix}^{-1} \begin{bmatrix} Re\{y_m^i[n]\} \\ Im\{y_m^i[n]\} \end{bmatrix} \tag{A.2}$$

$$c_m^i[n] = \breve{u}_m[n] \circledast h_m[n] \circledast x_m[n] + \breve{v}_m[n] \circledast h_m^*[n] + \acute{\varepsilon}_{T,m}^i[n][n] \tag{A.3}$$

In (4.9), $\breve{u}_m[n]$, $\breve{v}_m[n]$ and $\acute{\varepsilon}_{T,m}^i[n]$ represent, $u_m[n]$, $v_m[n]$, and $\varepsilon_{T,m}^i[n]$ respectively, that has been undergone I/Q imbalance correction. This forms the input of the FFT block. After the FFT on $c_m^i[n]$, the resulting frequency-domain signal can be expressed as,

$$C_m^i[k] = \breve{U}_m[k]H_m[k]X_m^i[k] + \breve{V}_m[k]H_m^*[-k]X_m^{*i}[-k] + \acute{\eta}_m^i[k] \tag{A.4}$$

With the frequency index k replaced by its corresponding pilot location k_p, the corrected signal for the i^{th} symbol in the m^{th} frame $C_m^i[k_p]$, can be expressed as,

$$\begin{bmatrix} C_m^i[k_p] \\ C_m^{i+1}[k_p] \end{bmatrix} = \begin{bmatrix} X_m^i[k_p] & X_m^{*i}[-k_p] \\ X_m^{i+1}[k_p] & X_m^{*i+1}[-k_p] \end{bmatrix} \begin{bmatrix} \breve{U}_m[k_p]H_m[k_p] \\ \breve{V}_m[k_p]H_m^*[-k_p] \end{bmatrix} + \begin{bmatrix} \acute{\eta}_m^i[k_p] \\ \acute{\eta}_m^{i+1}[k_p] \end{bmatrix} \tag{A.5}$$

Or in matrix form as,

$$\mathbf{C_p} = \bar{\mathbf{X}}_\mathbf{p}\boldsymbol{\beta}_\mathbf{p} + \boldsymbol{\eta}_\mathbf{p} \tag{A.6}$$

where, $\mathbf{C_p} = \begin{bmatrix} C_m^i[k_p] \\ C_m^{i+1}[k_p] \end{bmatrix}$, $\overline{\mathbf{X}}_\mathbf{p} = \begin{bmatrix} X_m^i[k_p] & X_m^{*i}[-k_p] \\ X_m^{i+1}[k_p] & X_m^{*i+1}[-k_p] \end{bmatrix}$, $\boldsymbol{\beta}_\mathbf{p} = \begin{bmatrix} \breve{U}_m[k_p]H_m[k_p] \\ \breve{V}_m[k_p]H_m^*[-k_p] \end{bmatrix}$,

and $\eta_p = \begin{bmatrix} \acute{\eta}_m^i[k_p] \\ \acute{\eta}_m^{i+1}[k_p] \end{bmatrix}$.

Assuming the noise to be white, by the help of best linear unbiased estimator (BLUE), I/Q and channel parameters can be estimated as,

$$\widehat{\boldsymbol{\beta}}_\mathbf{p} = [\overline{\mathbf{X}}_\mathbf{p}]^{-1}\mathbf{C_p} \tag{A.7}$$

$\widehat{\boldsymbol{\beta}}_\mathbf{p}$ is the estimated value of $\boldsymbol{\beta}_\mathbf{p}$ including error. Equivalently the complex conjugate of the corrected signal for $-k_p^{th}$ frequency index is given by,

$$\begin{bmatrix} C_m^{*i}[-k_p] \\ C_m^{*i+1}[-k_p] \end{bmatrix} = \begin{bmatrix} X_m^{*i}[-k_p] & X_m^i[k_p] \\ X_m^{*i+1}[-k_p] & X_m^{i+1}[p] \end{bmatrix} \begin{bmatrix} \breve{U}_m^*[-k_p]H_m^*[-k_p] \\ \breve{V}_m^*[-k_p]H_m[k_p] \end{bmatrix} + \begin{bmatrix} \acute{\eta}_m^{*i}[-k_p] \\ \acute{\eta}_m^{*i+1}[-k_p] \end{bmatrix} \tag{A.8}$$

Let, $\boldsymbol{\beta}_\mathrm{p}^\mathbf{c} = \begin{bmatrix} \breve{U}_m^*[-k_p]H_m^*[-k_p] \\ \breve{V}_m^*[-k_p]H_m[k_p] \end{bmatrix}$, $\overline{\mathbf{X}}_\mathbf{p}^\mathbf{c} = \begin{bmatrix} X_m^{*i}[-k_p] & X_m^i[k_p] \\ X_m^{*i+1}[-k_p] & X_m^{i+1}[k_p] \end{bmatrix}$, $\mathbf{C}_\mathbf{p}^\mathbf{c} = \begin{bmatrix} C_m^{*i}[-k_p] \\ C_m^{*i+1}[-k_p] \end{bmatrix}$

and $\boldsymbol{\eta}_\mathrm{p}^\mathbf{c} = \begin{bmatrix} \acute{\eta}_m^{*i}[-k_p] \\ \acute{\eta}_m^{*i+1}[-k_p] \end{bmatrix}$.

Equation (A.8) can be written in matrix form as,

$$\mathbf{C}_\mathbf{p}^\mathbf{c} = \overline{\mathbf{X}}_\mathbf{p}^\mathbf{c}\boldsymbol{\beta}_\mathbf{p}^\mathbf{c} + \boldsymbol{\eta}_\mathbf{p}^\mathbf{c} \tag{A.9}$$

Like (A.7), $\beta_\mathbf{p}^\mathbf{c}$ can also be estimated using BLUE as,

$$\widehat{\boldsymbol{\beta}}_\mathbf{p}^\mathbf{c} = [\overline{\mathbf{X}}_\mathbf{p}^\mathbf{c}]^{-1}\mathbf{C}_\mathbf{p}^\mathbf{c} \tag{A.10}$$

where, $\hat{\beta}_\mathrm{p}^\mathrm{c}$ is the estimate of $\beta_\mathrm{p}^\mathrm{c}$ with noise.

Step 2: Nominal gain and phase estimation

The nominal gain and phase can be estimated as follows:

The received signal after the I/Q distortion, at the various pilot frequencies for the for i^{th} and $(i+1)^{th}$symbols present in the m^{th}can be expressed as,

$$\begin{bmatrix} Y_m^i[k_p] \\ Y_m^{i+1}[k_p] \end{bmatrix} = \begin{bmatrix} X_m^i[k_p] & X_m^{*i}[-k_p] \\ X_m^{i+1}[k_p] & X_m^{*i+1}[-k_p] \end{bmatrix} \begin{bmatrix} U_m[k_p]H_m[k_p] \\ V_m[k_p]H_m^*[-k_p] \end{bmatrix} + \begin{bmatrix} \eta_m^i[k_p] \\ \eta_m^{i+1}[k_p] \end{bmatrix} \quad \text{(A.11)}$$

let, $\mathbf{Y_p} = \begin{bmatrix} Y_m^i[k_p] \\ Y_m^{i+1}[k_p] \end{bmatrix}$, $\overline{\mathbf{X}}_\mathbf{p} = \begin{bmatrix} X_m^i[k_p] & X_m^{*i}[-k_p] \\ X_m^{i+1}[k_p] & X_m^{*i+1}[-k_p] \end{bmatrix}$, $\boldsymbol{\lambda}_\mathbf{p} = \begin{bmatrix} U_m[k_p]H_m[k_p] \\ V_m[k_p]H_m^*[-k_p] \end{bmatrix}$,

and $\boldsymbol{\eta}_\mathbf{p} = \begin{bmatrix} \eta_m^i[k_p] \\ \eta_m^{i+1}[k_p] \end{bmatrix}$.

In the matrix form (4.13) can be written as,

$$\mathrm{Y_p} = \overline{\mathbf{X}}_\mathbf{p}\boldsymbol{\lambda}_\mathbf{p} + \boldsymbol{\eta}_\mathbf{p} \quad \text{(A.12)}$$

$\boldsymbol{\lambda}_\mathbf{p}$can be estimated from (4.22) as,

$$\hat{\boldsymbol{\lambda}}_\mathbf{p} = [\overline{\mathbf{X}}_\mathbf{p}]^{-\mathbf{1}}\mathrm{Y_p} \quad \text{(A.13)}$$

$\hat{\boldsymbol{\lambda}}_\mathbf{p}$ is the estimated version of $\boldsymbol{\lambda}_\mathbf{p}$ containing error. Similarly, for the corresponding image pilot frequencies, we have,

$$\hat{\boldsymbol{\lambda}}_\mathbf{p}^\mathbf{c} = [\overline{\mathbf{X}}_\mathbf{p}^\mathbf{c}]^{-\mathbf{1}}\mathrm{Y_p^c} \quad \text{(A.14)}$$

where, $\boldsymbol{\lambda}_\mathbf{p}^\mathbf{c} = \begin{bmatrix} U_m^*[-k_p]H_m^*[-k_p] \\ V_m^*[-k_p]H_m[k_p] \end{bmatrix}$, $\overline{\mathbf{X}}_\mathbf{p}^\mathbf{c} = \begin{bmatrix} X_m^{*i}[-k_p] & X_m^i[k_p] \\ X_m^{*i+1}[-k_p] & X_m^{i+1}[k_p] \end{bmatrix}$ and

$\mathrm{Y_p^c} = \begin{bmatrix} Y_m^{*i}[-k_p] \\ Y_m^{*i+1}[-k_p] \end{bmatrix}$. Likewise, $\hat{\boldsymbol{\lambda}}_\mathbf{p}^\mathbf{c}$ is the estimated value of $\boldsymbol{\lambda}_\mathbf{p}^\mathbf{c}$ including error. Through linear interpolation we could also calculate the parameter values at each of the subcarrier indexes k. Now, by dividing $V_m^*[-k]H_m[k]$ by $U_m[k]H_m[k]$, and $V_m[k]H_m^*[-k]$ by $U_m^*[-k]H_m^*[-k]$, and after substituting the values from (4.3) and (4.4), we obtain

$$\hat{\varphi}_e[k] = \frac{1}{2} \angle \frac{\left(1 + \frac{V_m^*[-k]}{U_m}\right)\left(1 - \frac{V_m[k]}{U_m^*[-k]}\right)}{\left(1 - \frac{V_m^*[-k]}{U_m[k]}\right)\left(1 + \frac{V_m[k]}{U_m^*[-k]}\right)} \tag{A.15}$$

Also, the estimated gain is,

$$g\frac{A_{I,m}[k]}{A_{Q,m}[k]} = e^{j\hat{\varphi}} \frac{\left(1 + \frac{V_m[k]}{U_m^*[-k]}\right)}{\left(1 - \frac{V_m[k]}{U_m^*[-k]}\right)} \tag{A.16}$$

Let,
$$\hat{g}_e[k] = g\frac{A_{I,m}[k]}{A_{Q,m}[k]} \tag{A.17}$$

The values of $\hat{g}_e[k]$ and $\hat{\varphi}_e[k]$ are averaged for all the subcarriers k to obtain a single value for gain $\acute{\hat{g}}_m$ and phase $\acute{\hat{\phi}}_m$ for m^{th} frame, such that

$$\acute{\hat{g}}_m = \frac{1}{N}\sum_{k=1}^{N} \hat{g}_e[k] \tag{A.18}$$

and
$$\acute{\hat{\phi}}_m = \frac{1}{N}\sum_{k=1}^{N} \hat{\varphi}_e[k] \tag{A.19}$$

The newly adopted gain $\acute{\hat{g}}_m$and phase $\acute{\hat{\phi}}_m$ value is then averaged with the nominal gain $\hat{g}_{m-1}$ and phase $\hat{\varphi}_{m-1}$ estimated in the previous frame i.e. $(m-1)^{th}$ frame to get more steady estimates and avoid drastic changes.

$$\hat{g}_m = \frac{\acute{\hat{g}}_m + \hat{g}_{m-1}}{2} \tag{A.20}$$

$$\hat{\varphi}_m = \frac{\acute{\hat{\phi}}_m + \hat{\varphi}_{m-1}}{2} \tag{A.21}$$

Finally, $\hat{g}_m$ and $\hat{\varphi}_m$ are used to correct upcoming $(m+1)^{th}$ frame.

Step 3: Frequency domain compensation

For example, the d^{th} data symbol of the m^{th} frame first undergoes time domain I/Q balance correction. Let $c_m^d[n]$ and $y_m^d[n]$ refers the corrected signal and the received signal, respectively, for d^{th} data symbol. The corrected signal can be expressed as,

$$\begin{bmatrix} Re\{c_m^d[n]\} \\ Im\{c_m^d[n]\} \end{bmatrix} = \begin{bmatrix} g_{m-1} & 0 \\ -sin\varphi_{m-1} & cos\varphi_{m-1} \end{bmatrix}^{-1} \begin{bmatrix} Re\{y_m^d[n]\} \\ Im\{y_m^d[n]\} \end{bmatrix} \quad \text{(A.22)}$$

Note that, the data symbols of the m^{th} frame is also corrected by the gain and phase estimated during the $(m-1)^{th\text{th}}$ frame. After that the corrected signal goes through FFT and the frequency domain signal $C_m^d[k]$ is obtained. Finally the compensated output for the d^{th} data symbol $\hat{X}_m^d[k]$ is obtained as,

$$\begin{bmatrix} \hat{X}_m^d[k] \\ \hat{X}_m^{*d}[-k] \end{bmatrix} = \begin{bmatrix} \breve{U}_m[k]H_m[k] & \breve{V}_m[k]H_m^*[-k] \\ \breve{V}_m^*[-k]H_m[k] & \breve{U}_m^*[-k]H_m^*[-k] \end{bmatrix}^{-1} \cdot \begin{bmatrix} C_m^d[k] \\ C_m^{*d}[-k] \end{bmatrix} \quad \text{(A.23)}$$

Let $\widehat{\mathbf{X}}^d$ denotes the vector containing $\hat{X}_m^d[k]$. After the IFFT of $\widehat{\mathbf{X}}^d$, the estimated data signal $\hat{\mathbf{x}}^d$can be obtained as,

$$\hat{\mathbf{x}}^d = \bar{\mathbf{F}}^* \widehat{\mathbf{X}}^d \quad \text{(A.24)}$$

APPENDIX B

PARALLEL CORRECTION AND EQUALIZATION OF I/Q IMBALANCE AND CHANNEL FOR SINGLE CARRIER MODULATIONS

In this appendix we have shown a method of correcting the I/Q imbalance as a feed-back loop and equalizing the channel afterwards. Frequency-flat I/Q imbalance has been considered only. It has been shown that, if an equalizer is capable of removing all the channel effect then I/Q parameter estimation becomes more accurate. The I/Q gain and phase can be estimated by using a simple training pattern. The estimated values are then fed back to do the correction. However, for having the equalizer perform better, it is necessary to get a close proximate of the gain and phase imbalance parameters. In this way, a few training frames are required for getting a close estimation of the actual gain and phase.

For analysis, it is assumed that the entire gain imbalance is present in the I branch and the phase imbalance is on the Q branch. Let, the complex baseband representation of the discrete time transmitted signal is $x[n]$, received signal before and after I/Q distortion is given by , $r[n]$, and $z[n]$ respectively. The channel is assumed to be multipath frequency-selective with Ricean distribution stated as follows [1],

$$r[n] = \frac{\sqrt{P_0}x[n] + \sum_{l=1}^{L}\sqrt{P_l}e^{-j\theta_l}x[n-\tau_l]}{\sqrt{\sum_{l=0}^{L}P_l}} + \eta[n] \qquad \text{(B.1)}$$

where, P_0 and P_l are the received power of the Line of sight (LOS) path and the l^{th} path respectively and τ_l represents the delay of the l^{th} path; $e^{-j\theta_l}$ represents the phase shift

of the l^{th} path and $\varepsilon[n]$ is the additive white Gaussian noise. The received signal after being I/Q distorted is written by,

$$z[n] = ur[n] + vr^*[n]. \tag{B.2}$$

where,
$$u = \frac{g + e^{-j\phi}}{2}, \tag{B.3}$$

and
$$v = \frac{g - e^{j\phi}}{2}. \tag{B.4}$$

Ideally if there is no I/Q imbalance then $g = 1$ and $\phi = 0$. That makes, $u = 1$ and $v = 0$. Now putting the value of u and v in (B.2) and doing some algebraic manipulation $z[n]$ becomes,

$$z[n] = \frac{1}{2}\{g(r[n] + r^*[n]) + cos\varphi(r[n] \tag{B.5}$$

$$-r^*[n] - jsin\varphi(r[n] + r^*[n])\}$$

Splitting the complex value into its real and imaginary part as $a = a_I + ja_Q$ where a_I and a_Q, are the real and imaginary part of a respectively, and $a_I = \frac{\{a+a^*\}}{2}$ and $a_Q = \frac{\{a-a^*\}}{2j}$, we get,

$$z_I[n] = gr_I[n] \tag{B.6}$$

and
$$z_Q[n] = (cos\varphi)r_Q[n] - (sin\varphi)r_I[n] \tag{B.7}$$

(B.6) and (B.7) can be written in as,

$$\begin{bmatrix} z_I[n] \\ z_Q[n] \end{bmatrix} = \begin{bmatrix} g & 0 \\ -sin\varphi & cos\varphi \end{bmatrix} \begin{bmatrix} r_I[n] \\ r_Q[n] \end{bmatrix} \tag{B.8}$$

If the imbalance coefficients g and φ are known then I/Q imbalance can be corrected by the above equation as,

$$\begin{bmatrix} \hat{r}_I[n] \\ \hat{r}_Q[n] \end{bmatrix} = \frac{1}{gcos\varphi} \begin{bmatrix} cos\varphi & 0 \\ sin\varphi & g \end{bmatrix} \begin{bmatrix} z_I[n] \\ z_Q[n] \end{bmatrix} \tag{B.9}$$

B. I/Q parameter Estimation and Correction

The block diagram of the simulation set up is given in Figure B-1. The channel equalization and I/Q estimation have been done in two modes successively. By the

help of training symbols, first the equalization is done and then the I/Q parameter is estimated. The estimation and correction strategies are as follows: At the beginning of the first frame, the I/Q imbalance is corrected, assuming $g_0 = 1$ and $\varphi_0 = 0$. (which means no correction is done at the very beginning).By the help of training sequence (TS), the received signal is equalized to get an output with less channel effect. I/Q imbalance parameters are then estimated using the same training symbols. After the equalizer converges, the equalized data output $z_{eq}[n]$ is used to estimate the gain and phase imbalance. The estimation of gain and phase is performed over several symbols, and averaged to reduce the noise effect. The averaged estimated values are fed back during the start of the next training frame to do the I/Q correction.

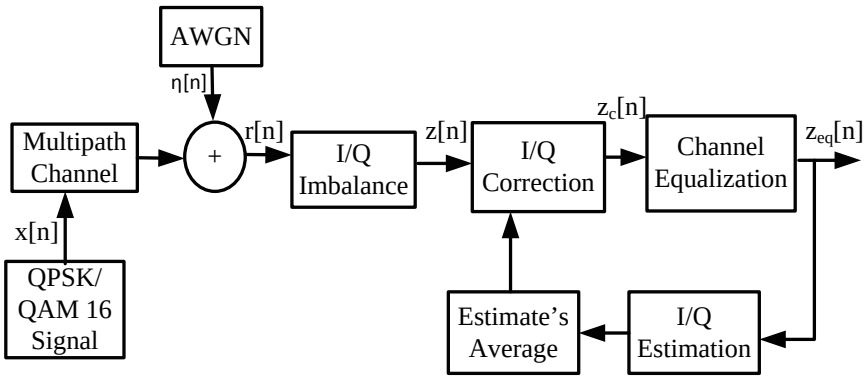

Figure B-2 Block diagram for parallel correction and equalization

Let, $x^i[n]$ and $z^i[n]$ represent the training and received signal respectively, for i^{th} frame ($i = 1,2,3 \ldots$). $z^i[n]$ contains the I/Q imbalance and multipath channel and goes through the correction process. The corrected signal $z_c^i[n]$, is input to the equalizer. The equalization is performed by least mean square (LMS) method. Let the equalizer coefficient for them^{th} tap is denoted by $w_m^i[n]$ where $m = 1,2,3 \ldots \ldots M$, and M is the total number of taps. The error signal is $e^i[n]$, u is the step size and $z_{eq}^i[n]$ is the equalized output. The equalizer coefficients at n^{th} iteration are updated as,

$$z_{eq}^i[n] = \sum_{m=1}^{M} w_m^i[n] z_c^i[n-m+1] \tag{B.10}$$

$$e^i[n] = x^i[n] - z_{eq}^i[n] \tag{B.11}$$

$$w_m^i[n+1] = w_m^i[n] + ue^i[n]z_c^{i*}[n-m+1] \quad \text{(B.12)}$$

After the equalizer converges, the received output $z_{eq}^i[n]$ would have less channel effect. As for first few frames the equalizer would not be able to remove the channel effect properly due to the presence of I/Q imbalance. Hence, the estimation will not be very accurate. Now assuming the channel has been removed completely and no noise is present, the real and imaginary part of the equalized output is given by (using (B.6) and (B.7)),

$$z_{eq_I}{}^i[n] = g^i x_I^i[n] \quad \text{(B.13)}$$

$$z_{eq_Q}{}^i[n] = (cos\varphi^i)x_Q^i[n] - (sin\varphi^i)x_I^i[n] \quad \text{(B.14)}$$

Taking the square of (B.14),

$$z_{eq_Q}{}^i[n] = cos^2\varphi^i\,(x_Q^i[n])^2 + +sin^2\varphi^i\,(x_I^i[n])^2 \quad \text{(B.15)}$$

$$-2\,cos\varphi^i\,sin\varphi^i x_Q^i[n]x_I^i[n]$$

The training symbols have been designed in such a way so that the real and imaginary parts are equal. This can be written as,

$$x_I^i[n] = x_Q^i[n] \quad \text{(B.16)}$$

Then (B.15) can be simplified as,

$$(z_{eq_Q}{}^i[n])^2 = (x_I^i[n])^2\{1 - \sin(2\varphi^i)\} \quad \text{(B.17)}$$

So, the estimated gain and phase can be written as,

$$\hat{g}^i = \frac{z_{eq_I}{}^i[n]}{x_I^i[n]} \quad \text{(B.18)}$$

$$\hat{\varphi}^i = \frac{1}{2}\left\{sin^{-1}\left(1 - \frac{(z_{eq_Q}{}^i[n])^2}{(x_I^i[n])^2}\right)\right\} \quad \text{(B.19)}$$

The estimated values have been averaged. Thus it reduces the effect of Gaussian Noise. The average estimated gain $\hat{g}_{av}^i$ and phase $\hat{\varphi}_{av}^i$, can be written as,

$$\hat{g}_{av}^{i} = \frac{1}{N_k}\sum_{k=1}^{Nk}\frac{{z_{eq}}_I^{\,i}[k]}{x_I^i[k]} \tag{B.20}$$

$$\hat{\varphi}_{av}^{i} = \frac{1}{N_k}\sum_{k=1}^{Nk}\frac{1}{2}\left\{sin^{-1}\left(1-\frac{({z_{eq}}_Q^{\,i}[k])^2}{(x_I^i[k])^2}\right)\right\} \tag{B.21}$$

where $k = 1,2,3 \ldots\ldots N_k$ and N_k is the number of the training symbols. The estimated gain $\hat{g}_i$ and phase $\hat{\varphi}_i$ which would be responsible for correcting the next frame is updated as follows:

$$\hat{g}_i = \frac{\hat{g}_{i-1} + \hat{g}_{i-1} + (\hat{g}_{av}^{i} - 1)}{2} \tag{B.22}$$

$$\hat{\varphi}_i = \frac{\hat{\varphi}_{i-1} + \hat{\varphi}_{i-1} + \hat{\varphi}_{av}^{i}}{2} \tag{B.23}$$

The term $\hat{g}_{i-1} + (\hat{g}_{av}^{i} - 1)$ and $\hat{\varphi}_{i-1} + \hat{\varphi}_{av}^{i}$ are averaged with $\hat{g}_{i-1}$ and $\hat{\varphi}_{i-1}$ (the gain and phase obtained during the $(i-1)^{th}$ frame) respectively to reduce the noise effect. Finally the $(i+1)^{th}$ frame is corrected as,

$$\begin{bmatrix} z_{cI}^{i+1}[n] \\ z_{cQ}^{i+1}[n] \end{bmatrix} = \frac{1}{\hat{g}_i cos\varphi}\begin{bmatrix} cos\hat{\varphi}_i & 0 \\ sin\hat{\varphi}_i & \hat{g}_i \end{bmatrix}\begin{bmatrix} z_I^{i+1}[n] \\ z_Q^{i+1}[n] \end{bmatrix} \tag{B.24}$$

APPENDIX C

LIST OF PUBLICATIONS

[1] **K. N. Haq** and C. Kah-Seng, "Correction and compensation of I/Q imbalance and multipath channel for OFDM receivers," in *9th IEEE International Symposium on Communication Systems, Networks & Digital Signal Processing, CSNDSP 2014*, Manchester, United Kingdom, July, 2014, pp. 966-971.

[2] **K. N. Haq** and C. Kah Seng, "Correction of in phase-quadrature imbalance in the presence of multipath fading," in *IEEE Australian Communications Theory Workshop, AusCTW 2014*, Sydney, Australia, February, 2014, pp. 79-83.

[3] **K. N. Haq** and C. Kah Seng, "An adaptive approach to mitigate the effects of I/Q imbalance and multipath channel," in *19th IEEE Asia-Pacific Conference on Communications, APCC 2013*, Bali, Indonesia, August, 2013, pp. 550-555.

REFERENCES

[1] R. B. Palipana, "A Direct-conversion Receiver for DVB-T," PhD Thesis, Department of Electrical and Computer Engineering, Curtin University of Technology, 2006.

[2] A. Tarighat, R. Bagheri, and A. H. Sayed, "Compensation schemes and performance analysis of IQ imbalances in OFDM receivers," *IEEE Transactions on Signal Processing*, vol. 53, pp. 3257-3268, 2005.

[3] J. Sevenhans, F. Op't Eynde, and P. Reusens, "The silicon radio decade," *IEEE Transactions on Microwave Theory and Techniques*, vol. 50, pp. 235-244, 2002.

[4] M. Loy, "Understanding and Enhancing Sensitivity in Receivers for Wireless Applications," *Texus instruments*, 1999.

[5] B. Narasimhan, W. Dandan, S. Narayanan, H. Minn, and N. Al-Dhahir, "Digital Compensation of Frequency-Dependent Joint Tx/Rx I/Q Imbalance in OFDM Systems Under High Mobility," *IEEE Journal of Selected Topics in Signal Processing*, vol. 3, pp. 405-417, 2009.

[6] E. Nemer and A. Said, "An iterative feedback algorithm for correcting the I/Q imbalance in DVB-S receivers," in *IASTED Conference on Communication Systems and Networks, CSN 2004*, Marbella, Spain, September, 2004.

[7] M. Valkama, M. Renfors, and V. Koivunen, "Blind source separation based I/Q imbalance compensation," in *The IEEE Adaptive Systems for Signal Processing, Communications, and Control Symposium, AS-SPCC 2000*, Lake Louise, Canada, October, 2000, pp. 310-314.

[8] M. Valkama, M. Renfors, and V. Koivunen, "Advanced methods for I/Q imbalance compensation in communication receivers," *IEEE Transactions on Signal Processing*, vol. 49, pp. 2335-2344, 2001.

[9] M. Valkama, M. Renfors, and V. Koivunen, "Blind I/Q signal separation-based solutions for receiver signal processing," *EURASIP Journal on Advances in Signal Processing*, vol. 2005, pp. 2708-2718, 2005.

[10] A. Schuchert, R. Hasholzner, and P. Antoine, "A novel IQ imbalance compensation scheme for the reception of OFDM signals," *IEEE Transactions on Consumer Electronics*, vol. 47, pp. 313-318, 2001.

[11] M. Mailand, R. Richter, and H.-j. Jentschel, "Blind IQ-Imbalance Compensation Using Iterative Inversion for Arbitrary Direct Conversion Receivers," in *IST Mobile & Wireless Communications Summit*, Dresden, Germany, June, 2005, vol. 14.

[12] L. Anttila, M. Valkama, and M. Renfors, "Circularity-Based I/Q Imbalance Compensation in Wideband Direct-Conversion Receivers," *IEEE Transactions on Vehicular Technology*, vol. 57, pp. 2099-2113, 2008.

[13] M. Valkama, M. Renfors, and V. Koivunen, "On the performance of interference canceller based I/Q imbalance compensation," in *IEEE International Conference on Acoustics, Speech, and Signal Processing, ICASSP 2000*, Istanbul, Turkey, June, 2000, vol.5, pp 2885-2888.

[14] H. A. Mahmoud, H. Arslan, M. K. Ozdemir, and F. E. Retnasothie, "IQ Imbalance Correction for OFDMA Uplink Systems," in *IEEE International Conference on Communications, ICC 2009*, Dresden, Germany, June, 2009, pp. 1-5.

[15] L. Anttila, M. Valkama, and M. Renfors, "Efficient Mitigation of Frequency-Selective I/Q Imbalance in OFDM Receivers," in *IEEE Vehicular Technology Conference, VTC 2008-Fall*, Calgary, Canada, September, 2008, pp. 1-5.

[16] B. Razavi, "Design considerations for direct-conversion receivers," *IEEE Transactions on Circuits and Systems II: Analog and Digital Signal Processing*, vol. 44, pp. 428-435, 1997.

[17] J. Ryynanen, K. Kivekas, J. Jussila, A. Parssinen, and K. A. I. Halonen, "A dual-band RF front-end for WCDMA and GSM applications," *IEEE Journal of Solid-State Circuits*, vol. 36, pp. 1198-1204, 2001.

[18] A. Pärssinen, *Direct Conversion Receivers in Wide-Band Systems*: Springer, 2001.

[19] F. E. Churchill, G. W. Ogar, and B. J. Thompson, "The Correction of I and Q Errors in a Coherent Processor," *IEEE Transactions on Aerospace and Electronic Systems*, vol. AES-17, pp. 131-137, 1981.

[20] J. P. F. Glas, "Digital I/Q imbalance compensation in a low-IF receiver," in *Global Telecommunications Conference, GLOBECOM 1998*, Sydney, Australia, November, 1998, vol.3, pp. 1461-1466.

[21] P. Kong-Pang, J. E. Franca, and C. Azeredo-Leme, "Wideband digital correction of I and Q mismatch in quadrature radio receivers," in *The IEEE International Symposium on Circuits and Systems, ISCAS 2000*, Geneva, Switzerland, May, 2000, vol.5, pp. 661-664.

[22] H. L. Van Trees, *Detection, Estimation, and Modulation Theory, Optimum Array Processing*: Wiley, 2004.

[23] M. Schwartz, *Information Transmission, Modulation, and Noise*: McGraw-Hill, 1990.

[24] Y. Li and W. M. Snelgrove, "A novel adaptive mismatch cancellation system for quadrature IF radio receivers," *IEEE Transactions on Circuits and Systems II: Analog and Digital Signal Processing*, vol. 46, pp. 789-801, 1999.

[25] P. Hyeong Getin, P. Chul, O. Hyunseo, and K. Mun Geon, "RF gain/phase and I/Q imbalance error correction technique for multi-channel array antenna systems," in *Vehicular Technology Conference, VTC 2001-Spring*, Rhodes, Greece, May, 2001, pp. 175-179 vol.1.

[26] J. K. Cavers and M. W. Liao, "Adaptive compensation for imbalance and offset losses in direct conversion transceivers," *IEEE Transactions on Vehicular Technology*, vol. 42, pp. 581-588, 1993.

[27] S. Il-Hyun, J. Eui-Rim, and Y. H. Lee, "Data-aided approach to I/Q mismatch and DC offset compensation in communication receivers," *IEEE Communications Letters*, vol. 6, pp. 547-549, 2002.

[28] M. Valkama and M. Renfors, "Advanced DSP for I/Q imbalance compensation in a low-IF receiver," in *IEEE International Conference on Communications, ICC 2000*, New Orleans, USA, June, 2000, vol.2, pp. 768-772.

[29] G. Gil, S. Il-Hyun, Y. H. Lee, S. Young Ik, and P. Jin Kyu, "Joint ML estimation of I/Q mismatch, DC offset, carrier frequency, and channel for direct-conversion receivers," in *IEEE Semiannual Vehicular Technology Conference, VTC 2003-Spring*, Jeju, Korea, April, 2003, vol.4, pp. 2348-2352.

[30] G. Gye-Tae, S. Il-Hyun, P. Jin-Kyu, and Y. H. Lee, "Joint ML estimation of carrier frequency, channel, I/Q mismatch, and DC offset in communication receivers," *IEEE Transactions on Vehicular Technology*, vol. 54, pp. 338-349, 2005.

[31] J.-F. Cardoso and B. H. Laheld, "Equivariant adaptive source separation," *IEEE Transactions on Signal Processing*, vol. 44, pp. 3017-3030, 1996.

[32] L. Anttila, M. Valkama, and M. Renfors, "Gradient-based blind iterative techniques for I/Q imbalance compensation in digital radio receivers," in *IEEE 8th Workshop on Signal Processing Advances in Wireless Communications, SPAWC 2007*, Helsinki, Finland, June, 2007, pp. 1-5.

[33] S. Kexuan, I. Darwazeh, H. Li-Ke, and A. Jones, "Optimal pilot based frequency-dependent I/Q imbalance compensation for wideband direct-conversion transmitters," in *IEEE Wireless Communications and Networking Conference, WCNC 2012*, Paris, France, April, 2012, pp. 226-231.

[34] U. Oruthota and O. Tirkkonen, "Effect of imperfect channel estimation in I/Q imbalanced OFDM system," in *6th International Wireless Communications and Mobile Computing Conference*, Caen, France, June, 2010.

[35] L. Chia-Liang, "Impacts Of I/Q Imbalance On Qpsk-ofdm-qam Detection," in *International Conference on Consumer Electronics, ICCE 1998*, Los Angeles, USA, June, 1998, pp. 384-385.

[36] S. Coleri, M. Ergen, A. Puri, and A. Bahai, "Channel estimation techniques based on pilot arrangement in OFDM systems," *IEEE Transactions on Broadcasting*, vol. 48, pp. 223-229, 2002.

[37] G. Auer, "Pilot-symbol aided channel estimation by Wiener filtering for OFDM systems with multiple transmit antennas," in *5th IEE International Conference on 3G Mobile Communication Technologies, 3G 2004*, London, United Kingdom, October, 2004, pp. 6-10.

[38] A. S. Mahdi and E. Ercelebi, "Reduced number of pilot in comb-type pilot arrangement by using modified least square channel estimation for OFDM system," in *21st Signal Processing and Communications Applications Conference, SIU 2013*, North Cyprus, Turkey, April, 2013, pp. 1-4.

[39] C. Tao, W. Min, and F. Yong, "A Novel Frequency-Domain Channel Parameters Estimation Method by Time-Domain Pilots Inserting for OFDM Systems," in *4th International Symposium on Wireless Pervasive Computing, ISWPC 2009,* Melbourne, Australia, February, 2009, pp. 1-5.

[40] W. Xianbin, P. Ho, and W. Yiyan, "Robust channel estimation and ISI cancellation for OFDM systems with suppressed features," *IEEE Journal on Selected Areas in Communications,* vol. 23, pp. 963-972, 2005.

[41] T. Yamamura and H. Harada, "High mobility OFDM transmission system by a new channel estimation and ISI cancellation scheme using characteristics of pilot symbol inserted OFDM signal," in IEEE *Vehicular Technology Conference, VTC 1999-Fall,* Amsterdam, Netherlands, September, 1999, vol.1, pp. 319-323.

[42] D. Linglong, W. Zhaocheng, and Y. Zhixing, "Time-Frequency Training OFDM with High Spectral Efficiency and Reliable Performance in High Speed Environments," *IEEE Journal on Selected Areas in Communications,* vol. 30, pp. 695-707, 2012.

[43] K. Ozaki, K. Tomitsuka, A. Okazaki, H. Sano, and H. Kubo, "Channel estimation technique for OFDM systems spread by chirp sequences," in *IEEE 23rd International Symposium on Personal Indoor and Mobile Radio Communications, PIMRC 2012,* Sydney, Australia, September, 2012, pp. 2125-2130.

[44] Z. Yaning, M. Valkama, and M. Renfors, "Pilot-Based Compensation of Frequency-Selective I/Q Imbalances in Direct-Conversion OFDM Transmitters," in *IEEE Vehicular Technology Conference, VTC 2008-Fall,* Calgary, Canada, September, 2008, pp. 1-5.

[45] O. Ozdemir, R. Hamila, and N. Al-Dhahir, "Digital baseband compensation of frequency-dependent joint TX/RX I/Q imbalance in beamforming MIMO OFDM transceivers," in *IEEE International Conference on Communications, ICC 2012,* Ottawa, Canada, June, 2012, pp. 3585-3589.

[46] B. Narasimhan, S. Narayanan, N. Al-Dhahir, and H. Minn, "Digital baseband compensation of joint TX/RX frequency-dependent I/Q imbalance in mobile

MIMO-OFDM transceivers," in *43rd Annual Conference on Information Sciences and Systems, CISS 2009*, Maryland, USA, March, 2009, pp. 545-550.

[47] B. Narasimhan, S. Narayanan, H. Minn, and N. Al-Dhahir, "Reduced-complexity baseband compensation of joint Tx/Rx I/Q imbalance in mobile MIMO-OFDM," *IEEE Transactions on Wireless Communications*, vol. 9, pp. 1720-1728, 2010.

[48] H. Jeng-Kuang, C. Wei-Ming, C. Yu-Lun, L. Shin-Ju, and L. Jien-Liang, "Adaptive Baseband Compensation for I/Q Imbalance and Time-Varying Channel in OFDM System," in *International Symposium on Intelligent Signal Processing and Communications, ISPACS 06*, Tottori, Japan, December, 2006, pp. 638-641.

[49] L. Jian, A. Kortke, and W. Keusgen, "Joint MIMO channel- and frequency-selective I/Q-imbalance estimation using a multi-functional preamble for OFDM systems," in *International Symposium on Signals, Systems, and Electronics, ISSSE 2012*, Potsdam, Germany, October, 2012, pp. 1-6.

[50] D. Juinn-Horng and F. Kuo-Tai, "Time-frequency-multiplex preamble design for joint I/Q imbalance, CFO and channel estimation in OFDM systems," in *15th International Conference on Advanced Communication Technology, ICACT* 2013, PyeongChang, Korea, January, 2013, pp. 295-300.

[51] R. B. Palipana and C. Kah-Seng, "Frequency Domain IQ Correction in a Direct conversion Receiver for DVB-T," in *Asia-Pacific Conference on Communications, APCC 2005*, Perth, Australia, October, 2005, pp. 590-594.

[52] R. B. Palipana and C. Kah-Seng, "IQ Cross-talk Compensation in Fading Channels," in *Asia-Pacific Conference on Communications, APCC 2006*, Busan, Korea, August, 2006, pp. 1-5.

[53] S. Traverso, M. Ariaudo, I. Fijalkow, J. L. Gautier, and C. Lereau, "Decision-Directed Channel Estimation and High I/Q Imbalance Compensation in OFDM Receivers," *IEEE Transactions on Communications*, vol. 57, pp. 1246-1249, 2009.

[54] J. Tubbax, B. Come, L. Van der Perre, S. Donnay, M. Engels, H. De Man, *et al.*, "Compensation of IQ imbalance and phase noise in OFDM systems," *IEEE Transactions on Wireless Communications*, vol. 4, pp. 872-877, 2005.

[55] O. Ozdemir, R. Hamila, and N. Al-Dhahir, "I/Q Imbalance in Multiple Beamforming {OFDM} Transceivers: SINR Analysis and Digital Baseband Compensation," *IEEE Transactions on Communications*, vol. 61, pp. 1914-1925, 2013.

[56] S. Simoens, M. de Courville, F. Bourzeix, and P. de Champs, "New I/Q imbalance modeling and compensation in OFDM systems with frequency offset," in *The 13th IEEE International Symposium on Personal, Indoor and Mobile Radio Communications, PIMRC 2002*, Lisbon, Portugal, September, 2002, vol.2, pp. 561-566.

[57] Y. Egashira, Y. Tanabe, and K. Sato, "A Novel IQ Imbalance Compensation Method with Pilot-Signals for OFDM System," in *IEEE Vehicular Technology Conference, VTC 2006-Fall*, Montreal, Canada, September, 2006, pp. 1-5.

[58] E. Lopez-Estraviz, S. De Rore, F. Horlin, and A. Bourdoux, "Pilot design for Joint Channel and Frequency-Dependent Transmit/Receive IQ Imbalance Estimation and Compensation in OFDM-Based Transceivers," in *IEEE International Conference on Communications, ICC 2007*, Glasgow, Scotland, June, 2007, pp. 4861-4866.

[59] H. Lanlan, M. Shaodan, W. Yik-Chung, Z. Yiqing, N. Tung-Sang, and H. V. Poor, "Pilot-Aided IQ Imbalance Compensation for OFDM Systems Operating Over Doubly Selective Channels," *IEEE Transactions on Signal Processing*, vol. 59, pp. 2223-2233, 2011.

[60] E. Lopez-Estraviz, S. De Rore, F. Horlin, and L. Van der Perre, "Optimal Training Sequences for Joint Channel and Frequency-Dependent IQ Imbalance Estimation in OFDM-based Receivers," in *IEEE International Conference on Communications, ICC 2006*, Istanbul, Turkey, June, 2006, pp. 4595-4600.

[61] G. Jingbo, Z. Xu, L. Hai, and A. K. Nandi, "Kalman Filtering Based Compensation for I/Q Imbalance and CFO in Time-Varying MIMO OFDM Systems," in *IEEE Global Telecommunications Conference, GLOBECOM 2009*, Hawaii, USA, December, 2009, pp. 1-6.

[62] L. Brötje, S. Vogeler, K.-D. Kammeyer, R. Rückriem, and S. Fechtel, "Estimation and correction of transmitter-caused I/Q imbalance in OFDM

systems," in *7th International OFDM workshop, InOWo 2002*, Hamburg, Germany, September, 2002, pp. 178-182.

[63] G. Jingbo, Z. Xu, L. Hai, and A. K. Nandi, "Blind I/Q Imbalance Compensation Using Independent Component Analysis in MIMO OFDM Systems," in *IEEE Wireless Communications and Networking Conference, WCNC 2009*, Budapest, Hungary, April, 2009, pp. 1-6.

[64] R. Sharma, H. Lalitha, and N. Kumar, "Design and development of non data aided estimation algorithm for carrier frequency-offset and I/Q imbalancing in OFDM-based systems," in *IEEE 10th International Conference on Wireless and Optical Communications Networks, WOCN 2013*, Bhopal, India, July, 2013, pp. 1-4.

[65] M. Valkama, L. Anttila, and M. Renfors, "Some radio implementation challenges in 3G-LTE context," in *IEEE 8th Workshop on Signal Processing Advances in Wireless Communications, SPAWC 2007*, Helsinki, Finalnd, June, 2007, pp. 1-5.

[66] M. Valkama, M. Renfors, and V. Koivunen, "Blind I/Q imbalance compensation in OFDM receivers based on adaptive I/Q signal decorrelation," in *IEEE International Symposium on Circuits and Systems, ISCAS 2005*, Kobe, Japan, May, 2005, vol. 3, pp. 2611-2614.

[67] M. Windisch and G. Fettweis, "Blind Estimation and Compensation of I/Q Imbalance in OFDM Receivers with Enhancements Through Kalman Filtering," in *IEEE 14th Workshop on Statistical Signal Processing, SSP 2007*, Wisconsin, USA, August, 2007, pp. 754-758.

[68] Z. Zhiwen, H. Xinping, and H. Leung, "Blind Compensation of Frequency-Dependent I/Q Imbalance in Direct Conversion OFDM Receivers," *IEEE Communications Letters*, vol. 17, pp. 297-300, 2013.

[69] P. Rabiei, N. Won, and N. Al-Dhahir, "Low-Complexity OFDM Channel Estimation in the Presence of I/Q Imbalance and Phase Noise," in *IEEE Global Telecommunications Conference, GLOBECOM 2009*, Hawaii, USA, December, 2009, pp. 1-5.

[70] M. Windisch and G. Fettweis, "On the performance of standard-independent I/Q imbalance compensation in OFDM direct-conversion receivers," in *13th*

European Signal Processing Conference, EUSIPCO 2005, Antalya, Turkey, September, 2005.

[71] LeonWcouch, II, "Complex Envelope Representations for Modulated Signals," in *Mobile Communications Handbook, Third Edition*, ed: CRC Press, 2012, pp. 55-70.

[72] A. Q. Kiayani, "DSP Based Transmitter I/Q Imbalance Calibration: Implementation and Performance Measurements," M.Sc Thesis, Tampere University of Technology, Tampere, 2009.

[73] *3GPP*. Available: http://www.3gpp.org/

[74] S. M. Kay, "Fundamentals of statistical signal processing: estimation theory," 1993.

[75] J. A. Srar, C. Kah-Seng, and A. Mansour, "Adaptive Array Beamforming Using a Combined LMS-LMS Algorithm," *IEEE Transactions on Antennas and Propagation*, vol. 58, pp. 3545-3557, 2010.

[76] W. Tranter, K. Shanmugan, T. Rappaport, and K. Kosbar, *Principles of communication systems simulation with wireless applications*: Prentice Hall Press, 2003.